MASTERS DISSERTATION

For the degree

Master of Science (MSc) in Environmental Science

at the

University of South Africa

TITLE:

Satellite based synthetic aperture radar and optical spatial-temporal information as aid for operational and environmental mine monitoring

By

Dr Corné ELOFF

(BA (Pol), BA Hons, LLB, MBA, D Litt et Phil)

Professional GISc Practitioner – PGP 1200

Student Number: 3034-380-1

Supervisor: Mr Maarten Jordaan

Date: April 2018

Mobile: +27 (0) 71 850 1610

E-mail: corne.eloff@airbus.com

Dedication

To my two sons Damian and Marcell whose support impelled me to undertake this research project.

To my mother and father, Mona and Gert, who continuously believe in me and who have provided their unselfish support to me over my academic career since 1994.

My Heavenly Father who gave me the opportunity and talent to study.

Declaration

I **Corné ELOFF** hereby declare that the dissertation which I hereby submit for the degree of Master of Science in Environmental Science at the University of South Africa, is my own work and has not been submitted by me for a degree at this or any other institution.

I declare that this dissertation does not contain any written work presented by other persons whether written, pictures, graphs or data or any other information without acknowledging the source.

I declare that my study adheres to the research ethics policy of the University of South Africa, as per approval received from the CAES Research Ethics Review Committee, Ref. 2017/CAES/002.

I declare that the content of my dissertation has been assessed through an electronic plagiarism detection program before final submission for examination.

Student signature: **Date: 5 April 2018**

Acknowledgements

I wish to declare full acknowledgement to the following people and organisations that supported me during this dissertation, without their devoted support this study would not have been possible:

- The University of South Africa, particularly the College of Agriculture and Environmental Sciences for its leadership and personnel for supporting me during this dissertation. Special thanks go to my supervisor **Mr Maarten Jordaan** for his invaluable guidance and support until the successful completion of this dissertation.
- Airbus Defence and Space, for the support and permission to use its satellite optical (Pléiades) and SAR (TerraSAR-X) products and services during this study. Special thanks to the SMM team in Postdam, Germany, **Dr Jan Anderson, Andreas Roesler and Maik Bindrich, for their support and for providing the SMM products**. Gratitude towards the Toulouse office, France for the extraction and delivery of the Pléiades imagery, with specific reference to **Vincent Garros** and **Philomene Jacquier**.
- Anglo American Kumba Iron Ore for their leadership and support to incubate the utilisation of satellite imagery as a solution for mine monitoring in South Africa. Special thanks to **Johan van Heerden** in his role as visionary to test the satellite imagery monitoring concept over the Sishen and Kolomela iron ore mines.
- Pinkmatter Solutions for their support in the utilisation of their advanced image processing system, FarEarth. The consistency in the quality of ortho-rectification, elevation and land cover classification products is a result of the quality of this system and the leadership demonstrated in the vision for automated image processing services, and certainly a result of excellence in software engineering. Special thanks to the management and technical team, **Thinus Prinsloo, Sonja Goosen, Chris Bhöme and Philip Bouwer**.
- PCI Geomatics and MapAfrica for their support in obtaining a software license to analyse the RS products during this study. Special thanks to **Kevin Melhuish and Wolfgang Lu̇ck**. Furthermore, full acknowledgement for the technical support and leadership in the technical workflow procedures during

the Pléiades elevation model generation and geometrical accuracy methodology provided by **Wolfgang Lu̇ck**.

- ESRI SA for the ArcGIS software license to enable various spatial analyses, statistics and the necessary layout view tools to transfer the results into the dissertation. Special thanks to **Marius Burger** for his support during the writing of this dissertation.
- GeoTerraImage for their assistance with the Landsat 8 2014/2015 land cover composite over the Sishen and Kolomela study areas. The accuracy and consistency of these products show true leadership in the science of RS land cover classification. Special thanks to **Mark Thompson** for his technical and product support during this dissertation.

Abstract

A sustainable society is a society that satisfies its resource requirements without endangering the sustainability of these resources. The mineral endowment on the African continent is estimated to be the first or second largest of world reserves. Therefore, it is recognised that the African continent still heavily depends on mineral exports as a key contributor to the gross domestic product (GDP) of various countries. These mining activities, however, do introduce primary and secondary environmental degradation factors. They attract communities to these mining areas, light and heavy industrial establishments occur, giving rise to artisanal activities.

This study focussed on satellite RS products as an aid to a mine's operations and the monitoring of its environment. Effective operational mine management and control ensures a more sustainable and profitable lifecycle for mines. Satellite based RS holds the potential to observe the mine and its surrounding areas at high temporal intervals, different spectral wavelengths and spatial resolutions. The combination of SAR and optical information creates a spatial platform to observe and measure the mine's operations and the behaviour of specific land cover and land use classes over time and contributes to a better understanding of the mining activities and their influence on the environment within a specific geographical area.

This study will introduce an integrated methodology to collect, process and analyse spatial information over a specific targeted mine. This methodology utilises a medium resolution land cover base map, derived from Landsat 8, to understand the predominant land cover types of the surrounding area. Using very high resolution mono- and stereoscopic satellite imagery provides a finer scale analysis and identifies changes in features at a smaller scale. Combining these technologies with the synthetic aperture radar (SAR) applications for precise measurement of surface subsidence or upliftment becomes a spatial toolbox for mine management.

This study examines a combination of satellite remote sensing products guided by a systematic workflow methodology to integrate spatial results as an aid for mining operations and environmental monitoring. Some of the results that can be highlighted is the successful land cover classification using the Landsat 8 satellite. The land cover that dominated the Kolomela mine area was the

“SHRUBLAND/GRASS” class with a 94% coverage and “MINE” class of 2.6%. Sishen mine had a similar dominated land cover characteristic with a “SHRUBLAND/GRASS” class of 90% and “MINE” class of 4.8%. The Pléiades time-series classification analysis was done using three scenes each acquired at a different time interval. The Sishen and Kolomela mine showed especially changes from the bare soil class to the asphalt or mine class. The Pléiades stereoscopic analysis provided volumetric change detection over small, medium, large and recessed areas. Both the Sishen and Kolomela mines demonstrated height profile changes in each selected category. The last category of results focused on the SAR technology to measure within millimetre accuracy the subsidence and upliftment behaviour of surface areas over time. The Royal Bafokeng Platinum tailings pond area was measured using 74 TerraSAR-X scenes. The tailings wall area was confirmed as stable with natural subsidence that occurred in its surrounding area due to seasonal changes of the soil during rainy and dry periods. The Chuquicamata mine as a large open pit copper mine area was analysed using 52 TerraSAR-X scenes. The analysis demonstrated significant vertical surface movement over some of the dumping sites.

It is the wish of the researcher that this dissertation and future research scholars will continue to contribute in this scientific field. These contributions can only assist the mining sector to continuously improve its mining operations as well as its monitoring of the primary as well as the secondary environmental impacts to ensure improved sustainability for the next generation.

Key words

Landsat 8, Pléiades, TerraSAR-X, Chuquicamata Mine, Sishen Mine, Kolomela Mine, Royal Bafokeng Platinum tailings pond, Africa, Airbus Defence and Space, mining, minerals, environment, land cover, monoscopic, stereoscopic, surface movement monitoring, elevation models, remote sensing, classification, image processing, image analysis, spatial information, temporal, Earth

Table of contents

List of figures

Chapter 4: Analytical optical results

List of tables

Chapter 4: Analytical optical results

Chapter 5: SAR surface movement monitoring results

List of graphs

List of equations

List of abbreviations

Centre National D'Etudes Spatiales	CNES
Charge-coupled device	CCD
Corner Reflector Interferometry SAR	CRInSAR
Differential Interferometric SAR	DInSAR
Differential SAR Interferometry	DInSAR
Digital Elevation Model	DEM
Digital Surface Model	DSM
Digital Terrain Model	DTM
Distinct Urban Mines	DUM
Environmental impact assessment	EIA
File Transfer Protocol	FTP
Food and Agriculture Organization of the United Nations	FAO
Gigabyte	GB
Ground Sampling Distance	GSD
Instantaneous Field Of View	IFOV
Interferometric Point Target Analysis	IPTA
Life of Mine	LoM
line-of-sight	LOS
Movement in line-of-sight	MLOS
National Land Cover	NLC
Normalized Difference Vegetation Index	NDVI
Persistent Scatterer Interferometry	PSI
Rational polynomial coefficient	RPC
Remote sensing	RS
Small Baseline approach	SBAS
Small Baseline Subset	SBAS
Surface movement monitoring	SMM
Synthetic Aperture Radar	SAR
Système Pour l'Observation de la Terre	SPOT
Time Delay Integration	TDI
Time Delay Integration	TDI
Top-of-atmosphere	ToA

United States Geological Survey	USGS
United States of America	USA

CHAPTER 1: INTRODUCTION

1.1 Background

Minerals, and the mining thereof, have been part of human life since ancient times and have expanded ever since. Holism is the belief that everything in nature is connected in some way. To look at things in a holistic way, means to look at the “big picture” and to come to systemic grips with the constituent parts and their inter-relationships (Steyn, 2012).

If the idea exists that progress will carry on without limits, it must be said that the unfettered growth in global human numbers has become unsustainable. A sustainable society is a society that satisfies its resource requirements without endangering the sustainability of these resources (Steyn & Buys, 2010).

Human creativity does not only evolve because of the increasing complexity of technology. It also arises from the increasing complexity and intensity of competition and conflict. Moreover, the succession of disruptive technological revolutions is compressed. An improvement in creativity should show a corresponding rapid exponential rise in the development of technology (Steyn & Buys, 2010).

Commodity prices continued to languish at historically low levels during 2015 and new investments have become harder to secure (Moore, 2016). Chinese GDP growth is set to dip below 7% and Africa has had its own challenges with terrorism, the Ebola outbreak and political instability. Mining companies are retrenching more and more labourers and taking cost-saving steps to be more efficient and profitable (Moore, 2016). Mechanisation, self-generating energy and environmental consciousness are some fundamental words that describe the next generation mines. According to the World Bank, an estimated 18% of mining projects are expected to supply their own power by 2020 (Cann, 2016).

Africa is richly endowed with mineral reserves and ranks first or second in quantity of world reserves of bauxite, cobalt, industrial diamonds, phosphate rock, platinum-

group metals (PGM), vermiculite, and zirconium. Gold mining is Africa's main mining resource (Yager, *et al.,* 2012).

According to Yager *et al, (2012)* strategic minerals and key producers in Africa during 2005 were:

- Diamonds: 46% of the world, divided as Botswana 35%; Congo (Kinshasa) 34%; South Africa 17%; Angola, 8%.
- Gold: 21% of the world, divided as South Africa 56%; Ghana, 13%; Tanzania, 10%; and Mali, 8%.
- Uranium: 16% of the world, divided as Namibia 46%; Niger 44%; South Africa less than 10%.
- Bauxite (for aluminium): 9% of the world, divided as Guinea 95%; Ghana 5%.
- Steel: 2% of the world, divided as South Africa 54%; Egypt 32%; Libya 7%; Algeria 6%.
- Aluminium: 5% of the world, divided as South Africa 48%; Mozambique 32%; Egypt 14%.
- Copper (mine/refined): 5%/ of the world, divided as Zambia 65%/77%; South Africa 15%/19%; Congo (Kinshasa) 13%/0%; Egypt 0%/3%.
- Platinum/Palladium: 62% of the world, divided as South Africa 97%/96%.
- Coal: 5% of the world, divided as South Africa 99%.

Africa as continent heavily depends on mineral exports as a key contributor to the gross domestic product (GDP) of various countries. Ongoing mining projects of more than US$1 billion are taking place in South Africa (PGM 69%; gold: 31%), Guinea (bauxite and aluminium), Madagascar (nickel), Mozambique (coal), Congo (Kinshasa) and Zambia (cobalt and copper), Nigeria and Sudan (crude petroleum), Senegal (iron), and many others (Yager, *et al.,* 2012).

Mining activities do introduce primary and secondary environmental degradation factors. Mining activities attract communities to the mining areas, formal industrial mining or even through artisanal[1] activities. According to the Food and Agriculture Organization of the United Nations (FAO), the large scale felling of trees and the

[1] Artisanal and Small-scale mining (ASM) refers to informal mining activities carried out using low technology or with minimal machinery. - See more at: http://www.miningfacts.org/communities/what-is-artisanal-and-small-scale-mining/#sthash.MjY5YvaC.dpuf

resulting decreases in forest areas are the main environmental challenges of the African Continent. Widespread clearing of the forest for agriculture, settlement and fuel needs are a reality. The rate of illegal logging, which is another main cause of deforestation, varies from country to country, such as 50% in Cameroon and 80% in Liberia. In the Democratic Republic of the Congo, desertification is primarily caused by the needs of the poor citizens, along with unsupervised logging and mining (Ahluwalia, 2007).

Direct environmental impacts from mining are the generated wastes. These wastes contain high concentrations of metals and metalloids which can be mobilised, and could potentially leaching into groundwater and surface water resources. Most of these heavy metals are highly toxic and are not biodegradable (Ahluwalia, 2007).

An open pit mine can be defined as an excavation or cut made at the surface of the ground for the purpose of extracting ore and which is open to the surface for the duration of the mine's life (Peck, 1999). To expose and mine the ore, it is generally necessary to excavate and relocate large quantities of waste rock. The main objective in any commercial mining operation is the exploitation of the mineral deposit at the lowest possible cost with a view to maximizing profits. The selection of physical design parameters and the scheduling of the ore and waste extraction program are complex engineering decisions of enormous economic significance. The planning of an open pit mine is, therefore, basically an exercise in economics, constrained by certain geologic and mining engineering aspects (Peck, 1999).

Mine planning must account for both environmental protection, beginning as early as the initial exploration, and for reclamation. It is critical that planning alleviate or mitigate potential impacts of mining for two key reasons (Barr and Cook, 2009):

- The cost of environmental protection is minimized by incorporating it into the initial design, rather than performing remedial measures to compensate for design deficiencies, and
- Negative publicity or poor public relations may have severe economic consequences.

From the start of the planning process, adequate consideration must be given to regulatory affairs. From the beginning of the mine design planning stage, data

gathering and permitting, environmental considerations are important, although benefits from a strictly economic sense may be intangible. From exploration, where core holes must be sealed and the site reclaimed, through plan development, the impacts on the environment must be considered. These impacts include aesthetics, noise, air quality (dust and pollutants), vibration, water discharge and runoff, subsidence, and process wastes; sources include the underground and surface mine infrastructure, mineral processing plant, access or haul roads, remote facilities, etc. If mining will cause quality deterioration of either surface water or groundwater, remedial and treatment measures must be developed to meet discharge standards.

The mine plan must include all the technical measures necessary to handle all the environmental problems from initial data gathering to the mine closure and reclamation of the disturbed surface area. Reclamation plans include many of the following concerns: drainage control, preservation of top soil, segregation of waste material, erosion and sediment control, solid waste disposal, control of fugitive dust and restoration of waste and mine areas. The plan must also consider the effects of mine subsidence, vibration (induced by mining, processing, transport, or subsidence), and impact on surface water and groundwater. These environmental items often dictate the economics of a planned mining operation and determine its viability (Barr and Cook, 2009).

Operational mining excellence is of immense importance to ensure viable and responsible mining. Operational excellence encompasses many functions and areas in a mining operation and requires the involvement of many people in order to be successfully supported in the operation. The seven drivers for excellence include the following (Barr and Cook, 2009):

- Performance measurement
- Continuous improvement
- Health, safety and environment (HES)
- Compliance and management
- Quality
- Knowledge management
- Human resource development

According to KPMG's Operational Excellence Framework it helps mining / resource companies to gain a strong position in markets, and retain a leading position in margins and return on investment through high levels of operations integration across functional verticals and cost competitiveness (Jansen, 2011).

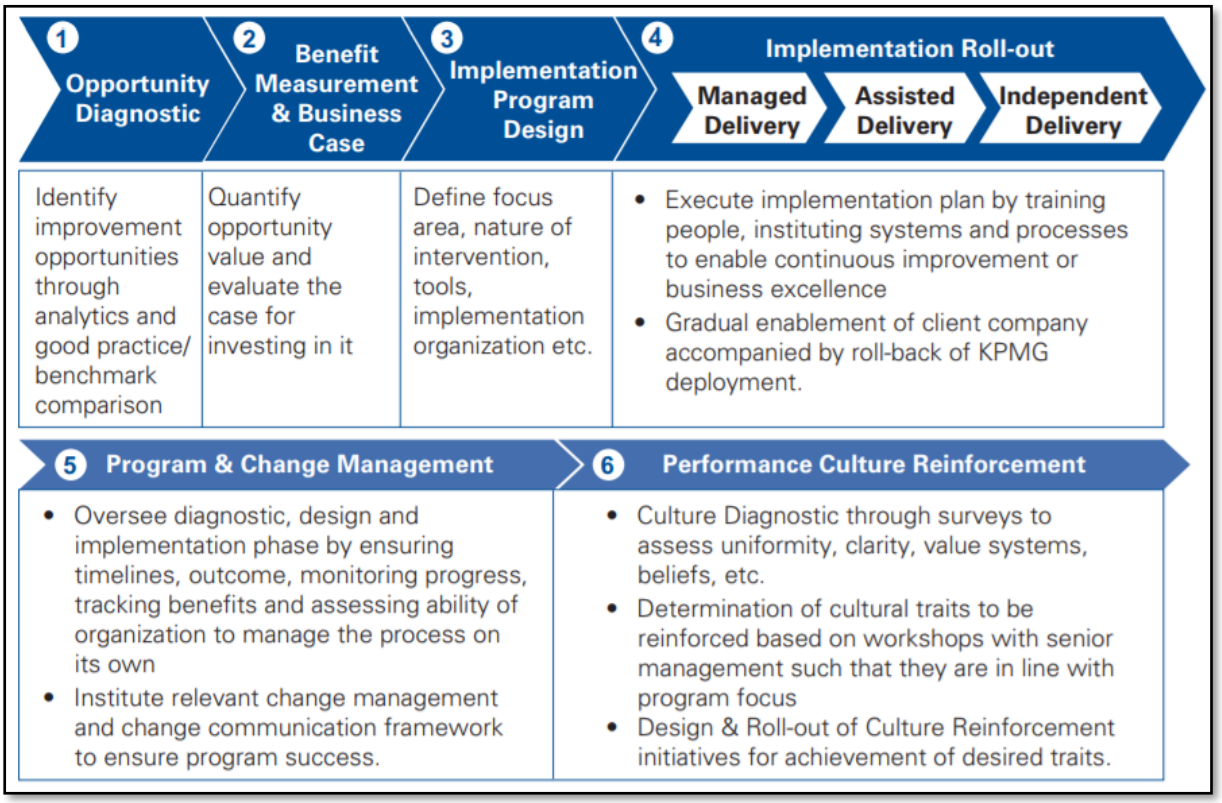

Figure 1.1: KPMG's approach towards operational excellence in mining
Source: ©2011 KPMG International Cooperative ("KPMG International") a Swiss entity. Member firms of the KPMG network of independent firms are affiliated with KPMG International. KPMG International does not provide any client service. All rights reserved.

Recognising the challenges faced by the mining sector to strive for operational excellence in combination with profitability and environmental responsibilities, a focus during this study was to demonstrate the aid that remote sensing (RS) technology can contribute to mine monitoring operations, specifically with open pit mines. An optical RS modelling will be applied over two open pit mines located in the Northern Cape, South Africa. The synthetic aperture radar (SAR) case studies were done over the Chuquicamata copper mine in Chile and the Royal Bafokeng tailings pond located near Rustenburg, South Africa.

1.2 Study Area

The **optical data** case studies focused on two prominent open pit mines in South Africa. The mines are situated in the Northern Cape near Kathu and Postmasburg.

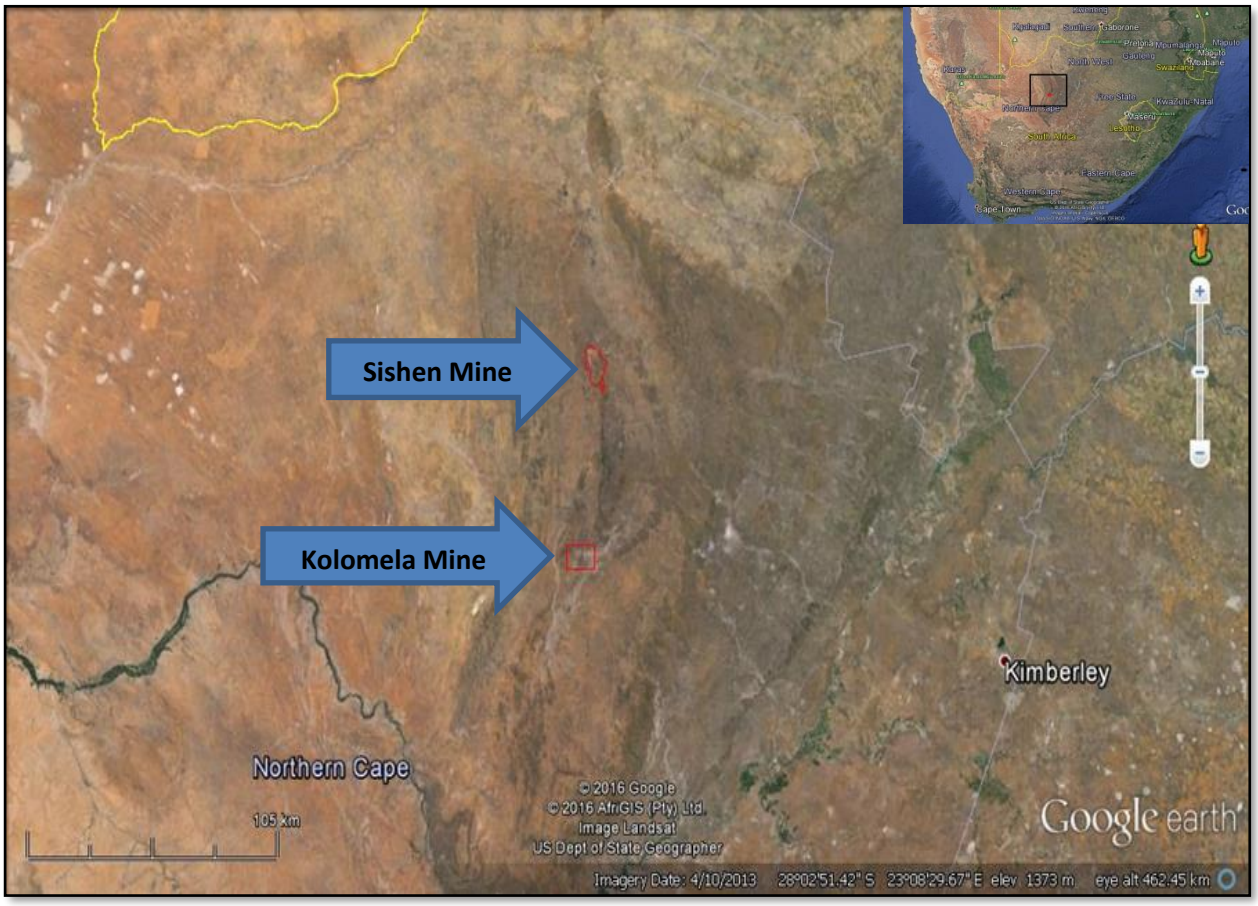

Figure 1.2: Location of two open pit mines in the Northern Cape, near Kathu and Postmasburg
Source: © Google Earth 2016

Figure 1.3: Kolomela iron ore mine near Postmasburg, Northern Cape, South Africa
Source: © PLEIADES (CNES) 2016, Distribution Airbus DS. All rights reserved.

Figure 1.4: Sishen iron ore mine near Kathu, Northern Cape, South Africa
Source: © PLEIADES (CNES) 2016, Distribution Airbus DS. All rights reserved.

The bulk of iron ore production in South Africa comes from **Sishen mine**, located in the Northern Cape Province near the mining town of Kathu. In production since 1953, Sishen mine remains a flagship operation and one of the largest open-pit mines in the world (Myburgh and Nortje, 2017).

Sishen mine has sufficient reserves to sustain a 19-year life of mine (LoM). Most of the iron ore mined here is exported, with about 3.9Mt of its production being supplied to Arcelor Mittal SA in 2013. All mining is done by opencast methods with ore transported to the beneficiation plant where it is crushed, screened and beneficiated. Sishen mine is the only haematite ore producer in the world to fully beneficiate its product (Myburgh and Nortje, 2017).

The jig plant at Sishen mine is the largest of its type in the world. Iron ore products, conforming to different chemical and physical specifications, are produced at this mine. The pictures below illustrate some of its mining equipment and operational activities.

Figure 1.5: Loader and tipping truck

Figure 1.6: Waste dumps

Figure 1.7: Motorised shovel

Figure 1.8: Drilling equipment

Figure 1.9: Open-pit mine activities, blasting
source: http://www.angloamericankumba.com/ourbusiness/operations.aspx

Kolomela mine is near Postmasburg in the Northern Cape Province. Kolomela is the latest mining operation of the Anglo American group, having been completed at the end of 2011. Its name means ‘to dig deeper’ or ‘to persevere’. Kolomela has a LoM of 25 years. Kolomela lump iron ore is in demand because of its excellent physical strength and high iron content.

Figure 1.10: Kolomela mine
Source: http://www.mining-technology.com/projects/kolomela-iron-ore-mine-northern-cape/kolomela-iron-ore-mine-northern-cape1.html

Surface movement monitoring using **SAR** technology will be illustrated based on available data-stacks collected from the TerraSAR-X satellite in the necessary interferometry mode. The Royal Bafokeng South Mine, located near Rustenburg, South Africa is a platinum mine with a perimeter more than 8km and approximate 4.6km² slime dam. The other case study is an analysis over an open pit copper mine based in Chile, named Chuquicamata mine. It is realised that the latter is not a mine based in Africa, yet the same scientific principles for a surface movement monitoring procedure apply.

Figure 1.11: Royal Bafokeng South Mine as illustration of a large slime dam
Source: © Google Earth 2016
Source: © DLR 2014 © Airbus DS GmbH 2014 © Google Earth2014

Figure 1.12: Chuquicamata open pit copper mine in Chile
Source : © Google Earth 2016

1.3 Problem statement

Mining introduces several primary and secondary environmental challenges within its geographical surroundings. Africa, being a rich mineral endowment continent, faces several challenges. Mining is seen as a potential solution to one such challenge – improving the socio-economic conditions of millions of people in Africa (Emuze and Hauptfleisch, 2014). Unfortunately, devastating effects on the environment occur due to these mining activities, especially in poorly regulated and/or poor law enforcement countries. Therefore, the intended research is to introduce a workflow methodology using satellite based RS technology as a contributor to better understand open pit mine operations and the impact on its geographical area. The researcher will attempt to answer the following question:

"What contribution can a workflow methodology provide to determine open pit mine operations and the detection of environmental changes within its geographical area by means of earth observation satellite based technologies?"

1.4 Motivation

Mineral endowment in Africa holds the potential to improve the socio-economic conditions of various African countries. It is also true that mining introduces various negative primary and secondary environmental issues within an area. If environmental policies and regulations are weak and badly enforced within a country, then the environmental degradation of that mining area is a logical consequence (Hames, 2015).

Effective operational mine management and control to ensure a sustainable and profitable lifecycle of these mines are also essential (Jansen, 2011). Satellite based RS holds the potential to observe these mines and its surrounding areas at high temporal intervals, different spectral wavelengths and spatial resolutions. The combination of SAR and optical RS information creates a spatial platform to observe and measure the mine operations and the behaviour of specific land cover and land use classes over time – thus to contribute to a better understanding of the mining activities and their influence on the environment within a specific geographical area.

The use of SAR SMM further adds value to mine operations to measure and to know what the stability of the surface is over specific topographic features within the mining area and its surroundings (Anderson, 2016).

Therefore, the design of a workflow methodology to detect and analyse changes within mining areas using satellite based technologies formed the fundamental contributor to this study.

1.5 Aim and objectives of the study

The aim of this study was to apply satellite based RS technology as an aid to contribute to the monitoring of an open pit mine, its operations and understanding of the changes within its surrounding geographical area. This provided spatial information on primary and secondary environmental impact factors within the mine and its surrounding area. These primary and secondary factors were further discussed in section 2.2.3.

Furthermore, the aim was not only to use satellite based technology in an unattached way, but to design a workflow methodology as contributor to demonstrate the integration potential of such spatial information products as an aid for mine monitoring and the detection of environmental changes.

This study will thereby allow mine managers to observe and manage their mine operations more regularly, to consider and manage environmental change factors as well as to understand the spatial-temporal changes of land cover and land use in its surroundings. Therefore the objectives of this study are as follows:

- Objective 1: Collect suitable temporal multi-sensor data stacks over two open pit mines.
- Objective 2: Pre-processing of the temporal data stacks to ensure good atmospheric normalisation and co-pixel registration during the ortho-rectification procedure.
- Objective 3: Produce a baseline land cover classification map over both the mines.

- Objective 4: Prepare and analyse a spatial-temporal stereoscopic elevation model over the open pit mine and calculate the relevant ore/waste volumetric cubicles.
- Objective 5: Apply and describe a SAR surface movement management model over two open pit mines to determine its surface upliftment and subsidence stability over time.
- Objective 6: Provide recommendations on how satellite based RS can be used to effectively contribute to the monitoring of mine operations and the surrounding environmental conditions.

1.6 Conclusion

This chapter introduced the background to this study and provided a perspective on the mineral endowment in Africa and the complexities to achieve excellence in operational mining. The mine study areas were also introduced during this chapter and consisted of the two mines (Sishen and Kolomela) that were used for the optical RS data analysis. The SAR mine examples that were used in this study were the Royal Bafokeng tailings pond and Chuquicamata mine. The SAR analytical focus was based on the concept of surface movement monitoring. The problem statement, motivation and objectives for this study concluded this chapter.

CHAPTER 2: LITERATURE STUDY

2.1 Introduction

This chapter will provide a more theoretical basis for this study. The literature study provided the reader with background information to better understand the actual landscape of minerals in Africa as well as the primary and secondary factors associated with mining. Furthermore, the description of a typical open pit mine and its operational challenges have been explained followed by RS as a space based technology.

2.2 Literature study

The literature study consists of four sections; The first section will focus on the landscape of minerals and mining on the African continent. Understanding this landscape will unlock the rationale for the importance of mining in Africa, and its potential. The second section contains information about the primary and secondary environmental impacts of mining. The third section pertains to the critical open pit mining operations as a rationale to understand the complexities of mining engineering and the quest for operational excellence. Finally, the fourth section will present information on RS, which will provide understanding of the techniques and methods that were employed during this study.

2.2.1 Landscape of minerals and mining in Africa

According to Morgan (2015), an agreement was reached during the launch of the African Minerals Development Centre in Maputo in 2013 to help the African Union's mission develop an African mining vision. The vision is to map all African resources in an advanced geo-scientific way. This project, which received the name of *The Trillion Dollar Map,* is a plan to invest $380 million to develop comprehensive knowledge of Africa's mineral endowment.

It is therefore recognised that Africa is mineral enriched and may unlock immense economic potential. The African continent is home to more than one billion people and is endowed with an estimate of 10% of the world's reserves of oil, 40% of its gold and 80% to 90% of known deposits of chromium and platinum group metals (Hames, 2015).

Despite this rich mineral endowment in Africa, it is also true that mining in Africa is also challenged by inadequate access to capital and problems pertaining to productivity improvement, resource nationalisation, a lack of skilled labour, poor infrastructure, reputational risk, maintaining a social and political license to operate, commodity prices and currency fluctuations and widespread fraud and corruption (Hames, 2015).

The precious metals, gemstones, metallic minerals and industrial minerals are commonly spread in Africa. These reserves and production of some minerals are significant in world terms. Examples include bauxite, chromium, cobalt, gold, manganese, phosphate, platinum group metals and titanium as well as diamonds. Copper and iron ore are typical exported commodities that contribute to world industrial consumption (Janneh and Ping, 2011).

It therefore remains the vision of the African Union and the Economic Commission for Africa to develop an African mineral policy with the following summarised objectives (Janneh and Ping, 2011):

- Enhancing retained value by promoting linkages;
- Obtaining an adequate share of mineral revenue;
- Improving public participation and accountability;
- Pursuing an integrated view of the rights of various stakeholders;
- Valuing environmental resources;
- Using mineral revenue efficiently;
- Promoting local development;
- Encouraging regional cooperation and harmonization; and
- Strengthening institutions: building capacity and developing networks.

2.2.2 Open pit mine operations

During this study applied RS science was tested over open pit mines. It was therefore necessary to understand the fundamentals of an open pit mine since the design, engineering and operational maintenance of an open pit mine are complex, with various assorted challenges.

Open pit mines primarily extract and mill ore. Ore can be defined as a natural aggregation of one or more solid minerals that can be mined, processed and sold at a profit. Furthermore, exploration can be defined as the search for a mineral deposit and the subsequent investigation of any deposit found until orebody, if such exists, has been established (Hustrulid and Kuchta, 2013). The production of an open pit mine means the mining of ores, and as required, the subsequent processing into products ready for marketing.

The mine development phases are illustrated in Figure 2.1 and Figure 2.2 below. A positive change in the market place creates a new or increased demand for a mineral product. In response to the demand, financial resources are applied in an exploration phase resulting in the discovery and delineation of deposits. These deposits must be thoroughly evaluated regarding their economic attractiveness. This is known as the **planning phase**. The result of this phase is a feasibility report that will indicate “go or no-go”. If the answer is positive, the **implementation phase** will start, that is the development of the mine and its concentrating facilities. In order to implement the program, investment, design and construction stages are the first logical parallel activities to establish the mine (Hustrulid and Kuchta, 2013).

The second stage of the implementation phase is commissioning. This is the trial operation of the individual components to integrate them into an operating system and ensure their readiness. The **production phase** consists of the start-up stage which commences the moment that feed is delivered to the plant with the express intention of transforming it into product. Start-up normally ends when the quality and quantity of the product is deemed sustainable at the desired level. Operation is the second stage of the production phase and commences after start up (Hustrulid and Kuchta, 2013).

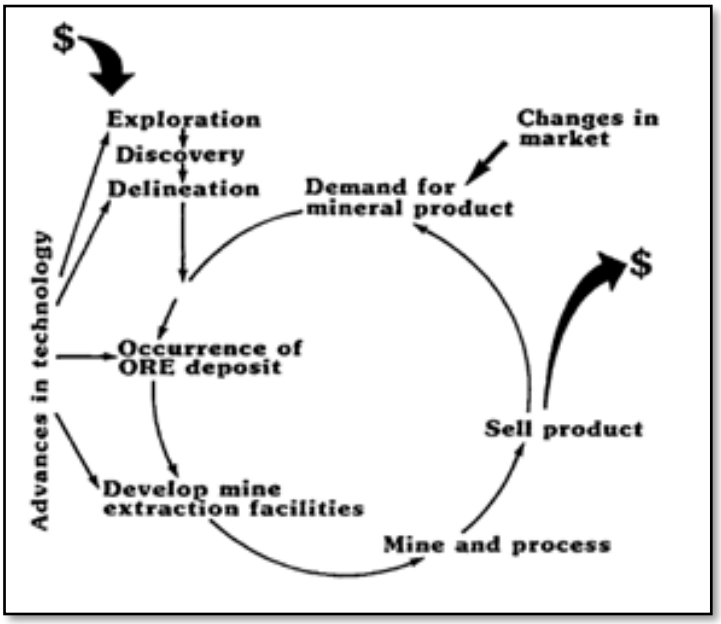

Figure 2.1: Diagrammatic representation of the mineral supply process
Source: Hustrulid and Kuchta, 2013.

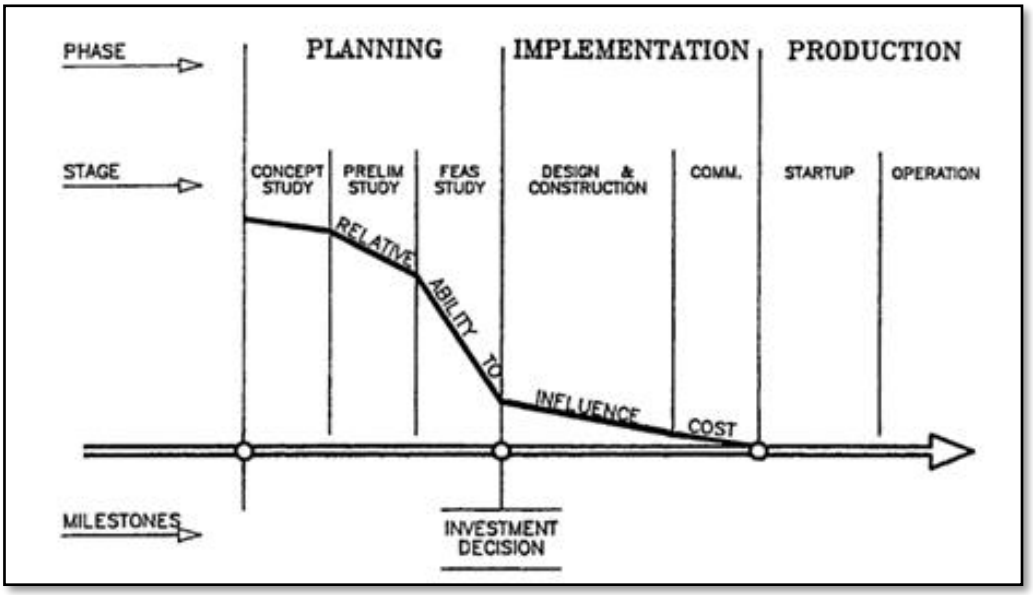

Figure 2.2: Relative ability to influence costs during mine establishment
Source: Hustrulid and Kuchta, 2013.

According to Hustrulid and Fernberg (2010) there is a distinction between quarrying and open pit mining. Where the product is rock, the operations are known as quarries. Where metallic ore or non-metallic minerals are involved, they are called open pit mines. Thus, two major differences between open pit mining and quarrying

are the geological conditions and the demands placed on the characteristics of the blasted material. For quarries, a majority of the rock products eventually delivered to the customers have only undergone crushing and screening in order to obtain the desired size fractions. An open pit metal mine, on the other hand, attempts to deliver the ore as pure as possible via crushers to contractors consisting of mills, separators, flotation and/or biochemical systems, see Figure 2.3.

Surface mining, which can be used when ore is close to the earth's surface, is an older and more productive method than underground mining. Open-pit mines differ depending on the nature of the material removed. Shallow mines from which gravel and sand are extracted are generally referred to as quarries, whereas deeper and longer mines from which coal is removed are known as strip mines. A deep surface mine is typical of mines with hard metal deposits such as copper and iron ore (see Figure 2.4. Overburden waste must be removed before extraction can begin. Haul roads wind up through the mine from the bottom of the pit to the surface. Extraction occurs from benches, in other words the open faces of material alongside the benches (Newman *et al,* 2010).

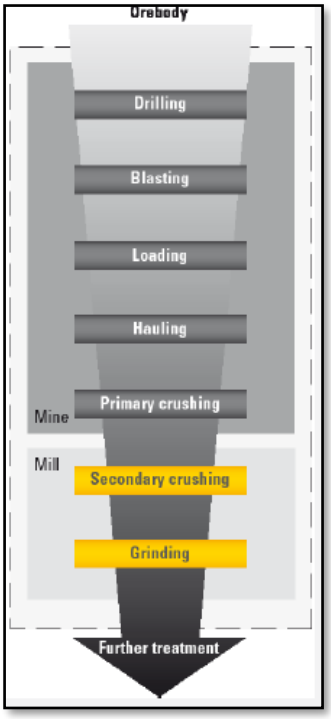

Figure 2.3: Diagrammatic representation of the open pit mine overall mine-fragmentation system and the mine and mill subsystem
Source: Hustrulid and Fernberg, 2010.

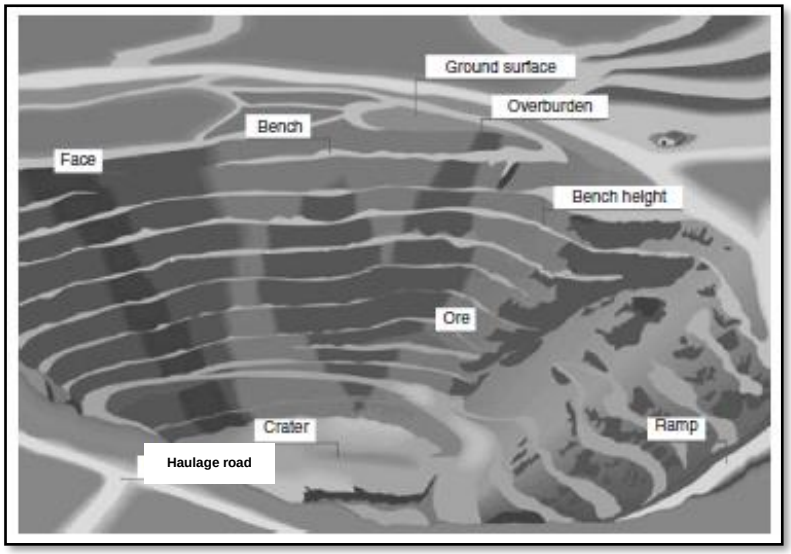

Figure 2.4: Schematic illustration of an open-pit mine
Source: http://www.visualdirectoryonline.com © QA International, 2010.

2.2.3 Primary and secondary impacts of mining on the environment

During the establishment of an open pit mine the top soil and all vegetation are removed, leaving only bare ground and a deep hole in the ground due to excavations. Deep mines, such as gold mines, do not create such extensive top surface devastation, but establish slime dams containing high levels of acid water that holds several environmental risks, such as ground water contamination (Emuze and Hauptfleisch, 2014).

The direct operations of a mine can be classified as primary impact factors on the environment. Secondary impact factors on the environment are the result of the mining activity. People are attracted to these mines hoping to find employment. One may define this as mine urbanisation (Emuze and Hauptfleisch, 2014). Mines also establish infrastructure such as roads, railways, power stations, etc. to meet their energy and logistical needs. These roads introduce a new economic corridor and people will also use the infrastructure to access areas that were difficult to reach in the past.

It is also true that conflict occurs between people where mineral resources are found. According to Maystadt *et al* (2014) conflict events recorded in the Democratic Republic of the Congo at geo-located mining concession areas between 1997 and

2007 revealed an “ecological fallacy”. In other words, whereas, concessions have no effect on the number of conflicts at the territory level (lowest administrative level), they do foster violence at the district level (higher administrative unit).

Distinct Urban Mines (DUM) has high concentrations of specific products/minerals. The fear of scarcity of resources highlights the need to exploit secondary materials from urban mines in the anthroposphere, one of the earth's spheres. The anthroposphere (sometimes also referred as technosphere) is that part of the environment that is made or modified by humans for use in human activities and human habitats.. Maximising resource recovery from excavation waste dumps is a novel approach to optimising the resource value from these areas. This type of recycling method ensures less environmental damage from primary mining activities (Ongondo, *et al.* 2015).

Commerce, migration, employment and industry configuration and population growth are factors that contribute significantly to the urbanization phenomenon. Mining activities are part of these factors and have led to the advancement and regression of cities. An abundance of literature exists on the negative effects of urbanisation and mining on the environment. A study that was done in the mining town of Kathu, in the Northern Cape of South Africa confirmed that centralisation of employment, resources and trade lead to urbanisation, which is primarily driven by the mining industry. During this study it was observed that mining as a factor that accelerates urbanisation, also impacts negatively on the environment. Thus, there is a need to better understand mining-induced urbanisation so as to reduce pollution and the adverse effects of secondary activities that support the primary industry of mining (Emuze and Hauptfleisch, 2014).

Secondary factors such as the influence of open pit mines, e.g. coal mines, on public health and air pollution were studied. According to Hendryx (2015) surface coal mining causes local air and water pollution, as confirmed during a study conducted in the USA. Environmental and public health impacts are pronounced in mountaintop removal mining areas. Evidence during this study showed epidemiological disease patterns for populations living in proximity to surface mining. Environmental evidence has shown that surface waters and biota are harmed by mountaintop removal, while

other environmental studies have shown that water and air pollution exists in residential areas close to mining (Hendryx, 2015).

In order to manage primary and secondary impact factors of mining on the environment, proper assessment procedures and tools are essential. Environmental impact assessment (EIA) was identified as an important instrument for facilitating environmental protection and sustainable development (Gwimbi and Nhamo, 2016). Applying correct and improved mitigation measures during an EIA and applying it in practice, will contribute to improved planning conditions for mining and processing. The latter was successfully tested in the Great Dyke of Zimbabwe's platinum mines.

Incorporating and enforcing substantive mitigation measures in environmental impact statements and planning conditions are essential for future mining sustainability. This will contribute to the early detection of primary and secondary negative environmental factors and assist with reactive and pro-active environmental management plans (Gwimbi and Nhamo, 2016). In China a fuzzy neural network (TSFNN) model was designed to classify EIA results into three categories: slight, moderate and heavy. Furthermore, a routine management system was developed for mining geo-environmental information managers and officials based on a client/server model and component-based Geographic Information Systems (GIS) secondary development technology. According to Zhang *et al* (2015) the system has five main capabilities:

- Mine enterprise and geo-environment information management;
- GIS map display and analysis;
- Data querying and statistical analysis;
- Geo-environmental impact assessment and classification; and
- Document query and management

According to a study by Appiah and Osman (2014), an EIA is an essential tool to manage primary and secondary mining impacts, especially during the exploration and pre-establishment phase of a mine. The study was conducted in Ghana to determine how communities affected by large-scale mining perceive EIA compliance. Mineral exports in Ghana account for an estimated 37% of its exports and are dominated by gold. It is recognised that an EIA is a tool used to identify the

environmental, social and economic impacts of a project prior to decision-making. The impact of mining starts with exploration, and extends through extraction and processing of minerals to decommissioning of operations. Also, it stresses that the environmental impact of mining operations is far beyond the initial exploited mineralised zone. Thus, each stage of the mining process has the potential of causing different impacts of various magnitudes. Problems also exist with small-scale mining in Ghana, due to its clandestine nature not amenable to monitoring. These activities therefore are also responsible for substantial levels of environmental damage in the mining communities. They conclude in their study that EIA from a mining perspective does not evaluate whether mineral investments can be effective in reducing poverty and raising living standards. It does not consider how project level impacts on environment, local economies and public health can contribute to poverty aggravation (Appiah and Osman, 2014).

The researcher therefore recognises that an EIA needs to be considered as a tool to manage primary and secondary impact factors throughout the mining cycle. Furthermore, in order to play an efficient role in environmental and communal sustainability clear and strict regulatory policies from a country's government must be properly enforced. In addition, the Environmental Protective Agencies (EPA's) of a specific country need to be committed to enforcing environmental rules and regulations and mining companies should prioritize compliance to the EIA regulations.

2.2.4 Remote sensing

According to the National Oceanic and Atmospheric Administration (NOAA), RS is defined as the science of obtaining information about objects or areas from a distance, typically from aircraft or satellites. The European Space Agency (ESA) describes RS as a way of collecting and analysing data to get information about an object without the instrument used to collect the data being in direct contact with the object. From an Earth science perspective, RS is a technology that primarily aims to observe and study the Earth system, the environment and its dynamics. In RS, four elements are essential. They are:

- a platform to hold the instrument;
- a target object to be observed;
- an instrument or a sensor to observe the target; and
- the information that is obtained from the acquired data, and how it is used and stored.

Platforms are all means used to be 'at a distance' from the Earth's surface, such as manned and unmanned airborne and spaceborne platforms. The target is our planet itself, the sensors are contained in all the instruments used to observe the Earth (cameras, scanners, radars, etc.) and finally the information obtained is everything that increases our knowledge about our planet, such as the increase in the ozone layer, the progress of deforestation, drought, or operational activities such as the monitoring of an open pit mine (Mather and Koch, 2011).

ESA adds that remote sensors collect data by detecting the energy that is reflected from Earth. Remote sensors can be either passive or active. Passive sensors respond to external stimuli. They record natural energy that is reflected or emitted from the Earth's surface. The most common source of radiation detected by passive sensors is reflected sunlight. In contrast, active sensors use internal stimuli to collect data about Earth. For example, a laser-beam RS system projects a laser onto the surface of Earth and measures the time that it takes for the laser to reflect back to its sensor.

According to Mather and Koch (2011) RS is the analysis and interpretation of data derived from electromagnetic radiation that is reflected from, or emitted by an object, which is observed and recorded by an instrument not in contact with the object. Different surface materials, such as vegetation and water bodies, have different amounts of electromagnetic radiation that is reflected, absorbed, transmitted or emitted within different wavelengths of the electromagnetic spectrum (Lillesand *et al,* 2007; Liang, 2004). The ability to differentiate features or objects such as vegetation types, structures such as roads, industrial or residential classes allows for the identification, quantification and modelling of trends associated with a specific feature class, through identifying the spectral signature, linked to that specific object or feature within the electromagnetic spectrum (Jones and Vaughan, 2010).

The above mentioned electromagnetic spectral signatures are true for passive optical sensors. The evolvement in synthetic aperture radar (SAR) as active systems complements the geo-information application prospects. According to Chen (2012) SAR image understanding and interpretation are essential for RS of Earth environment and target detection. Weng (2011) further emphasises that SAR is one of the key sensors currently positioned on satellites for Earth and planetary exploration. A SAR system radiates chirped pulses from different equispaced positions along the azimuth, which is usually a straight line, a linear array is thus synthesized. After raw data processing, the (microwave) image of the illuminated area is obtained, where the range and azimuth resolutions are calculated by the following formula:

$$\Delta r = [2\lambda/(\frac{\Delta f}{f})] \quad \text{AND} \quad \Delta x = L/2$$

λ = wavelength
ƒ = frequency of pulse carrier
Δƒ = chirp bandwidth
L = length of the radiating antenna
Δx = azimuth resolution

Equation 2.1: Range and azimuth resolution
Source: Weng (2011)

The use of RS dates back to the 1950s with the launch of Sputnik-1. The first RS sensors were a basic television camera that captured crude panchromatic images at a low resolution. Technology evolved to include images using a wider electromagnetic spectrum beyond just visual bands but also into infrared and thermal ranges (Avery and Berlin, 1992). The first metrological satellite was launched on 1 April 1960. The Television Infrared Observation Satellite (TIROS-1). TIROS-1 had a lifespan of 78 days and a spatial resolution of 2.5 to 3km (Kramer, 2002).

The Earth Resource Technology Satellite (ERTS-1), later known as Landsat MSS and operated by USGS was indeed a leader in its field. The second generation Landsat consists of two satellites, Landsat 4 and 5. Only Landsat 5 continued operationally with its newly introduced *thematic mapper* system, which includes seven spatial resolution bands of 30m that include infrared and thermal. The Landsat series of satellites contributed to one of the largest and oldest consistent archives of

the Earth, until today with Landsat-8. Europe responded to the space race and established the Système Pour l'Observation de la Terre (SPOT) programme. The SPOT-1 satellite was launched in 1986 and introduced the highest spatial resolution from an earth observation satellite, 10m panchromatic and 20m multispectral ground sample distance (GSD), operated by Centre National D'études Spatiales (CNES) the French space agency. The SPOT satellites were an along-track scanner with linear arrays of charge-coupled detectors (CCD). An innovation in SPOT is the off-nadir viewing capability, up to 27º incident angle and 26-day revisit cycle (Floyd and Sabins, 1986).

Radar RS from space began with the launch of *Seasat* in 1978 and continued with the Shuttle Imaging Radar (SIR) and Soviet Cosmos experiments in the 1980's. During 1991 three radar satellites were launched, *Almaz-1* (Soviet Union), *ERS-1* (European Space Agency) and *JERS-1* (Japan). These systems were followed by the first Canadian radar satellite, *Radarsat-1* in 1995. A trend in new systems followed with the USA Shuttle Radar Topography Mission (SRTM) and *Envisat* from ESA. Since the first decade of the 21st century advanced radar systems have followed, launched by Canada *(Radarsat-2),* Japan *(ALOS)* and Germany (*TerraSAR-X and TanDEM-X)* (Lillesand et al, 2007).

Today, commercial satellites have evolved to 30cm GSD, super multispectral capabilities with high agility, geometrical and radiometrical accuracies, for example WorldView-3 from Digital Globe. Satellites in twin, triplet or even quadric constellation orbits provide increased temporal revisits over any specific target on Earth, daily and even intra-daily acquisitions. The Airbus Defence and Space constellation of Pléiades 1A &1B complemented with the SPOT 6 and SPOT 7 satellites serves as a good example. These satellites have advance agility capabilities and can also acquire scenes in stereoscopic or tri-stereoscopic modes. It is these latter modes that enables the generation of digital elevation models.

The agility of a satellite can be defined as its manoeuvre ability to acquire oblique viewing imagery (up to 45° angle) which allows the satellites to revisit any point on the globe daily - ideal for anticipating risks, managing crises effectively or speed up large areas coverage (Astrium, 2012). The stereoscopic cover can be described as acquiring within the same pass over a specific area, a homogeneous product

composed of two images for which the angular difference (Base-over-Height) can be adjusted. Stereoscopic imaging with an additional quasi vertical image (tri-stereoscopy), allow the user to have an image and its stereoscopic environment. The Base-over-Height ratio reflects the angular difference between the two images. It should be high for rather flat areas and low for urban or mountainous areas (Astrium, 2012).

A futuristic view of space-based RS shows a trend of smaller micro-satellites with high quality payloads and in some cases video streaming solutions. Constellations of hundreds of satellites monitoring the Earth at a specific target for example every hour will become a reality within the next decade. The Hodoyoshi microsatellites, a constellation of 10, were launched during 2014 in one single year to observe the Earth. Planet Labs has already launched more than 113 satellites with a 3m to 5m GSD in the visual spectrum range. The prediction is that Planet Labs will have enough satellites in orbit after 2016 to image the globe once per day. The Google Skybox Imaging (renamed Terra Bella) introduces a concept of 24 CubeSat based satellites that will provide optical images (0.85m panchromatic, 2m multi-spectral) as well as video streaming of 1.1m GSD for 90 seconds at 30 frames per second. UrtheCast, a company based in Canada, announced that it wants to put an OptiSAR constellation of eight optical and eight two-band radar satellites in constellation once enough funding has been raised from prospective customers.

The trend of space-based RS data is that spatial resolution will continuously improve. Availability of a wider range of spectral bands, immense improvement in temporal revisits over specific targets as well as globe coverages is a near-future reality. Superior geometrical accuracies and the combination of optical, SAR and video capabilities open a whole new application field for geo-applications. It is these technological trends that will certainly contribute to the mining industry from an operational as well as from an environmental monitoring perspective.

2.3 Conclusion

In the literature review several authors emphasised the rich mineral endowment on the African continent (Yager, *et al.,* 2012; Morgan, 2015; Hames, 2015; Janneh and Ping, 2011). It is true that mining has introduced several primary and secondary factors that challenge the surrounding natural environment. These environmental impact factors include soil and vegetation removal, pollution of water and air, health risks, mine urbanisation, etc. (Emuze and Hauptfleisch, 2014; Ongondo, *et al.* 2015; Gwimbi and Nhamo, 2016; Maystadt *et al,* 2014; Appiah and Osman, 2014).

Open pit mines primarily extract and mill ore. The production of an open pit mine involves the mining of ores, and as required, the subsequent processing into products ready for marketing. The theme of an open pit mine will be used during this study as a focus point for the contribution of RS to the mining industry (Hustrulid and Kuchta, 2013; Hustrulid and Fernberg, 2010; Newman *et al,* 2010).

RS was described from an optical as well as a SAR perspective. A synopsis of the history of RS satellites was given, followed by a futuristic view of RS and its changing technological landscape. The current available satellites and those that will follow in the next decade will enable an innovative observation platform to contribute to the strategic and operational management of open pit mines and beyond (Mather and Koch, 2011; Lillesand *et al,* 2007; Kramer, 2002; Floyd and Sabins, 1986; Chen, 2012; Weng, 2011).

CHAPTER 3: METHODOLOGY

3.1 Introduction

The methodology chapter provides details on how the research was undertaken. The research design and image processing techniques with their associated workflows will be described followed later by the results in chapter 4 and 5. The approach here will focus on four major workflows, starting with the Landsat 8 time-series analysis in order to produce a reliable land cover base layer. The Pléiades monoscopic imagery workflow is then explained when designed as a mine monitoring aid. This is followed by the Pléiades stereoscopic data preparation that produced very high resolution elevation models to compute volumetric cubicles within the mine. The SAR data preparation and SMM analytics will provide a fine scale subsidence and upliftment measurement solution over the mine. In conclusion the integration of these workflows to create an ultimate mine monitoring and environmental impact model will conclude this chapter.

3.2 Research design

The research design focused on the integration of four different RS workflows to demonstrate a mine monitoring and environmental impact model concept. The model consisted of advanced data pre-processing computer processing techniques as well as statistical analysis for optical as well as SAR imagery. The four workflows can be described as follows:

- Workflow 1: Baseline land cover;
- Workflow 2: Change detection;
- Workflow 3: Calculate volumetric cubicle values;
- Workflow 4: SMM.

The research design diagram below highlights the proposed processing steps for each workflow, see Figure 3.1. The legend key for this diagram is as follows:

Input source data type	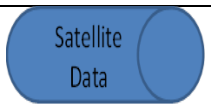
Master computer processing step	
Secondary computer processing step	
Satellite image product type	
Satellite description and sensor type	
Mine monitoring & environmental impact model – integrated end point	

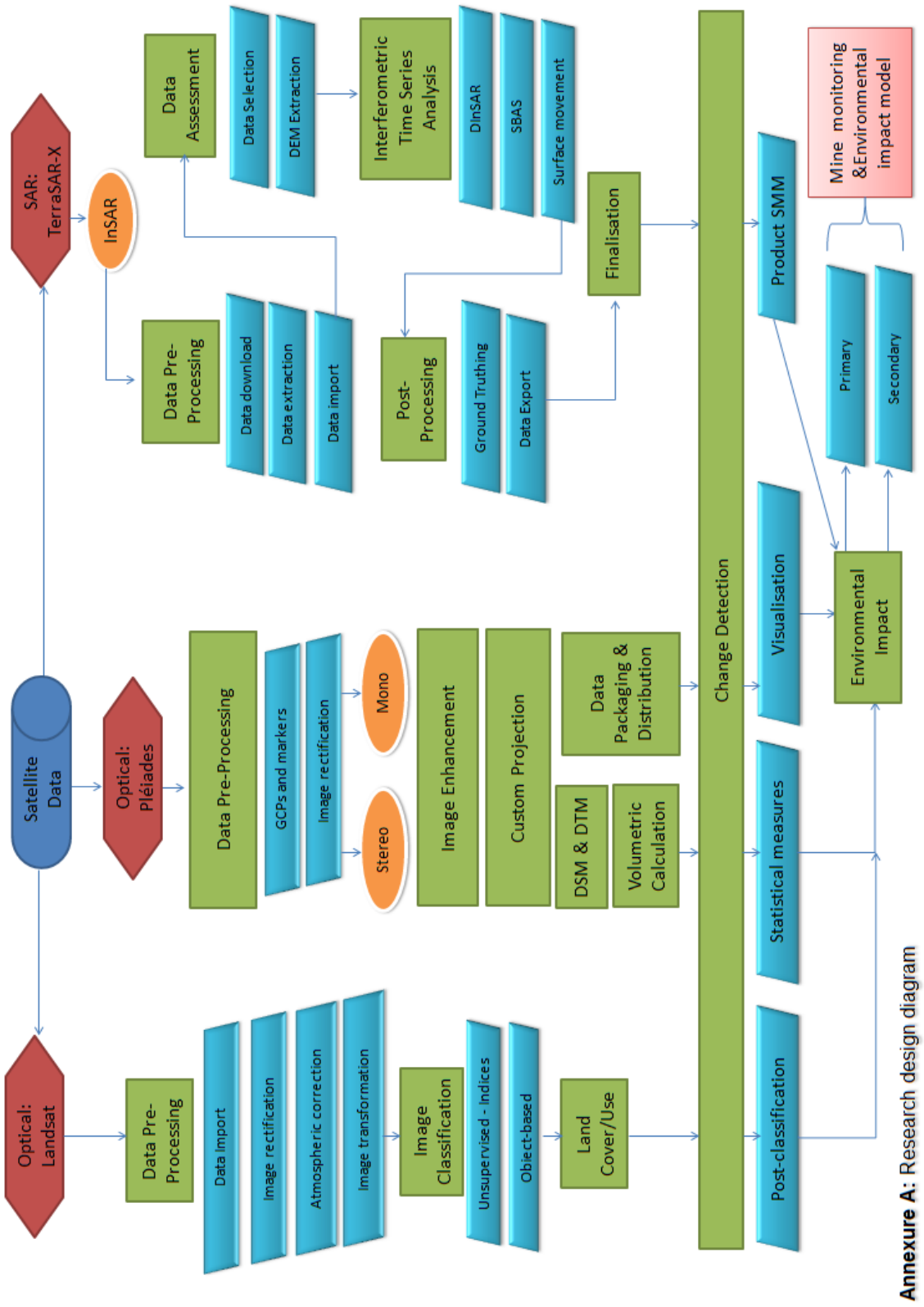

Figure 3.1: Research design diagram for this study, see Annexure A

3.3 Methodology

Satellite based RS consists of various satellite platforms, instrumentation and sensing modes. During this study the optical satellites of Landsat 8 and Pléiades will be used as well as the demonstration of the surface movement monitoring application as derived from TerraSAR-X. Literature reveals various image processing techniques, algorithms and workflow procedures (Mather, 2011; Lillesand, 2007; Weng, 2011 and Chen, 2012). Thus, no single procedure exists as the alpha image processing procedure of all. It is the combination of various image processing techniques relevant to producing a specific result applicable to fit the final application. The four workflow procedures mentioned will be applied as spatial-temporal output data for a mine monitoring and environmental impact concept model. Each different workflow methodology will be discussed in the following four sections.

3.3.1 Landsat optical image classification for a baseline land cover layer

According to Thompson (2015), land cover is a key information requirement for a wide range of landscape planning, inventory and management activities, ranging from environmental resource management to telecommunication planning. The recent global availability of Landsat 8 satellite imagery offered the opportunity to create a new, national land cover dataset for South Africa, circa 2013-14, replacing and updating the previous 1994 and 2000 South African National Land cover datasets. The 2013-14 national land cover dataset is based on 30mx30m raster cells, and is ideally suited for ± 1:75 000 - 1:250 000 scale GIS-based mapping and modelling applications. The dataset has been derived from multi-seasonal Landsat 8 imagery, using operationally proven, semi-automated modelling procedures developed specifically for the generation of this dataset, based on repeatable and standardised modelling routines.

Automated modelling procedures offer significant advantages in terms of ensuring data standards, minimising processing time, allowing improved repeatability and facilitating accurate change detection; when compared to more conventional image mapping approaches where there is a greater reliance on individual image analyst

knowledge and inputs. To this end, a series of automated image-based modelling steps were developed that utilise the seasonal dynamics associated with the broad landscape characteristics across South Africa. These were then used to rapidly produce a set of "foundation" cover classes that could be easily converted into more meaningful land cover information categories, using pre-defined geographic masks in the GEOTERRAIMAGE data libraries (Thompson, 2015).

The “foundation” cover classes represent the basic building blocks associated with all landscape characteristics, namely water, bare ground, grass and tree-bush-shrub cover types, with each being defined in terms of seasonal occurrence or permanence. These basic foundation cover classes represent the initial output from the automated modelling approach. The foundation cover classes are then converted into more conventional land cover information classes, i.e. urban, forest plantation etc, as part of the post-automated modelling data processing steps (Thompson, 2015).

The foundation cover classes are essentially “spectrally dependent” classes, since they are generated from automated modelling procedures that are based directly on the spectral characteristics associated with each image pixel over time (i.e. seasonal) and space (i.e. within an image frame). The final land cover information classes are referred to as “spectrally independent” classes since different cover classes can share similar foundation class spectral characteristics in a one-to-many type relationship, see Figure 3.2. For example, the “bare ground” spectrally dependent cover classes could represent non-vegetated built-up urban areas, natural rock exposures, beach sand or a mine pit and tailings dam. Similarly the tree-bush classes could represent a natural vegetation cover, a timber plantation or a fruit orchard. The advantage of this approach is that the conversion of the initial, spectrally dependent foundation cover classes into the final, spectrally independent land-cover information classes can be tailored to suit a variety of end-user information requirements; simply by using a different set of pre-determined masks and foundation class sub-divisions and amalgamations (Thompson, 2015).

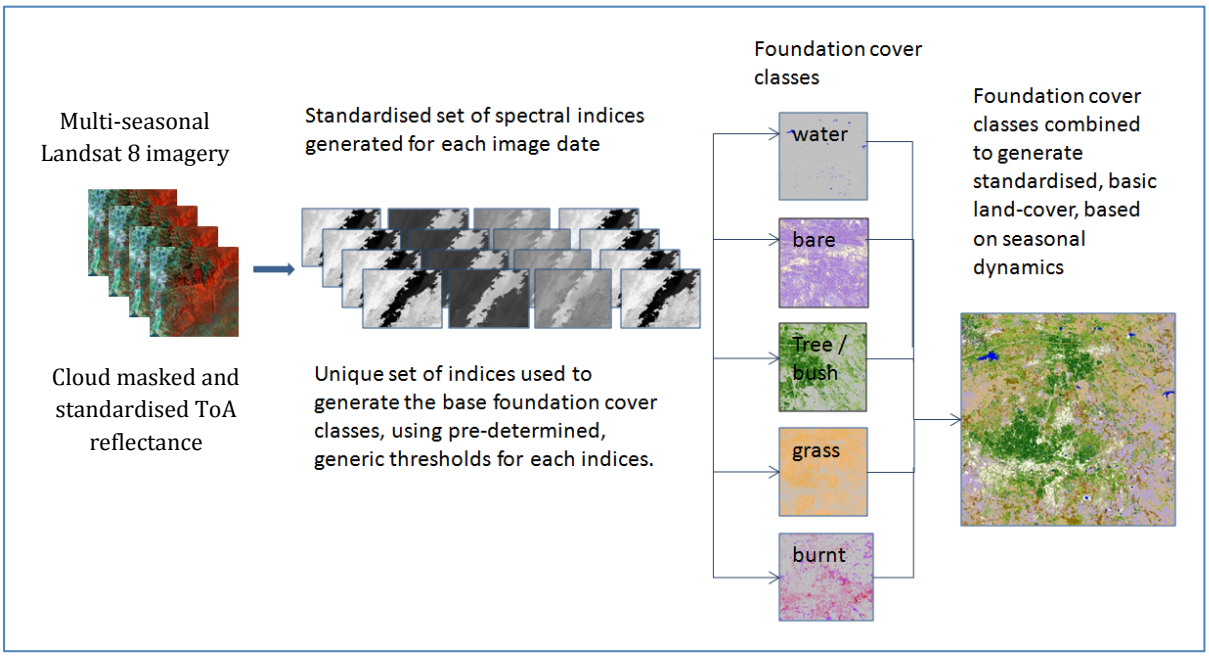

Figure 3.2: Summary of the full spectral land cover modelling process
Source: © GeoTerraImage

3.3.2 Pléiades monoscopic optical mine monitoring imagery and visualisation

3.3.2.1 Data acquisition

Airbus Defence and Space operates two Pléiades satellites acquiring imagery at a 50cm spatial resolution in the panchromatic band, and 2m resolution in the multispectral bands covering the blue, green, red and near-infrared parts of the electromagnetic spectrum, sees Figure 3.3. These satellites are spaced equally in an orbital plane and fly over the Sishen and Kolomela mines between 9h00 and 11h00 (GMT+2), depending on the orbit number. To ensure a good geometric fidelity and accuracy of the resulting products, imagery was only acquired at viewing angles of less than 15 degrees which is possible only at an approximately three-day interval. For mine management purposes an image acquired in the middle of the week is most favourable. Attempts were made to find the best compromises between the desired satellite viewing geometry and ideal observation times.

The acquired weekly images over the Kolomela and Sishen mines date back to mid-2014. A selective data-stack during 2015/2016 of five scenes over each mine will be used during this study to demonstrate the mine monitoring principles.

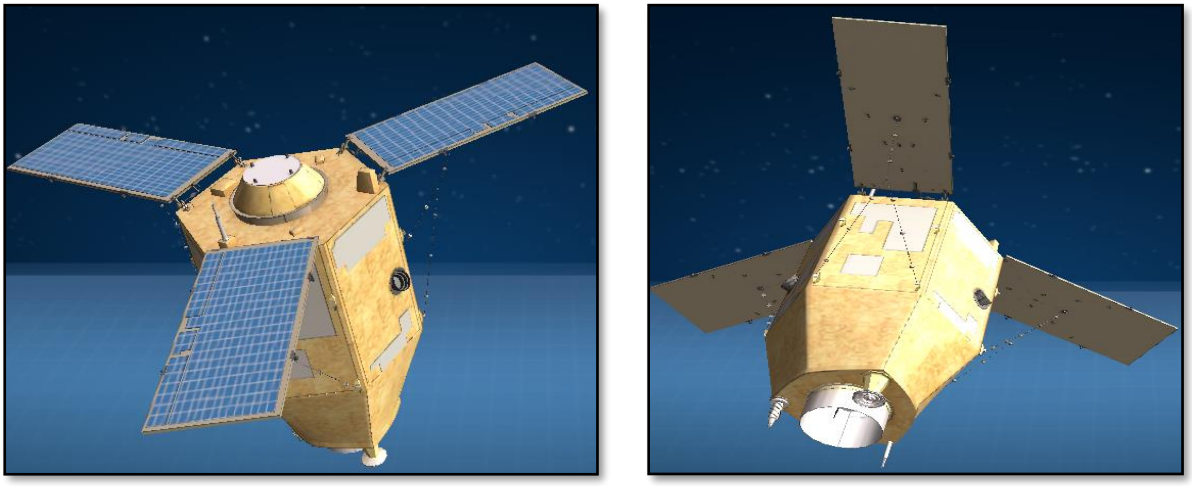

Figure 3.3: Pléiades 1A & Pléiades 1B twin satellite constellation
Source : © PLEIADES (CNES) 2016, Distribution Airbus DS. All rights reserved.

3.3.2.2 Ground control and reference data

According to Lück (2015) the precise geo-location of the geo-information products is critical. The Pléiades satellite's pointing accuracy is measured at 10m with a 90% confidence interval. Normally to increase the geo-location accuracy, additional ground control points are essential. The standard physical surveying beacons based at a mine often protrude several meters above the ground and renders them unsuitable as ground control points (GCPs) for precise triangulation of satellite imagery. They are difficult to identify in the imagery and their height above the ground introduces an error at oblique angles. According to Mather *et al* (2011) ground control must be well defined and easily recognisable features that can be located accurately both on a map and on the corresponding image.

Good satellite imagery GCPs has the following properties (Lück, 2015):

- The targets are placed level on the ground.
- The targets are the size of at least six times the pixel resolution of the satellite image in each dimension. For the Pleiades data, this translates to a square structure of at least 3m x 3m.
- The targets must consist of very high contrast features, such as white or silver features on a black background.

- Each feature should have a length of at least three times the pixel resolution of the satellite image, and have a width one third of the pixel resolution of the image.
- The targets should not be obstructed from view by objects above the ground and shadows may not be cast onto or near the targets.
- The targets should be evenly distributed over the area of interest.
- The targets should be placed in a geometric pattern in such a way that imaginary equal-angular triangles can be formed by connecting three reference points at a time (i.e. a triangular mesh).
- The targets should cover a range of elevation with the same triangle principle described above applying to the elevation.
- The centre of the marker is surveyed with a differential GPS with an accuracy of less than 10cm.

To comply with the good GCP principles, twelve 3m x 3m targets from black shade cloth and 20cm wide aluminium strips were manufactured and placed in an evenly spaced pattern at the mines on surfaces that were not expected to change in the near future. Such a marker is illustrated in Figure 3.4. The result of this marker on a Pléiades satellite scene is illustrated in Figure 3.5.

Figure 3.4: Satellite GCP target/marker made from shade netting and aluminium strips, placed on a cleared flat area at the mines

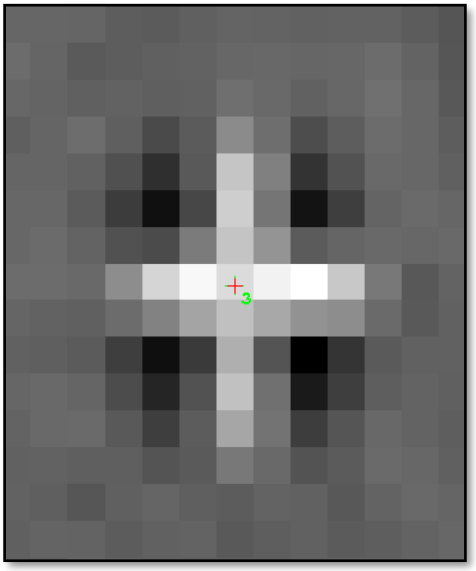

Figure 3.5: Reference targets as installed at the mines captured by a Pléiades panchromatic scene at scale 1:500

The placement of these markers is illustrated in Figures 3.6 and 3.7, ensuring a well distributed triangulated structure.

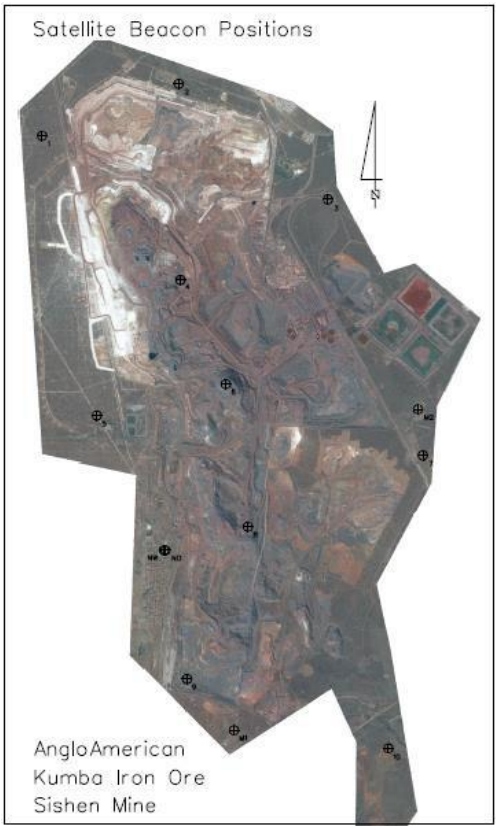

Figure 3.6: GCP markers positioned within the Sishen mining area
Source : © PLEIADES (CNES) 2016, Distribution Airbus DS. All rights reserved.

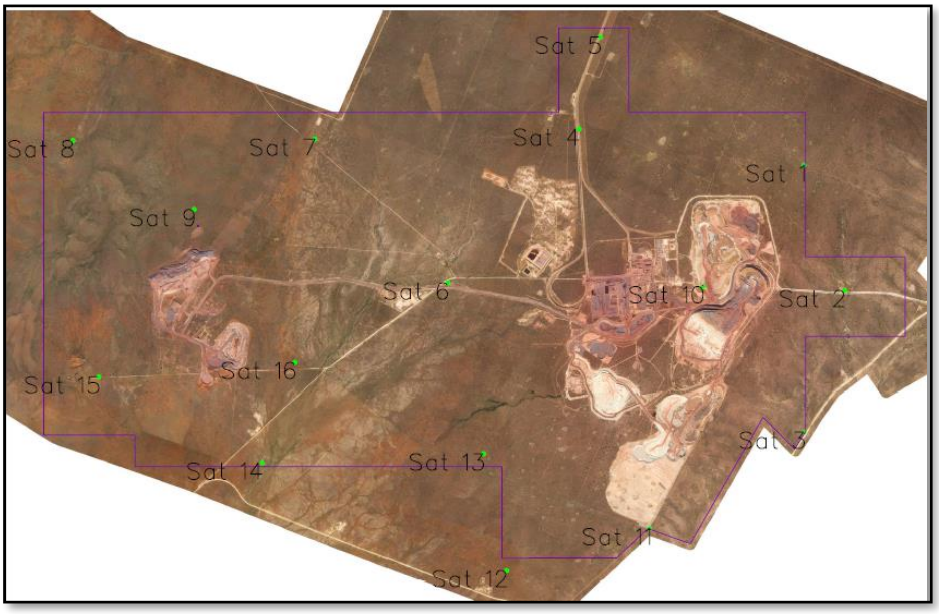

Figure 3.7: GCP markers positioned within the Kolomela mining area
Source : © PLEIADES (CNES) 2016, Distribution Airbus DS. All rights reserved.

According to Mather *et al* (2011) geometrical referencing based on GCP's and map values can be done by the least-squares transformation algorithm or using a polynomial function.

$$\hat{S} = a0 + a1t1i + a2t2i$$

Equation 3.1: Bivariate least-squares regression
Source: Mather *et al* (2011)

$$\hat{S} = a00 + a10t + a01u + a20t^2 + a11tu + a02u^2 + a30t^3 + a21t^2u + a12tu^2 + a03u^3$$

Equation 3.2: Third-polynomial function
Source: Mather *et al* (2011)

The geometric rectification of satellite RS imagery is the process of projecting one original image into a specific reference coordinate system, eliminating the geometric distortions of the original image and producing a new image that satisfies the requirements of the map projection or the graphical expression. According to Liang, Li and Wang (2012) the process of geometric rectification of RS imagery proceeds as follows:

- Determine an appropriate geometric processing model between the image-space coordinates and the object-space coordinates according to the imaging mode of the RS imagery. These models can be classified into two general types:
    - Rigorous Geometric Processing Models
    - Empirical Geometric Processing Models
        - The General Polynomial Model
        - The Direct Linear Transformation Model
        - The Affine Transformation Model
        - The Rational Function Model

- Confirm the geometrical rectification formulas according to the above-mentioned geometric processing models.
- Implement adjustments to solve the model parameters according to the coordinates of the GCP's and the corresponding image points, and evaluate the accuracy.

- Implement the geometric transformation and resampling of the original image.
    - The following image resample techniques exist:
        - Nearest-Neighbour Interpolation
        - Bilinear Interpolation
        - Bi-cubic Convolution

According to the *Pléiades User Guide*, as produced by Airbus Defence and Space, the rational polynomial coefficient (RPC) model is an analytical model which gives a relationship between:

- Image coordinates + altitude and ground coordinates (direct model: image _→ ground)
- Ground coordinates + altitude and image coordinates (inverse model: ground _→ image)

The RPC file contains the coefficients and normalization parameters for the Rational Polynomial Coefficients (also called Rapid Positional Capability, Rational Function Model) geometric analytic model. This file is only given for images supporting sensor geometry i.e. the primary product. The primary product has been designed to remove this complexity and offer end-users a simple product with state-of-the-art geometric and radiometric accuracy. Technically, the primary processing is also called Sensor, Perfect Sensor or Virtual Sensor. The geometric reference frame for Primary imagery simulates the imaging geometry of a single pushbroom linear array, located very close to the raw Panchromatic Time Delay Integration (TDI) arrays. Besides, this ideal array is supposed to belong to a perfect instrument with no optical distortion and carried by a platform with no high altitude perturbations. This altitude variation correction (made with a polynomial fitting) allows for both simple altitude modelling and more accurate precision of the imaging geometry by the **rational function sensor model**.

When using the **inverse localization algorithm model** (ground → image), the user supplies geographic coordinates (longitude, latitude) and altitude (alt). The results of the application model are image coordinates (col, lin). These algorithmic steps were described in the *Pléiades User Guide* for image geometrical correction using ground control points. This is the preferred method to geometrically correct Pléiades imagery

as these algorithms have been provided by the satellite manufacturer and engineered to provide high quality results (Astrium, 2012).

3.3.2.3 Image processing and packaging

Pléiades data has been received by Airbus Defence and Space in Primary product format. The Primary product is the processing level closest to the natural image acquired by the sensor. The Primary product is (Astrium, 2012):

- In sensor geometry, synthesized on a perfect single and linear pushbroom array,
- With an equalized radiometry on the native dynamic range of the sensor, 12 bits (4 096 values).

This processing entails a relative radiometric correction converting relative voltage readings to relative radiation readings to produce a uniform image. The data is then ortho-corrected, pansharpened, re-projected in a custom mine projection and then tiled in the relevant file format. The final step is to ingest the data into the packaging and distribution system. The aim of the system is to process the data from primary to final customer orientated product within one hour, thus from data acquisition in France, data FTP transfer to final product delivery within one working day (Lück, 2015).

Processing procedures can be summarised as follows (Lück, 2015):

- Metadata is extracted from the imagery.
- GCPs are collected from a chip database or reference image.
- GCPs are refined, where poor matches are identified, using an orbit defined sensor model for the calculation of residuals, and rejected.
- The panchromatic band is orthorectified using a reference DTM, onto the mine cartographic projection.
- GCPs are collected and refined from the multispectral imagery before orthorectification using the orthorectified panchromatic band as reference.

- The high-resolution panchromatic band is fused with the low-resolution multispectral bands, producing a pan-sharpened colour image at 50cm resolution. This technique does not corrupt the colour values (radiometric accuracy) of the multispectral image, as illustrated in Figure 3.8.
- The image is normalised radiometrically, where Digital Numbers (in relative radiance) are converted to Top of Atmosphere Reflectance values, by compensating for light intensities affected by the solar elevation, earth-sun distance and Lambertian scattering. Lambertian reflectance is the property that defines an ideal "matte" or diffusely reflecting surface. The apparent brightness of a Lambertian surface to an observer is the same regardless of the observer's angle of view.
- The product is packaged, which entails:
    - Data is rescaled from 16- to 18-bit values.
    - Tiles are generated in ECW file format.
    - 8-bit images are generated in TIFF format.
    - Full-resolution browse images are created in JPEG format.

Figure 3.8: Illustration of Image Fusion, with panchromatic image (left), multispectral image (middle), and fused product (right)
Source: © PLEIADES (CNES) 2016, Distribution Airbus DS. All rights reserved.

3.3.3 Pléiades stereoscopic optical image to generate very high resolution elevation models

3.3.3.1 Elevation model processing procedure

According to Lück (2015) the following additional stereoscopic image processing steps were proposed. When a Digital Surface Model (DSM) is generated, the same

pre-processing steps as described in section 3.3.2.3 apply, followed by the next additional steps:

- Tie-points between the two stereo datasets are collected.
- The tie-points are refined, referencing the two datasets.
- Final triangulation of the imagery is performed.
- Epipolar image pairs are generated.
- DSMs of different resolutions are extracted.
- DSMs that have been produced are then geo-coded.

Once spectral classification is completed, the set of DSM raster's are produced and then merged into a single DSM. The following procedures are applied during the merging of DSMs:

- Areas of poor correlation, due to the effect of shadows or homogenous surfaces, such as very smooth stockpiles, roads and water, are identified and masked in each DSM.
- The DSMs are normalised to one another and then merged into a single product.
- The spectral pre-classification information as well as derived DSM slope values is used to identify features above the ground automatically, which allows for the creation of a mask of all the features above the ground.
- A Digital Terrain Model (DTM) is produced, interpolating areas previously identified as being features above the ground.
- The DSM products are then packaged using the following process:
    - The fused DSM and resulting DTM data are exported to an ASCII text file.
    - A mask for areas with no data is generated as a GeoTIFF file.
    - Full resolution browse products are created which are hill-shaded and in pseudo- colour, as geo-referenced JPEG images.

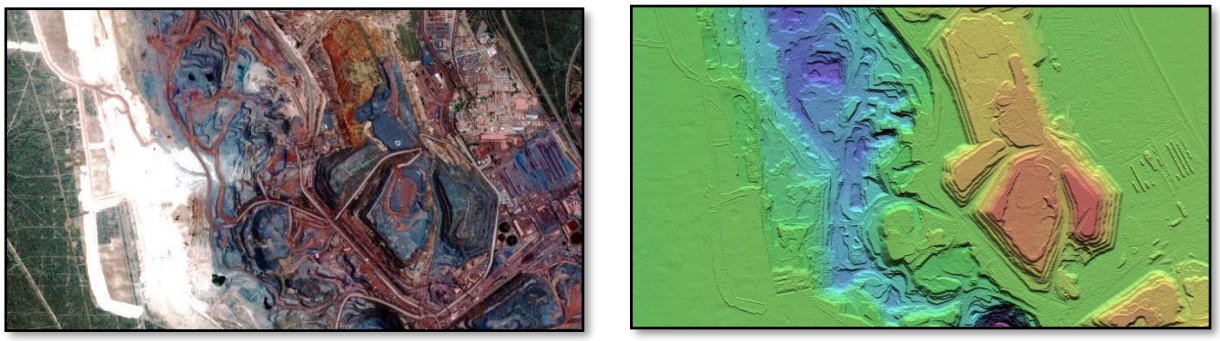

Figure 3.9: Stereo image over Sishen mine (left), DSM generated from Stereo (right)
Source: © PLEIADES (CNES) 2016, Distribution Airbus DS. All rights reserved.
© Pinkmatter Solutions 2016

3.3.3.2 DEM differencing

A comparison between DSMs generated from Pléiades stereo imagery acquired on 28 November 2014 and 24 December 2015, as illustrated in Figure 3.10 below, gives a good overview of volume changes, both in terms of mined material, and dump deposits of waste material (Lück, 2015).

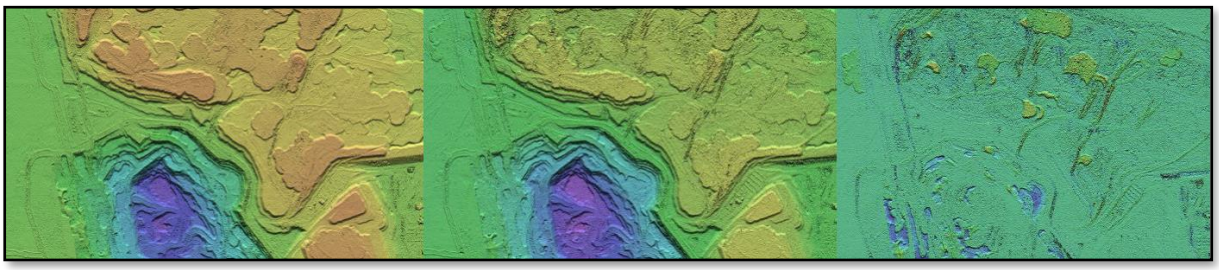

Figure 3.10: Pleiades DSM 28 November 2014 (left), Pleiades DSM 24 December 2014 (middle), Volume Change Product (right)
Source: © PLEIADES (CNES) 2016, Distribution Airbus DS. All rights reserved.
© Pinkmatter Solutions 2016

3.3.3.3 Image differencing

Pléiades satellite imagery can be used to detect changes on the surface of the mine, which is essential for operational management purposes. Automatic change detection can highlight changes that occurred and indicate where infrastructure, such as drill rigs and excavators, has been relocated from one location to another. Change detection in optical imagery can be performed by measuring changes in

brightness (intensity) or texture at pixel level. The concept of brightness change detection as the preferred method is illustrated in Figure 3.11 below (Lück, 2015).

Figure 3.11: Illustration of intensity change detection: 21 November 2015 (left), 28 November 2015 (middle), Change detection product (right), decrease in brightness (blue), increase in brightness (yellow)

3.3.4 TerraSAR-X InSAR imagery for interferometric time series analysis to generate a surface movement monitoring product

Interferometric time series analysis exploits phase information of a number of SAR satellite datasets for the derivation of ground movement. A network of measurement pixels spreaded over wide areas is provided. Time series analysis is preferred to a common differential interferometry approach, as it allows the removal of atmospheric errors, increases the theoretical precision (repeatability of measurements) to 2mm to 4mm for TerraSAR-X data. There are at least fifteen radar images necessary to achieve this precision, see Figures 3.12 and 3.13 (Anderson, 2016).

The Small Baseline Subset (SBAS) method was chosen for the processing of the areas of interest within this study. The SARscape software (Version No. 5.2) from Sarmap S.A. was used for processing. The SBAS approach (Berardino *et a*l, 2002) extends the technique presented in (Lundgren *et al*, 2001) and (Usai, 2001) to the case of multiple short-baseline (SB) acquisitions via an easy and effective combination of all the available SB interferograms (Anderson, 2016).

Primary input datasets were delivered by the customer service team of Airbus Defence and Space and downloaded via a File Transfer Protocol (FTP) server. After data extraction from the FTP server the data were imported into the software. The data was then subject to a general assessment before processing. All useful

datasets, which were free of errors were subsequently be used for further processing. An external DEM was introduced into the workflow to correct the data for the topography, in this case the WorldDEM™ at 12m resolution (Anderson, 2016).

After the pre-processing steps different interferometry approaches can be applied in order to derive ground deformation estimations, such as DInSAR, PSI, IPTA, SBAS or CRInSAR (Anderson, 2016). As mentioned above, the SBAS technique was selected as neither precision scatters nor corner reflectors were placed physically on the ground within the area of interest. After the interferometry processing a post-processing was carried out to undertake a plausibility control and to integrate available ground truth information. As a last step in the post-processing the ground deformation analysis outcomes were exported to specific usable file formats such as KMZ, GeoTiff or SHP (Anderson, 2016).

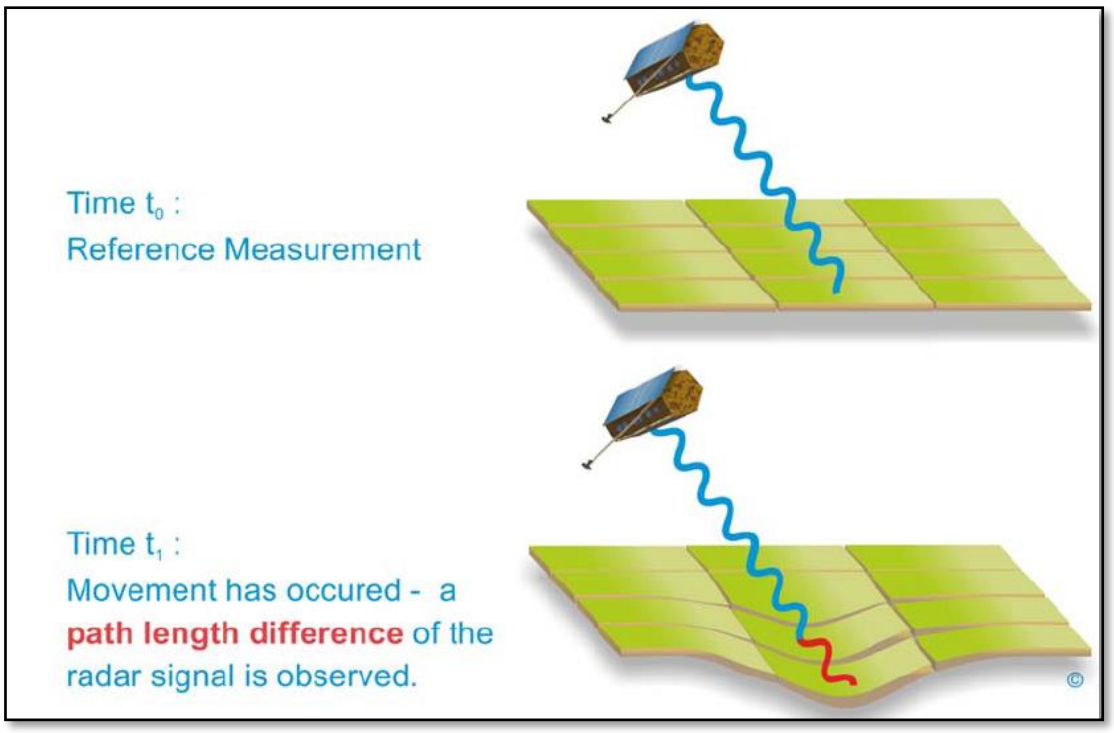

Figure 3.12: Principle of radar interferometry to measure surface movements.
Source: © DLR e.V. 2014 and © Airbus DS / Infoterra GmbH 2014

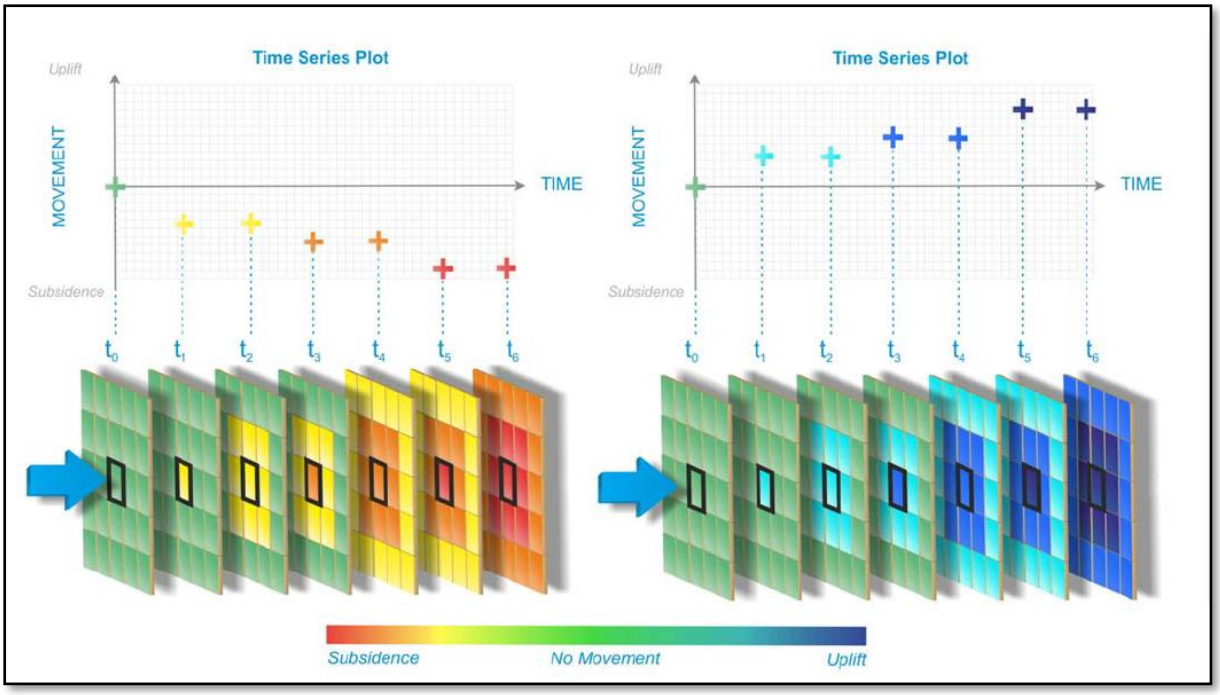

Figure 3.13: Time series analysis using multiple acquisitions. A time series will be available for every measurement pixel.
Source: © DLR e.V. 2014 and © Airbus DS / Infoterra GmbH 2014

3.3.4.1 Processing workflow for surface movement monitoring

The workflow of Airbus Defence and Space surface movement monitoring service consists of different processing sections and single steps. The interferometric processing core contains different time series analysis approaches to derive the optimum deformation estimation for different conditions at a given AOI. The flowchart in Figure 3.14 gives an overview of the main sections and steps of the processing workflow based on the SBAS method. The collection of multiple SAR interferometric imagery enables the monitoring of a specific targeted area every eleven days. Collecting the SAR data at precisely the same viewing angle ensures the processing of a surface movement monitoring product. Airbus Defence and Space have launched its third SAR satellite named PAZ on 22 February 2018 *via* the Falcon 9 rocket launcher of Space-X. This will further improve temporal collection of interferometric SAR imagery to around seven days.

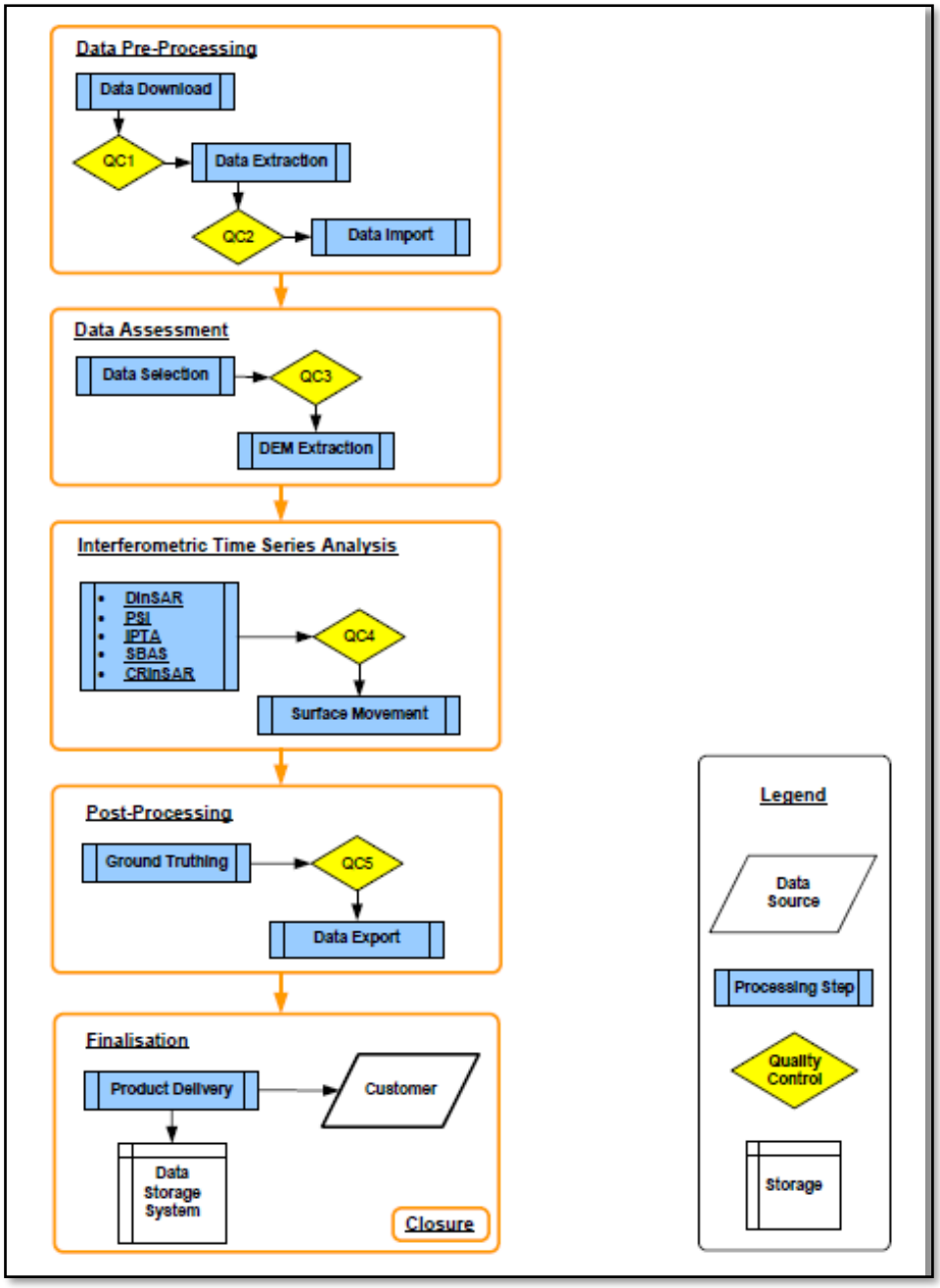

Figure 3.14: Generic surface movement monitoring workflow overview with quality control (QC) breakpoints displayed in yellow.
Source: © DLR e.V. 2014 and © Airbus DS / Infoterra GmbH 2014

3.3.4.2 Precision and accuracy of surface movement monitoring from TerraSAR-X

The interferometric surface movement monitoring in general estimates an average annual (linear) movement rate, the velocity, from a number of time series points. The theoretical precision, i.e. the repeatability of measurements, of the velocity can be given to be about 1mm - 2mm per year, the precision of individual time series points

about 2mm - 4mm (using TerraSAR-X data). For each measurement pixel, the precision of the velocity value is estimated and given in the column ‘V_Precisio’ in the digital results file of the SMM product (Anderson, 2016).

The accuracy, i.e. the difference between measurements and reality, of a time series point depends on several measurement parameters, such as data availability, surface signal reflection properties, temporal and spatial movement characteristics, processing method and the assumed stable reference pixel. The accuracy can be estimated in comparison to true measurements, e.g. resulting from a terrestrial levelling campaign. However, under optimal conditions, e.g. in an urban environment, it can be shown that an accuracy of about 3mm for a time series point can be achieved. Under ‘normal’ measurement conditions, the technique is estimated to produce an accuracy of about 1cm for a time series point. That is, in this result, only the precision (and not the accuracy) is given for the pixels’ velocity: velocity ± precision (e.g. -46.9 ± 4.4mm/year) (Anderson, 2016).

SAR-interferometry (InSAR) is a relative surveying method and its results have to be referenced to reference points (RPs) in order to derive absolute measurements. The RPs themselves are assumed to be stable. All other measurement pixels represent the movement values with respect to these defined zero movement locations. Actually one RP would be enough to refer the InSAR result, but from a technical point of view it is advisable to define several RPs within a small area of zero movement (Anderson, 2016). According to Casu et al. (2006) the theoretical increase of standard deviation, depending on the distance to the RPs, for single measurements within a time series is: the longer the distance to the RP, the smaller the precision of a measurement.

3.3.4.3 Understanding the TerraSAR-X satellite viewing geometry

The one dimensional SAR-satellite viewing geometry has to be considered in the interpretation of the surface movement results: The real three dimensional surface movement phenomena are projected into a one dimensional measurement into the satellite line-of-sight (LOS). A decomposition of the one dimensional LOS

measurement into a three dimensional surface movement is generally not possible using one satellite viewing geometry. Figure 3.15 depicts the viewing geometry in terms of potential subsidence bowls in the study area (Anderson, 2016).

The satellite measures the surface movement in line-of-sight of satellite (MLOS) under a certain incidence angle. A 3D deformation phenomenon is characterized by a combination of horizontal and vertical surface movement components. As shown in Figure 3.15, while having almost comparable values, the horizontal surface movement components for an exemplary subsidence bowl yield different amounts of MLOS depending on their location on the bowl. Therefore, a simple transformation of LOS measurements into the vertical direction under the assumption of only vertical surface movement introduces a certain inaccuracy. This issue cannot be overcome without any additional information about the real three dimensional surface movement components (Anderson, 2016).

One technical way to overcome this issue is the exploitation of two viewing geometries, i.e. ascending and descending, as depicted in Figure 3.16. The merge of the ascending and descending MLOS allows a decomposition of the real three dimensional surface movement into two components: vertical (MV) and almost east-west directed horizontal (MEW). The north-south component cannot be derived due to the polar orbit of SAR-satellites and the related viewing geometry (Anderson, 2016).

Based on this technical explanation it is worthwhile to consider the acquisition of both ascending and descending viewing geometries over the study area to have movement estimates in both vertical and horizontal directions.

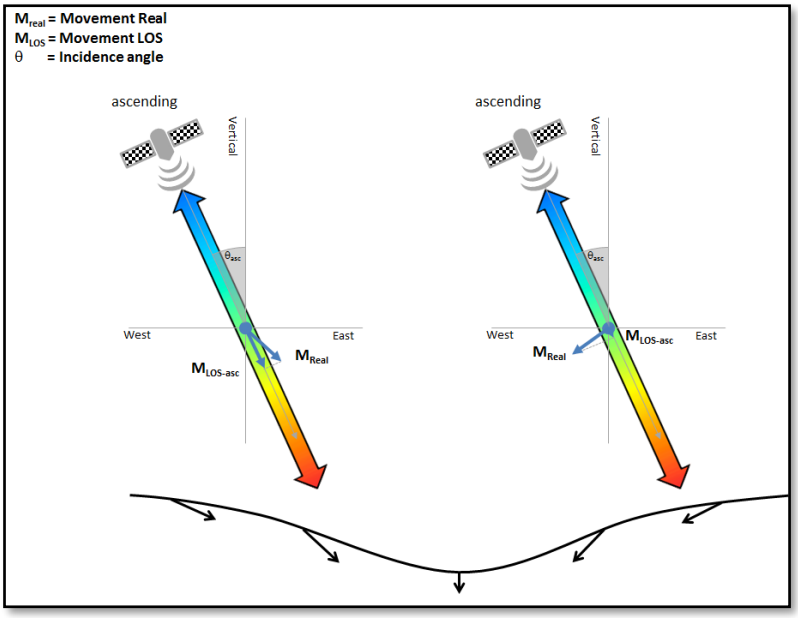

Figure 3.15: Exemplary ascending viewing geometry for a subsidence bowl. The colour coding of arrows (line-of-sight of satellite) corresponds to that of the velocity maps.
Source: © DLR e.V. 2014 and © Airbus DS / Infoterra GmbH 2014

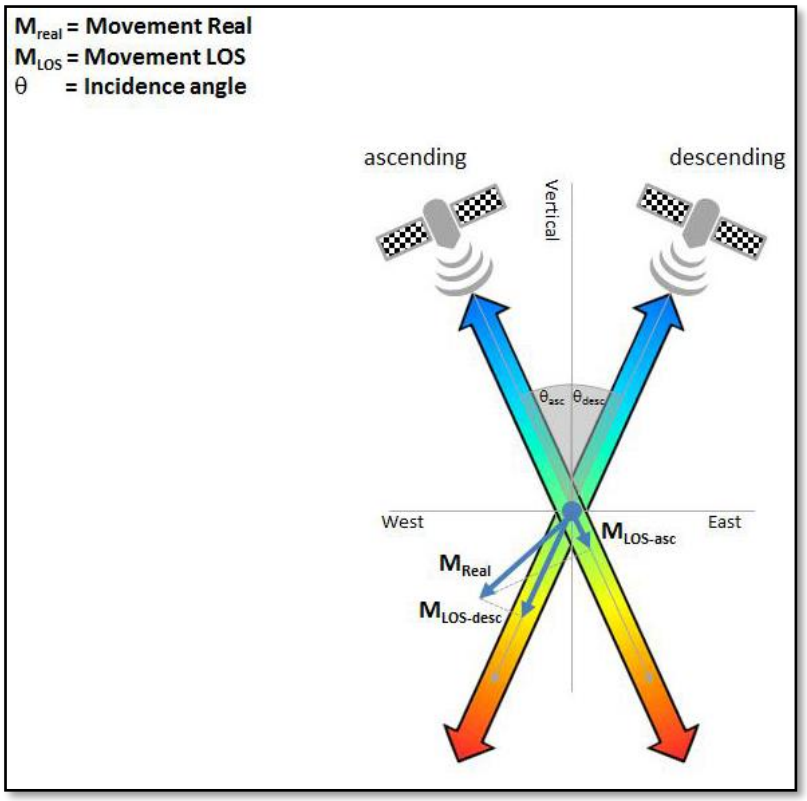

Figure 3.16: Ascending and descending viewing geometry in terms of an exemplary vertical and horizontal composed surface movement. The colour coding of arrows (line-of-sight of satellite) corresponds to that of the velocity maps.
Source: © DLR e.V. 2014 and © Airbus DS / Infoterra GmbH 2014

3.3.5 Mine monitoring and environmental impact model

The final step will be the integration of the findings of the Landsat land cover baseline, the Pléiades monoscopic monitoring images, the Pléiades stereoscopic elevation and volumetric calculations as well as the concept of the TerraSAR-X SMM product as spatial input to monitor a mine and to understand the primary and secondary activities that impact on its environment.

3.4 Conclusion

This chapter introduced the methodology applied during this study. A detailed research design diagram was provided to explain the workflow methods to ultimately create an environmental mine monitoring model through the use of RS technology. A description of each major workflow was provided. Firstly, the Landsat 8 time-series analysis to produce a reliable land cover base layer. Secondly, the Pléiades monoscopic imagery as a monitoring aid over the mine to provide high temporal change layers. Thirdly, the Pléiades stereoscopic data produced a very high resolution elevation model to enable the calculation of volumetric cubicles in the mining area. Lastly, the SAR data preparation and SMM analytics provided a fine scale subsidence and upliftment measurement solution over the Royal Bafokeng, Rustenburg and Chuquicamata, Chile mines. The later SMM case studies served as a concept model, although they were not part of the Kolomela and Sishen mine study areas. Combining all these workflow methods provided a mine monitoring tool to detect changes and serves as a contributor to the monitoring of the mine operations.

CHAPTER 4: ANALYTICAL OPTICAL RESULTS

4.1 Introduction

This chapter will comprise of the analytics done based on the processed optical imagery. The Landsat 8 imagery was used to derive the baseline land cover information and the Pléiades imagery as a very high resolution time-series information stack.

Land cover is a key information requirement for a wide range of landscape planning, inventory and management activities, ranging from environmental resource management to telecommunication planning. The recent global availability of Landsat 8 satellite imagery offered the opportunity to create a new, national land-cover dataset for South Africa, circa 2013-14, replacing and updating the previous 1994 and 2000 South African National Land Cover datasets. The 2013-14 National Land Cover Dataset is based on 30mx30m raster cells, and is ideally suited for ± 1:75 000 to 1:250 000 scale GIS-based mapping and modelling applications (Thompson, 2015).

The dataset has been derived from multi-seasonal Landsat 8 imagery, using operationally proven, semi-automated modelling procedures developed specifically for the generation of this dataset, based on repeatable and standardised modelling routines. The dataset has been created by GEOTERRAIMAGE (GTI) and is available as a commercial data product (Thompson, 2015).

The Pléiades imagery was used to analyse spatial-temporal changes over each study area based on the monoscopic and stereoscopic imagery. The interpretation of these changes will conclude this chapter.

4.2 Landsat 8 imagery as National Land Cover baseline, 2013/2014

The dataset used in this study contains 72 x land cover / use information classes, covering a wide range of natural and man-made landscape characteristics. Each data cell contains a single code representing the dominant land cover class (by area) within that 30mx30m unit, as determined from analysis of the multi-date imagery acquired over that image frame (Thompson, 2015).

Land use classes such as cultivated lands, forest plantations, mines and settlements were all derived as separate modelling procedures, typically using independently sourced and generated geographical masks to control where and how the original 51 seasonally defined, spectral foundation classes were re-coded and modified into the final land use classes. The masking process allowed the geo-location of the re-coding process to be accurately controlled and managed (Thompson, 2015).

The foundation land cover classes that were detected in the Sishen mine and Kolomela mine study areas will be described in the following paragraphs. According to Thompson (2015) these classes can be described as per 2013-14 South African National Land Cover legend.

4.2.1 Foundation National Land Cover classes

The fundamental National Land Cover classes that were described in this study can be found as Annexure B. These fundamental classes were the following:

- Water
- Base vegetation
- Cultivated
- Forest plantations
- Mines
- Bare
- Built-up / Settlements

4.2.2 National Land Cover 2013/2014 assessment over study areas

The National Land Cover 2013/2014 consisted of 72 defined land cover class types (see Table 4.1). Each class has a unique class code allocated to a specific pixel, as derived from the multi-seasonal Landsat 8 images. The count of the total pixels that belong to a specific class code, representing a geographical size of 30m x 30m, provides the ability to calculate its geographical extent within the study area.

The 72 classes were combined into 14 foundation classes to represent the predominant land cover/land use activities within each study area. These foundation classes are described in Table 4.2 below.

Class Code	ClassName
1	WATER: Permanent Water
2	WATER: Seasonal Water
3	WETLAND
4	FOREST: Indigenous Forest
5	THICKET & DENSE BUSH
6	WOODLAND / OPEN-BUSH
7	GRASSLAND
8	LOW SHRUBLAND Fynbos
9	LOW SHRUBLAND: Other
10	CULTIVATED: Commercial Annuals (rainfed)
11	CULTIVATED: Commercial Annuals (rainfed)
12	CULTIVATED: Commercial Annuals (rainfed)
13	CULTIVATED: Commercial Pivot
14	CULTIVATED: Commercial Pivot
15	CULTIVATED: Commercial Pivot
16	CULTIVATED: Commercial Permanent
17	CULTIVATED: Commercial Permanent
18	CULTIVATED: Commercial Permanent
19	CULTIVATED: Commercial Permanent
20	CULTIVATED: Commercial Permanent
21	CULTIVATED: Commercial Permanent
22	CULTIVATED: Commercial Permanent
23	CULTIVATED: Subsistence
24	CULTIVATED: Subsistence
25	CULTIVATED: Subsistence
26	CULTIVATED: Sugarcane pivot
27	CULTIVATED: Sugarcane pivot
28	CULTIVATED: Sugarcane non-pivot
29	CULTIVATED: Sugarcane non-pivot
30	CULTIVATED: Sugarcane non-pivot
31	CULTIVATED: Sugarcane non-pivot
32	FOREST: Forest Plantations: Mature Trees
33	FOREST: Forest Plantations: Young Trees
34	FOREST: Forest Plantations: Temporary Clearfelled
35	MINE: Bare
36	MINE: Semi-Bare
37	MINE: Mine water seasonal
38	MINE: Mine water permanent
39	MINE: Mine Buildings
40	BARE: Erosion dongas and gullies
41	BARE: Bare (Non Vegetated)
42	BUILT-UP: Commercial
43	BUILT-UP: Industrial
44	BUILT-UP: Informal
45	BUILT-UP: Informal
46	BUILT-UP: Informal
47	BUILT-UP: Informal
48	BUILT-UP: Residential
49	BUILT-UP: Residential
50	BUILT-UP: Residential
51	BUILT-UP: Residential
52	BUILT-UP: Schools & Sports Grounds
53	BUILT-UP: Smallholding
54	BUILT-UP: Smallholding
55	BUILT-UP: Smallholding
56	BUILT-UP: Smallholding
57	BUILT-UP: Sports & Golf
58	BUILT-UP: Sports & Golf
59	BUILT-UP: Sports & Golf
60	BUILT-UP: Sports & Golf
61	BUILT-UP: Township
62	BUILT-UP: Township
63	BUILT-UP: Township
64	BUILT-UP: Township
65	BUILT-UP: Village
66	BUILT-UP: Village
67	BUILT-UP: Village
68	BUILT-UP: Village
69	BUILT-UP: Built-up other
70	BUILT-UP: Built-up other
71	BUILT-UP: Built-up other
72	BUILT-UP: Built-up other

Table 4.1: 72 National land cover classes 2013/2014

CLASS NAME	CLASS CODE
WATER	1,2
BUSH	5,6
CULTIVATED	10,11,12,13,14,15
FOREST	32,33
MINE	35,36
MINE_WATER	37,38
MINE_BUILDINGS	39
BARE	40,41
BUILT_UP_TOWNSHIP	44,45,46,47,61,62,63,64
BUILT_UP_IND/COM	42,43
BUILT_UP_RESIDENTIAL	48,49,50,51
BUILT_UP_SCH_SPORT	52,57,58,59,60,
BUILT_UP_OTHER	67,68,69,70,71,72
SHRUBLAND/GRASS	7,9

Table 4.2: National land cover classes combined into 14 foundation classes

4.2.2.1 Kolomela mine study area

The Kolomela mine area selected during this study was calculated to an approximate size of 1 755km². This area was used to subset the associated National Land Cover Dataset to ensure an assessment relevant to the surroundings of the actual mine.

$$\text{Total study area} = (C \times LPx) \times (R \times LPy)$$

$$= (1\,430 \times 30) \times (1\,364 \times 30)$$

$$= 1\,755\,468\,000\text{m}^2 / 1\,000\,000$$

$$= 1\,755\text{km}^2$$

C = Column
LPx = Pixel size of Landsat 8 (horizontal pixel size)
R = Row
LPy = Pixel size of Landsat 8 (vertical pixel size)

Equation 4.1: Kolomela study area calculation

It is the opinion of the researcher that an area greater than 40km x 40km represents the predominant foundation land cover classes that surround the target area, in this case the actual mine.

The relationship between a specific National Land Cover (NLC) class and the study area was calculated based on its geographical size *versus* the total area, 30m x 30m pixel count values. The measurement units used to calculate the results were done in square metre and expressed in percentage. The calculations were done based on the original National Land Cover 2013/2014 pixel class value, thus raster based calculations *versus* vector.

CLASS NAME	CLASS CODE	M²	M² CLASS PERCENTAGE
FOREST	32,33	30 600	0.00%
WATER	1,2	59 400	0.00%
MINE_WATER	37,38	219 600	0.01%
BUILT_UP_SCH_SPORT	52,57,58,59,60,	733 500	0.04%
MINE_BUILDINGS	39	913 500	0.05%
BUILT_UP_IND/COM	42,43	1 050 300	0.06%
CULTIVATED	10,11,12,13,14,15	1 150 200	0.07%
BUILT_UP_OTHER	67,68,69,70,71,72	1 360 800	0.08%
BUILT_UP_RESIDENTIAL	48,49,50,51	2 180 700	0.12%
BUILT_UP_TOWNSHIP	44,45,46,47,61,62,63,64	3 748 500	0.21%
BUSH	5,6	18 745 200	1.07%
BARE	40,41	30 086 100	1.71%
MINE	35,36	44 908 200	2.56%
SHRUBLAND/GRASS	7,9	1 650 281 400	94.01%

Table 4.3: Kolomela Mine study area - 14 Foundation NLC classes

- CLASS NAME = A description of the foundation class type
- CLASS CODE = The original 72 class codes as per NLC 2013/2014 legend
- M² = The m² calculation per foundation class
- M² CLASS PERCENTAGE = The percentage geographical coverage (m²) of a foundation class within the total study area (1 755 468 000m²)

The combination of “SHRUBLAND/GRASS” dominates the base vegetation land cover within the study area and represents an estimate of 94%. The “BUSH” foundation class (thicket/ dense bush & woodland/open bush) has a low value of 1.07%.

The “MINE” foundation class is the largest land use class and represents an estimate of 2.56%. The largest built-up foundation class is “TOWNSHIP”, 0.21%, followed by “RESIDENTIAL”, 0.12%.

Kolomela mine is situated in the Northern Cape, an arid area, thus the reason for the low “WATER”, 0.00%, “FOREST”, 0.00% and “CULTIVATED”, 0.07% results. The rocky outcrops in this area were detected under the “BARE”, 1.71% foundation class, see Figures 4.1 to 4.3, Graphs 4.1 to 4.3.

Figure 4.1: Kolomela Mine, Landsat 8 (2013) Red = Band 4; Green = Band 3; Blue = Band 2 (Natural colour composite)
Source: © USGS 2013

Figure 4.2: Kolomela Mine, Landsat 8 (2014) Red = Band 4; Green = Band 3; Blue = Band 2 (Natural colour composite)
Source: © USGS 2014

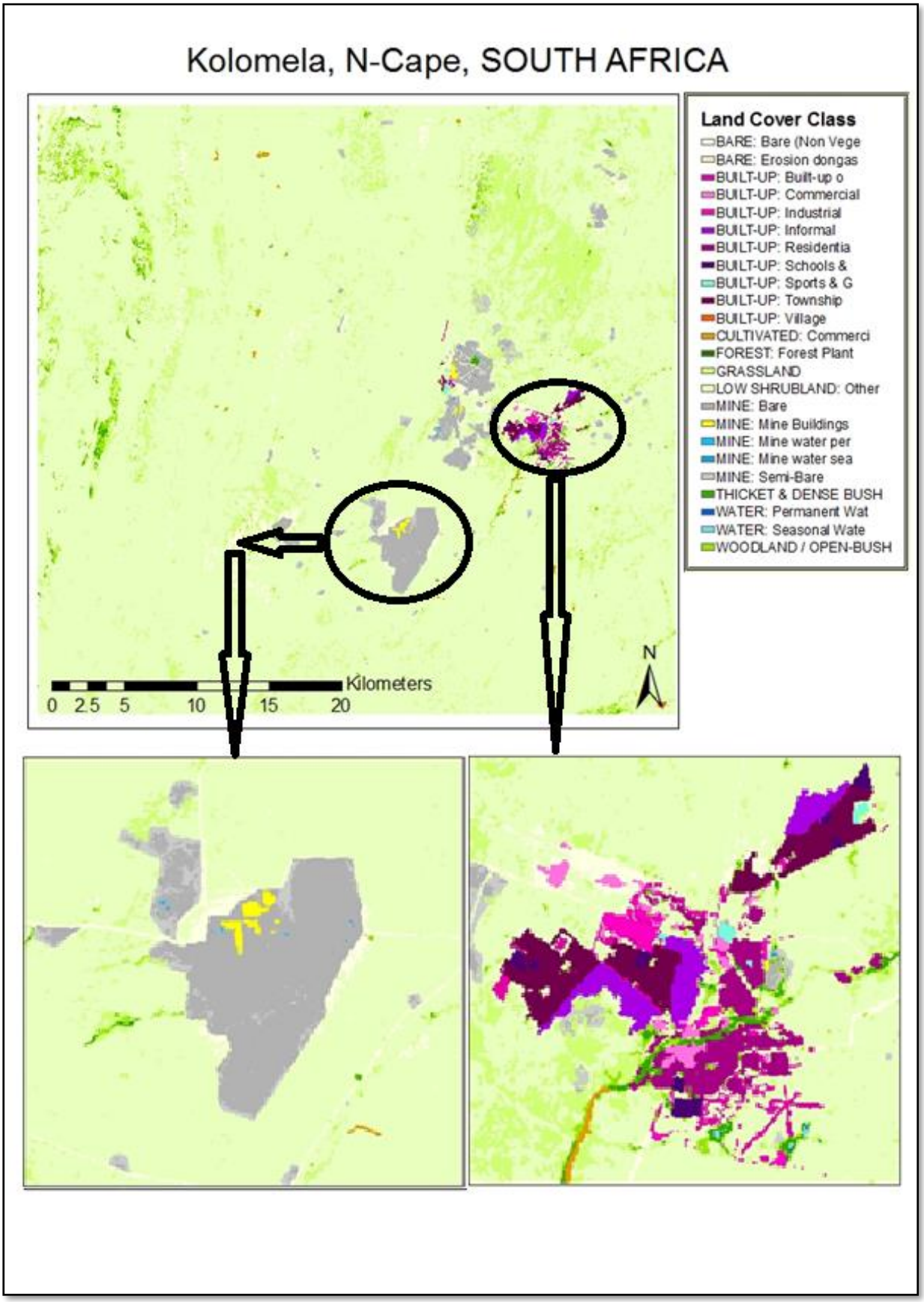

Figure 4.3: Kolomela Mine study area, NLC 2013/2014
Source: © GEOTERRAIMAGE - 2014

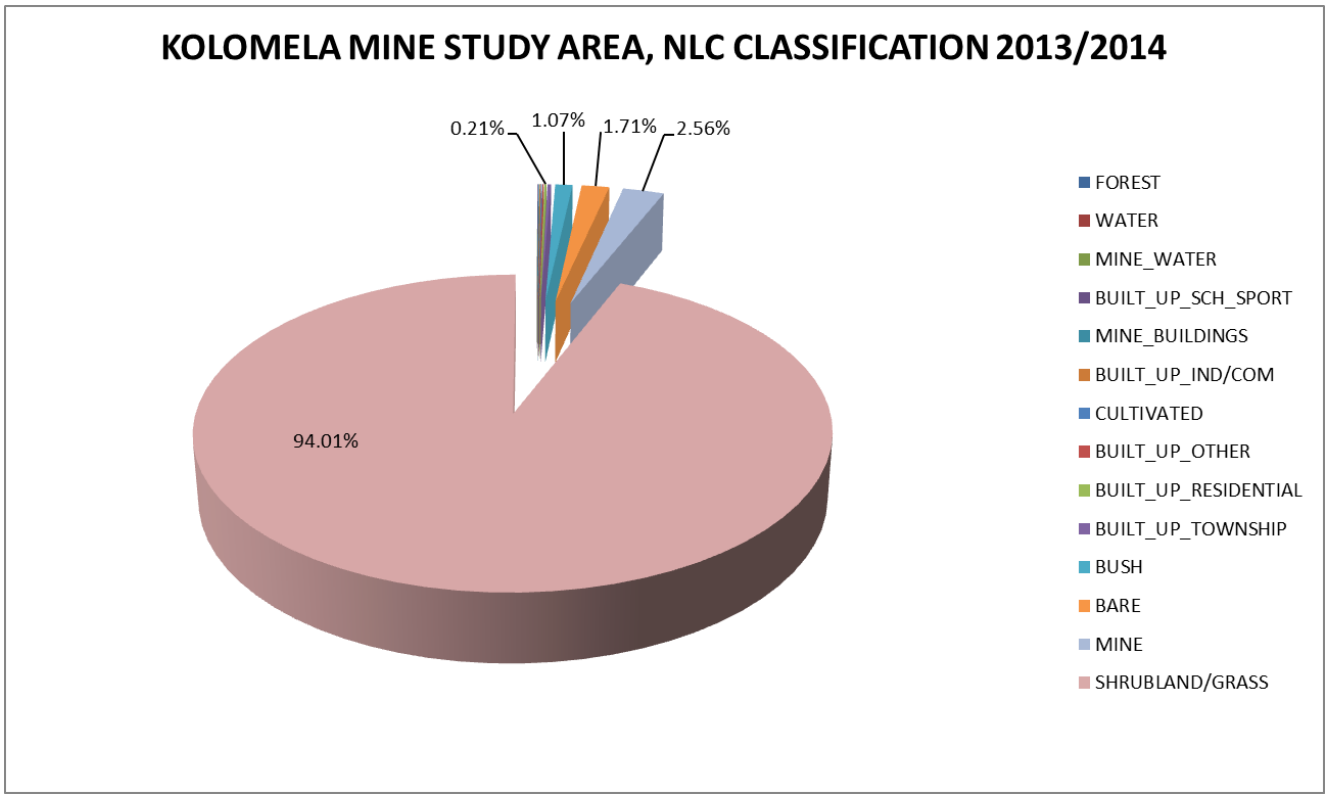

Graph 4.1: Graph representing 14 NLC foundation classes, Kolomela Mine study area

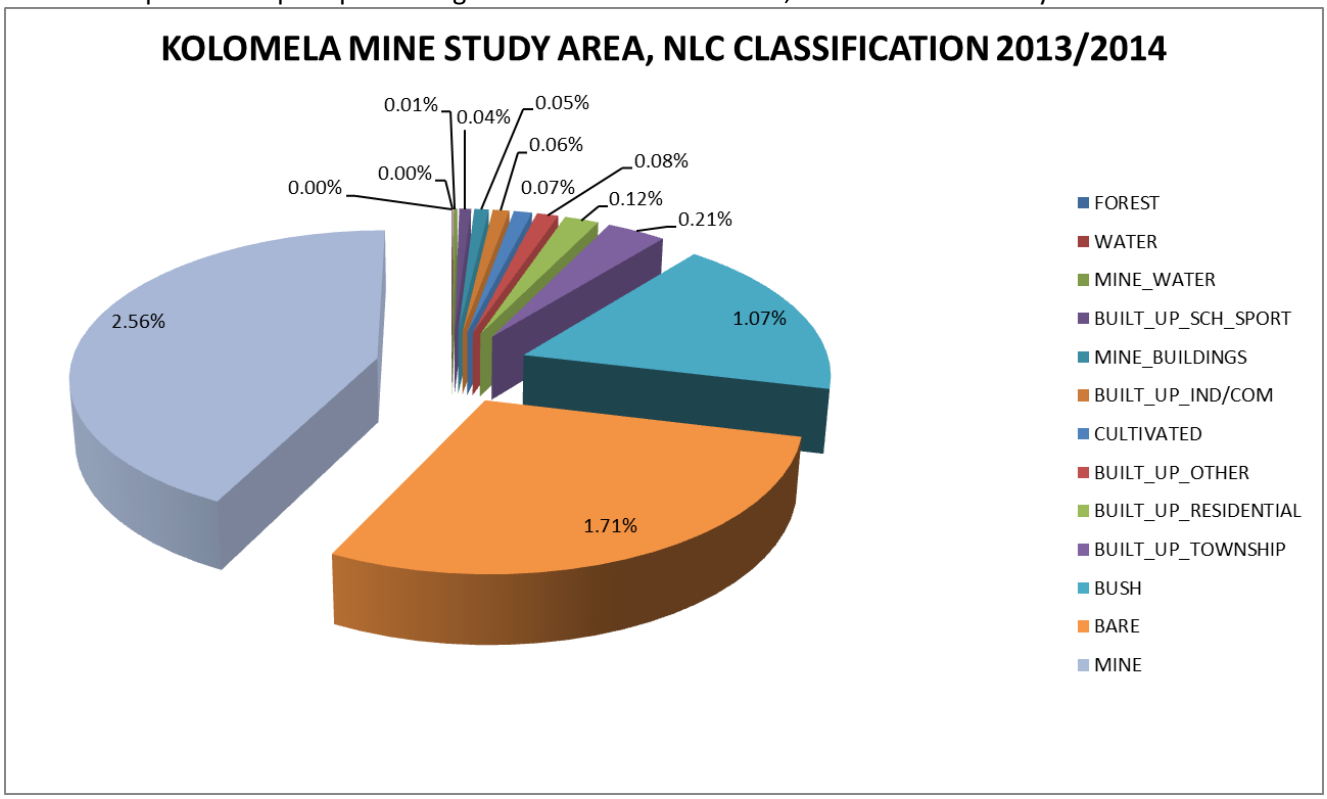

Graph 4.2: Graph representing 13 NLC foundation classes (SHRUBLAND/GRASS excluded), Kolomela study area

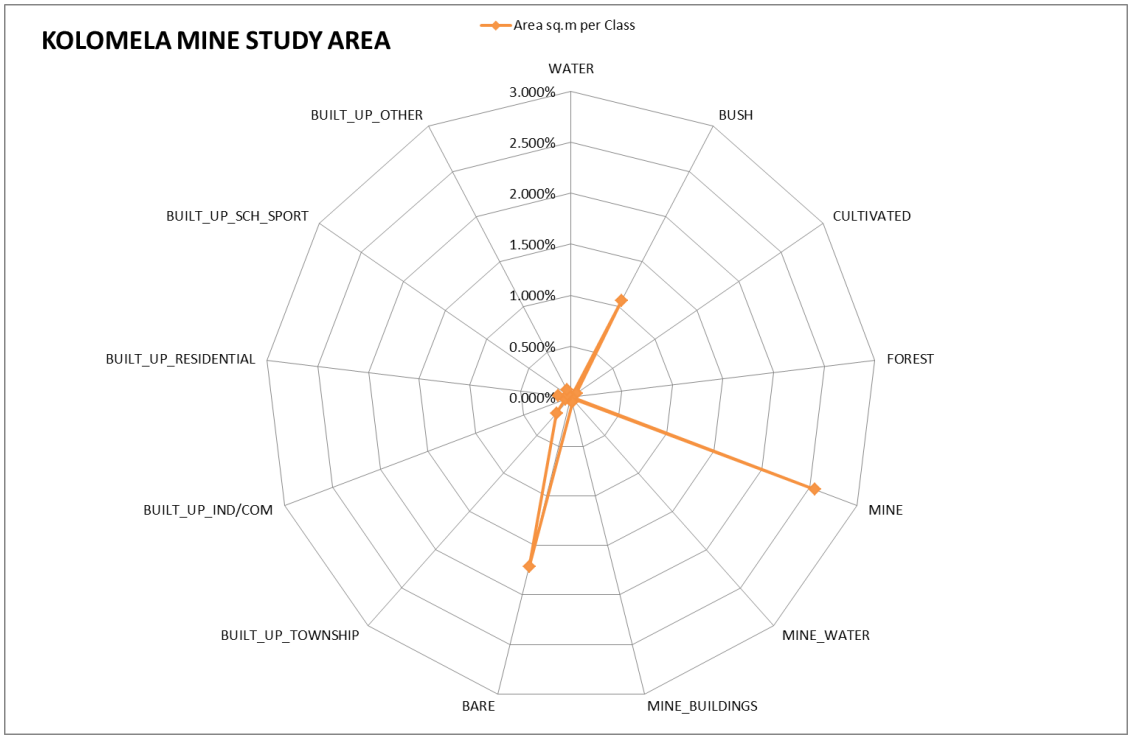

Graph 4.3: Radar graph representing 13 NLC foundation classes, SHRUBLAND/GRASS excluded, Kolomela study area

The SHRUBLAND/GRASS foundation class dominates the study area with a 94% coverage. This class was excluded from Graphs 4.2 and 4.3 to illustrate the position of the other foundation classes within the study area. These other classes that dominate the study area, yet with a percentage of less than 3% each, are the following:

- MINE = 2.56%
- BARE = 1.71%
- BUSH = 1.07%
- BUILT-UP TOWNSHIP = 0.21%
- BUILT-UP RESIDENTIAL = 0.12%
- BUILT-UP IND/COM = 0.06%

4.2.2.2 Sishen mine study area

The Sishen mine area selected during this study was calculated to an approximate size of 1 680km². This area was used to subset the associated National Land Cover Dataset to ensure an assessment relevant to the surroundings of the actual mine.

$$\text{Total study area} = (C \times LPx) \times (R \times LPy)$$

$$= (1\,334 \times 30) \times (1\,400 \times 30)$$

$$= 1\,680\,840\,000\text{m}^2 / 1\,000\,000$$

$$= 1\,680\text{km}^2$$

C = Column
LPx = Pixel size of Landsat 8 (horizontal pixel size)
R = Row
LPy = Pixel size of Landsat 8 (vertical pixel size)

Equation 4.2: Sishen study area calculation

The relationship between a specific National Land Cover class and the study area was calculated based on its geographical size *versus* the total area, 30m x 30m pixel count values. The measurement units used to calculate the results were done in m² and expressed in percentage. The calculations were done based on the original National Land Cover 2013/2014 pixel class value, thus raster based calculations *versus* vector.

CLASS NAME	CLASS CODE	M²	M² CLASS PERCENTAGE
FOREST	32	9 000	0.00%
WATER	1,2	250 200	0.01%
MINE_WATER	37,38	454 500	0.03%
CULTIVATED	10,11,12,13,14,15	522 000	0.03%
BUILT_UP_IND/COM	42,43	1 383 300	0.08%
BUILT_UP_SCH_SPORT	52,57,58,59,60,	1 459 800	0.09%
BUILT_UP_TOWNSHIP	46,61,62,63,64	2 059 200	0.12%
BUILT_UP_OTHER	53,54,55,56,69,70,71,72	2 235 600	0.13%
MINE_BUILDINGS	39	2 877 300	0.17%
BUILT_UP_RESIDENTIAL	48,49,50,51	6 107 400	0.36%
BARE	41	18 806 400	1.12%
BUSH	5,6	46 764 000	2.78%
MINE	35,36	80 978 400	4.82%
SHRUBLAND/GRASS	7,9	1 516 932 900	90.25%

Table 4.4: Sishen Mine study area - 14 Foundation NLC classes

- CLASS NAME = A description of the foundation class type
- CLASS CODE = The original 72 class codes as per NLC 2013/2014 legend
- M² = The m² calculation per foundation class
- M² CLASS PERCENTAGE = The percentage geographical coverage (m²) of a foundation class within the total study area (1 680 840 000m²)

The combination of “SHRUBLAND/GRASS” dominates the base vegetation land cover within the study area and represents an estimate of 90%. The “BUSH” foundation class (thicket/ dense bush & woodland/open bush) has a low value of 2.78%.

The “MINE” foundation class is the largest land use class and represents an estimate of 4.82%. The largest built-up foundation class is “RESIDENTIAL”, 0.36%, followed by “TOWNSHIP”, 0.12%.

Sishen mine is also situated in the Northern Cape, an arid area, thus the reason for the low “WATER”, 0.01%, “FOREST”, 0.00% and “CULTIVATED”, 0.03% results. The rocky outcrops in this area were also detected under the “BARE”, 1.12% foundation class, see Figures 4.4 to 4.6 and Graphs 4.4 to 4.6.

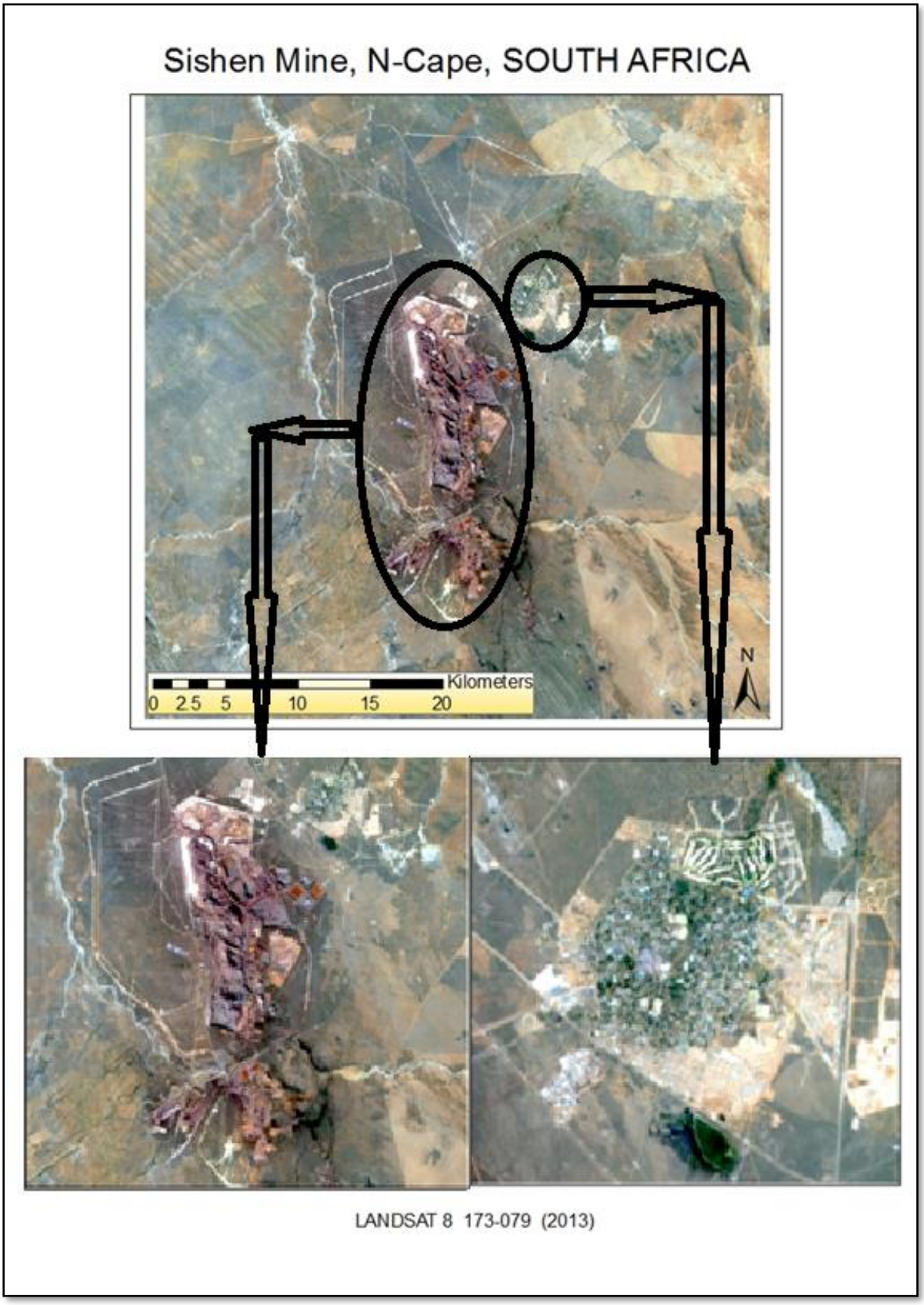

Figure 4.4: Sishen Mine, Landsat 8 (2013) Red = Band 4; Green = Band 3; Blue = Band 2 (Natural colour composite)
Source: © USGS 2013

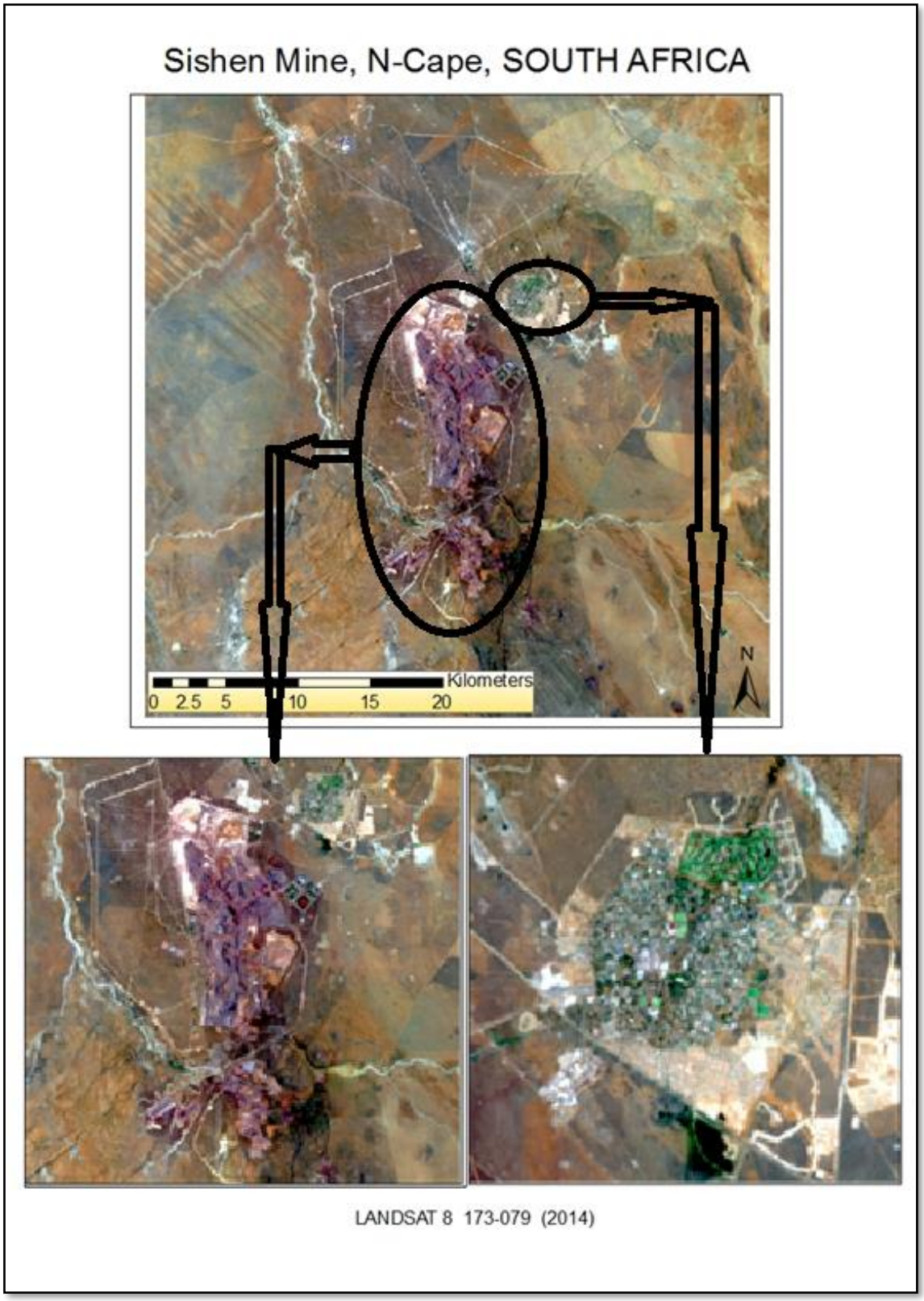

Figure 4.5: Sishen Mine, Landsat 8 (2014) Red = Band 4; Green = Band 3; Blue = Band 2 (Natural colour composite)
Source: © USGS 2014

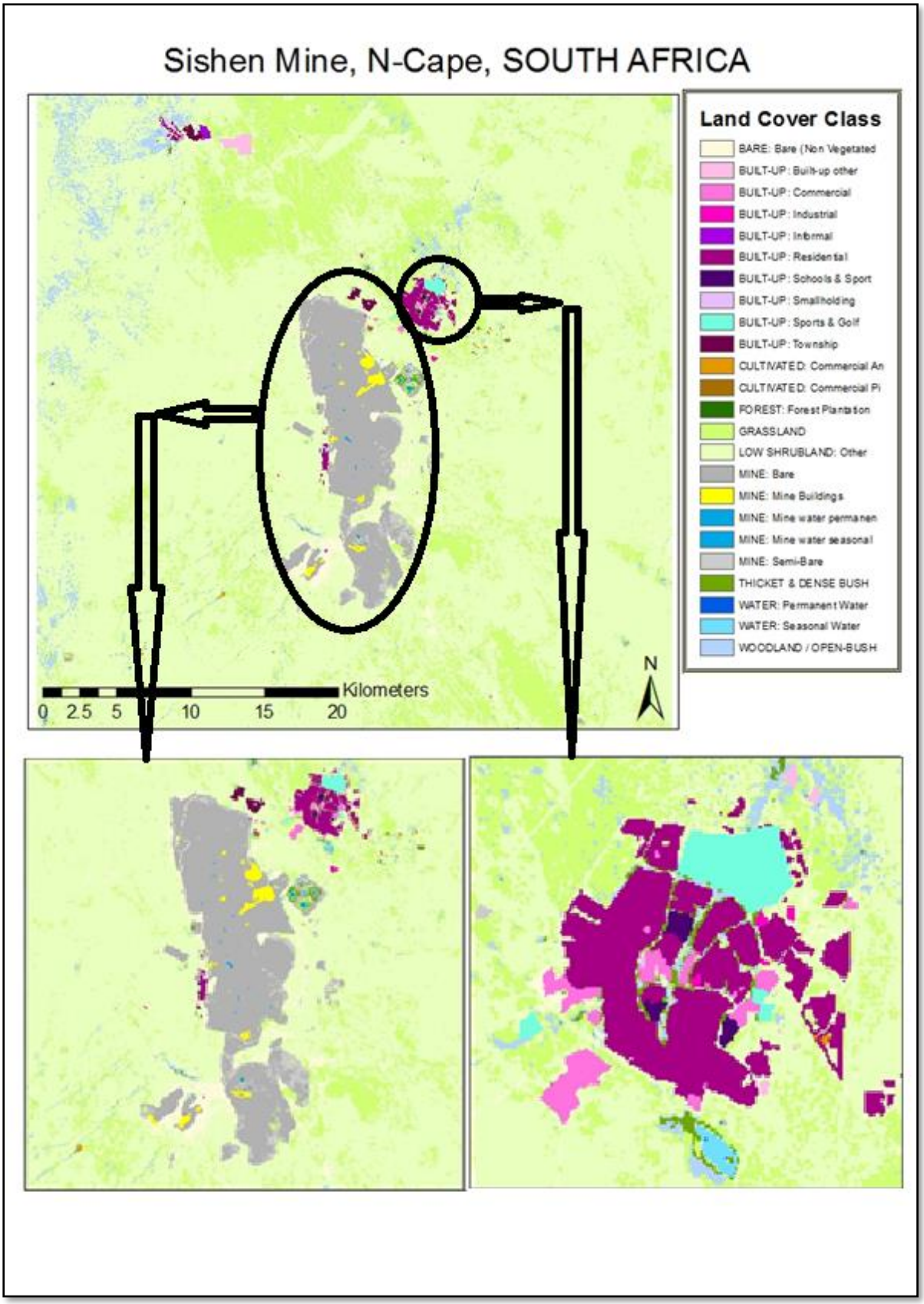

Figure 4.6: Sishen Mine study area, NLC 2013/2014
Source: © GEOTERRIMAGE - 2014

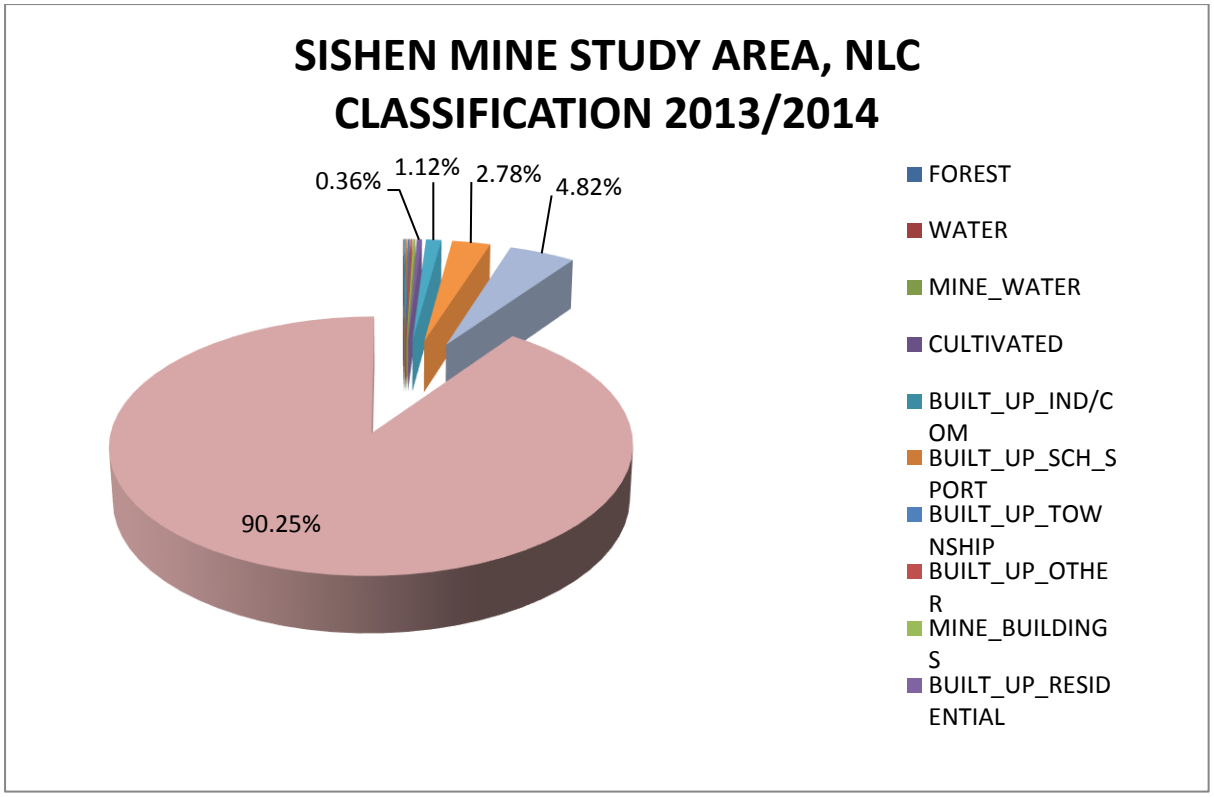

Graph 4.4: Graph representing 14 NLC foundation classes, Sishen Mine study area

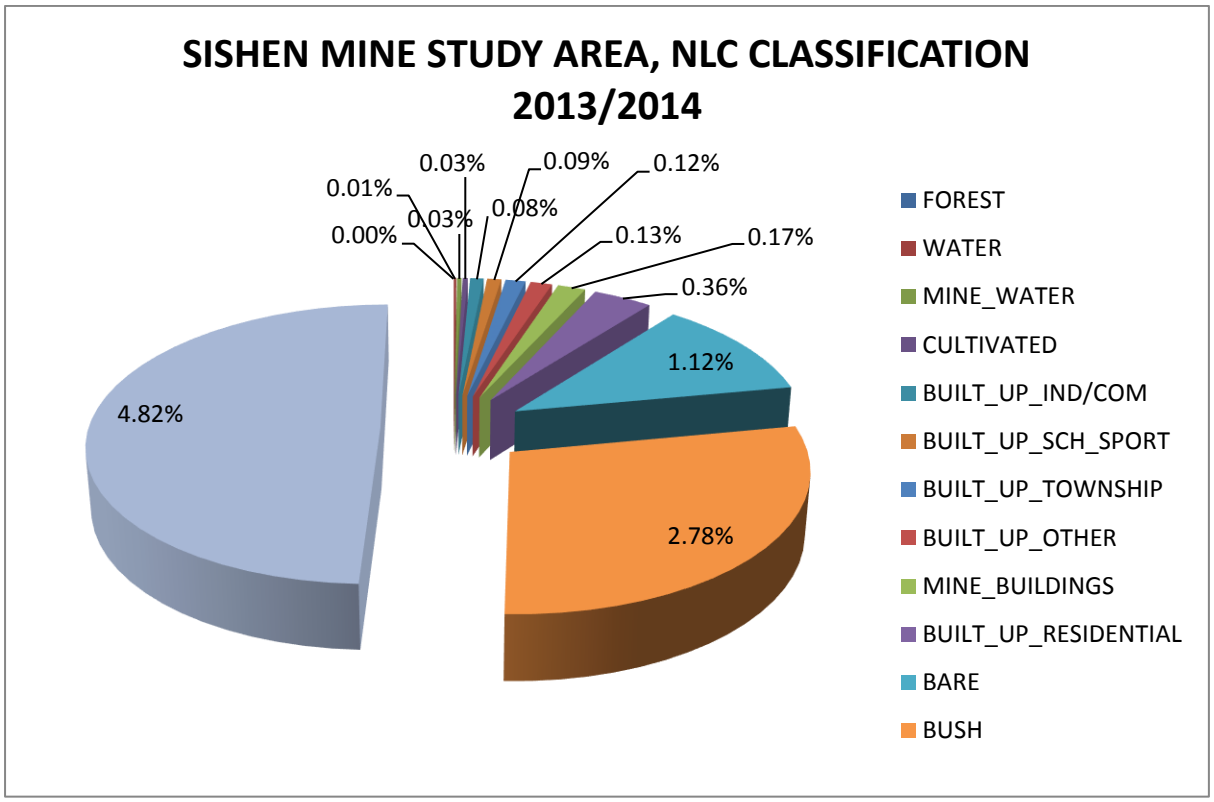

Graph 4.5: Graph representing 13 NLC foundation classes (SHRUBLAND/GRASS excluded), Sishen study area

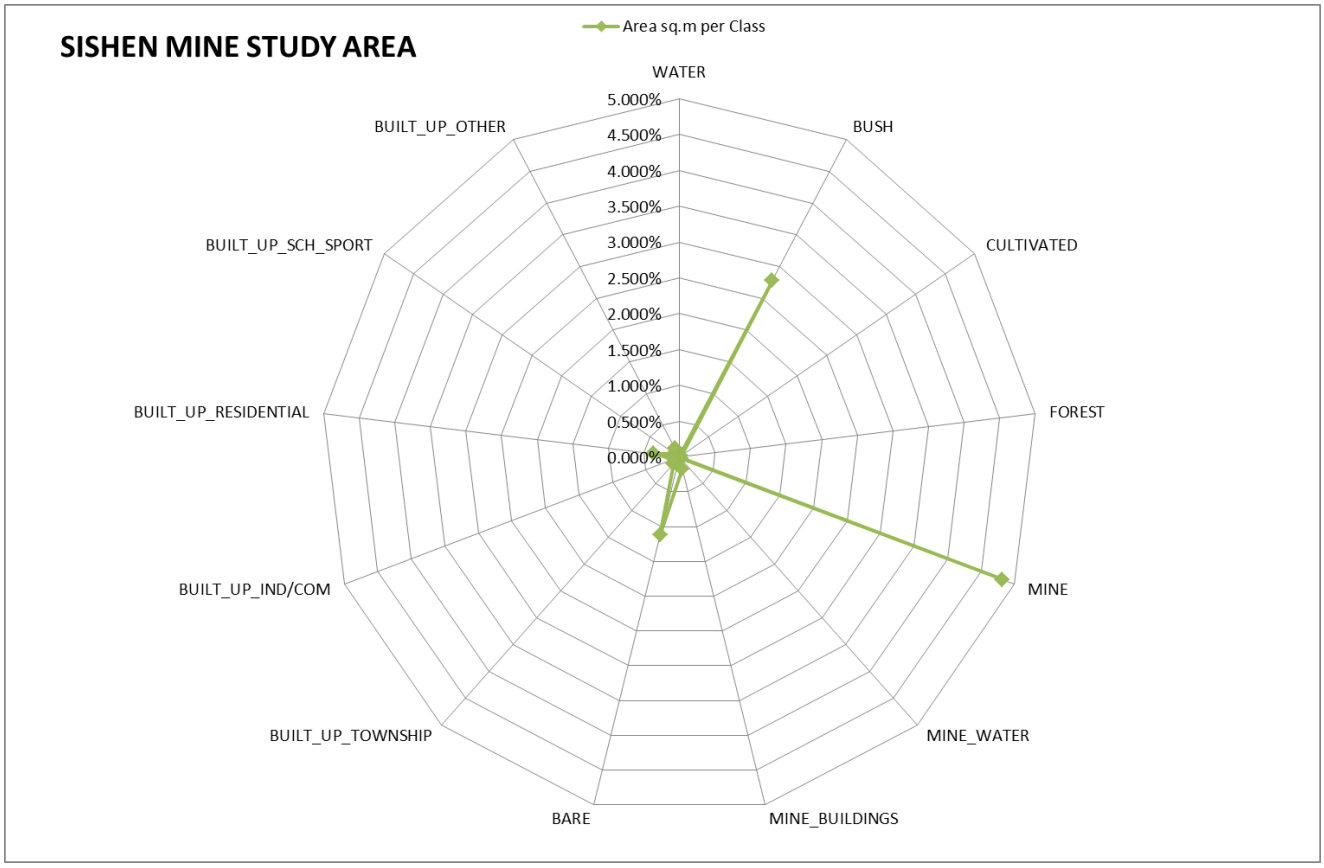

Graph 4.6: Radar graph representing 13 NLC foundation classes, SHRUBLAND/GRASS excluded, Sishen study area

The SHRUBLAND/GRASS foundation class dominates the study area with a 90% coverage. This class was excluded from Graphs 4.5 and 4.6 to illustrate the position of the other foundation classes within the study area. These other classes that dominate the study area, yet with a percentage of less than 5% each, are the following:

- MINE = 4.82%
- BUSH = 2.78%
- BARE = 1.12%
- BUILT-UP RESIDENTIAL = 0.36%
- BUILT-UP TOWNSHIP = 0.12%
- BUILT-UP IND/COM = 0.08%

4.3 Pléiades assessment over study areas

The Pléiades satellites are a constellation owned by the Centre National D'Etudes Spatiales (CNES), France. CNES took over the responsibility of project manager for the Pléiades program. Airbus Defence and Space was appointed prime contractor for the satellite manufacturing, interacting with Thales Alenia Space, who designed the optical instrument. In an agreement signed in 2008, the CNES appointed Airbus Defence and Space as the civilian operator and the exclusive worldwide distributor of Pléiades data. The Pléiades 1A spacecraft was launched on December 16, 2011 on a Soyuz ST from Europe's spaceport in Kourou, French Guiana. It was followed by Pléiades 1B during 2012. The Pléiades twins are very high resolution satellites delivering 50cm Ortho products as a standard. The technical specifications for the e Pléiades satellites are available as Annexure C.

4.3.1 FarEarth data processing and data handling system

The processing of the Pléiades imagery introduced serious challenges due to the file size of each scene. A single scene from Pléiades, 400km² 4-band pansharpened, averages a size of 12Gb. A time series of 20 scenes over each mine introduced a processing volume of over 240Gb per mine. Processing these scenes using homogeneous algorithms and the same reference dataset required a more advanced solution compared to traditional desktop processing. It was therefore the rationale to use the FarEarth system to produce the ortho-rectified and 4-band pansharpened Pléiades scenes. It was also used to produce the primary classification layers. The FarEarth system also provided the solution to derive the very high resolution elevation models from the stereoscopic imagery of Pléiades.

The FarEarth system designed by Pinkmatter Solutions, a software engineering company based in South Africa, provides the advanced RS data processing and management solution. The FarEarth system provides a lightweight and robust framework for archiving, cataloguing, processing and dissemination of data products, see Figure 4.7. Processing workflows can easily be configured to fit various standard

production methodologies. Both automatic as well as manual, human driven production workflow steps, are also supported (Böhme, Goosen, Lück, and Prinsloo, 2014).

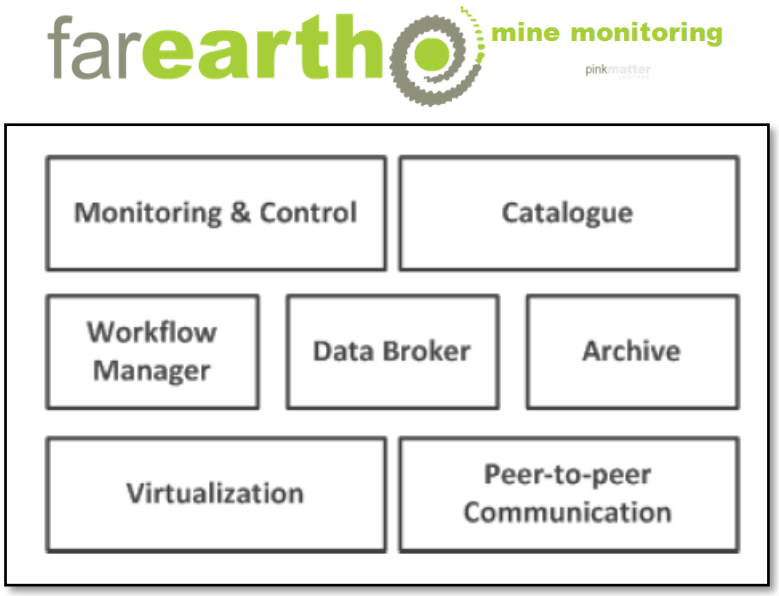

Figure 4.7: Main components of the FarEarth System.
Source:© Pinkmatter Solutions, 2014. All rights reserved.

The core components of the FarEarth data handling system are the workflow manager, archive and data broker. The workflow manager orchestrates the timely execution of tasks, the data broker is responsible for moving data between nodes, and the archive contains a spatial and temporal index of the available data, be that raster data, vector data or documents (Böhme *et al,* 2014).

Various levels of data processing are essential if RS data is to be turned into conceptual information products. During this study the focus was on the workflow process for specific Pléiades image processing products. The change detection processing chain for vegetation degradation can be used as an example. The steps normally involved would be radiometric correction, geometric correction, orthorectification, image co-registration, topographic normalization, classification, and finally change determination. Performing all these processing steps typically requires disparate processing resources and sometimes manual steps (Böhme *et al,* 2014).

The FarEarth processing system can deliver results in a robust and reliable way by capturing expert knowledge in reproducible workflows. Workflows were configured using Excel spreadsheets that present the operators with a familiar interface for documenting their processing requirements. Even if all steps in a production workflow were to be performed manually by human operators, an organization would still benefit if a management system aided operators by prompting them to perform certain steps, ensuring that the steps are executed in the correct sequence, tracking the overall progress in the production chain and ensuring that resources are utilized effectively. The FarEarth system has been designed with support for human as well as machine-performed steps in mind and to provide operators and managers with a clear view of the production status. Steps performed by RS or GIS technicians were modelled in the system just as automated steps are. Technicians were notified when a manual step needs to be performed. A single click opens the configured GIS or RS software package with the correct files and settings already configured. The workflow system monitors the software application and continues with the next step in the process when the technician's work is done (Böhme *et al,* 2014).

4.3.2 Pléiades monoscopic analysis

The Pléiades monoscopic image processing methodology was described in section 3.3.2 of this study. This temporal Pléiades dataset also enabled the classification of specific land cover class types. These classes were derived from a pixel based unsupervised classification technique. Each scene was classified into 19 classes according to their spectral reflectance values, see Table 4.6 and Figures 4.8 to 4.9. These classes were:

Class Code	Colour	Description
0		unknown/shadow
1		snow/ice
2		cloud
3		dark-bare-soil
4		bright-bare-soil
5		average-vegetation

6		bright-vegetation
7		dark-vegetation
8		yellow-vegetation
9		mix-vegetation/soil
10		asphalt/dark-sand
11		bright-sand/bare-soil/cloud
12		sand/bare-soil/cloud
13		dry-vegetation/soil
14		sparse-vegetation/soil
15		clear-water
16		turbid-water
17		clear-water-over-sand
18		other

Table 4.6: Land cover classes derived from the FarEarth system

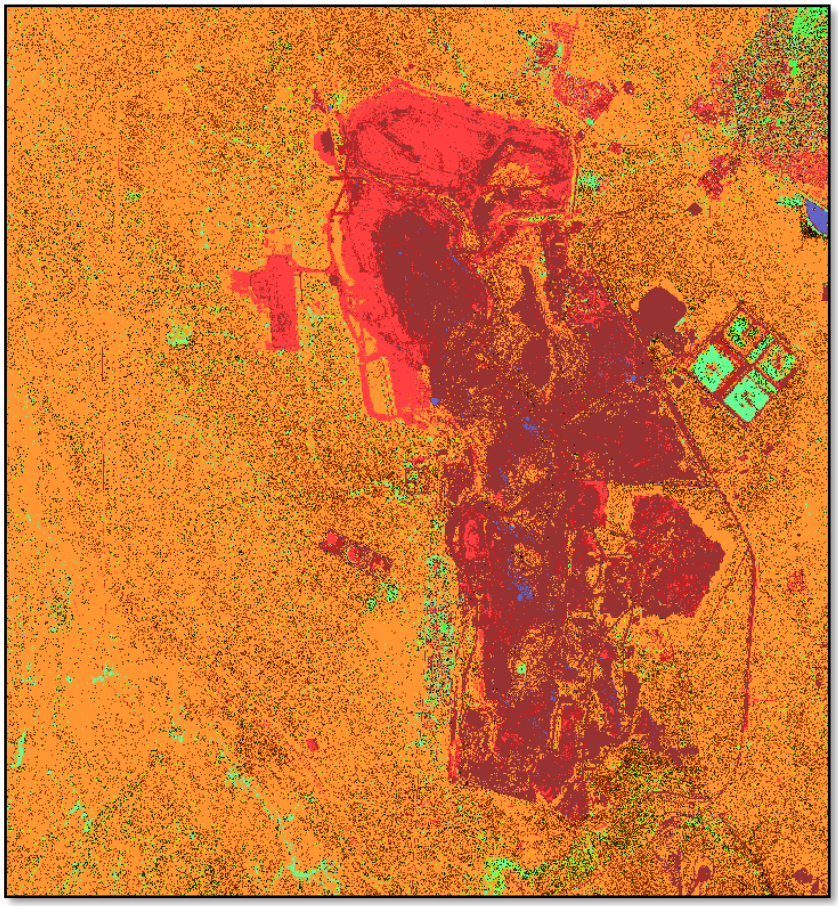

Figure 4.8: Sishen Mine area land cover classification, derived from a Pléiades image dated 2016/03/30

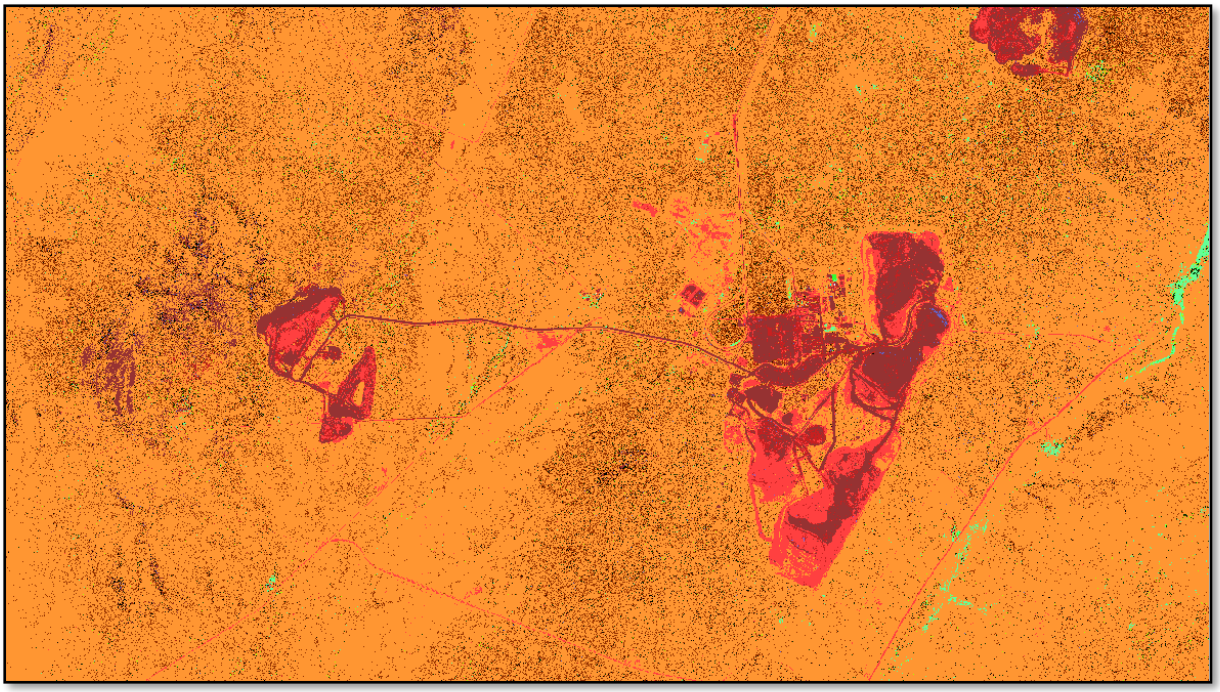

Figure 4.9: Kolomela Mine area land cover classification, derived from a Pléiades image dated 2016/03/30

These land cover classes were generated from the original 2m multispectral bands and 0.5m panchromatic band from Pléiades. A raster classification grid of 0.5m x 0.5m size pixels was produced as an end result. It was realised during this spectral classification process that the arid conditions over both mine areas generated difficulties to distinguish between bare soil, mining area, dry vegetation, dark sand, asphalt and some of the building structures.

The rationale was to reclassify the 19 classes into 6 primary classes to produce a super class representing the dominating class type, see Table 4.7 and Figures 4.10 to 4.11. The aim of this study from an environmental perspective was to determine, in this case, if the decrease in vegetation was due to the removal of it by human activity such as new mining areas, settlement growth or removal for fuelwood. If vegetation removal was detected, was it within the primary mining area or secondary, thus outside the perimeter of the mine? These concepts will be illustrated in the following paragraphs.

New Class Code	Combined Class	Colour	Description
0	0; 18		Unknown/shadow/other
1	1;2		snow/ice/cloud
2	3;4,13,14		bare-soil
3	5;6;7;8;9		vegetation
4	10,11,12		asphalt/mine/built-up
5	15,16,17		waterbodies

Table 4.7: Newly grouped land cover classes, 6 prime classes

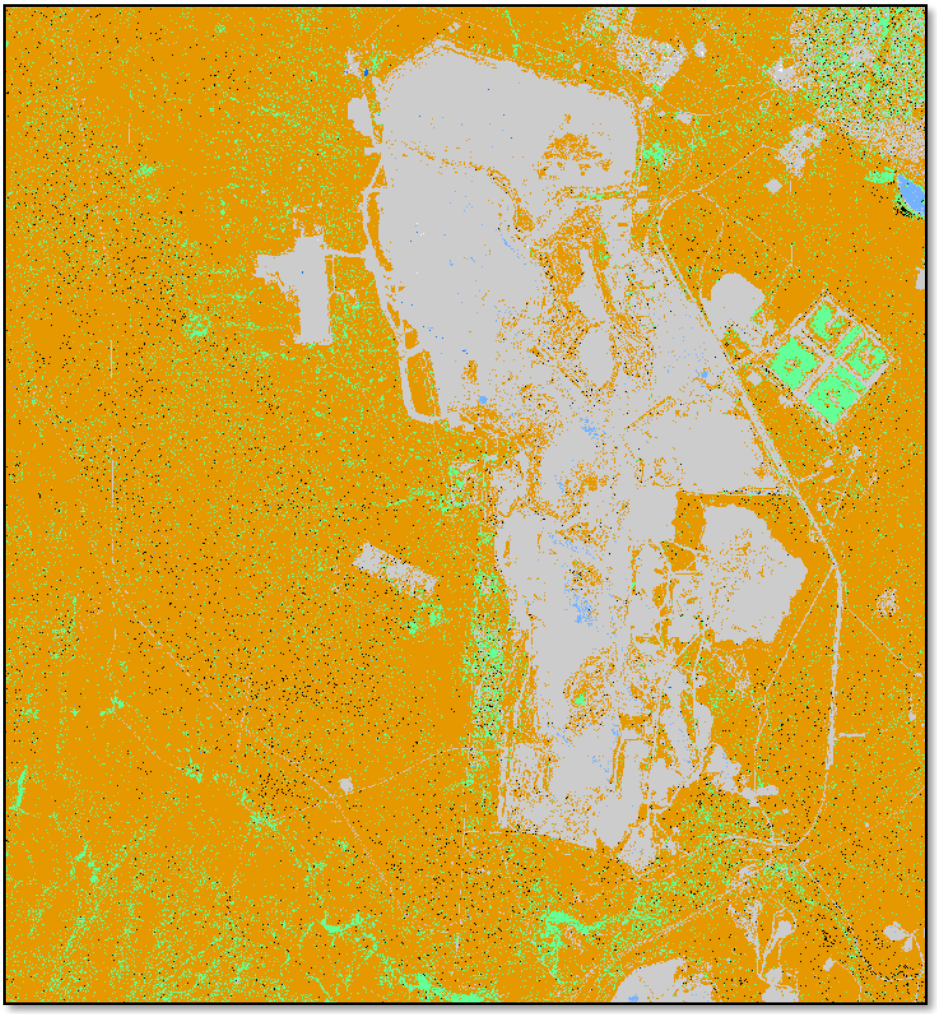

Figure 4.10: Sishen Mine area with new combined land cover classification codes, derived from a Pléiades image dated 2016/03/30

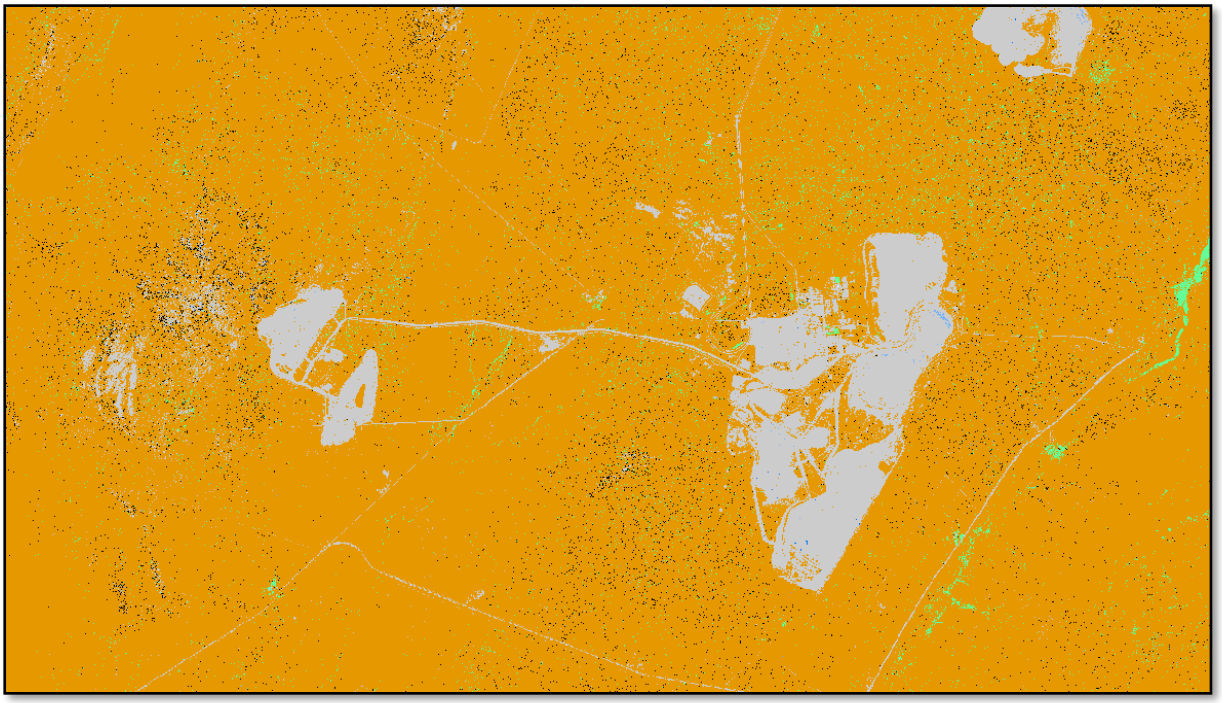

Figure 4.11: Kolomela Mine area with new combined land cover classification codes, derived from a Pléiades image dated 2016/03/30
Source:© Pinkmatter Solutions, 2014. All rights reserved.

4.3.2.1 Pléiades temporal dataset

The Pléiades imagery used during this monoscopic imagery time series analysis consisted of five images selected in terms of availability and to take seasonal changes into account. The scene date stamp over each mine was as follows, see Table 4.8:

	Scene 1	Scene 2	Scene 3	Scene 4	Scene 5
Sishen	10/05/2015	27/07/2015	19/10/2015	5/01/2016	30/03/2016
Kolomela	16/05/2015	19/10/2015	5/01/2016	30/03/2016	28/12/2016

Table 4.8: Pléiades temporal monoscopic imagery

The changes in the mining landscape over each mine are clearly visible during this period and can be illustrated in the figures below. The primary changes occurred mainly within the mining perimeter when compared to the rural landscape. As various changes are visible, two subsets over each mine will be used to zoom in on

specific changes that relate to environmental changes, followed by the land cover temporal changes analysis over these focus areas in the next paragraph.

4.3.2.2 Pléiades land cover classification

The Sishen and Kolomela mines are situated in a predominantly arid area, see Table 4.9. The typical vegetation in the rural areas is sparse low scrubland and during the dry season it matches the signature of the bare soil. The infrared band of Pléiades distinguishes soil and vegetation more accurately when moisture conditions exist. It enables the vegetation to produce more chlorophyll which is sensitive to the infrared and red spectral signatures. The Pléiades optical sensor does detect and classify water and vegetation spectral signatures accurately, especially as its bit dynamic depth per pixel is 12 bit values, thus 4 096 distinctive values. The latter was part of the decision to demonstrate the water and vegetation classification results in this study. The vegetation class calculated in m² over the Sishen mine area was displayed in Figure 4.12 and Graph 4.7 below. The relationship between the waterbodies class and vegetation was also visible in the graph below.

Winter 10/05/2015

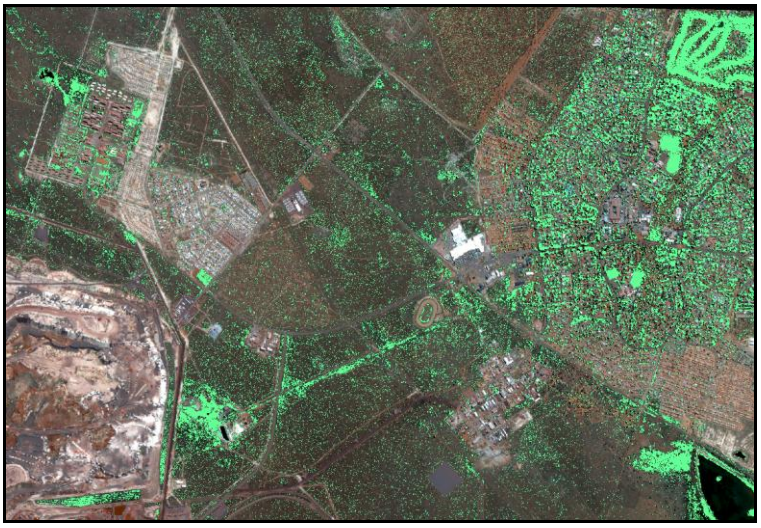
Summer 30/03/2016

Figure 4.12: Vegetation classification over Sishen mine area [bright green pixels], Pléiades image 10/05/2015 compared to 30/03/2016
Source: © CNES 2016, distribution rights Airbus DS, All rights reserved

Month	Temperature °C				Average Rainfall (mm)	
	Average		Absolute		Daily	Monthly
	max	min	max	min		
January	30.4	16.1	38.9	10.2	2.4	72
February	27.5	14.6	38.9	6.4	2.7	81
March	26.7	13	38	0.5	1.9	57
April	22.6	8.7	32	-1.4	1.4	42
May	19.5	4.4	30.4	-3	0.3	9
June	17	0.9	25	-10	0.3	9
July	17.1	0.6	29	-6	0	0
August	20.2	3.1	29.3	-3.6	0.3	9
September	22.8	6.8	33.5	-4	0.2	6
October	23.8	10	35	0.8	0.8	24
November	27.1	12.9	36	5.5	1.4	42
December	27.9	14.1	39.4	5.8	1.4	42

Table 4.9: Average temperature and rainfall from 2014 to 2016 over the Kathu district area.
Source: http://www.meoweather.com/

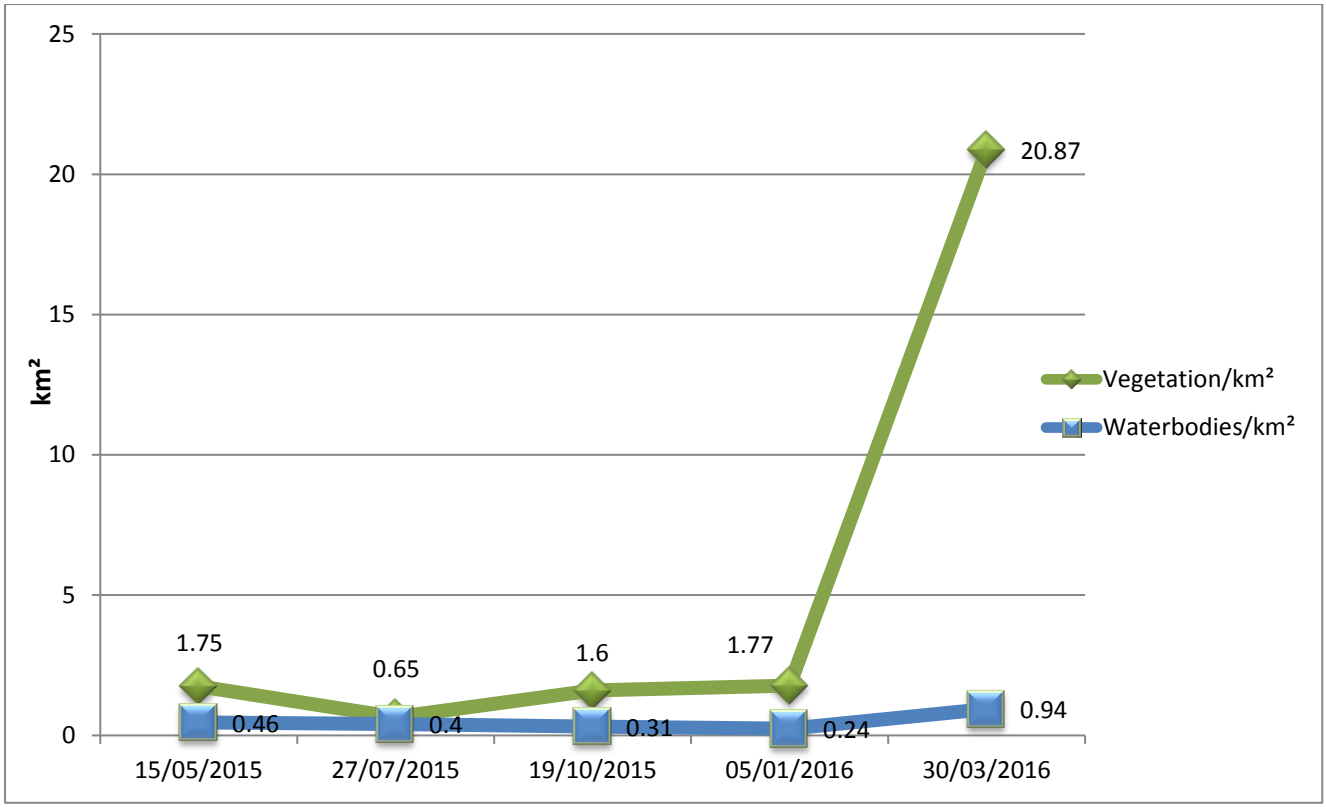

Graph 4.7: Vegetation and waterbodies class over Sishen mine as per Pléiades temporal dataset

According to the average rainfall data from 2014 to 2016 (see Table 4.9) peak rainfall was recorded from January to March. In Graph 4.7 the vegetation curve was low from 15/05/2015 until 05/01/2016. A significant increase between 05/01/2016 and 30/03/2016 was calculated, confirming the correlation between the rainfall data and vegetation growth. The increase in the vegetation class from January 2016 to March 2016 was clearly visible as well as the increase in waterbodies. The vegetation curve is fairly constant from May 2015 to January 2016. It is also well known that South Africa experienced extreme drought conditions during 2015. An interesting fact for the Sishen mine area is the dominance of vegetation within the residential areas of Kathu, the town close to the mine. The residents of Kathu planted various tree species over the years and established a good urban vegetation footprint within the area, compared to the natural rural vegetation consisting of sparse low scrubland. Figure 4.13 below provides an illustration of the urban vegetation compared to the natural rural vegetation.

30/03/2016 (Residential)

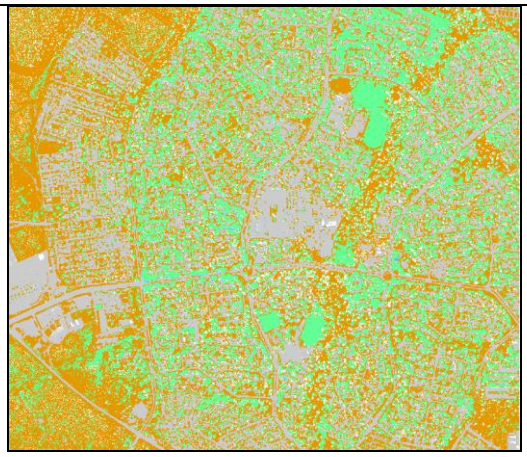

Vegetation (Green), Bare-soil (brown), Built-up (Grey)

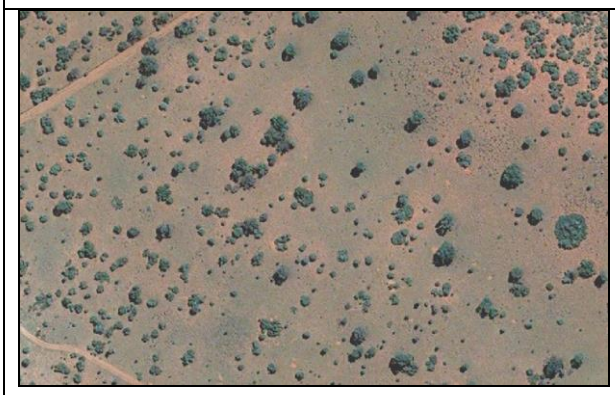

30/03/2016 (Rural)

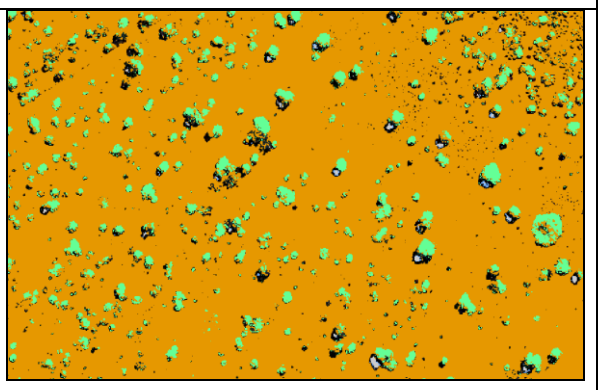

Vegetation (Green), Bare-soil (brown), black (shadow)

Figure 4.13: Comparing the vegetation landscape of rural and residential areas in the Kathu area near Sishen mine, Pléiades image 30/03/2016

The temporal change detection case studies that were addressed in section 4.3.2.1 formed the baseline data for this analysis, calculating the land cover classification results. These areas were within the primary mining area with the aim do demonstrate the classification methodology, the same method can be applied at any other area within the satellite image, thus also over secondary areas. The following change detection case studies were focussed on:

a) Sishen mine: New mining waste dump [A1] – Figure 4.14
b) Sishen mine: New power plant area [A2] - Figure 4.15
c) Kolomela mine: New mining waste dump [B1] - Figure 4.16
d) Kolomela mine: New parking area [B2] - Figure 4.17

4.3.2.2.1 Sishen mine: New mining waste dump [A1]

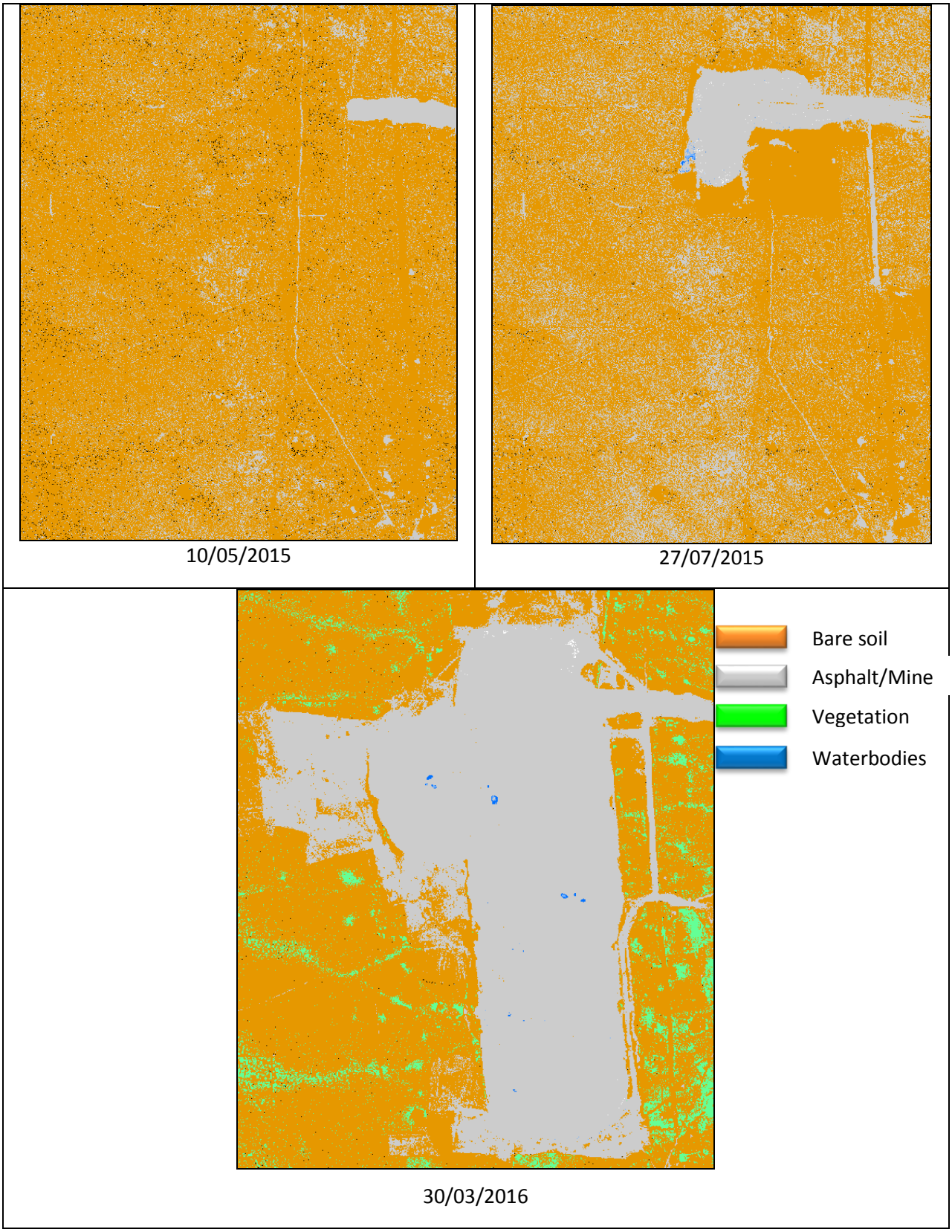

Figure 4.14: New waste dumping area within the Sishen mining area, bare soil (brown), vegetation (green), asphalt/mine (grey), waterbodies (blue)

Scene Date	Bare soil (m²)	Vegetation (m²)	Asphalt/mine (m²)	Waterbodies (m²)
10/05/2015	2 638 700	200	457 000	2 500
27/07/2015	2 190 900	0	928 700	3 500
30/03/2016	1 597 800	123 500	1 360 000	1 700
AVERAGE	2 142 400	41 200	915 200	2 600
STD DEV	426 300	58 200	368 800	700

Table 4.10: Temporal comparison of land cover class changes due to the new mining waste dump area in the Sishen mining area, expressed in m²

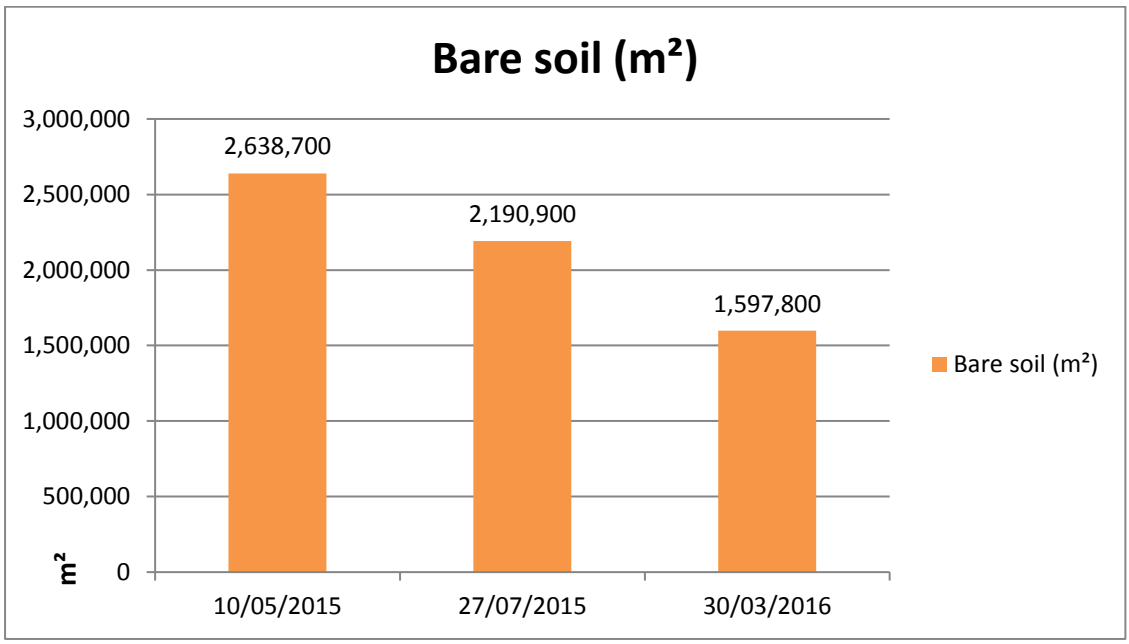

Graph 4.8: Bare soil changes per m² over the new mining waste dump area, Sishen mine

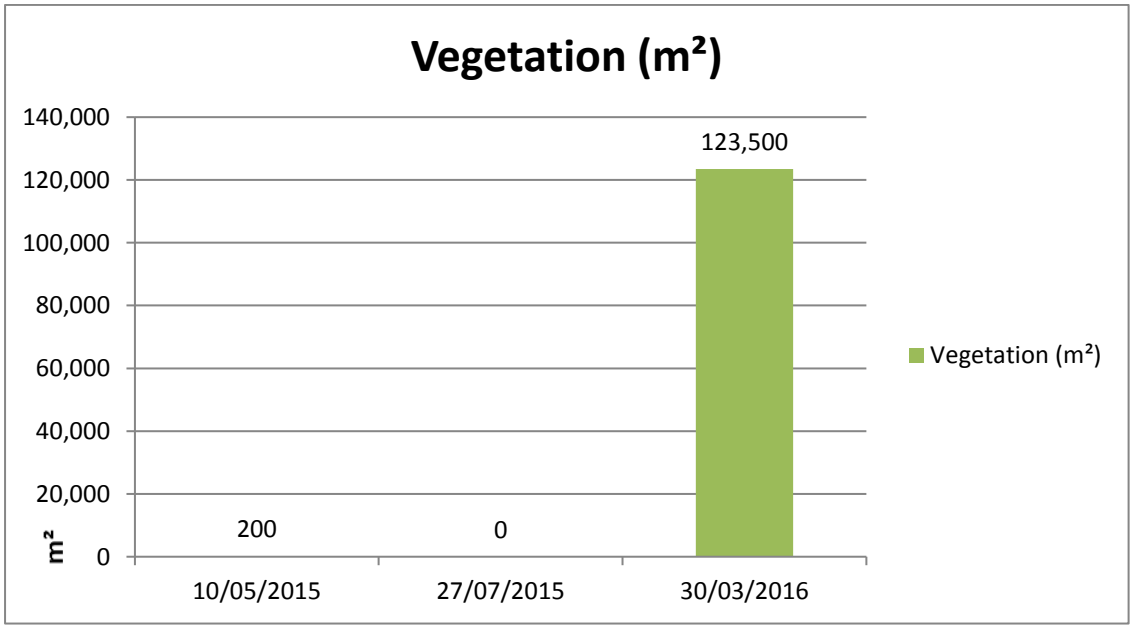

Graph 4.9: Vegetation changes per m² over the new mining waste dump area, Sishen mine

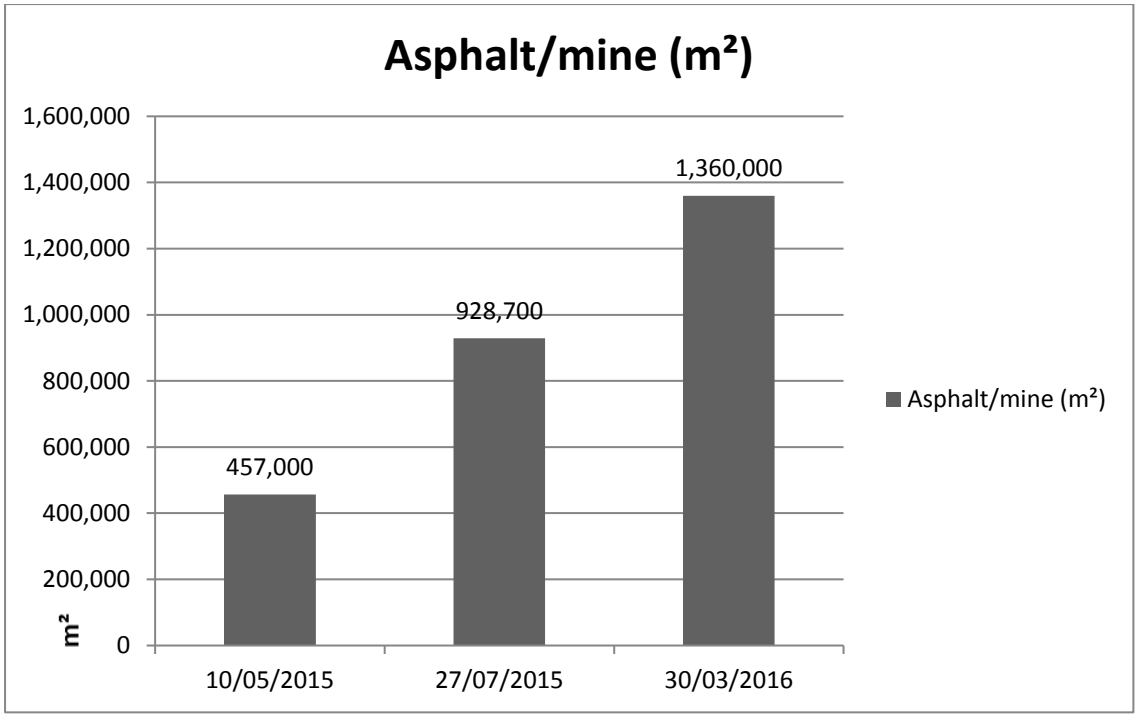

Graph 4.10: Asphalt (dark sand) or mine changes per m² over the new mining waste dump area, Sishen mine

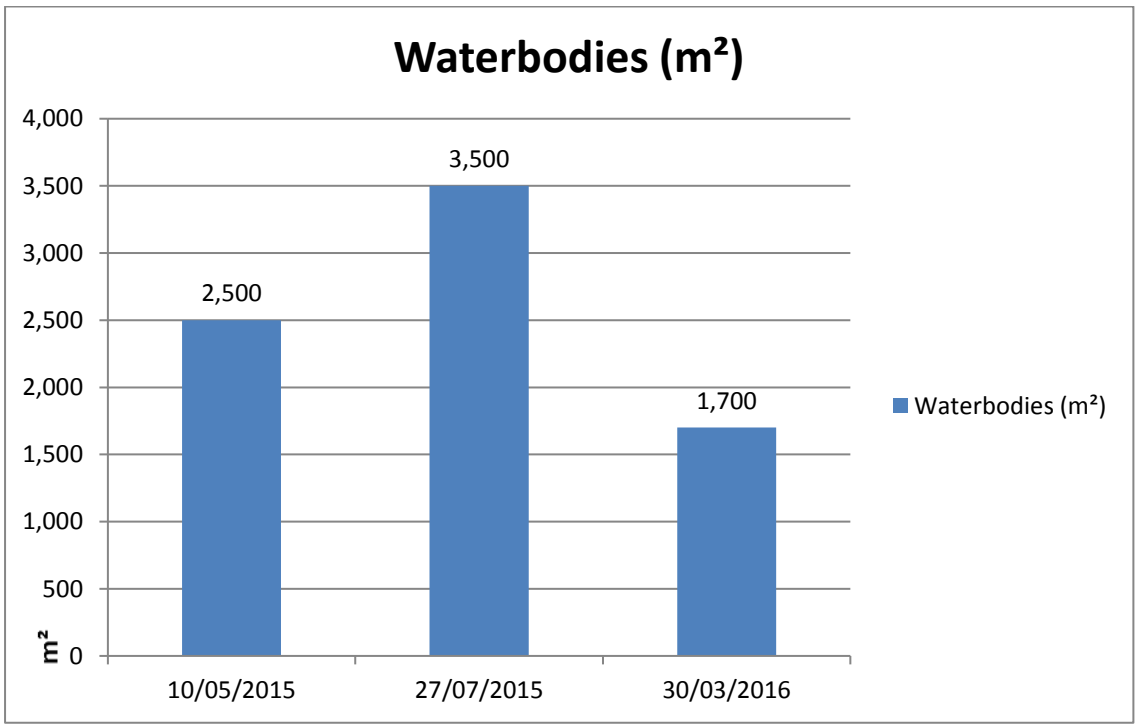

Graph 4.11: Waterbody changes per m² over the new mining waste dump area, Sishen mine

The new mining waste dump area [A1] within Sishen reveals that the bare soil dominates this area (scene 10/05/2015 and 27/07/2015) and increases to the asphalt (dark sand) or mine class (scene 30/03/2016), see Figure 4.14 and

Table 4.10. The bare soil difference between 10/05/2015 and 30/03/2016 was a decrease of -39.44%. The opposite is true of the increase in asphalt or mine class between 10/05/2015 and 30/03/2016, 197.60%, see Graphs 4.8 to 4.11. This was an example of natural changes due to primary mine activities within the mining permit area.

4.3.2.2.2 Sishen mine: New power plant area [A2]

10/05/2015

27/07/2015

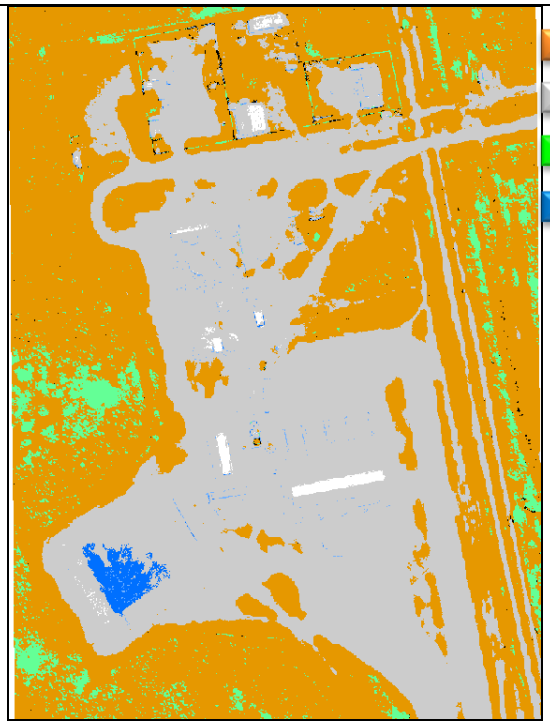

Figure 4.15: New power plant area within the Sishen mining area, bare soil (brown), vegetation (green), asphalt/mine (grey), waterbodies (blue)

Scene Date	Bare soil (m²)	Vegetation (m²)	Asphalt/mine (m²)	Waterbodies (m²)
10/05/2015	129 200	0	44 300	100
27/07/2015	97 400	0	75 200	500
30/03/2016	89 600	7 700	73 600	1 700
AVERAGE	105 400	2 600	64 400	800
STD DEV	17 200	3 600	14 200	700

Table 4.11: Temporal comparison of land cover class changes due to the new power plant area within the Sishen mining area, expressed in m²

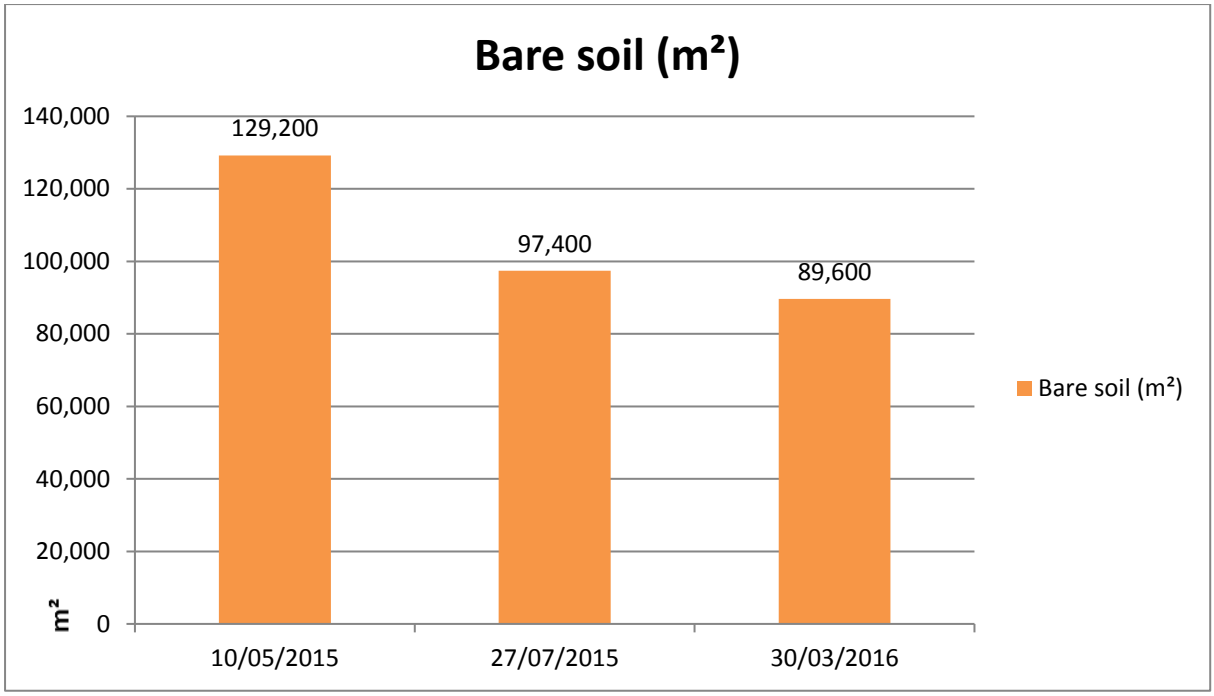

Graph 4.12: Bare soil changes per m² over the new power plant area, Sishen mine

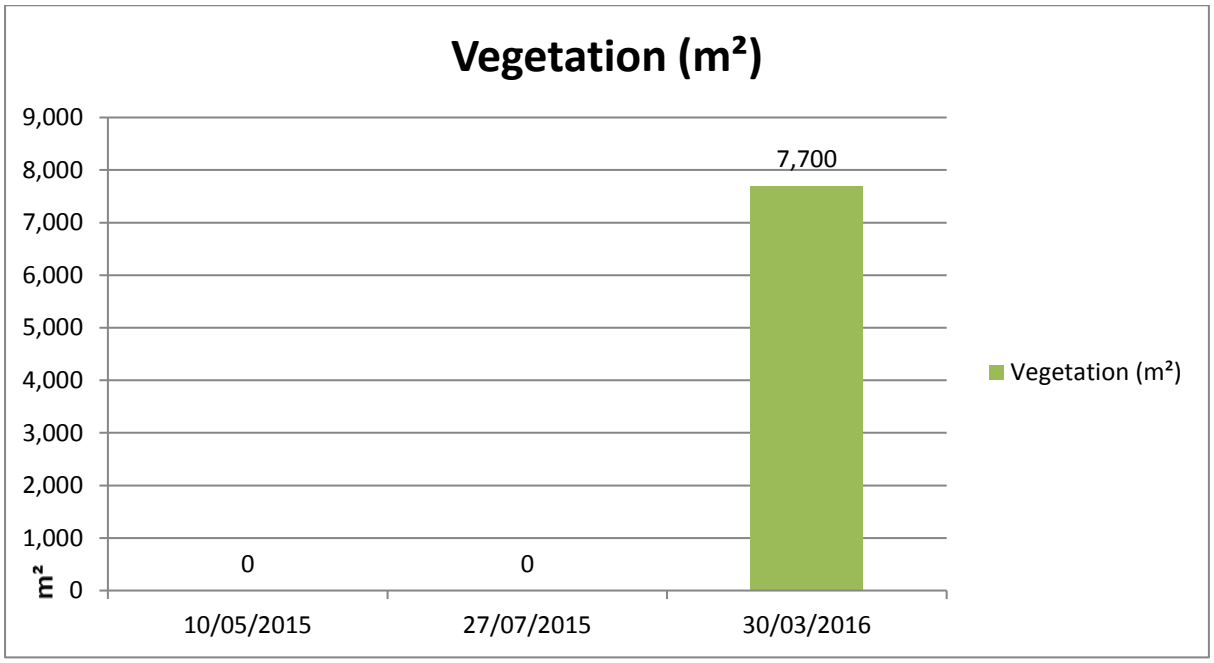

Graph 4.13: Vegetation changes per m² over the new power plant area, Sishen mine

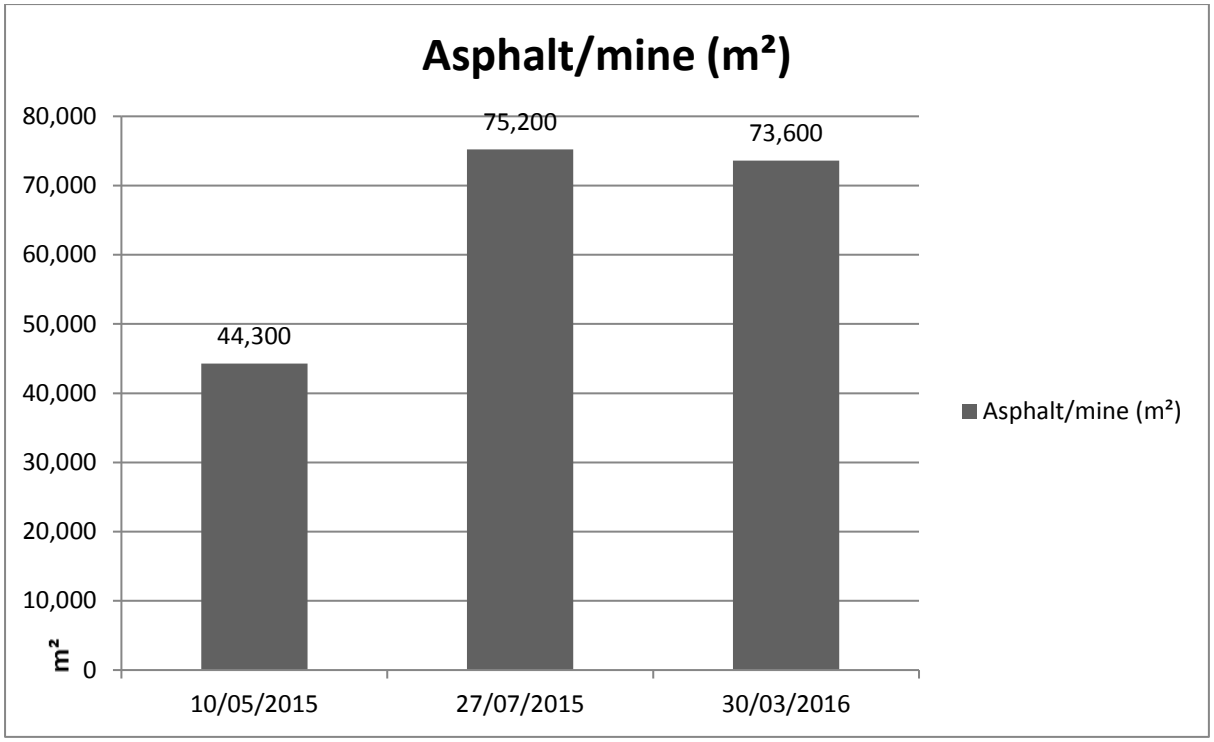

Graph 4.14: Asphalt (dark sand) changes per m² over the new power plant area, Sishen mine

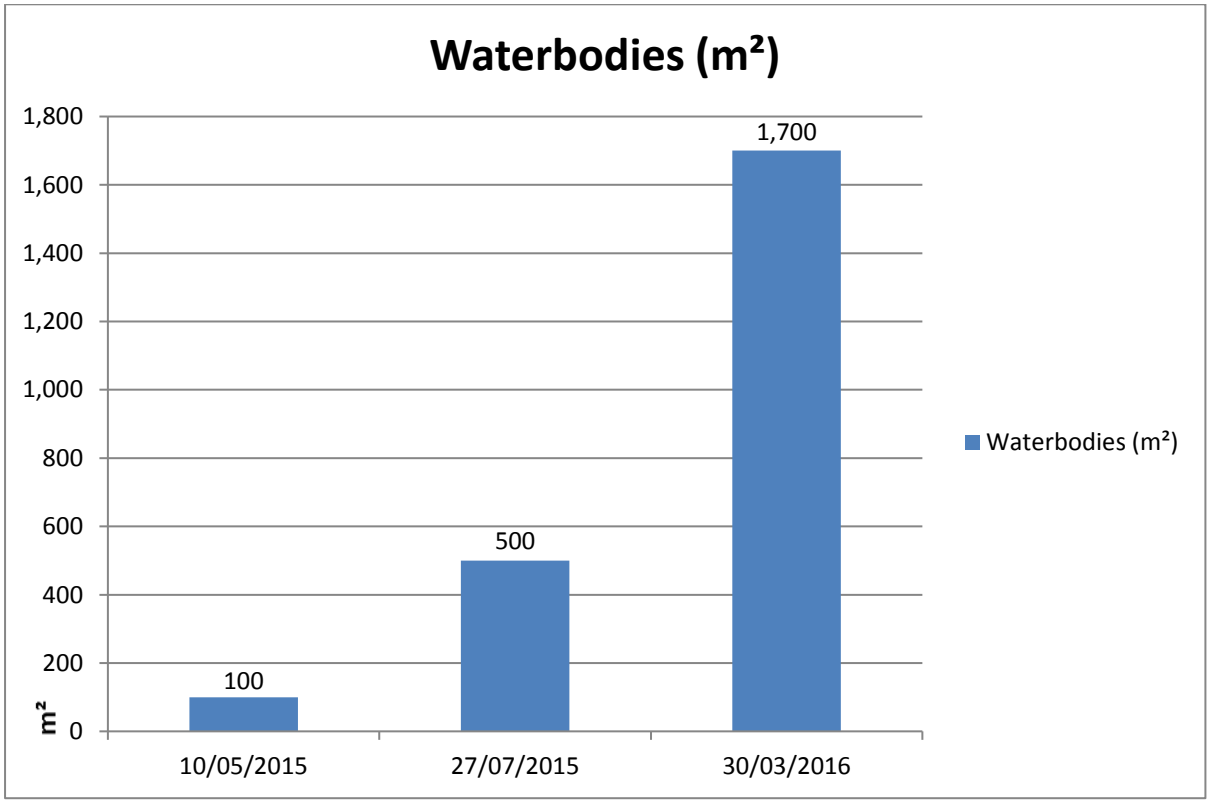

Graph 4.15: Waterbody changes per m² over the new power plant area, Sishen mine

The new power plant area [A2] primarily changed bare soil dominant values (scene 10/05/2015) to asphalt (dark sand) (scene 27/07/2015 and 30/03/2016), see Figure 4.15 and Table 4.11. The bare soil difference between 10/05/2015 and 27/07/2015 was a decrease of -24.64%. An increase in asphalt (dark sand) class between 10/05/2015 and 27/07/2015 was 69.66%. The difference in the asphalt class between 10/05/2015 and 30/03/2016 was an increase of 66.19%, see Graphs 4.12 to 4.15. This example highlights again the change from natural bare soil area to an asphalt class during the construction of a new power plant area.

4.3.2.2.3 Kolomela mine: New mining waste dump [B1]

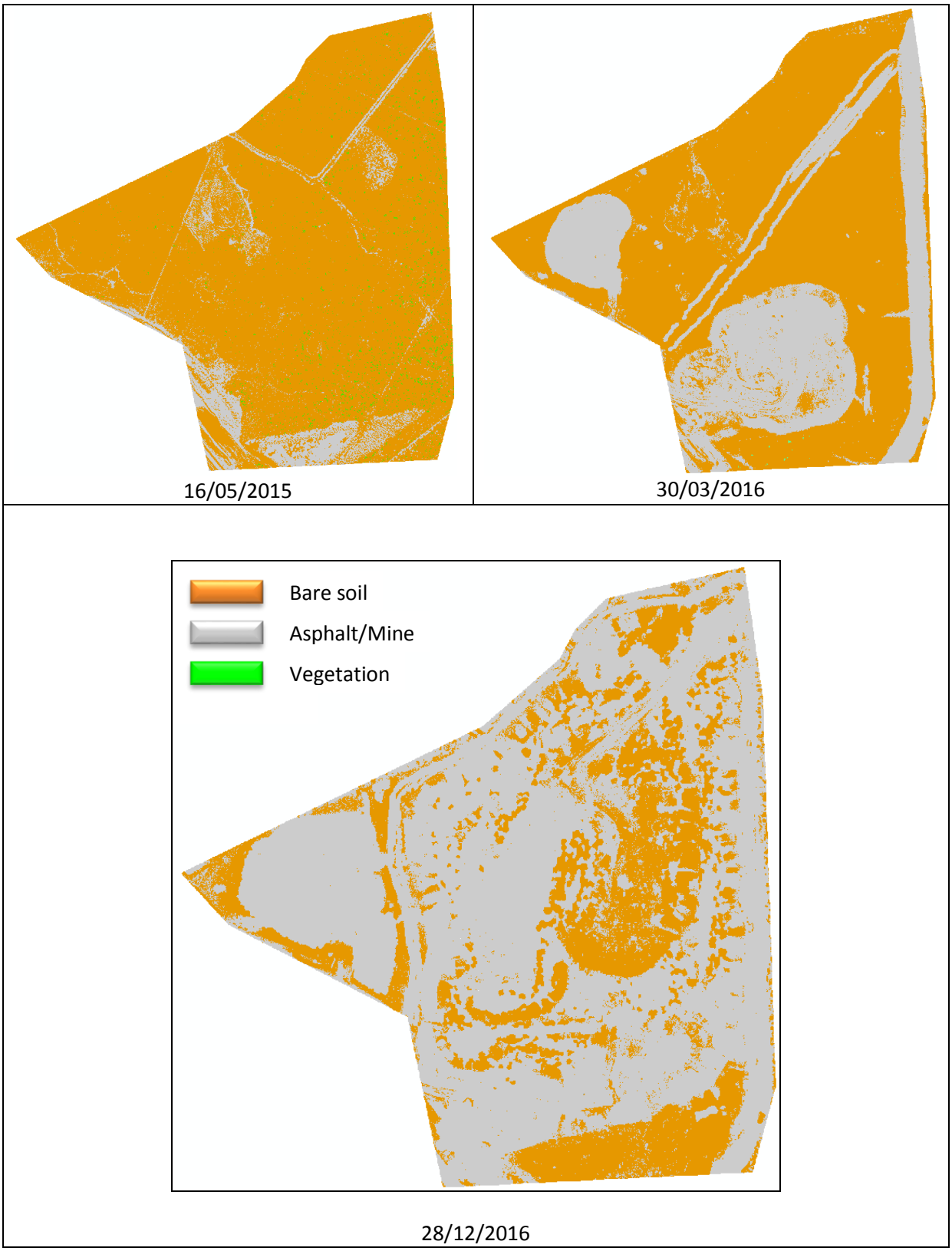

Figure 4.16: New mining waste dump at the Kolomela mining area, bare soil (brown), vegetation (green), asphalt/mine (grey)

Scene Date	Bare soil (m²)	Vegetation (m²)	Asphalt/mine (m²)
16/05/2015	585 300	4 400	64 100
30/03/2016	430 100	100	227 400
28/12/2016	197 100	0	461 700
AVERAGE	404 200	1 500	251 200
STD DEV	159 500	2 000	163 200

Table 4.12: Temporal comparison of land cover class changes due to the new mining dumping area within the Kolomela mining area, expressed in m²

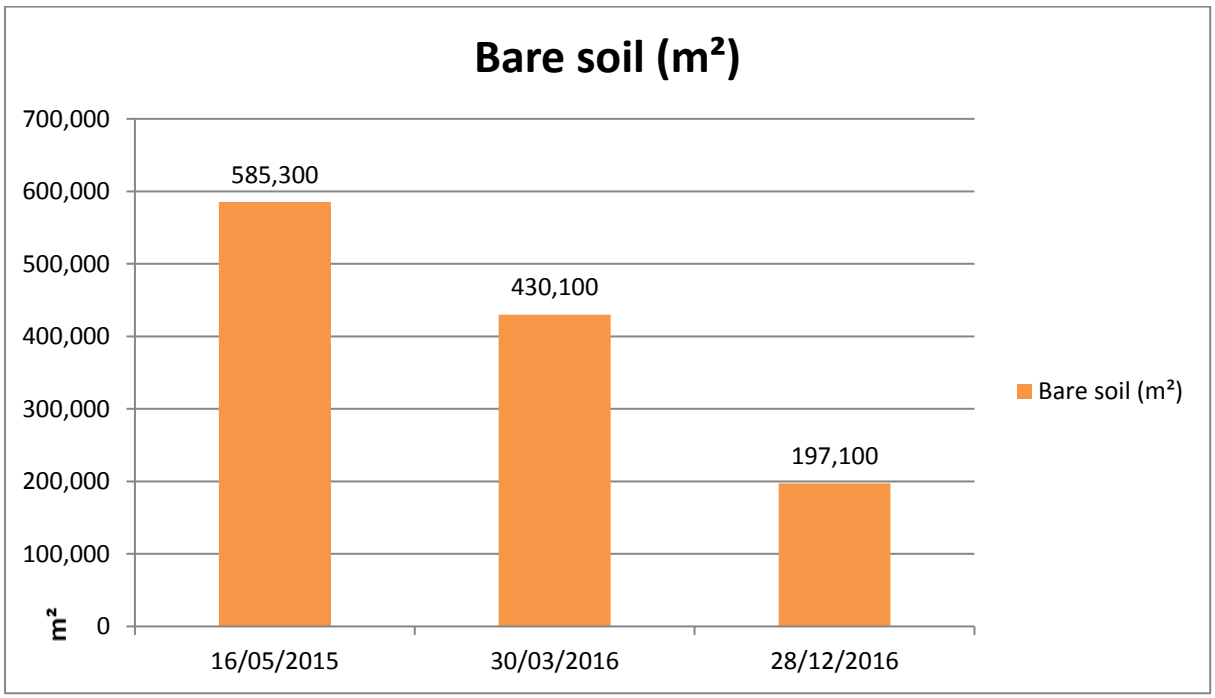

Graph 4.16: Bare soil changes per m² over the new mining dumping area, Kolomela mine

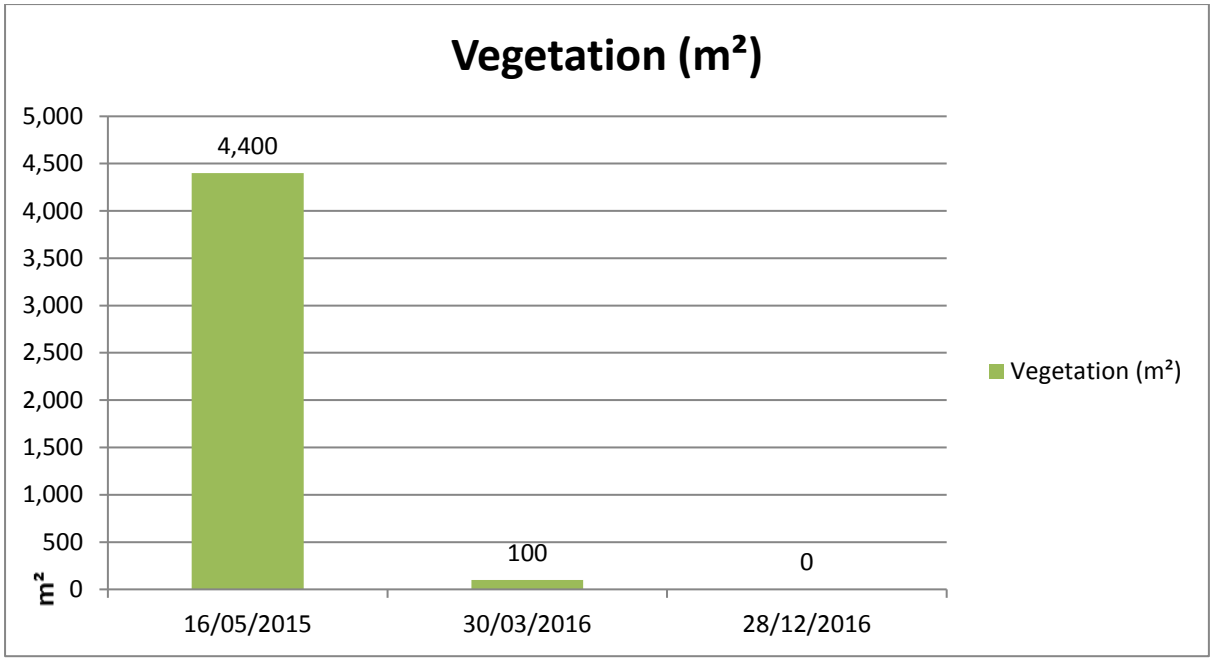

Graph 4.17: Vegetation changes per m² over the new mining dumping area, Kolomela mine

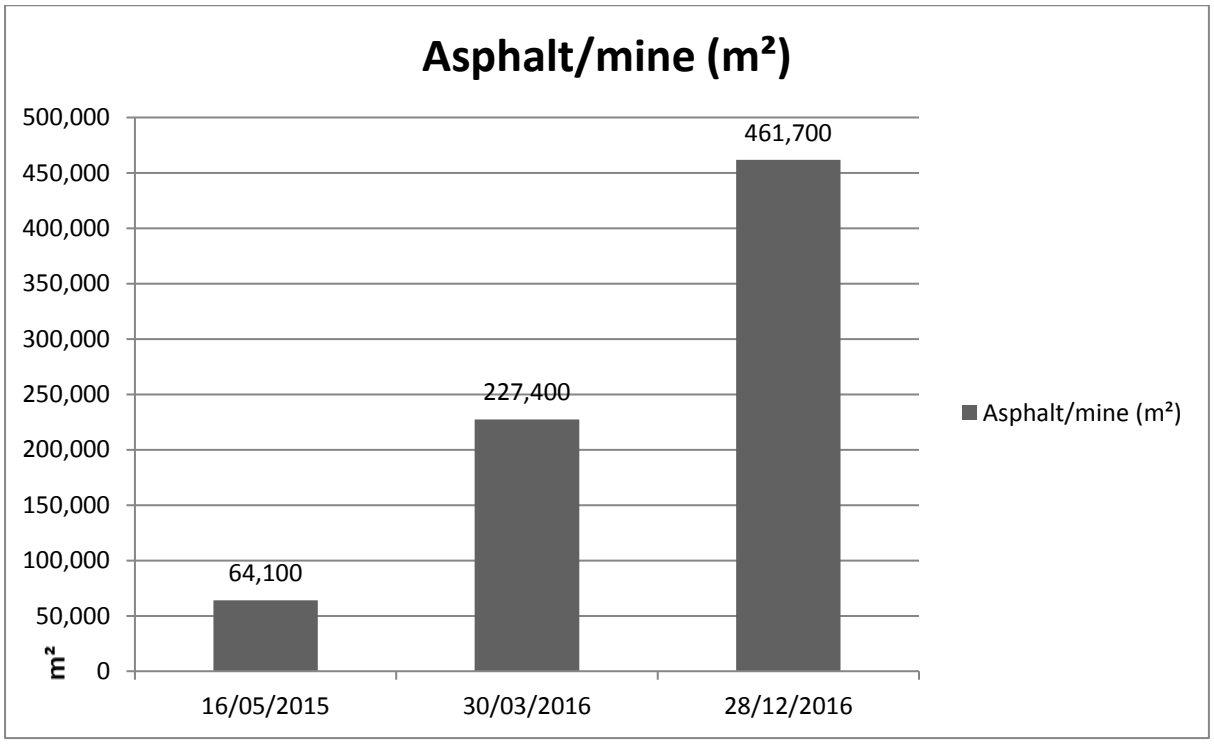

Graph 4.18: Asphalt (dark sand) changes per m² over the new mining dumping area, Kolomela mine

The new mining waste dump area [B1] within Kolomela mine was dominated by bare soil (scene 16/05/2015) and decreased against the asphalt (dark sand) or mine class (scene 30/03/2016 and 28/12/2016), see Figure 4.16 and Table 4.12. The bare soil difference between 16/05/2015 and 30/03/2016 was a decrease of -26.51%. A further difference exists between 16/05/2015 and 28/12/2016 and was calculated as

a decrease of -66.32%. The vegetation class resulted in very low numbers per m², thus rather the focus on the asphalt (dark sand) or mine class growth. The increase in asphalt or mine class against the bare soil class was clearly visible. The asphalt or mine class difference between 16/05/2015 and 30/03/2016 was 254.82%. This trend continuously grows as calculated between 16/05/2015 and 28/12/2016 - a 620.34% increase. The asphalt or mine class growth between 30/03/2016 and 28/12/2016 was 103%, thus confirming the continuous transformation of bare soil into the asphalt or mine class, see Graphs 4.16 to 4.18. This confirms the natural changes due to primary mine activities within the mining area.

4.3.2.2.4 Kolomela mine: New parking area [B2]

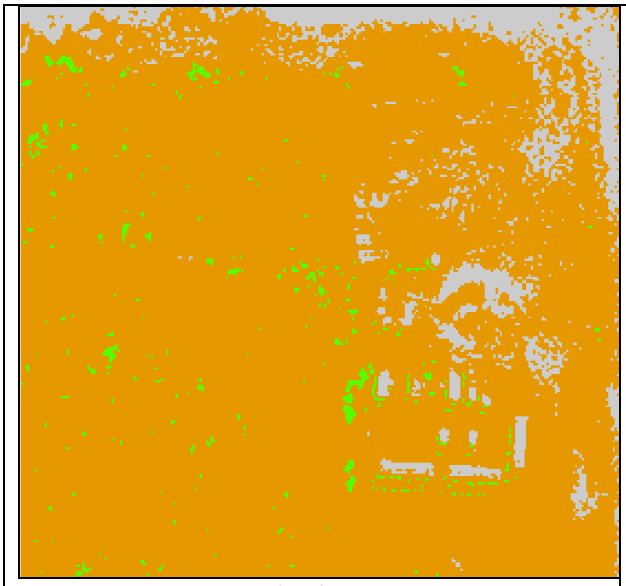

16/05/2015

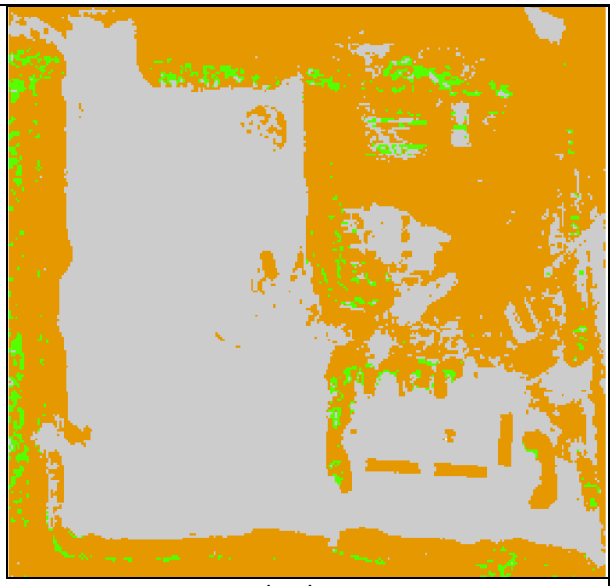

30/03/2016

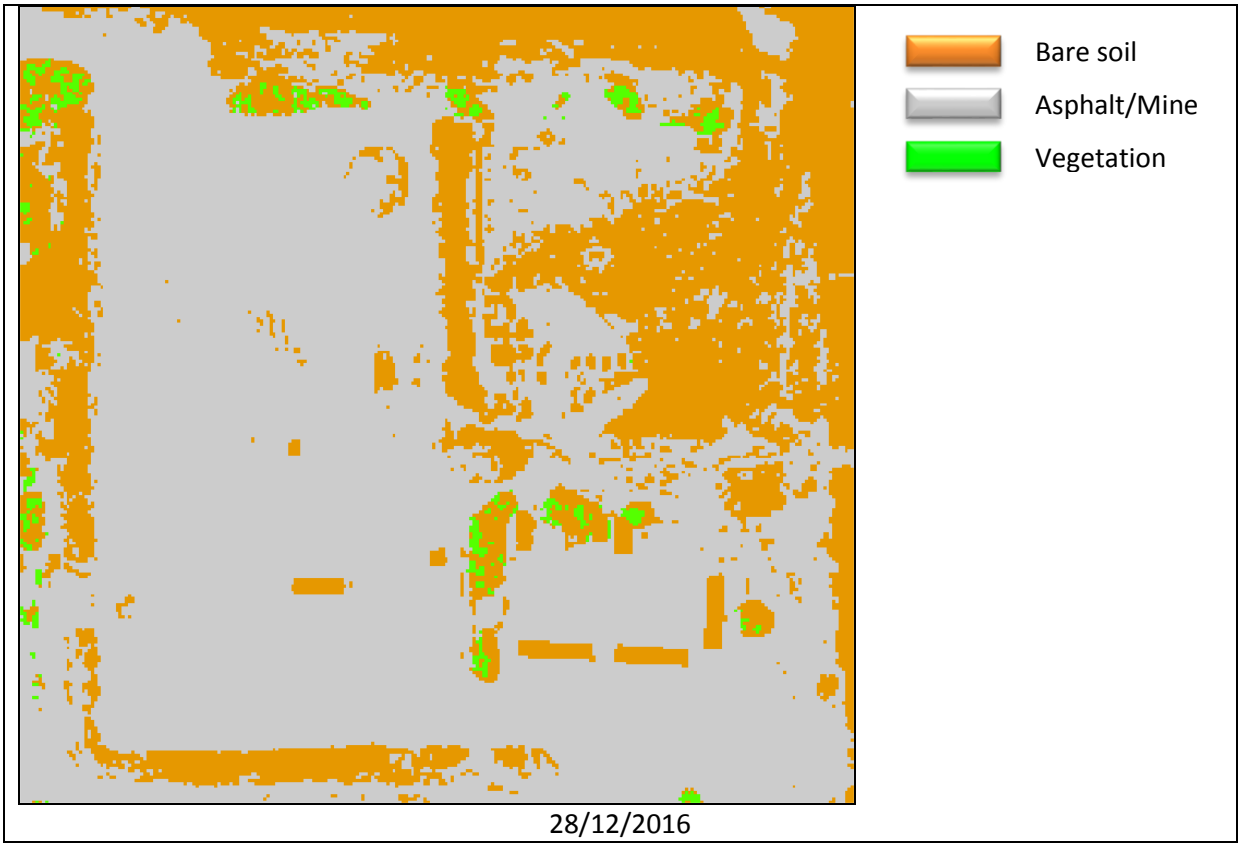

Figure 4.17: New parking area in the Kolomela mining area, bare soil (brown), vegetation (green), asphalt/mine (grey)

Scene Date	Bare soil (m²)	Vegetation (m²)	Asphalt/mine (m²)
16/05/2015	15 600	300	1 700
30/03/2016	8 300	400	8 800
28/12/2016	5 300	200	12 000
AVERAGE	9 800	300	7 500
STD DEV	4 300	100	4 300

Table 4.13: Temporal comparison of land cover class changes due to the new parking area within Kolomela mining area, expressed in m²

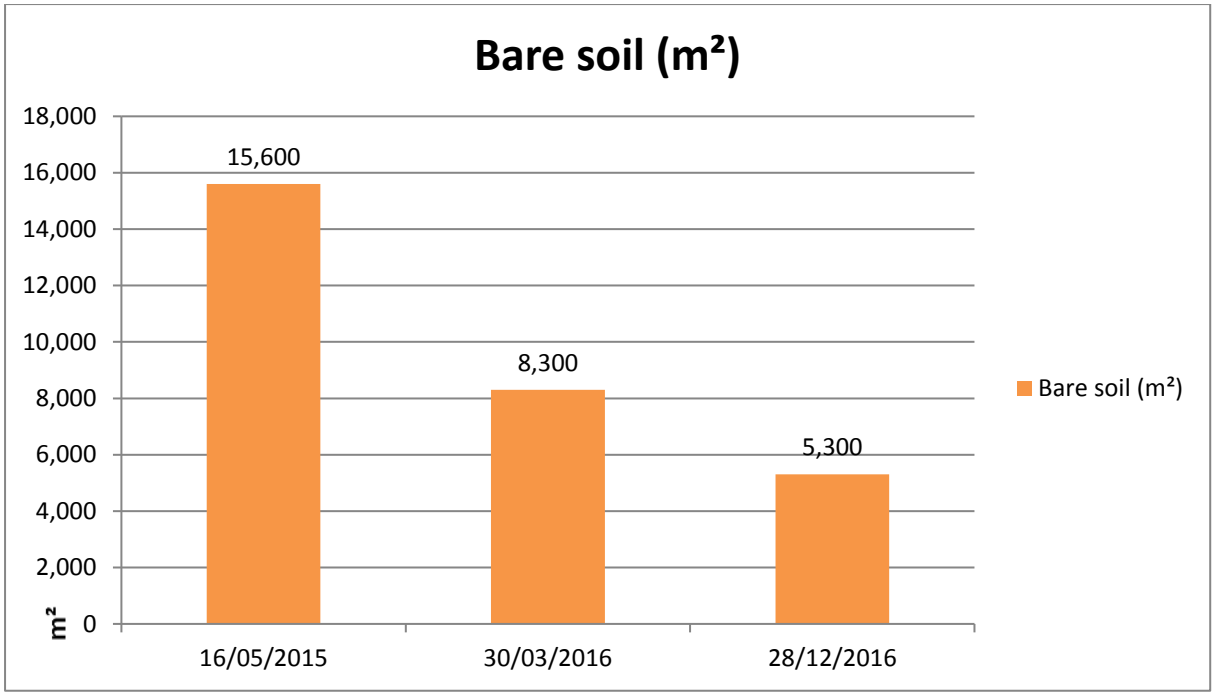

Graph 4.19: Bare soil changes per m² over the new parking area, Kolomela mine

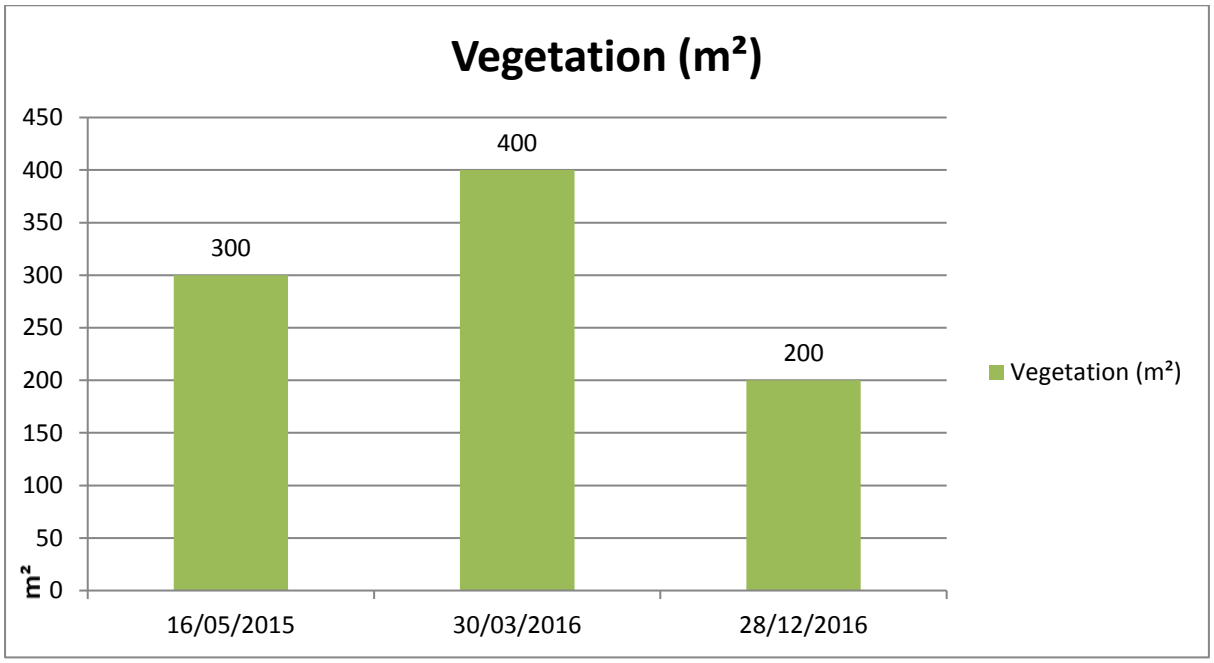

Graph 4.20: Vegetation changes per m² over the new parking area, Kolomela mine

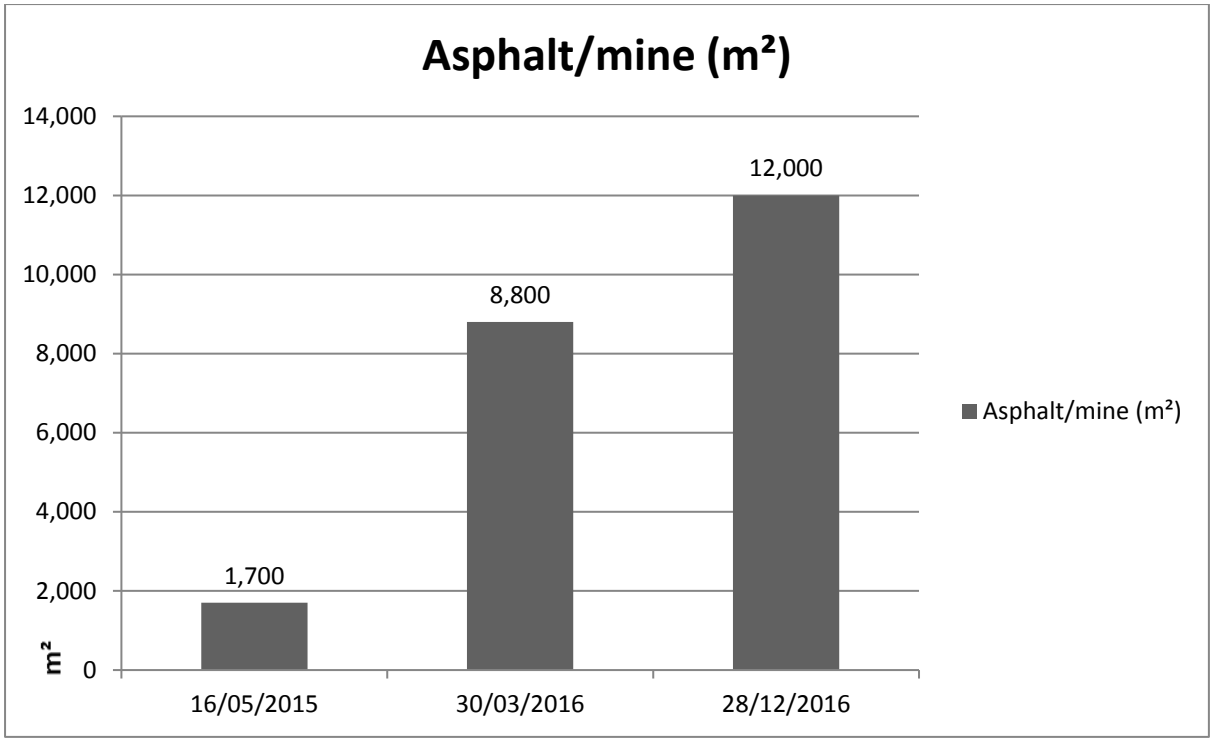

Graph 4.21: Asphalt (dark sand) or mine changes per m² over the new parking area, Kolomela mine

The new parking area [B2] at Kolomela mine was dominated by bare soil (scene 16/05/2015) and decreased against the asphalt (dark sand) or mine class (scene 30/03/2016 and 28/12/2016), see Figure 4.17 and Table 4.13. The bare soil difference between 16/05/2015 and 30/03/2016 was a decrease of -46.90%. A further difference existed between 16/05/2015 and 28/12/2016 and was calculated as a decrease of -65.85%. The calculations per m² for the vegetation class was again very low, thus rather the focus on the asphalt (dark sand) or mine class growth. The increase in asphalt or mine class against the bare soil class was evident. The asphalt or mine class difference between 16/05/2015 and 30/03/2016 was 431.58%. This trend continuously grows as calculated between 16/05/2015 and 28/12/2016, a 624.58% increase. The asphalt or mine class growth between 30/03/2016 and 28/12/2016 was 36.31%, thus confirming the continuous transformation of bare soil into the asphalt or mine class, see Graphs 4.19 to 4.21. In this case study the bare soil was removed to make space for a new parking area within the mining area, dominated by asphalt.

4.3.2.3 Rapid visualisation of mine operational activities

The aim of this paragraph is to highlight specific mine operational activities. These activities can be detected and identified by RS imagery. By employing high resolution satellite imagery, it provides mine managers with the opportunity to confirm the geolocation of specific mine operations as well as their progress, see Figures 4.18 to 4.21. The following extractions from the study areas confirmed the identification of specific mine operations during and after specific operations:

a) Drilling activities in preparation for blasting and excavation

10/05/2015 (drilling holes)

27/07/2015 (excavation and second stage blasting)

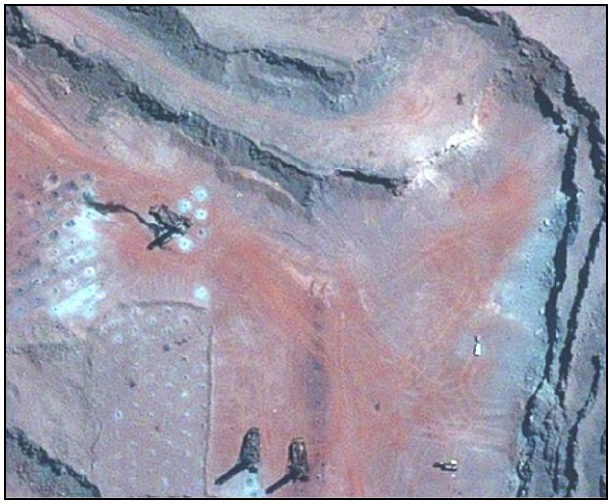

19/10/2015 (new drilling holes)

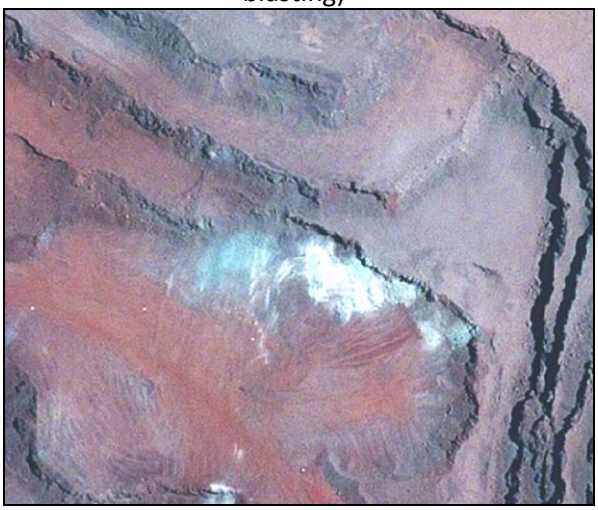

05/01/2016 (excavation complete)

30/03/2016 (Filling activities and new mine road established)
Figure 4.18: Mine operational activities over a specific area monitored from 10/05/2015 until 30/03/2016, Sishen mine
Source: © CNES 2016, distribution rights Airbus DS, All rights reserved

b) Mine equipment detection and identification

Shovel and loader equipment

Drilling equipment

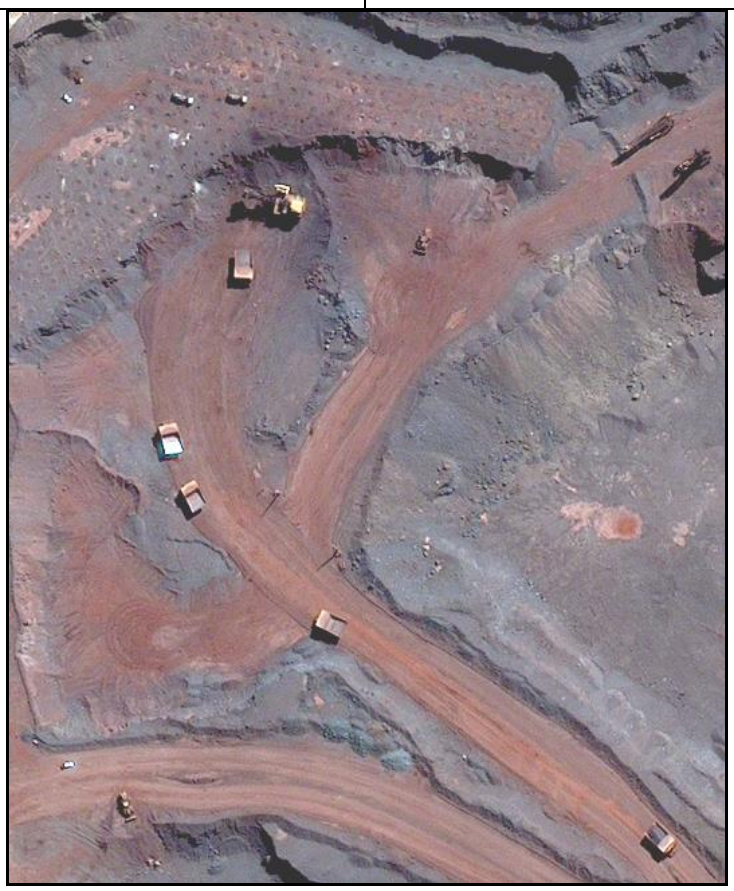

Soil loading and hauling activities, shovel and loaders visible

Figure 4.19: Detecting and identifying mine equipment

Source: © CNES 2016, distribution rights Airbus DS, All rights reserved

c) Iron ore dumping and shipment area

10/05/2015 (Iron ore dumping and shipment area)

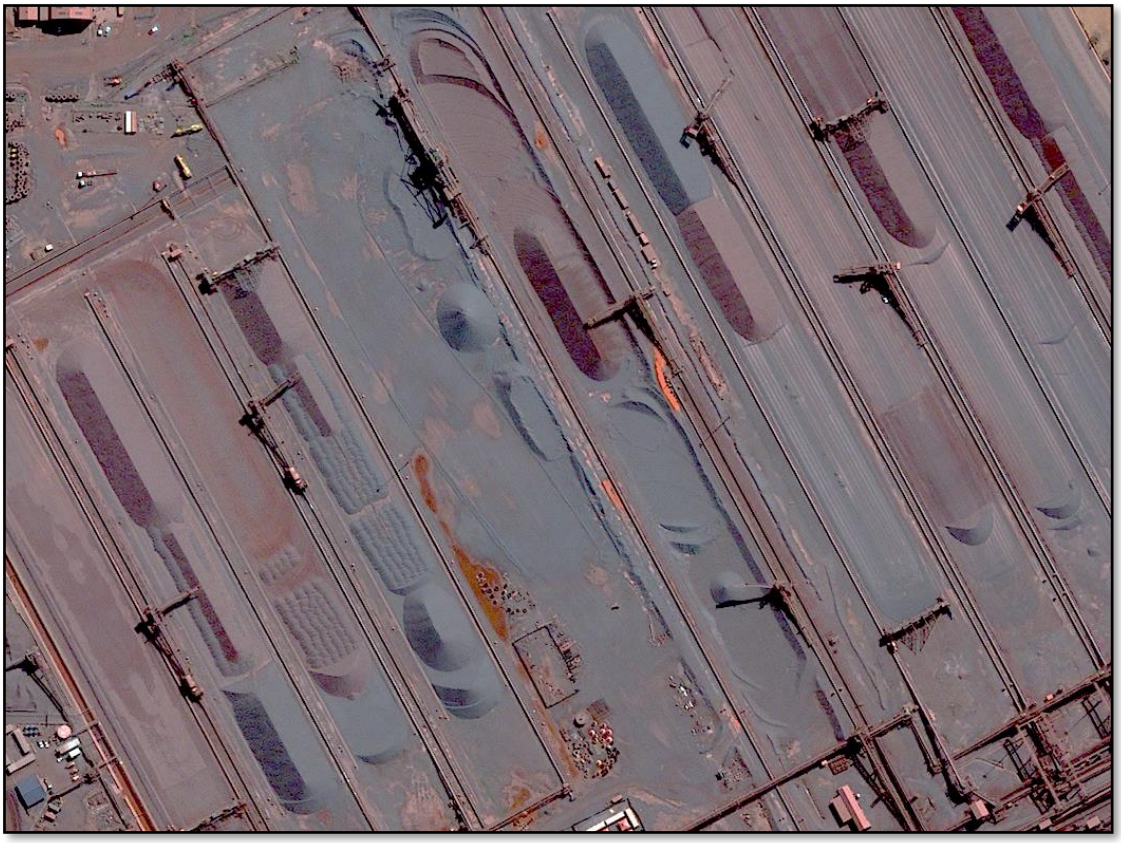

30/03/2016 (Iron ore dumping and shipment area)

Figure 4.20: Iron ore dumping and shipment area, Sishen mine

d) Waste dumping area

10/05/2015 (Waste dumping area, Sishen Mine)

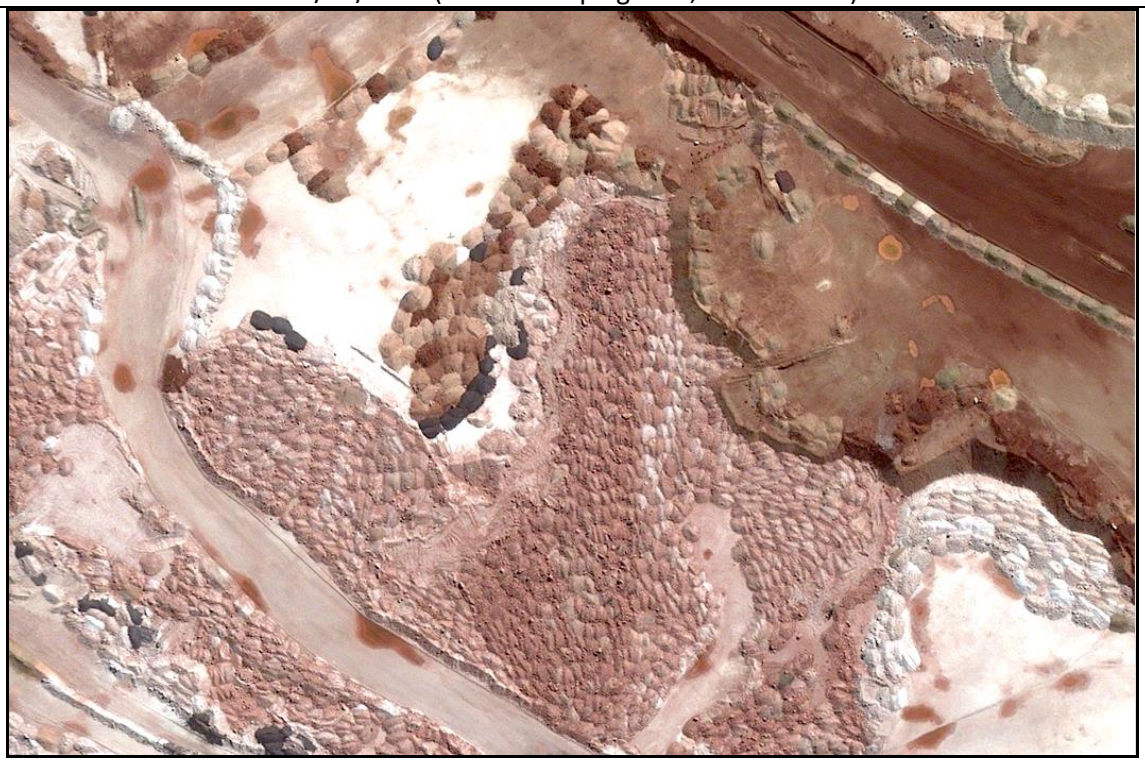

30/03/2016 (Waste dumping area, Sishen Mine)

Figure 4.21: Waste dumping area, Sishen mine

4.3.3 Pléiades stereoscopic analysis

In this section of the study the stereoscopic imagery of Pléiades over the Sishen and Kolomela mine applies. The stereoscopic imagery was used to generate one metre elevation models to enable volumetric calculations. The stereo pair data available during this study were the following:

- 2014/07/28 = Sishen mine
- 2016/01/25 = Sishen mine
- 2016/01/25 = Kolomela mine

The two stereo pairs available over Sishen mine were used to illustrate the use of the digital terrain model (DTM) to calculate height profiles and volumetric change between the temporal dataset, see Figure 4.22. In section 2.2.3 the open pit mine operations were discussed. The danger of stock piles and excavation slope areas are well-known in the mining industry and the measurement of the changes and stability of these areas is part of the rational to include this technical aspect within the overall methodology introduced in this study. As only a single stereo pair was available over Kolomela mine, it was used to illustrate its DTM as well as height profile measurement, see Figure 4.23. This last portion of this section will conclude with an illustration of change detection applications using the Normalised Difference Vegetation Index (NDVI) as an index for vegetation and a brightness-difference product to highlight regions of activity where the properties of the underlying area have changed. Lastly, elevation data between two timestamps over Sishen mine were used to subtract elevation values from each other to highlight the earth-surface changes over a specific selected area.

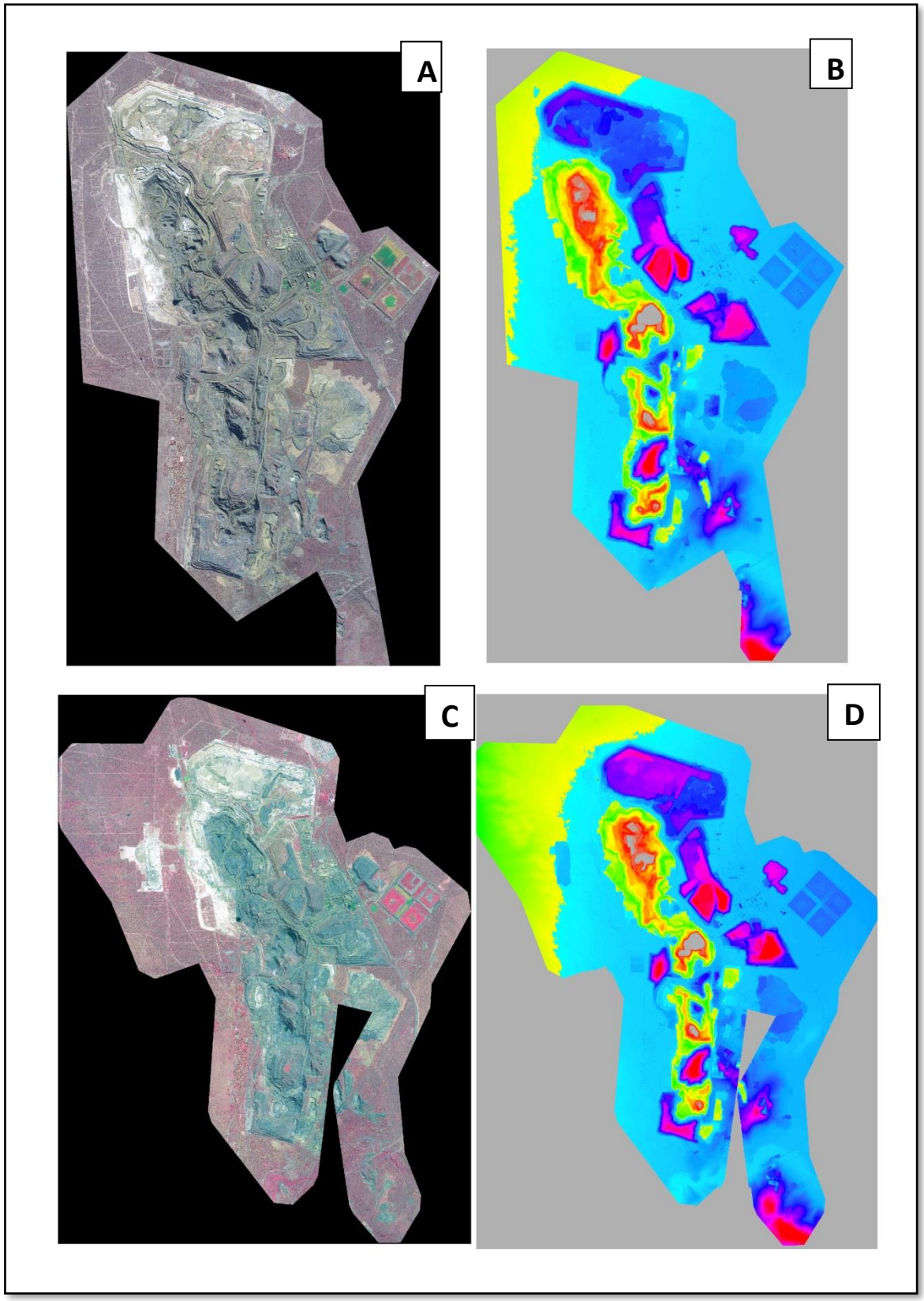

Figure 4.22: Sishen Mine (A) Pléiades image false colour (R G NIR), 2014-07-28 (B) Pléiades 1m DTM 2014-07-28 (C) Pléiades image false colour (R G NIR), 2016-01-25 (D) Pléiades 1m DTM 2016-01-25

Source: © CNES 2016, distribution rights Airbus DS, All rights reserved

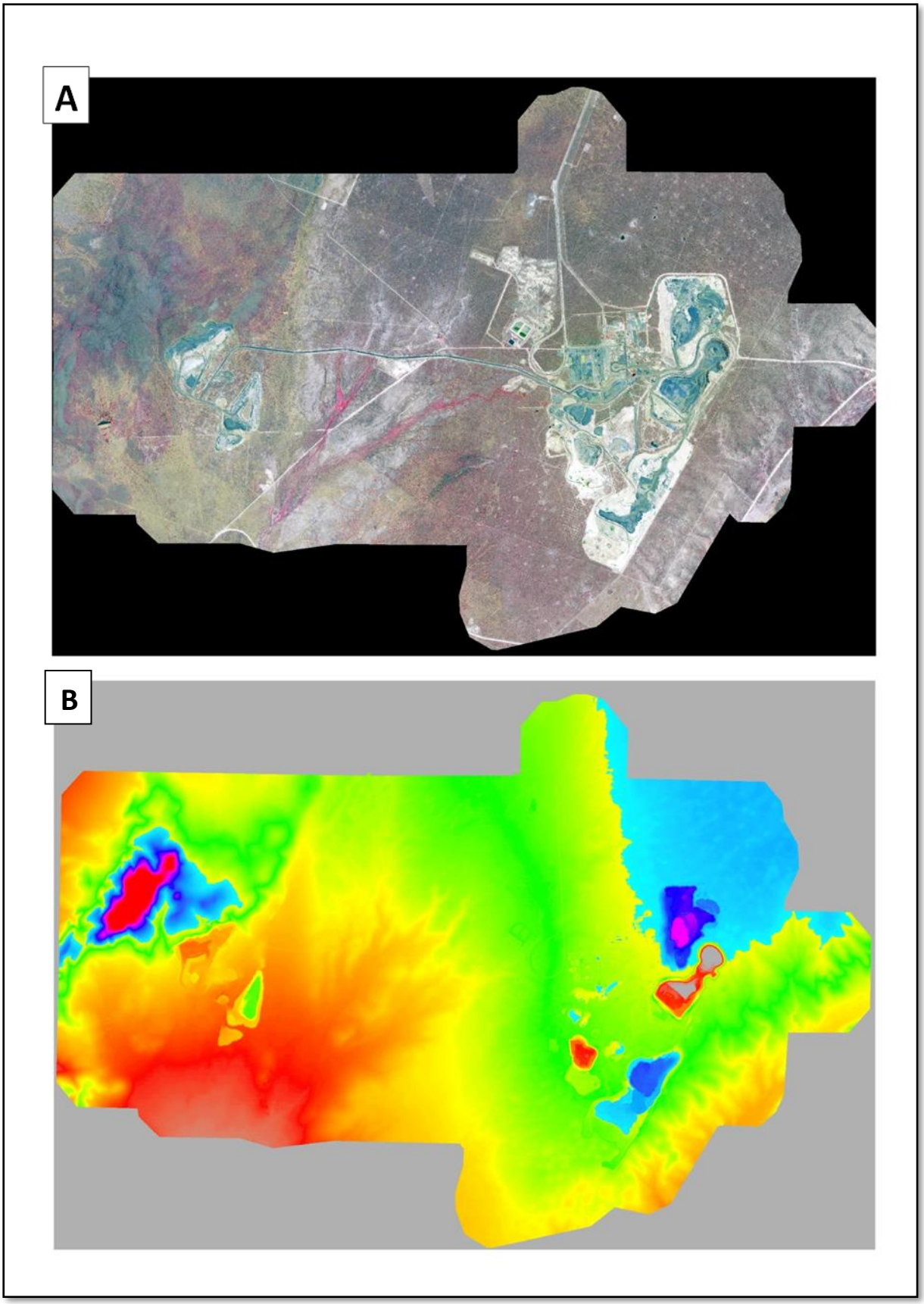

Figure 4.23: Kolomela Mine (A) Pléiades image false colour (R G NIR), 2016-01-25 (B) Pléiades 1m DTM 2016-01-25
Source: © CNES 2016, distribution rights Airbus DS, All rights reserved

4.3.3.1 Height profile measurement over selected large waste dump at the Sishen mine

A height profile over a first selected large waste dump at the Sishen mine is illustrated in Figure 4.24 below. The selected large waste dump area can be viewed in A1 [DTM 1m derived from the 2014/07/28 Pléiades stereo dataset] and B1 [DTM 1m derived from the 2016/01/25 Pléiades stereo dataset]. The selected height line can be viewed in A2 and B2, illustrated as a black line. It illustrates the side profile of the large waste dump and is just over 900m in length. The graph can be viewed in A3 and B3. The result clearly shows how the waste dump expanded in height and overall size between the two timestamps.

The measurement was done from a northern to a southern direction. The northern foot of the waste dump during 2014/07/28 [A3] showed that the first ± 100m at 1 210m height was fairly at flat surface level compared to the 2016/01/25 graph [B3] that indicated an immediate vertical climb of the height value at the 1 210m height point until 1 270m before it reached a first horizontal plateau, thus a 60m vertical rise within the first ±100m.

Noticeable is the difference in the size of the top plateau. The 2014/07/28 elevation model illustrates that the top plateau is around 300m to 500m at 1280m height [A3] compared to 2016/01/25 elevation model that illustrates the plateau between 200m to 600m at 1280m, almost 200m longer in horizontal length. This top plateau can be viewed in [A2 and B2], visible light white colour coded area in the centre of the waste dump.

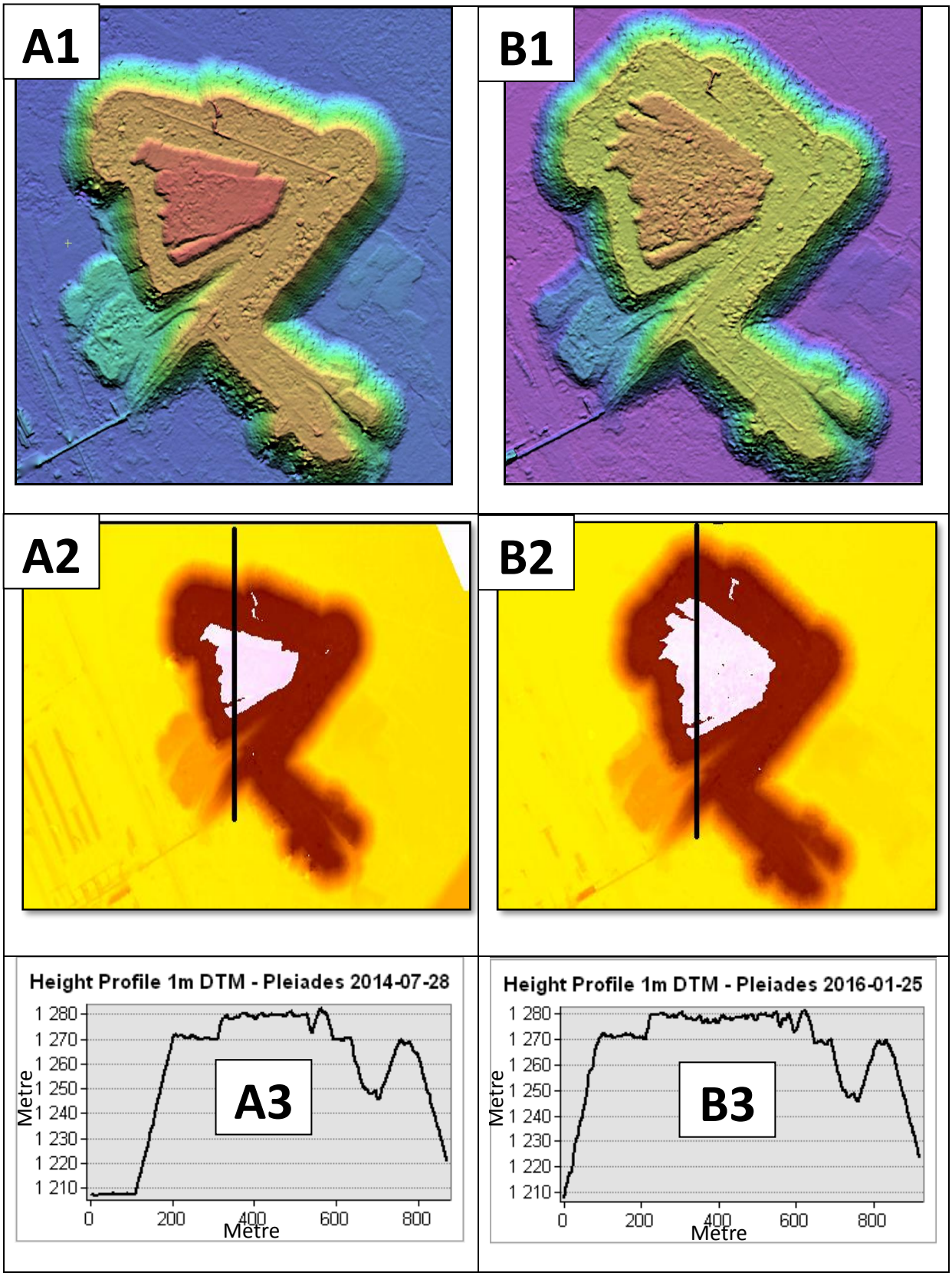

Figure 4.24: First height profile over a large heap at the Sishen mine, comparing 2014/07/28 [A1, A2,A3] with 2016/01/25 [B1,B2,B3]

A height profile over a second selected waste dump at the Sishen mine was illustrated in Figure 4.25 below. The selected area can be viewed in A1 [DTM 1m derived from the 2014/07/28 Pléiades stereo dataset] and B1 [DTM 1m derived from the 2016/01/25 Pléiades stereo dataset]. The selected height profile line can be viewed in A2 and B2, illustrated as a black line. This line generates a height graph to illustrate the height side profile of the area and is just over 1 200m in length. The graph can be viewed in A3 and B3. The result clearly shows how the waste dump shrunk at its north-western foot, yet the overall area became bulkier in size compared between the two timestamps. Thus, it seems that the waste soil at the foot of the area was extracted and dumped at a higher point..

The measurement was done from a north-western to a south-eastern direction. The north-western foot of the area during 2014/07/28 [A3] showed that the first ± 20m had a vertical climb from 1 200m to 1 220m, thus an immediate steep edge at the foot of the waste dump. Compared to the 2016/01/25 graph [B3], it indicates a levelled area for the first 80m, yet at a recessed height value of 1 180m. Thus, removal of soil took place between the two timestamps at the same starting measurement point of almost 20m.

Furthermore, the area also reached 1 260m in height within the first 200m [B3], compared to 1 250m within the first 200m of the 2014/07/28 dataset [A3]. Thus, the gradient of the area from 200m to 400m became steeper between the timestamps. The 2014/07/28 elevation model illustrates that a distance from the starting point to around 200m a height value of 1 250m was reached and at 400m a height value of 1 280m, thus a less steep slope. Comparing this to the 2016/01/25 elevation model a distance from the starting point to around 200m a height value of 1 260m was reached already and at 400m a height value of 1 280m was reached, thus a raised value of ±20m in height within 200m, indicating a much steeper slope and an increase in overall volume size.

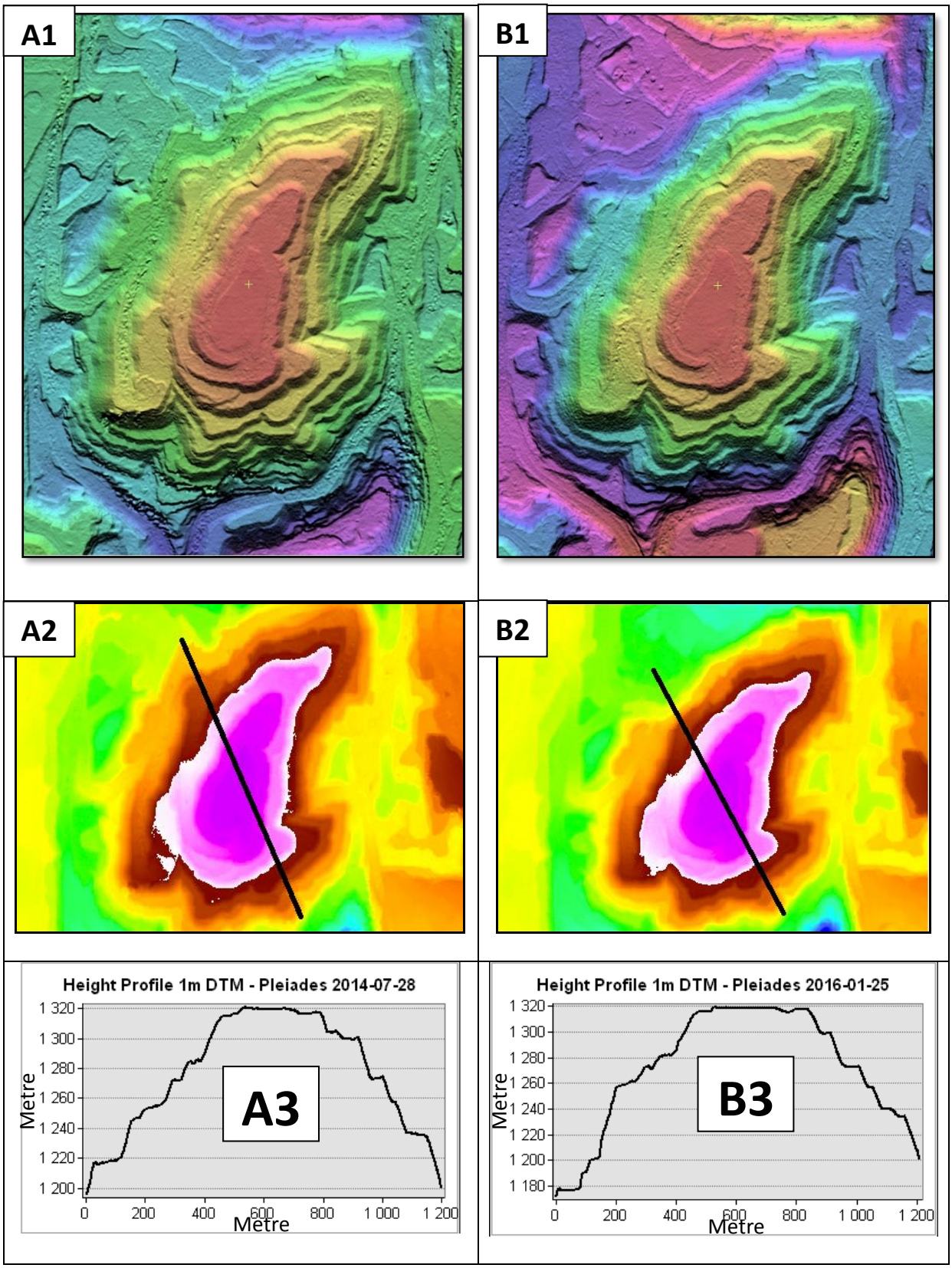

Figure 4.25: Second height profile over a large heap at the Sishen mine, comparing 2014/07/28 [A1, A2,A3] with 2016/01/25 [B1,B2,B3]

4.3.3.2 Volumetric calculations over Sishen mine

The volumetric differences were illustrated using two Pléiades DTM1 elevation datasets over the Sishen mine. The Pléiades stereo acquisitions occurred on 2014/07/28 (see Figure 4.26) and 2016/01/25 (see Figure 4.27) respectively. Four areas of varying topographic properties were selected over which the volume for each elevation dataset was calculated. The volume differences were then calculated for each area. The four selected topographical areas can be described as a flat area, medium waste dump, large waste dump and recessed area.

In order to compute the volume of an area the following must be known:

a) The elevation surface representing the heap, expressed in meters above a fixed known reference.
b) The size of the "pixels" in terms of surface area in which the elevation profile is expressed (ground sampling distance).
c) The zero-plane above which the volume is calculated, expressed in meters above the same known reference as in step (a) above.

Knowing the height of each pixel above the zero-plane, and the width and length of the pixel, the height for that particular pixel is simply its area multiplied by the height. The summation of this volume for all of the pixels in the area determined to form part of the heap gives the volume of the heap. This volume algorithm is expressed and described below.

$$VH = \Sigma[\Delta xij \times \Delta yij \times (Eij - Pij)]H$$

VH = Volume of heap
H, Δxij and Δyij = Size of pixel at coordinate $(i,)$
Eij = Elevation value at coordinate $(i,)$
Pij = Zero-plane value at coordinate $(i,)$

Equation 4.3: Volume algorithm
Source: Lück (2015)

Where VH is the volume of heap H, Δxij and Δyij are the size of the pixel at coordinate (i,j) forming part of the area in H in the x and y directions respectively, Eij is the elevation value at coordinate (i,j) and Pij the zero-plane value at coordinate (i,j).

In order to compare volume differences between elevation models, the zero-plane has to be chosen in such a way that it is identical to both the elevation models being compared. To calculate the volume of a heap, a reference plane is selected and the volume calculated as a positive value above the plane. Two methods for selecting the reference plane were used:

a) Create a horizontal plane starting at the lowest point of the area in question for heaps, or the highest point of the area for recesses.
b) Create a plane by interpolating the elevation of the outer-rim of the area in question.

Figure 4.26: Pléiades 1m DTM 2014-07-28 over Sishen Mine
Source: © CNES 2016, distribution rights Airbus DS, All rights reserved

Figure 4.27: Pléiades 1m DTM 2016-01-25 over Sishen Mine
Source: © CNES 2016, distribution rights Airbus DS, All rights reserved

4.3.3.2.1 Selected areas

For the study of volume differences, four areas have been selected: a flat area, a recessed area and two waste dump areas of different sizes. The location of these areas on the mine and a close-up view of these four study areas can be viewed in Figure 4.28 below.

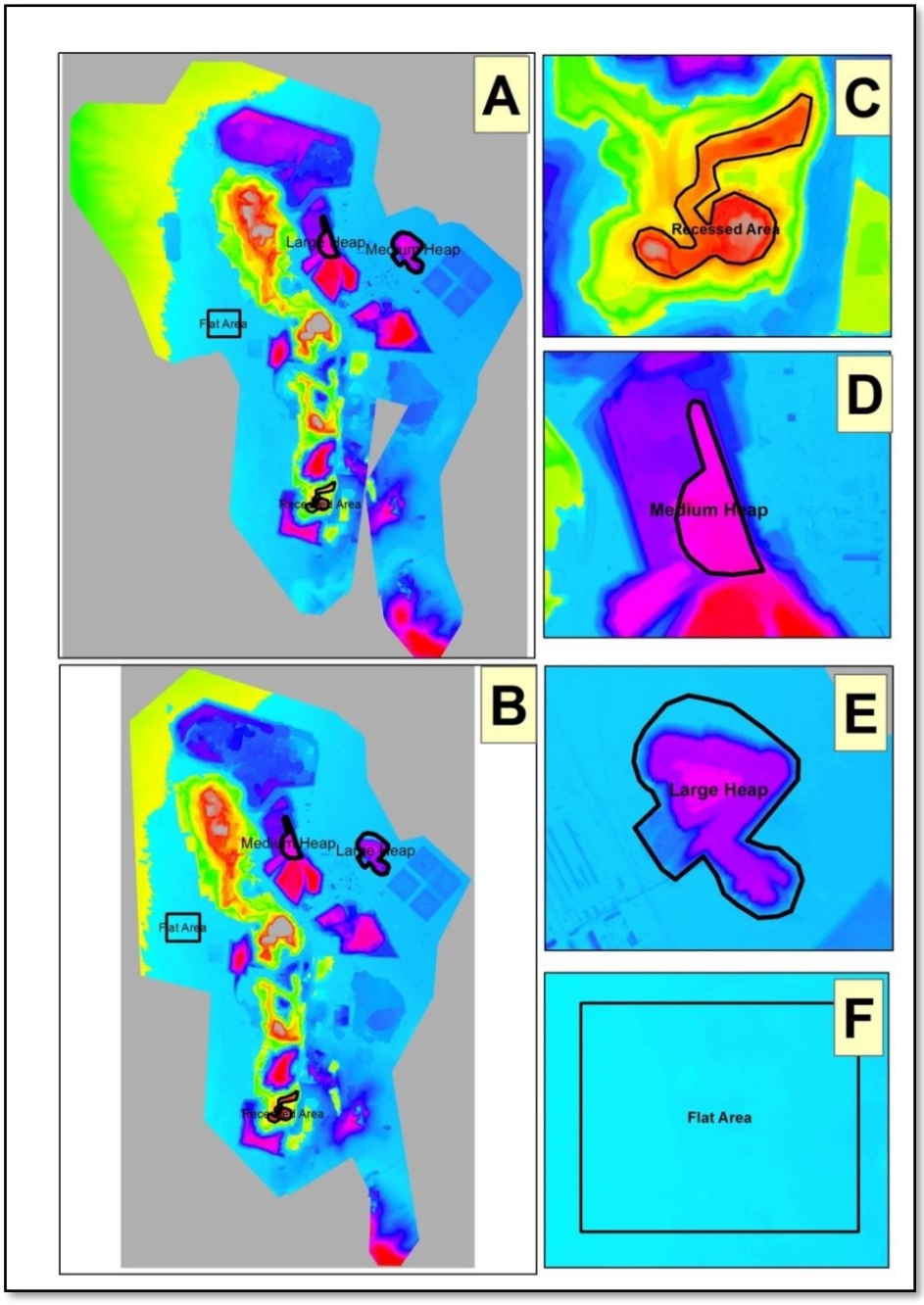

Figure 4.28: Selected areas over the Sishen mine area, [A] Pléiades DTM1 2016/01/25 [B] Pléiades DTM1 2014/07/28 [C] Recessed area [D] Medium heap [E] Large heap [F] Flat area

4.3.3.2.2 Flat area

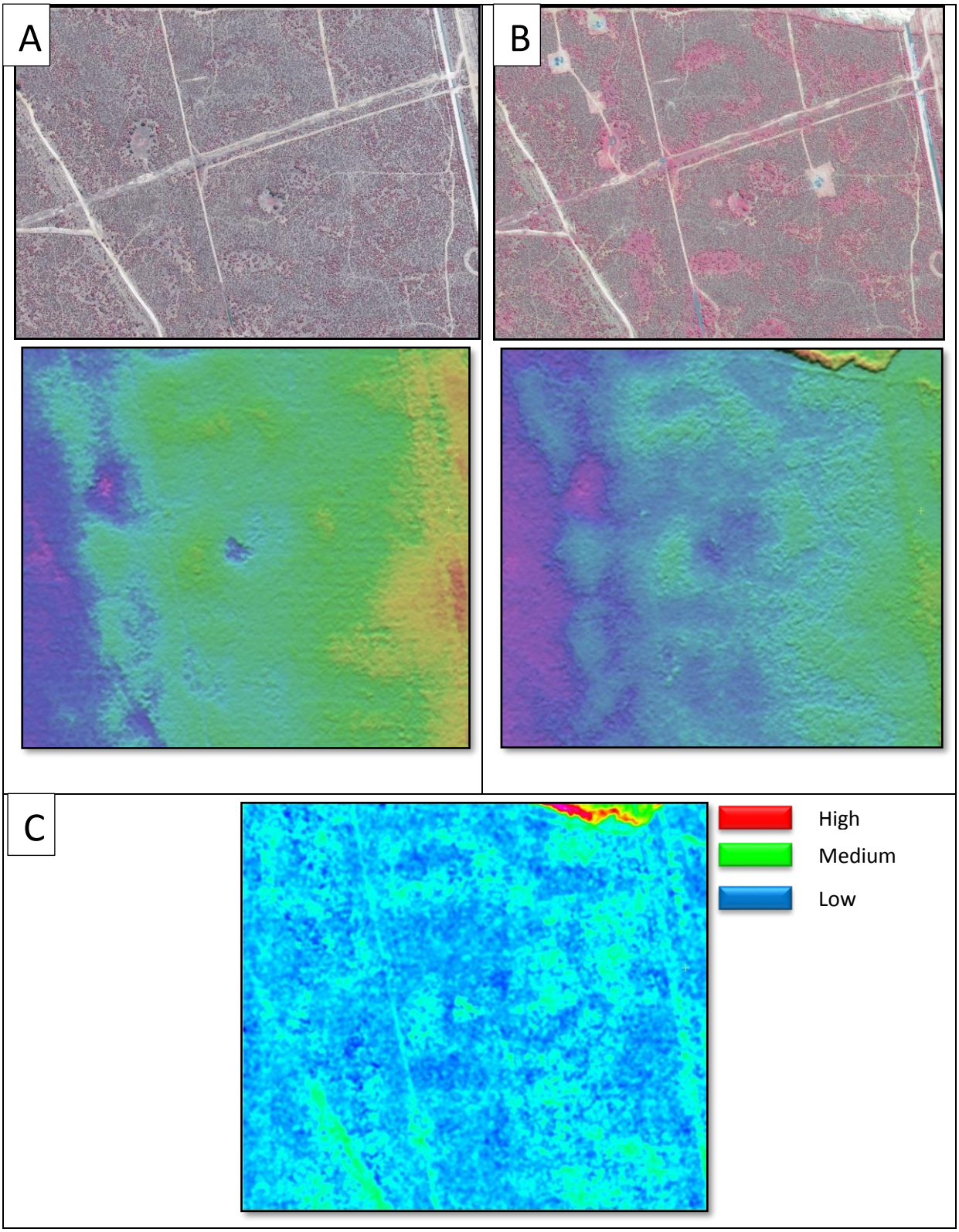

Figure 4.29: [A] Flat area subset of Pléiades image and DTM1 2014/07/28, [B] Flat area subset of Pléiades image and DTM1 2016/01/25, [C] Pléiades DTM1 2016/01/25 minus Pléiades DTM1 2014/07/28

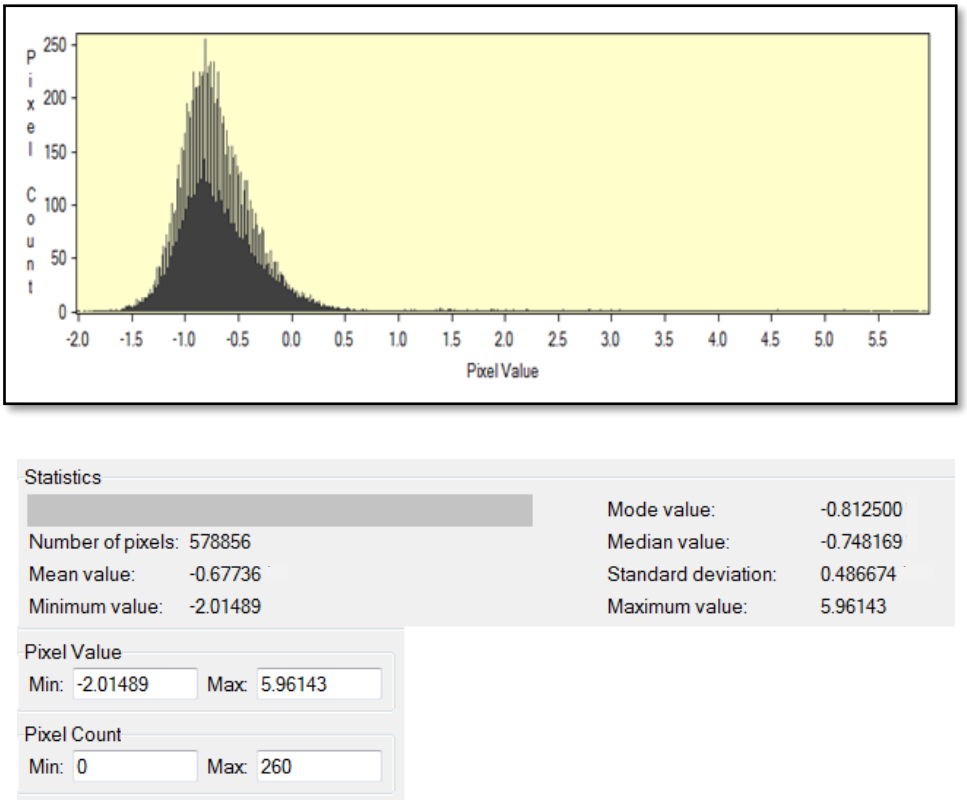

Graph 4.22: Pléiades DTM 1 2016/01/25 minus Pléiades DTM 1 2014/07/28, pixel count as Y-axis and pixel value (height in metres) as X-axis

The analysis illustrates that the difference between dataset 2014/07/28 and 2016/01/25 over the flat area has an average change of -0.68m and median of -0.75m calculated over 578 856 pixels of 1m x 1m each, see Figure 4.29 and Graph 4.22. The minimum height value is -2.015m (recessed area) and the maximum height value 5.96m (new waste dump area formed in the northern side during 2016).These statistics therefore illustrate various surface changes that occurred from 2014 to 2016 over this area. The statistical values are represented in the Table 4.14 below.

Area	Data	Min(m)	Max(m)	StdDev(m)	Mean(m)	Median(m)	Area(m²)
Flat Area:	2016/01/25	1193.21	1204.23	2.2	1197.5	1197.41	578 856
	2014/07/28	1193.79	1201.71	1.87	1197.8	1197.8	578 856
	2016-2014	-2,01	5.96	0.49	-0.68	-0.75	578 856

Table 4.14: Statistical calculations over flat area

4.3.3.2.3 Medium heap area

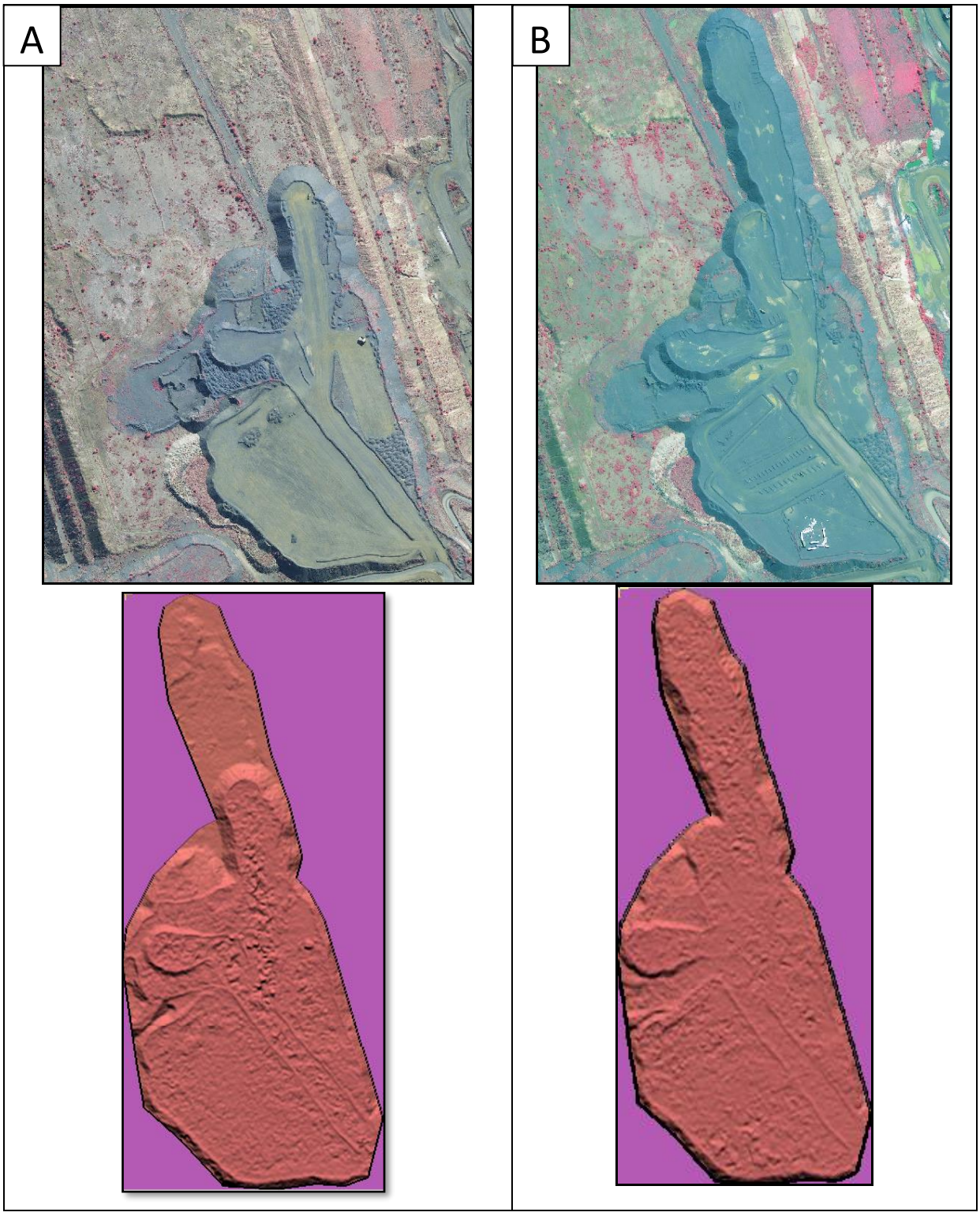

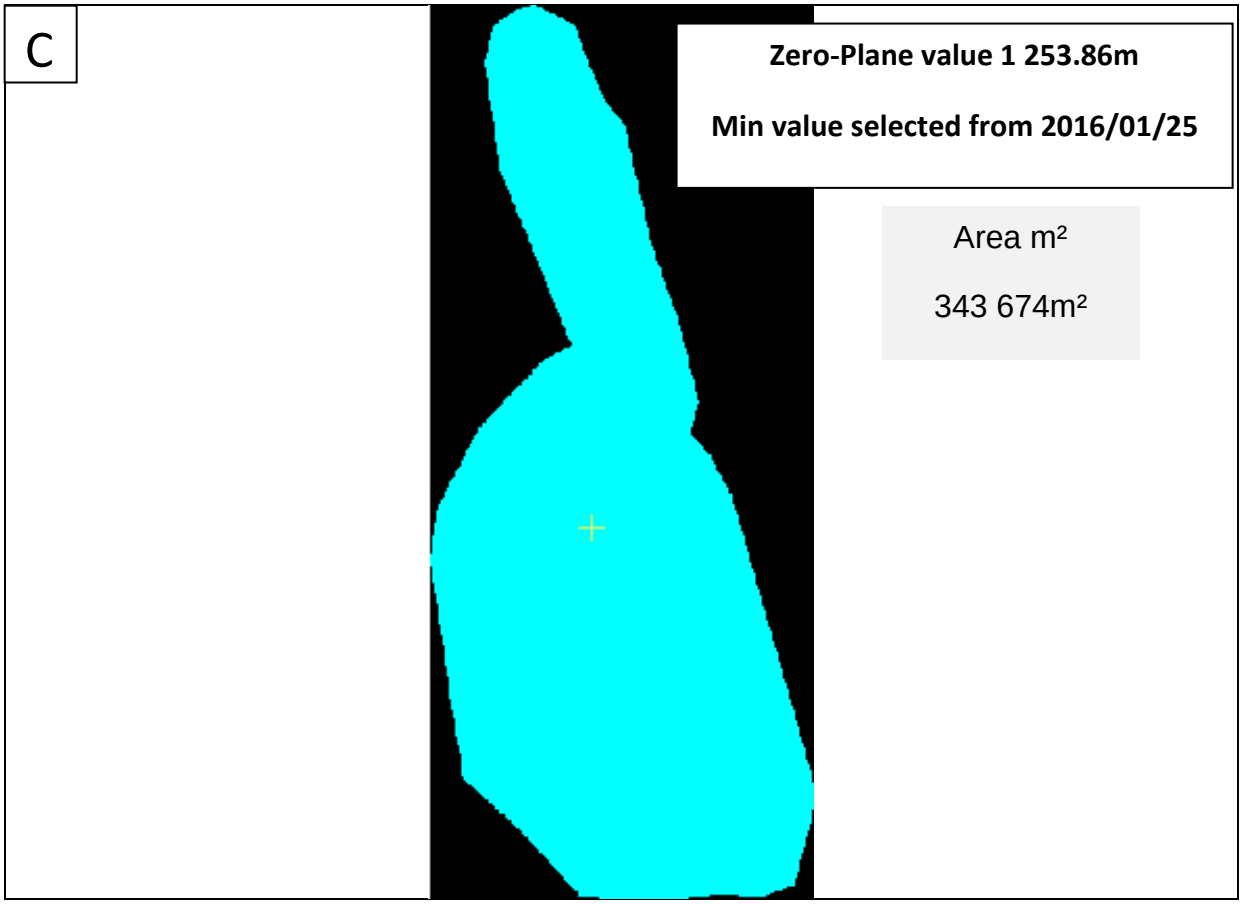

Figure 4.30: [A] Medium heap subset of Pléiades image and DTM1 2014/07/28, [B] Medium heap subset of Pléiades image and DTM1 2016/01/25, [C] Zero-plane vector selected over the subset using the 2016/01/25 DTM1 with height value of 1 253.86m above mean sea surface.
Source: © CNES 2016, distribution rights Airbus DS, All rights reserved

The analysis between the two elevation datasets, Pléiades DTM1 2014/07/28 and Pléiades DTM1 2016/01/25 over the medium waste dump subset highlights the growth of the heap from 2014 to 2016. The zero-plane value selected from the minimum pixel value of the 2016/01/25 elevation model was 1 253.86m above mean sea level, 343 674m² area, see Figure 4.30. The zero-plane value was used to calculate the height value difference from the 2014/07/28 elevation model as well as the 2016/01/25 elevation model. The volume calculation for 2016/01/25 was 8 019 990m³ and 7 449 012m³ for 2014/07/28, thus a difference of 520 978m³ which represents a volume growth of 6.95%, see Table 4.15. These results can be summarised as follows:

Area	Data	Min(m)	Max(m)	StdDev(m)	Mean(m)	Median(m)	Zero-Plane	Area(m)	Volume(m)	Diff (%)
Medium Heap:	2016/01/25	1253.86	1288.29	6.9	1275.35	1276.99	1253.86	343 674	8 019 990	
	2014/07/28	1253.04	1288.96	9.9	1271.92	1275.62	1253.86	343 674	7 499 012	6.95%

Table 4.15: Statistical calculations over medium heap

4.3.3.2.4 Large heap area

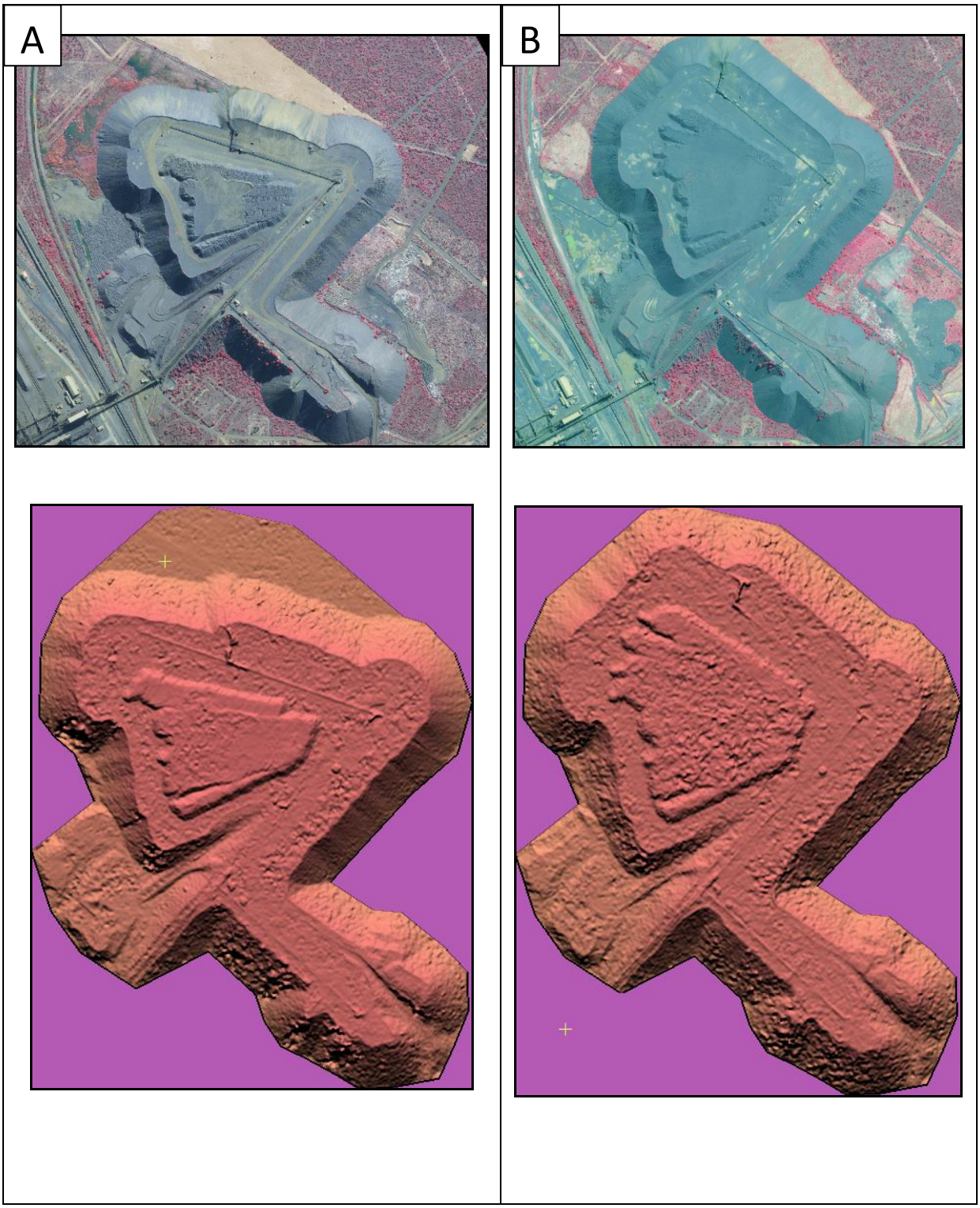

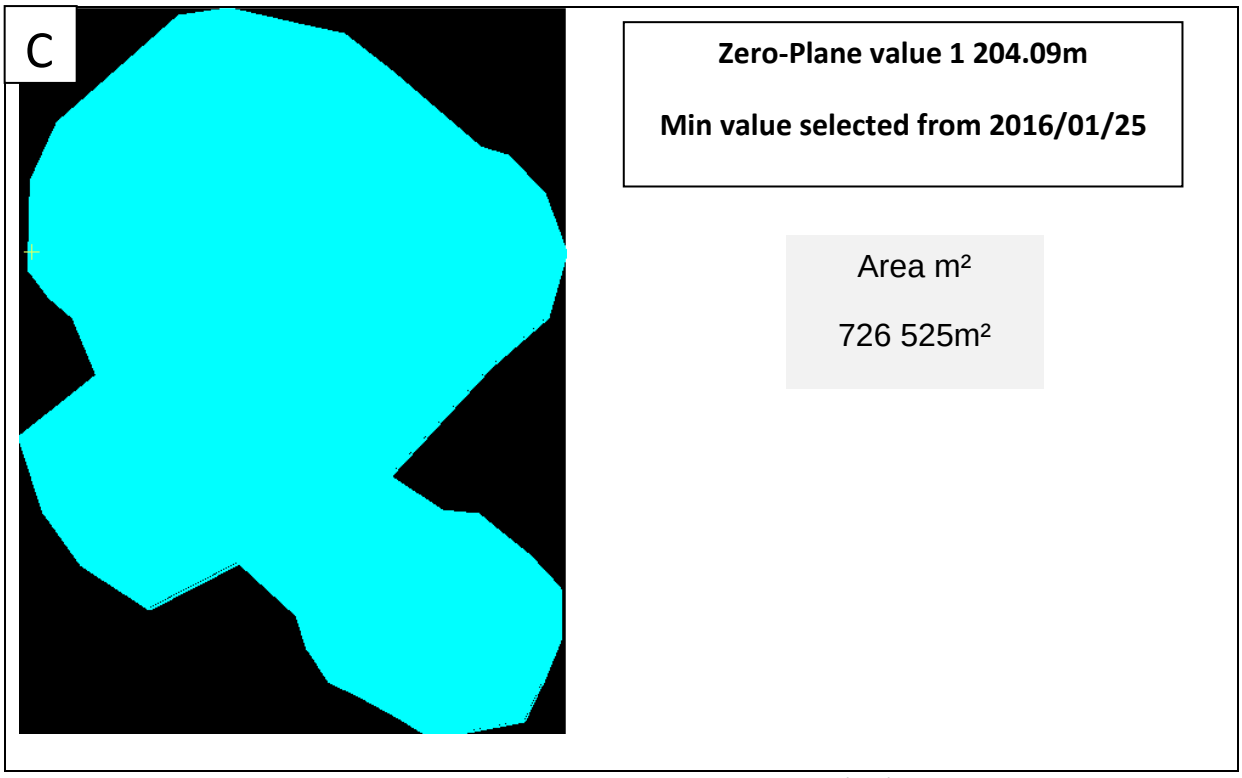

Figure 4.31: [A] Large heap subset of Pléiades image and DTM1 2014/07/28, [B] Large heap subset of Pléiades image and DTM1 2016/01/25, [C] Zero-plane vector selected over the subset using the 2016/01/25 DTM1 with height value of 1 204.09m above mean sea surface.
Source: © CNES 2016, distribution rights Airbus DS, All rights reserved

The analysis between the two elevation datasets, Pléiades DTM1 2014/07/28 and Pléiades DTM1 2016/01/25 over the large waste dump subset highlights the significant growth of the heap from 2014 to 2016. The zero-plane value selected from the minimum pixel value of the 2016/01/25 elevation model was 1 204.09m above mean sea level, 726 525m² area, see Figure 4.31. The zero-plane value was used to calculate the height value difference from the 2014/07/28 elevation model as well as the 2016/01/25 elevation model. The volume calculation for 2016/01/25 was 37 176 983m³ and 33 337 946m³ for 2014/07/28, thus a difference of 3 839 037m³ which represents a volume growth of 11.52%, see Table 4.16. These results can be summarised as follows:

Area	Data	Min(m)	Max(m)	StdDev(m)	Mean(m)	Median(m)	Zero-Plane	Area(m)	Volume(m)	Diff (%)
Large Heap:	2016/01/25	1206.02	1289.14	21.71	1247.81	1248.57	1204.09	726 525	37 176 983	
	2014/07/28	1193.51	1282.57	22.41	1245	1244.88	1204.09	726 525	33 337 946	11.52%

Table 4.16: Statistical calculations over large heap

4.3.3.2.5 Recessed area

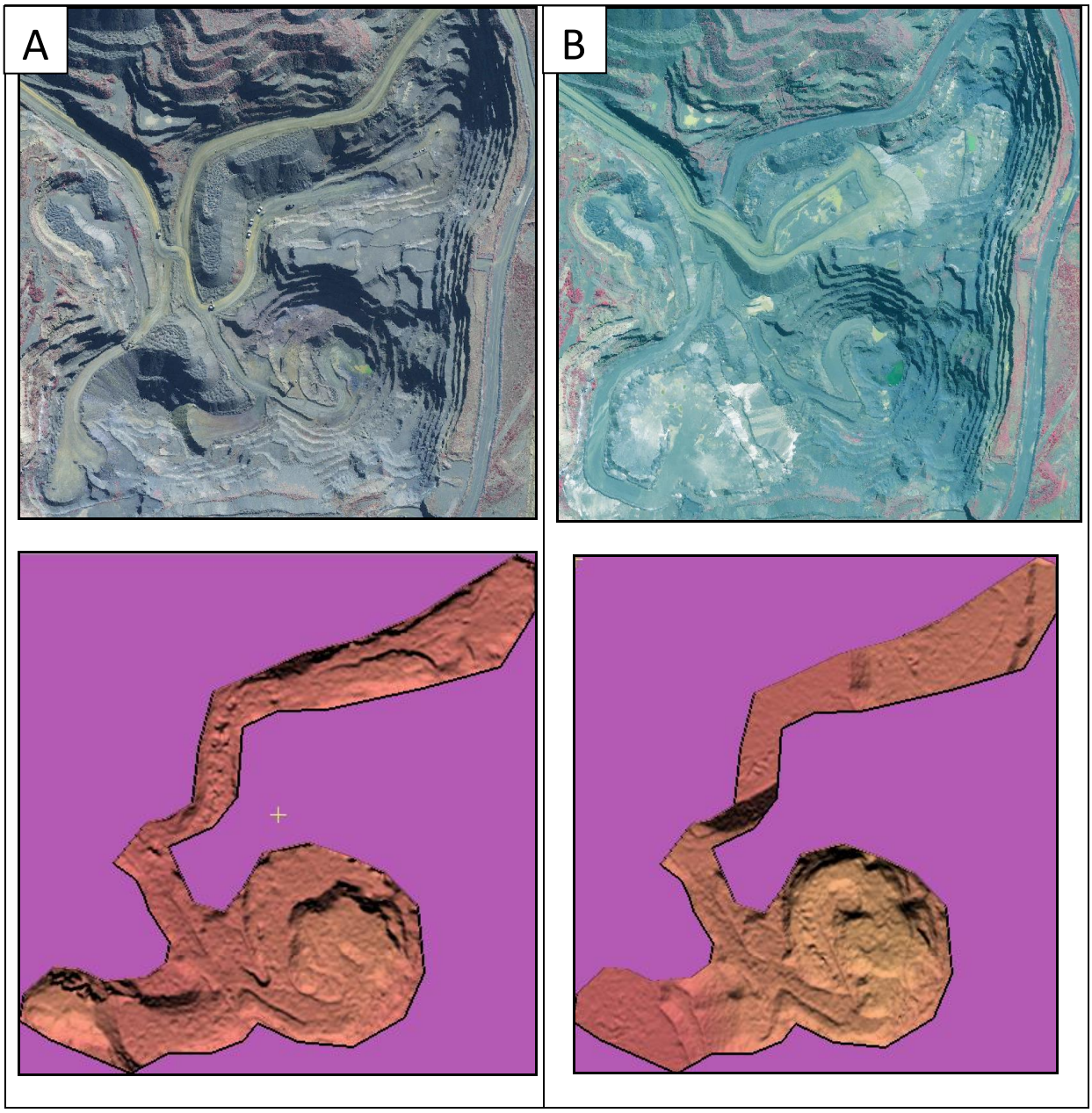

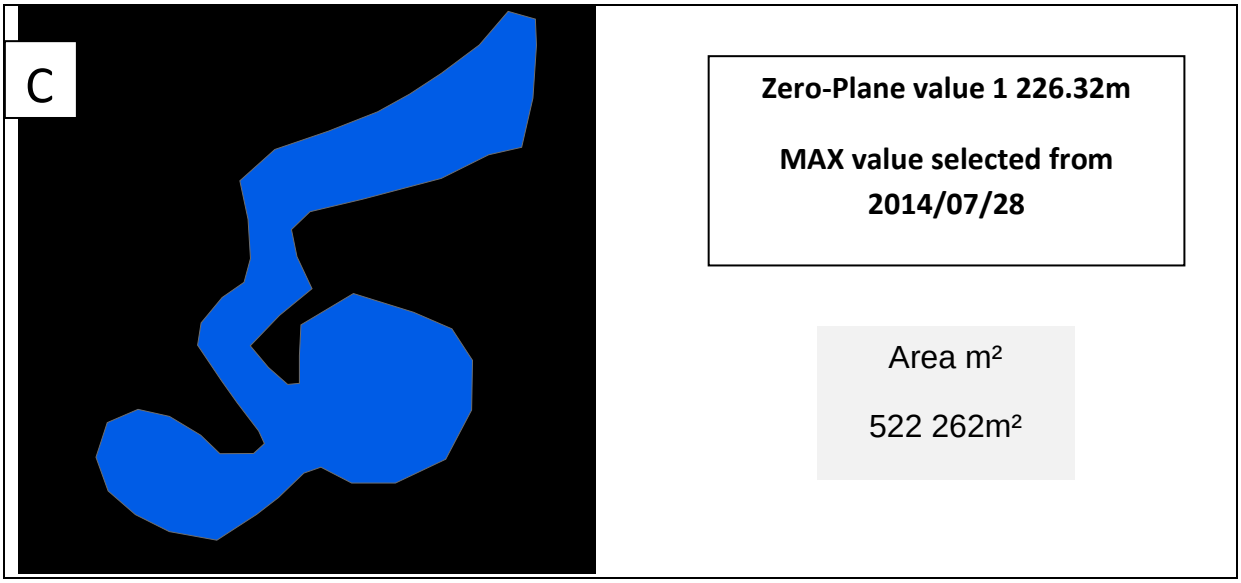

Figure 4.32: [A] Recessed area subset of Pléiades image and DTM1 2014/07/28, [B] Recessed area subset of Pléiades image and DTM1 2016/01/25, [C] Zero-plane vector selected over the subset using the 2014/07/28 DTM1 with height value of 1226.32 metres above mean sea surface. Source: © CNES 2016, distribution rights Airbus DS, All rights reserved

The analysis between the two elevation datasets, Pléiades DTM1 2014/07/28 and Pléiades DTM1 2016/01/25 over the recessed area subset highlights the volume change in the recessed mine area from 2014 to 2016. The zero-plane value selected from the maximum pixel value of the 2014/07/28 elevation model was 1 253.86 above mean sea level, it represented the highest surface height value over the 522 262m² squared area, see Figure 4.32. The zero-plane value was used to calculate the recessed difference from the 2014/07/28 elevation model as well as the 2016/01/25 elevation model. The volume calculation for 2016/01/25 was -28 859 487m³ and -32 407 931m³ for 2014/07/28, thus a difference of -3 548 444m³ which represents a decrease in the recessed growth of -10.95%. This decrease in the recessed area can be explained by the filling that took place in the south-western area of this area from 2014 to 2016, see Table 4.17. These results can be summarised as follows:

Area	Data	Min(m)	Max(m)	StdDev(m)	Mean(m)	Median(m)	Zero-Plane	Area(m)	Volume(m)	Diff (%)
Recessed:	2016/01/25	1033.88	1147.79	31.85	1087.18	1085.87	1226.32	213 182	-28 859 487	
	2014/07/28	1041.98	1108.05	14.37	1073.75	1076.26	1226.32	213 182	-32 407 931	-10.95%

Table 4.17: Statistical calculations over recessed area

4.3.3.2.6 Result summary of volumetric calculations

The use of stereoscopic imagery from Pléiades to generate high resolution elevation models proved to be valuable during the calculation of volumes and associated volumetric changes between temporal datasets. The calculations were done over different topographical areas with different characteristics. Table 4.18 below highlights the results of these calculations. The flat area showed various surface changes from 2014 to 2016. The medium waste dump outstretched by 6.95% followed by the large waste dump of 11.52%. The measurement of the recessed area showed filling activities as a result from 2014 to 2016 as the recessed area decreased in volume by -10.95%.

Area	Data	Min(m)	Max(m)	StdDev(m)	Mean(m)	Median(m)	Zero-Plane	Area(m)	Volume(m)	Diff (%)
Flat Area:	2016/01/25	1193.21	1204.23	2.2	1197.5	1197.41	N/A	578 856	N/A	
	2014/07/28	1193.79	1201.71	1.87	1197.8	1197.8	N/A	578 856	N/A	
	2016-2014	-2.01	5.96	0.49	-0.68	-0.75	N/A	578 856	N/A	
Medium Heap:	2016/01/25	1253.86	1288.29	6.9	1275.35	1276.99	1253.86	343 674	8 019 990	
	2014/07/28	1253.04	1288.96	9.9	1271.92	1275.62	1253.86	343 674	7 499 012	6.95%
Large Heap:	2016/01/25	1206.02	1289.14	21.71	1247.81	1248.57	1204.09	726 525	37 176 983	
	2014/07/28	1193.51	1282.57	22.41	1245	1244.88	1204.09	726 525	33 337 946	11.52%
Recessed:	2016/01/25	1033.88	1147.79	31.85	1087.18	1085.87	1226.32	213 182	-28 859 487	
	2014/07/28	1041.98	1108.05	14.37	1073.75	1076.26	1226.32	213 182	-32 407 931	-10.95%

Table 4.18: Summary of statistical calculations over all elevation study areas

4.3.3.3 Height profile measurement over selected large heaps at the Kolomela mine

Two height profiles over Kolomela mine were illustrated in Figure 4.33 below. Both areas include a large waste dump as well as a recessed area and can be viewed in A1 [DTM 1m derived from the 2016/01/25 Pléiades stereo dataset] and B1 [DTM 1m derived from the 2016/01/25 Pléiades stereo dataset]. The selected height profile lines can be viewed in A,A2 and B,B2, illustrated as a black line. These lines generated a height graph to illustrate the height profile of the large waste dump and recessed areas. The A-line is about 2 600m in length and the B-line is about 2 000m. The graphs A3 and B3 can be viewed in Figures 4.34 and 4.35.

The A-line measurement [A] was done from a northern to a southern direction, see Figure 4.34. The northern foot starts at 1 310m height above mean sea level and immediately shows a constant increase in height until it reaches the top plateau as

from 600m to 1 200m reaching close to 1 360m in height. A steep fall in height over the recessed area is visible in the graph [A3] as from about 1 800m to 2 100m in distance, decreasing in height from 1 390m to around 1 170m.

The B-line measurement [B] was done from a western to an eastern direction, see Figure 4.35. The western point starts at the recessed area, 1 240m height above mean sea level and reduces rapidly in height value within about 10m to 1 200m. As from about 500m to 1 100m the ground surface is reached again measured at an approximate height value of 1 275m. The area is reached at a distance of approximately 1 100m with a steep raise within approximately 200m. The height value rises from 1 275m to about 1 325m. It reaches the plateau at a distance of approximately 1 300m and continues until about 1 800m, thereafter a steep decline can be observed again as the heap ends, passing the 2 000m distance mark [B3].

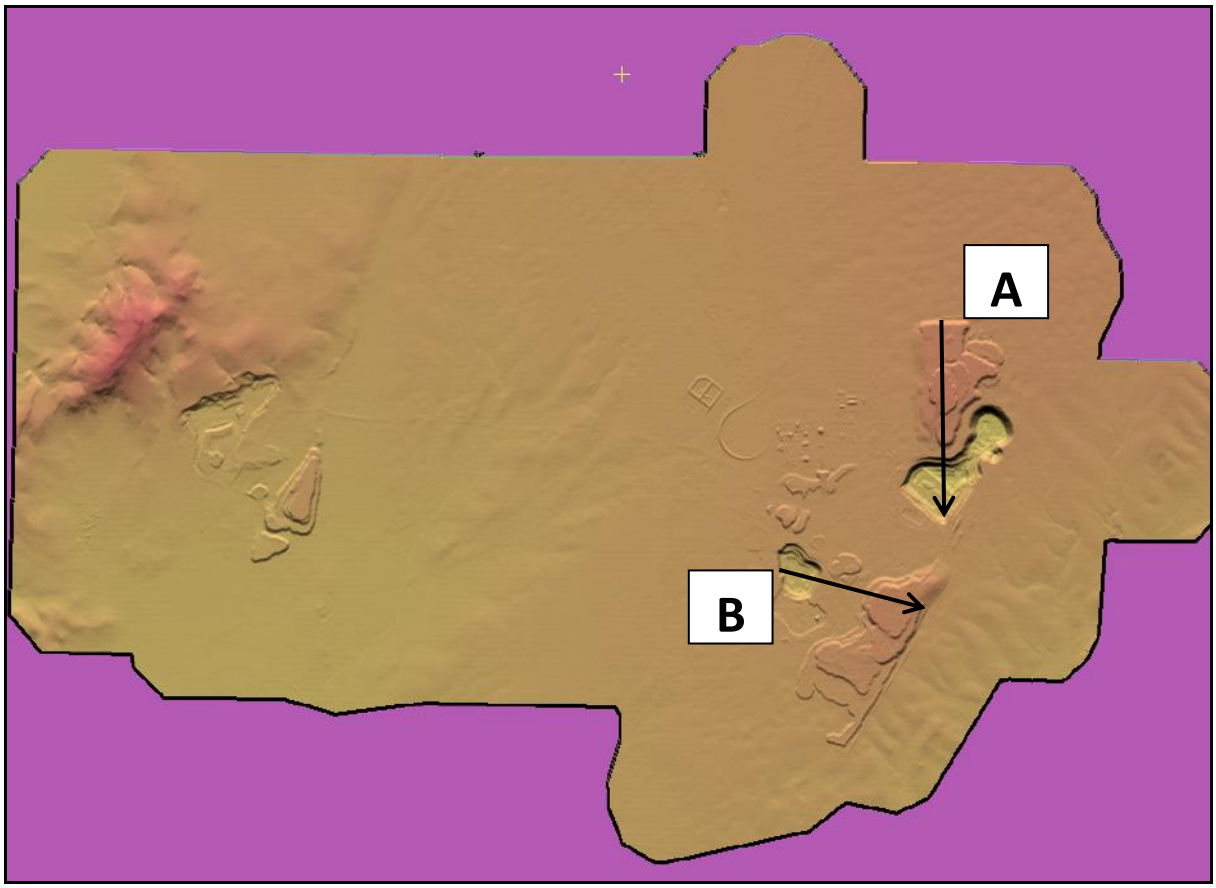

Figure 4.33: Height profiles over the Kolomela Mine, Pléiades DTM1 2016/01/25, measurement lines A and B.

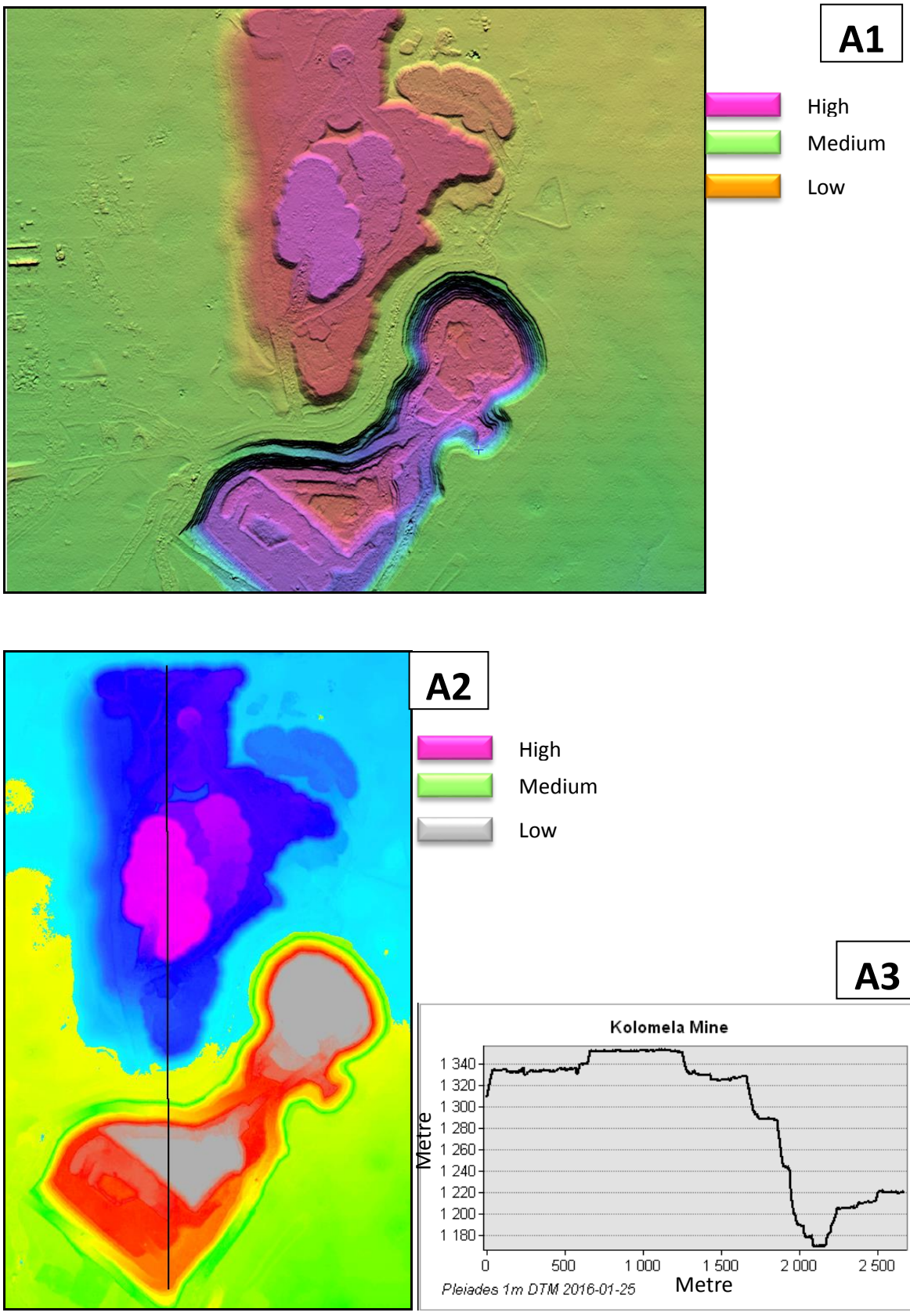

Figure 4.34: Subset over the Kolomela Mine, Pléiades DTM1 2016/01/25, A1 represents the DTM1 elevation view, A2 illustrates the linear measurement visible as the black line, A3 illustrates the height profile in graph format.

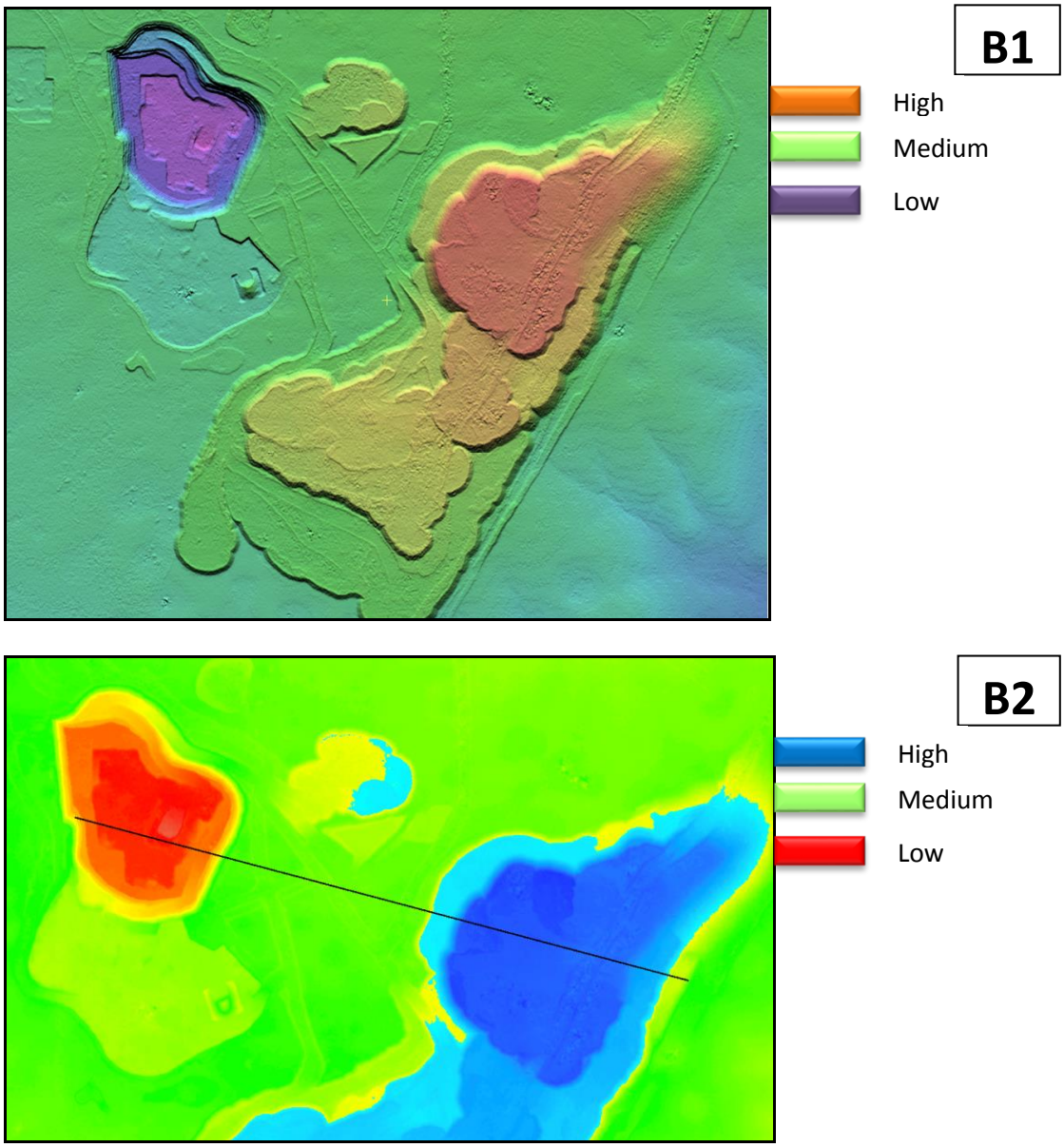

Figure 4.35: Subset over the Kolomela Mine, Pléiades DTM1 2016/01/25, B1 represents the DTM1 elevation view, B2 illustrates the linear measurement visible as the black line, B3 illustrates the height profile in graph format.

4.3.3.4 Change detection applications

In this section change detection products were illustrated over the Sishen mine. These change products were created from both monoscopic and stereoscopic imagery. The ultimate test was to generate these products using automated algorithms and processing chains (Far Earth System, as per section 4.3.1) to deliver operational products for the monitoring of mining operations. The Far Earth System applied pre-processing algorithms to produce from primary processing level to ortho-rectified ready image, which includes top of atmosphere corrections. Once the ortho-rectified image has been produced, then it is ready for further thematic classification. These change detection products attempted to highlight changes that took place in the mining area over a specific time period. Products to detect changes in human and/or mining activity, vegetation and elevation will be described in the next paragraphs.

The processing of these change products started with the accurate production of orthorectified and radiometrically comparable products. For these, indices and elevation models are calculated. The NDVI indices are combinations of the values for various spectral bands. For brightness values, the average of all the spectral bands was calculated. Pixel-based difference products were calculated on a set of such indices. This produced a change product for a specific type of class between two timestamps. The choice of which timestamps were to be used in the generation of difference products needs to be considered carefully to account for seasonal changes and other temporally-associated differences.

4.3.3.4.1 Vegetation change

A Normalized Difference Vegetation Index (NDVI) is an index with values between 0 and 1 which highlights the intensity of vegetation. These change products were produced from the pre-processed and top-of-atmosphere (ToA) corrected images. The NDVI highlights the degree of plant growth and/or chlorophyll reflectance. By comparing the difference in the NDVI between two timestamps, the relative gain or loss of vegetation can be visualised. An area with an increase in the NDVI indicates

more vegetation growth than in the past. An area with a decrease in the NDVI indicates a decrease in the vegetation in the area.

A positive gain in NDVI could be an indication of vegetation recovery in an area. After periods of rain a natural increase in NDVI is also observed and consequently the seasonal changes will be visible in the NDVI.

In Figure 4.36 a subset over an area close to the Sishen open pit mine has been used to demonstrate the vegetation change product. The Pléiades image visible in [A] was acquired on 2014/07/28, the Pléiades image in [B] was acquired on 2016/01/25 and the Pléiades image in [C] was acquired on 2016/03/30. The NDVI change between [B] and [C] is illustrated in [D]. It is clear that new waste dumping took place between 2014/07/28 and 2016/01/25 over this area. The area was all natural vegetation and changed into a mine operational activity. The vegetation growth on these waste dumps between [B] and [C] is clearly visible in the green coloured layer in [D]. Further waste dumping within the [C] image in the north-eastern area compared to [B] is also visible. This is a typical example of breaking new areas, thus the removal of vegetation to be replaced by specific mine activities.

In Figure 4.37 another subset over the Sishen mine area illustrates a vegetation recovery example. This recovery can be explained as a seasonal vegetation recovery due to rain in this area from January 2016 until March 2016. The Pléiades image [A] was acquired on 2016/01/25 and the Pléiades image [B] was acquired on 2016/03/30. The 2016/03/30 image was used to overlay the NDVI change layer highlighting the recovered vegetation in the bright green colour [C].

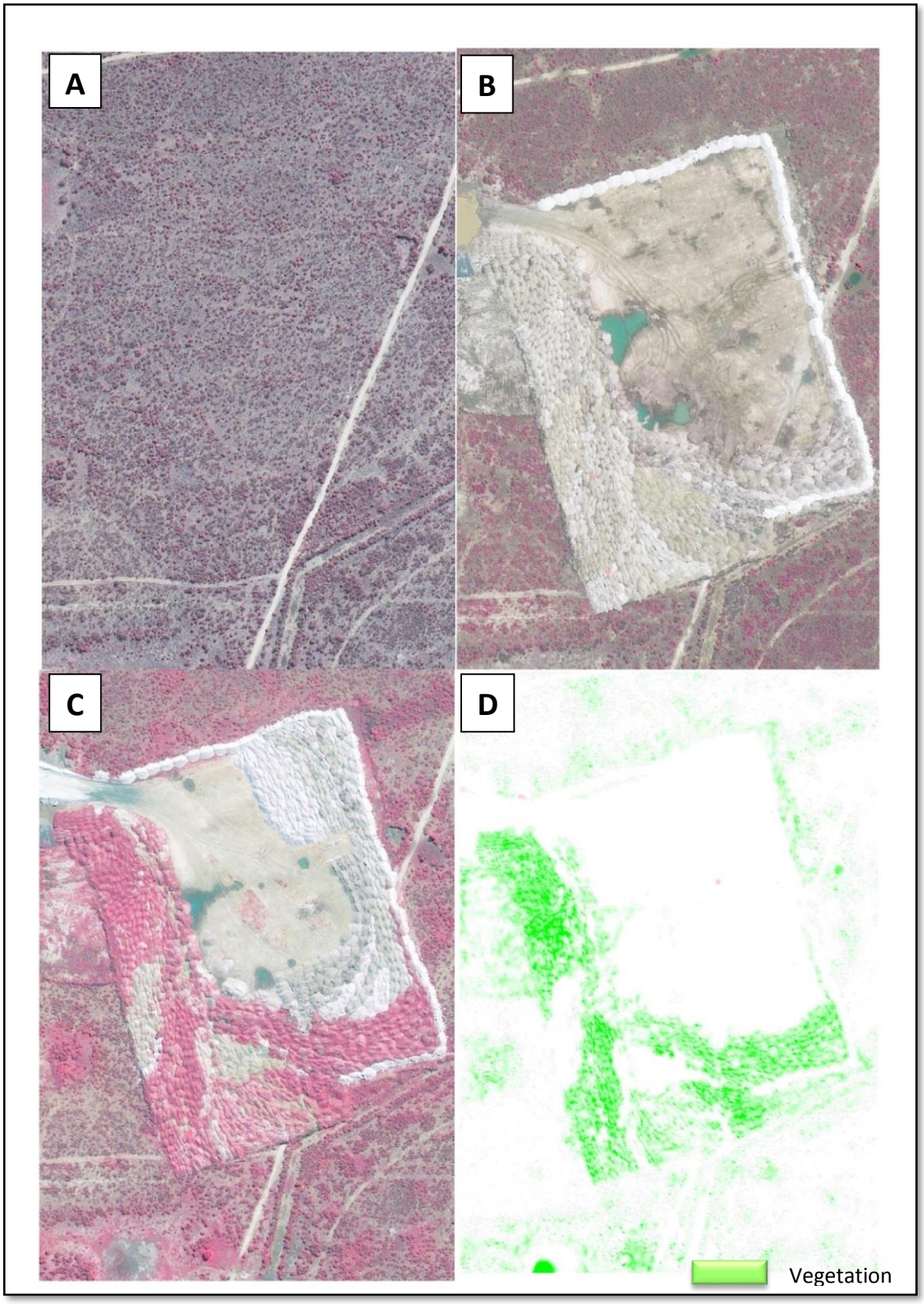

Figure 4.36: [A] Pléiades false colour image 2014/07/28, [B] Pléiades false colour image 2016/01/25, [C] Pléiades false colour image 2016/03/30, [D] NDVI change product between [B] and [C]
Source: © CNES 2016, distribution rights Airbus DS, All rights reserved

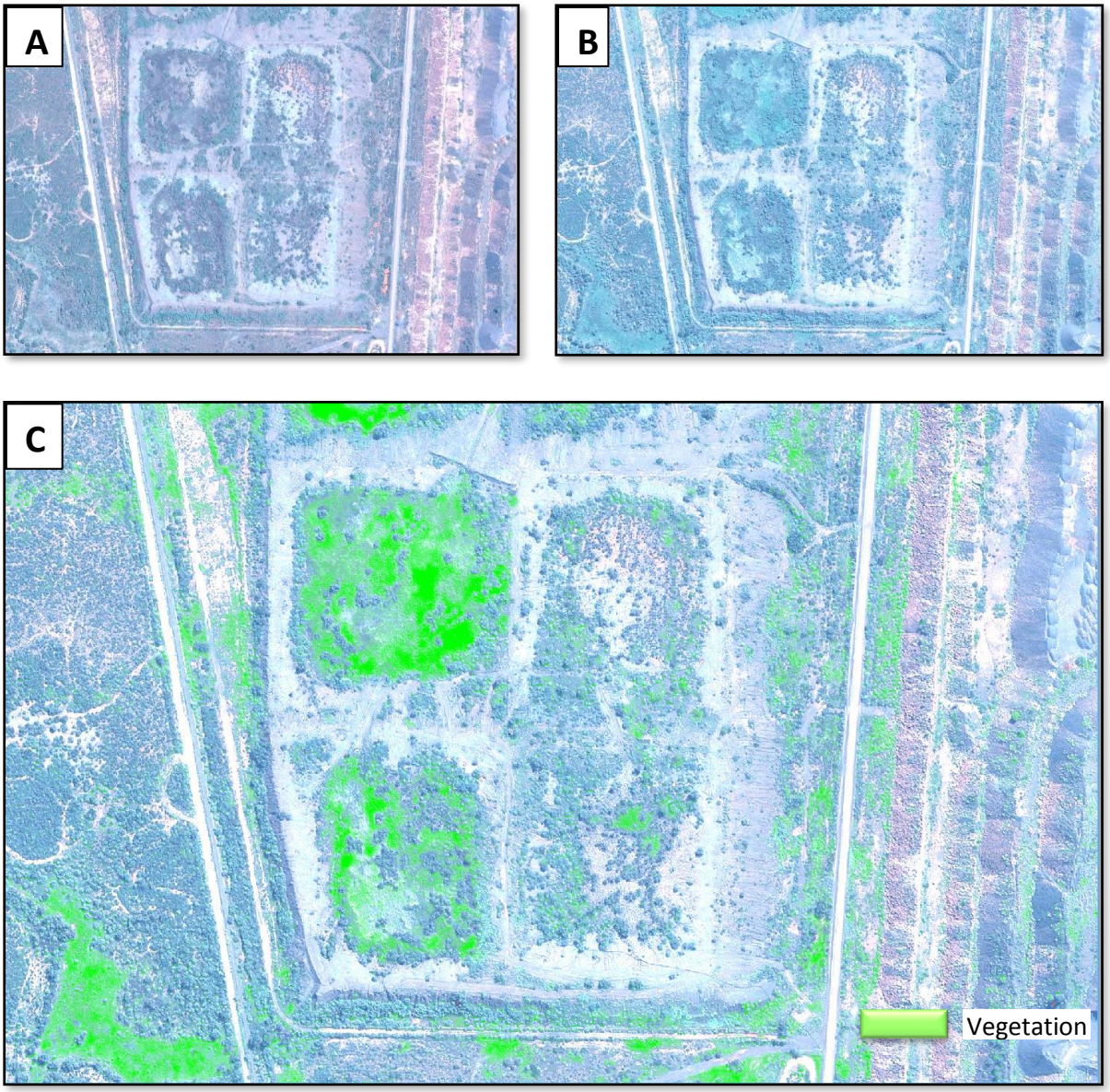

Figure 4.37: [A] Pléiades natural colour image 2016/01/25, [B] Pléiades natural colour image 2016/03/30, [C] NDVI change product between [A] and [B] (bright green)
Source: © CNES 2016, distribution rights Airbus DS, All rights reserved

4.3.3.4.2 Brightness change

The purpose of a brightness change product is to highlight areas of activity using the radiometric data intensity values. An area of activity, where soil has been disturbed, is often visually recognisable due to the change in colour of the soil – freshly exposed soil tends to be darker in colour. These changes might not manifest

themselves as a change in NDVI, and therefore a comparison of the relative brightness between two timestamps is useful.

In Figure 4.38 below a brightness change product between the Pléiades image acquired during 2016/01/25 [A] and 2016/03/30 [B] indicates a significant change in mine activity during this period. Blue indicates an increase in brightness and orange a decrease in brightness [C].

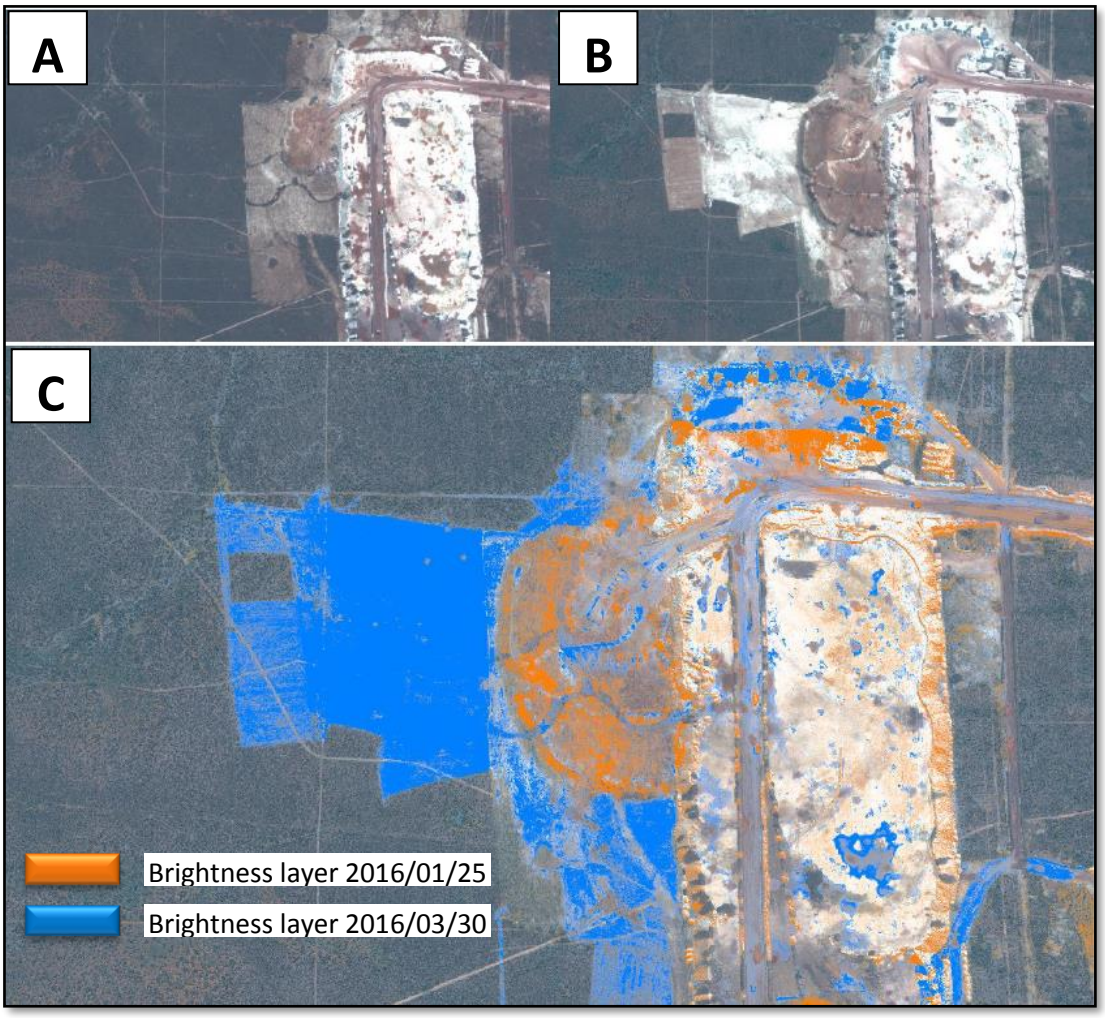

Figure 4.38: [A] Pléiades natural colour image 2016/01/25, [B] Pléiades natural colour image 2016/03/30, [C] Brightness change product between [A] (orange) and [B] (blue)
Source: © CNES 2016, distribution rights Airbus DS, All rights reserved

4.3.3.4.3 Absolute activity change

Using the change detection algorithm in PCI Geomatica accurate change between two timestamp images can be determined. This change detection reveals the

differences between two images of the same content from different dates. This feature is useful to determine changes such as the construction of new infrastructure around the mine or large vegetation removal. It is also useful to determine the movement of equipment and vehicles such as loaders during the comparable timestamps. These comparisons can be expressed simply as “before versus after”.

The output of the change can be displayed in three available options: red, green, and blue (RGB), pseudocolor, or grayscale. To perform change detection, a working image as well as a reference image needs to be selected. The working image is typically the more recent image. The reference image is the older image. In this case the Pléiades 2016/03/30 image [C] was selected as the working image and the Pléiades 2016/01/25 image [B] was selected as the reference image.

With each image - working and reference - you can select whether to compare all layers in the image, or one specific layer. When you compare all layers, each channel in the file is used as input data, and you must specify the same number of channels as input for both files. The channels are compared sequentially (difference: A1-B1, A2-B2) before being amalgamated into the output change layer. In this example a RGB output with a difference algorithm was applied to all four bands of the Pléiades imagery. RGB: maps red to the working layer [C], green to the reference layer [B], and blue to the change layer. In this example the change layer was exported as a single layer and an orange colour was used to display the results [D].

The image difference method compares images of the same location from different dates, and then subtracts the imagery of one date from that of the other. In addition to the type of change detection, a selection of the absolute value as output was also confirmed. The absolute value is, as the name implies, the fixed value of the computed change layer. The magnitude of change is reported, but not the direction. When the difference method is used in combination with absolute value, an output value of zero represents the pixels that changed the least and hundred corresponds to the pixels that changed the most.

To ensure further accuracy to the change detection results a subset over a specific area within the Pléiades images was selected and used as an input mask. A mask can define one or more areas to include, such as the pixels under the inclusion

mask. For example, when interest is shown only in a specific area, you can use an inclusion mask to limit the change detection to that area.

Change detection in Figure 4.39 was performed using the difference algorithm, with absolute values as output. The Pléiades image in [A] was collected during 2014/07/28. This image clearly shows no human activities and is all natural. The image during 2016/01/25 illustrates that specific construction started and the progress until 2016/03/30.

Various change detection changes are visible [D]. Vehicles/trucks have moved within the two timestamps in the northern parking areas. The construction of the tanks progressed from only the walls to the completion of the rooftops. The warehouse building had only its metal frame completed in image [B] and progressed to a completed rooftop in image [C]. These changes have been clearly detected in the change detection layer [D]. The dark orange colours illustrate absolute change versus the lighter orange colours that show a less significant change between the two comparable images, see Figure 4.39.

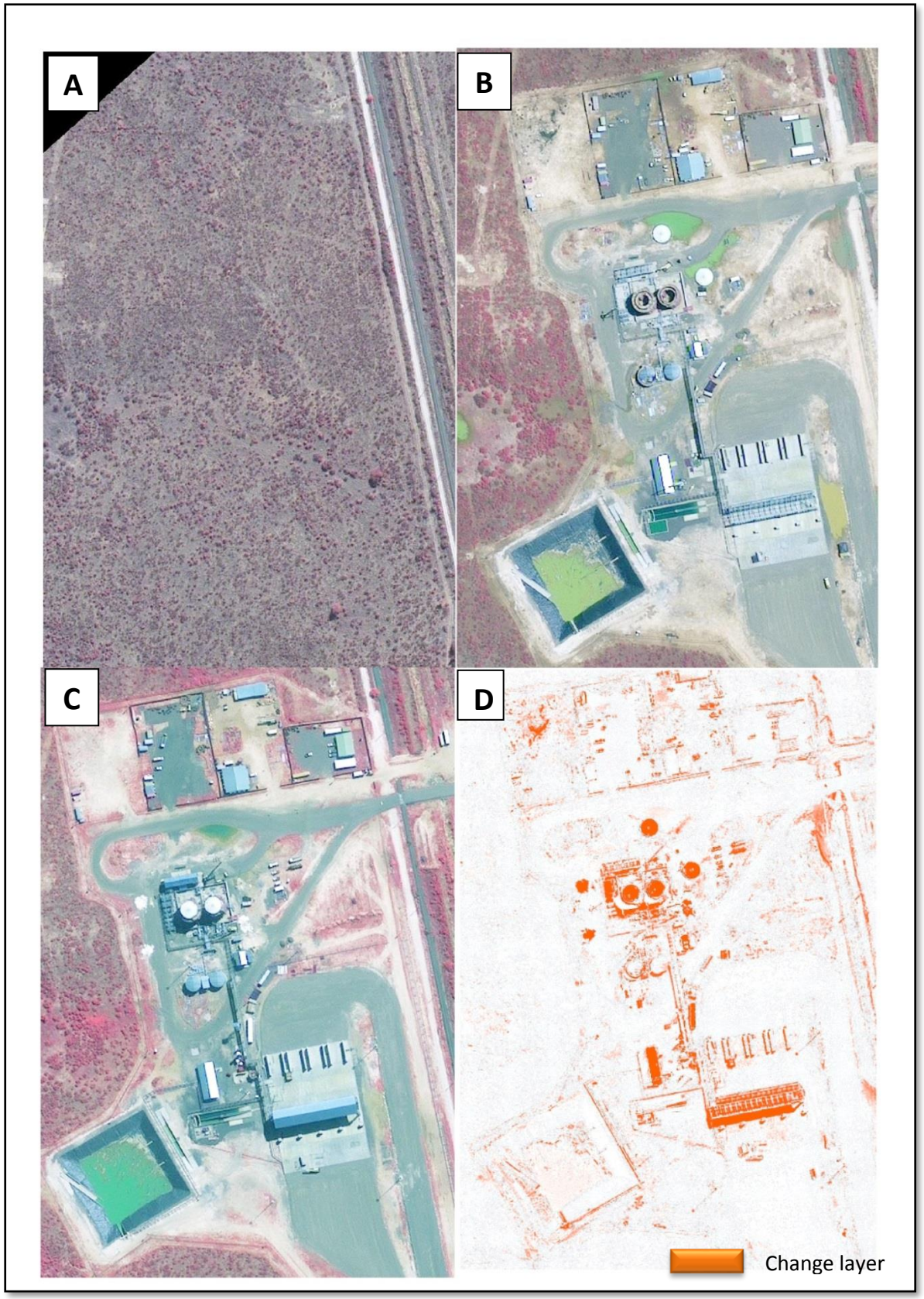

Figure 4.39: [A] Pléiades false colour image 2014/07/28, [B] Pléiades false colour image 2016/01/25, [C] Pléiades false colour image 2016/03/30, [D] Change detection product between [B] and [C]
Source: © CNES 2016, distribution rights Airbus DS, All rights reserved

4.3.3.4.4 Elevation change detection

DEM differencing is dependent on two available elevation sources that were collected during two different timestamps. In this example the Pléiades stereo imagery collected on the 2014/07/28 [A1] and 2016/01/25 [B1] was used to generate the DTM 1m products. The latest DTM 1m was then subtracted from the oldest DTM 1m (B2 – A2) to generate a change elevation model [C]. The end result was a new DTM 1m that only retained the elevation values that will illustrate increased areas as well as recessed areas (see Figure 4.40).

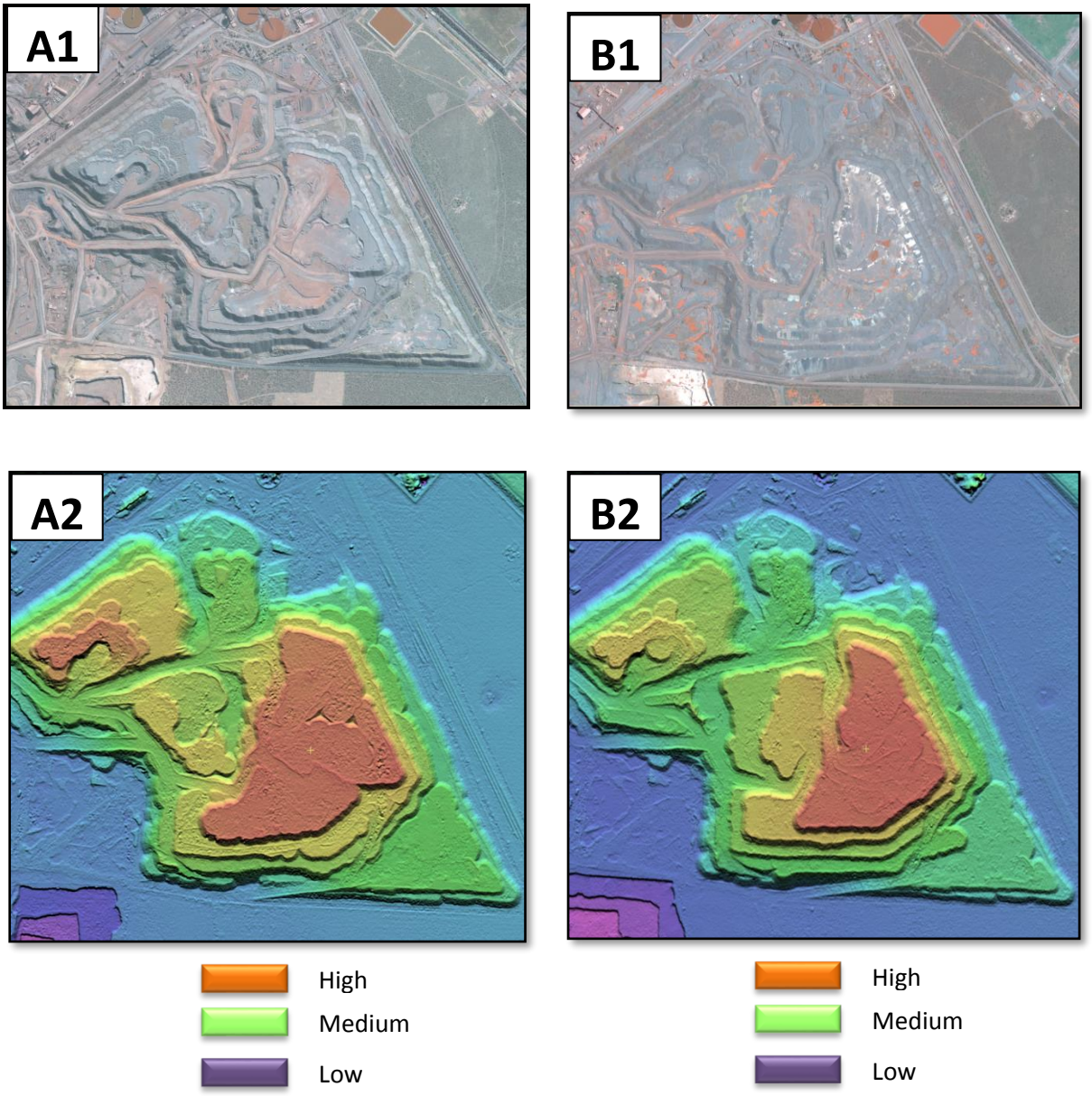

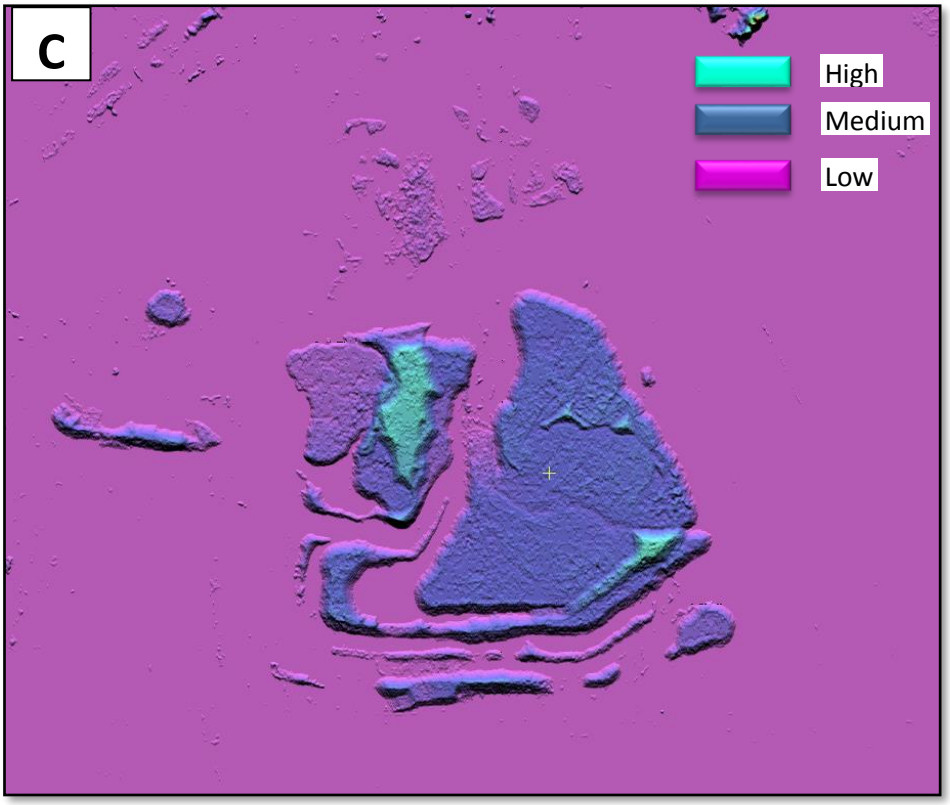

Figure 4.40: [A1] Pléiades image 2014/07/28, [A2] Pléiades DTM 1m 2014/07/28, [B1] Pléiades image 2016/01/25, [B2] Pléiades DTM 1m 2016/01/25 [C] Elevation change product between [A2] and [B2], light purple (low), dark purple (medium), green (high)

4.4 Conclusion

This chapter introduced various optical analytical possibilities applicable to the monitoring of mine operations as well as the environmental and operational changes that occurred over the open mine pit and its surroundings over time. The Landsat 8 imagery was firstly used to analyse the dominant land cover classes over the applicable mine study areas. These land cover classes assisted the researcher to understand the landscape, comparing its natural behaviour to changes due to human activities.

The monoscopic analysis of the very high resolution satellite Pléiades enabled a fine scale analysis of important land cover classes to visualise, analyse and measure changes in vegetation, bare soil, asphalt or mine areas as well as waterbodies. The monoscopic analysis was followed by the stereoscopic analysis of Pléiades elevation models. The derived one metre digital terrain models were used to understand

changes not only at ground level but also to include the height factor. The changes in height profiles over various different topological areas were demonstrated.

This chapter concluded with some change detection products such as vegetation changes, brightness changes, absolute activity changes and elevation change products. The combination of all these RS analytic methods using different satellite sensors, acquisition modes and algorithmic methods generates a wealth of geo-spatial information that can contribute to the understanding of the behaviour of mine operations and their impact on the surroundings. These changes relate to primary as well as secondary factors that introduce different pressure points to the environment. Understanding these constant changes in environmental and human activities can assist mine managers during decision making processes and continuous efforts to improve mining operations.

CHAPTER 5: SAR SURFACE MOVEMENT MONITORING RESULTS

5.1 Introduction

In this chapter Surface Movement Monitoring (SMM) results, using SAR technology from the X-band TerraSAR-X satellite, will be discussed. Although the archive interferometric SAR imagery were not available over the Sishen or Kolomela mines, other two areas were selected to demonstrate the methodology. These two case study areas will highlight the principles of SMM and how they can be applied within the mining sector. The focus was therefore more on the SMM application potential than the actual geographical location of these study areas. The interferometric scenes were processed by the specialist team of Airbus Defence and Space, based in Postdam, Germany, to produce the SMM results.

The Time Series Interferometric Analysis was applied to derive the movement measurement over the Royal Bafokeng tailings pond near Rustenburg, South Africa and the open surface Chuquicamata Mine in Chile. The methodology was described in section 3.3.4 of this study.

5.2 Royal Bafokeng Platinum tailings pond case study

The Royal Bafokeng tailings pond is situated near the platinum deep pit mine of Bafokeng South Mines. The tailings pond is about 4.5km² with a perimeter of more than 7km, see Figures 5.1 and 5.2. This pond holds several million litres of mine waste water. The purpose of applying the SMM over this area was to determine the stability of the tailings pond side walls as well as to determine the stability of the surface that surrounds the pond, especially to determine if underground percolation occurred.

Figure 5.1: Royal Bafokeng Tailings pond, yellow rectangular illustrates the area of interest for the study area.
Source: © Google Earth 2016

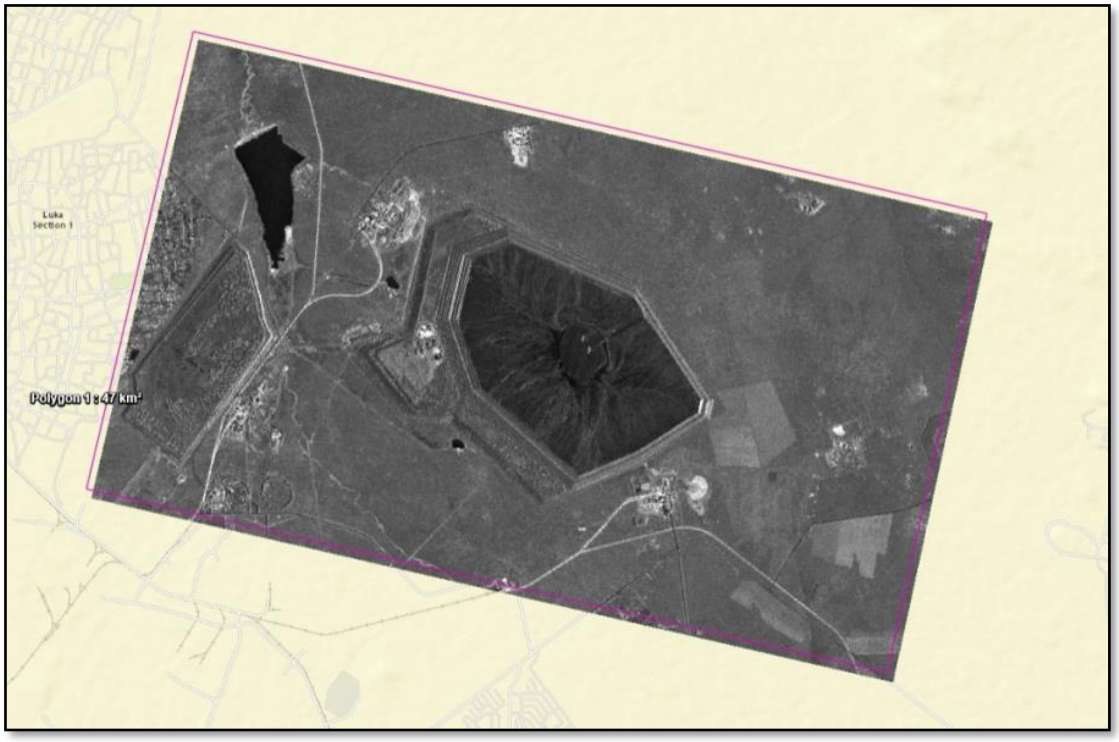

Figure 5.2: TerraSAR-X High Resolution Spotlight scene, 5km x 10km over the tailings pond.
Source: © DLR e.V. 2014 and © Airbus DS / Infoterra GmbH 2014

Since the case study commenced, 74 scenes were collected over the area, see Graph 5.1. The data collection occurred from May 2013 until March 2016. The data collection was done in descending mode, Horizontal Horizontal (HH) polarization, relative orbit number 107, right looking direction, 11day revisit cycles as prime objective. Quality was ensured by using the scientific TerraSAR-X orbit data to ensure maximum accuracy during image processing.

According to the Jet Propulsion Laboratory, California Institute for Technology a radar antenna can be designed to transmit and receive electromagnetic waves with a well-defined polarization, which is defined as the orientation of the electric field vector in the plane orthogonal to the wave propagation direction. By varying the polarization of the transmitted signal, SAR systems can provide information on the polarimetric properties of the observed surface. These polarimetric properties are indicative of the structure of the surface elements within a resolution element. A polarimetric radar can be designed to operate as a single-pol system, where there is a single polarization transmitted and a single polarization received. A typical single-pol system would transmit horizontally or vertically polarized waveforms and receive the same (giving HH or VV imagery).

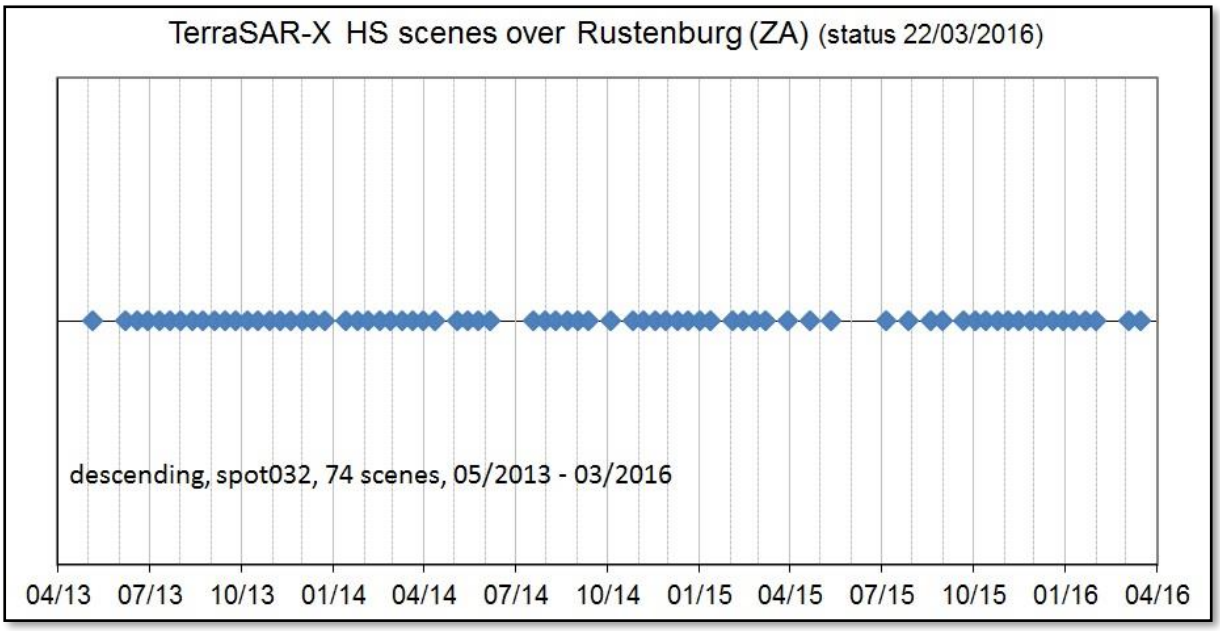

Graph 5.1: Interferometric data collection by TerraSAR-X over the tailings pond since May 2013 until March 2016

5.2.1 Surface movement monitoring result

The SMM results to be shared during this study are based on the first six months' data collection, May to October 2013 [14 scenes] to produce the baseline result. The SMM focus was to measure the vertical movement over time. In Figure 5.3 the SMM results are shown on a monthly basis. It is clear that subsidence occurred during this period within the surroundings of the tailings pond. The important aspect is the interpretation of these results. The subsidence in this case study is a very good example of the behaviour of the natural soil and drying river beds during the dry season. A natural shrinking of the soil took place (see Figures 5.4 and 5.5). The focus point was also the stability of the tailing pond walls. The constant green movement index around the tailings pond confirms the stability of these walls, compared to the adjacent soil areas (see Figures 5.4 and 5.5). Upliftment was detected to the southern parts of the dam, it can be defined as swelling due to the moisture being absorbed by the soil (see Figures 5.4 and 5.5).

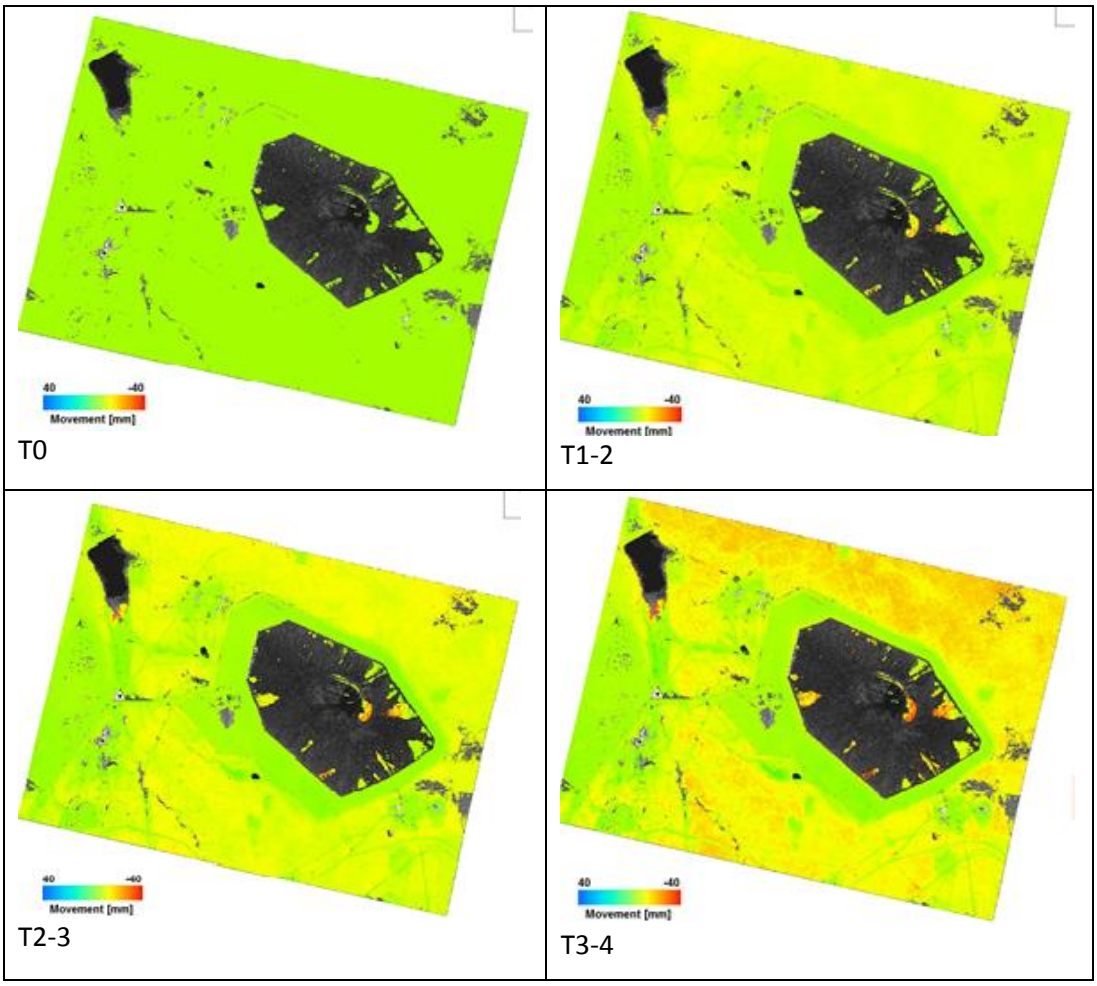

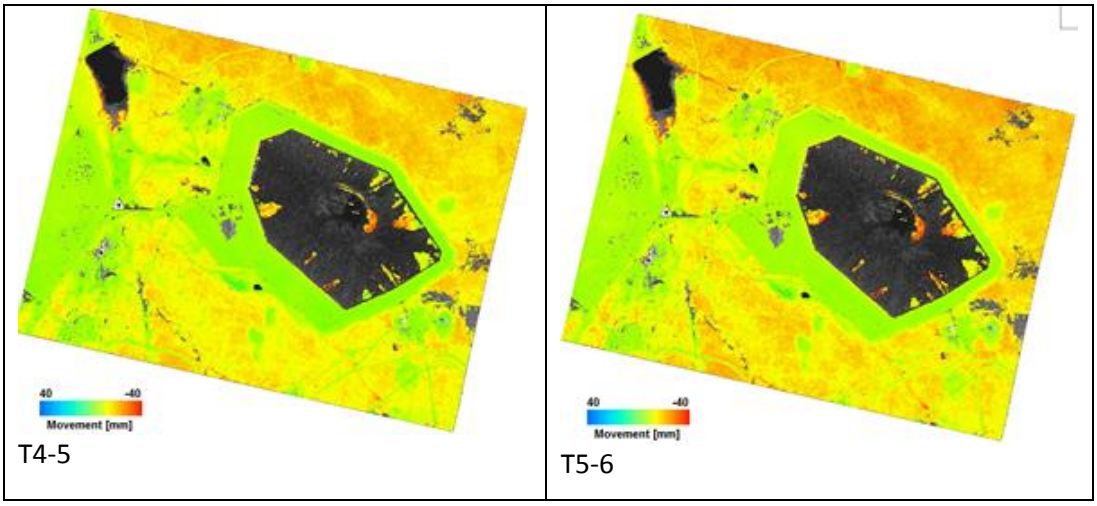

Figure 5.3: Time series SMM analysis for over 6 months (T0 to T6) [May to Oct 2013], Movement scale (mm): Blue upliftment, Green stable or low upliftment, Yellow low subsidence, Red high subsidence.
Source: © Airbus DS Geo GmbH

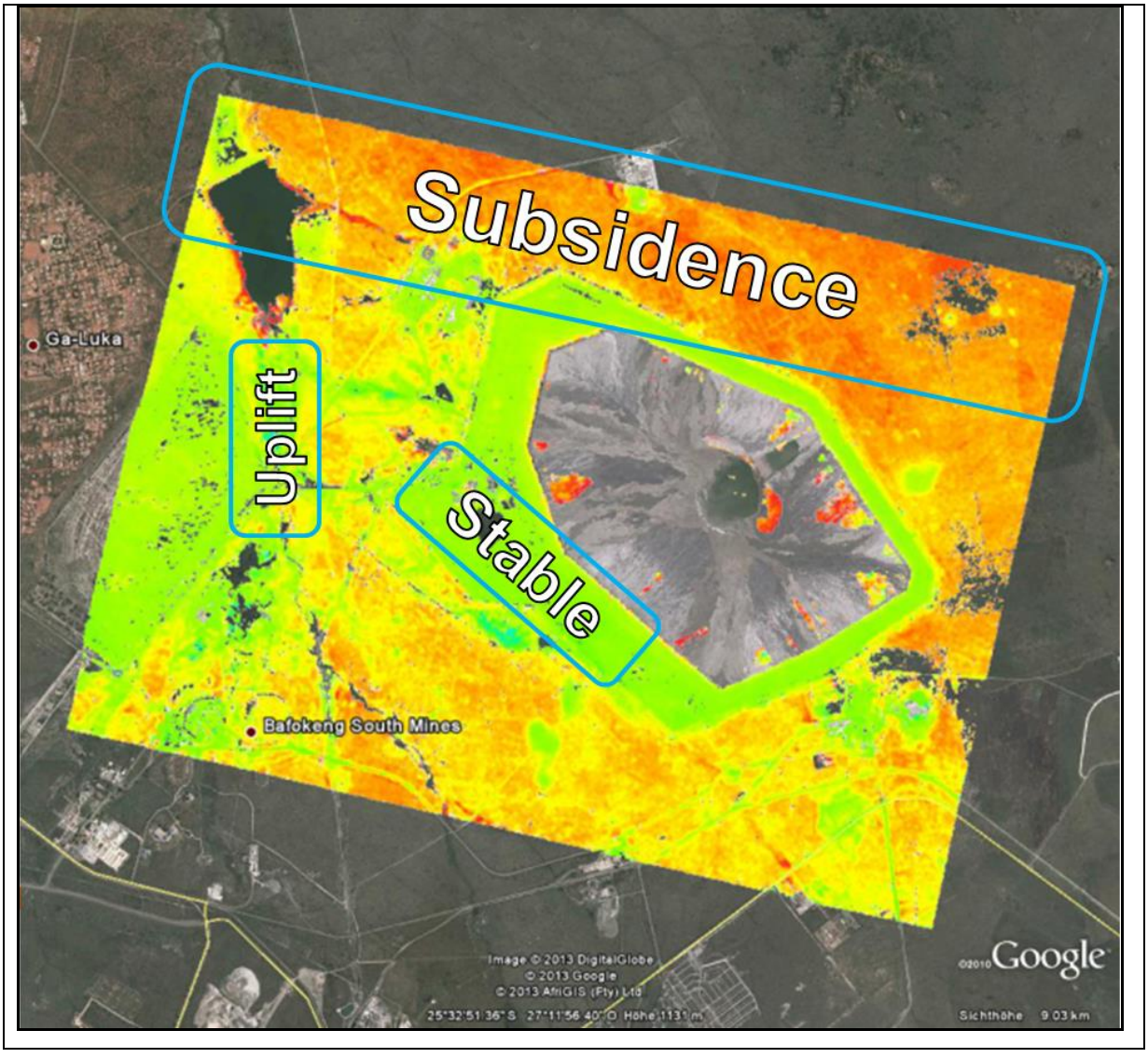

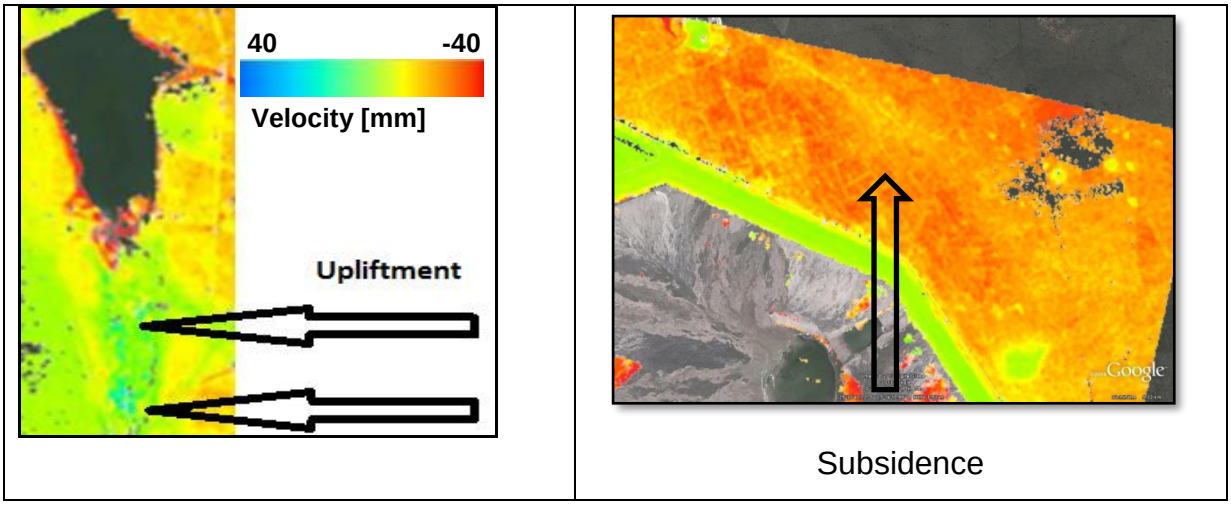

Figure 5.4: Illustrating the subsidence, upliftment and stable areas over the study area after 6 months (May to Oct 2013).
Source: © Airbus DS Geo GmbH, © Google Earth 2016

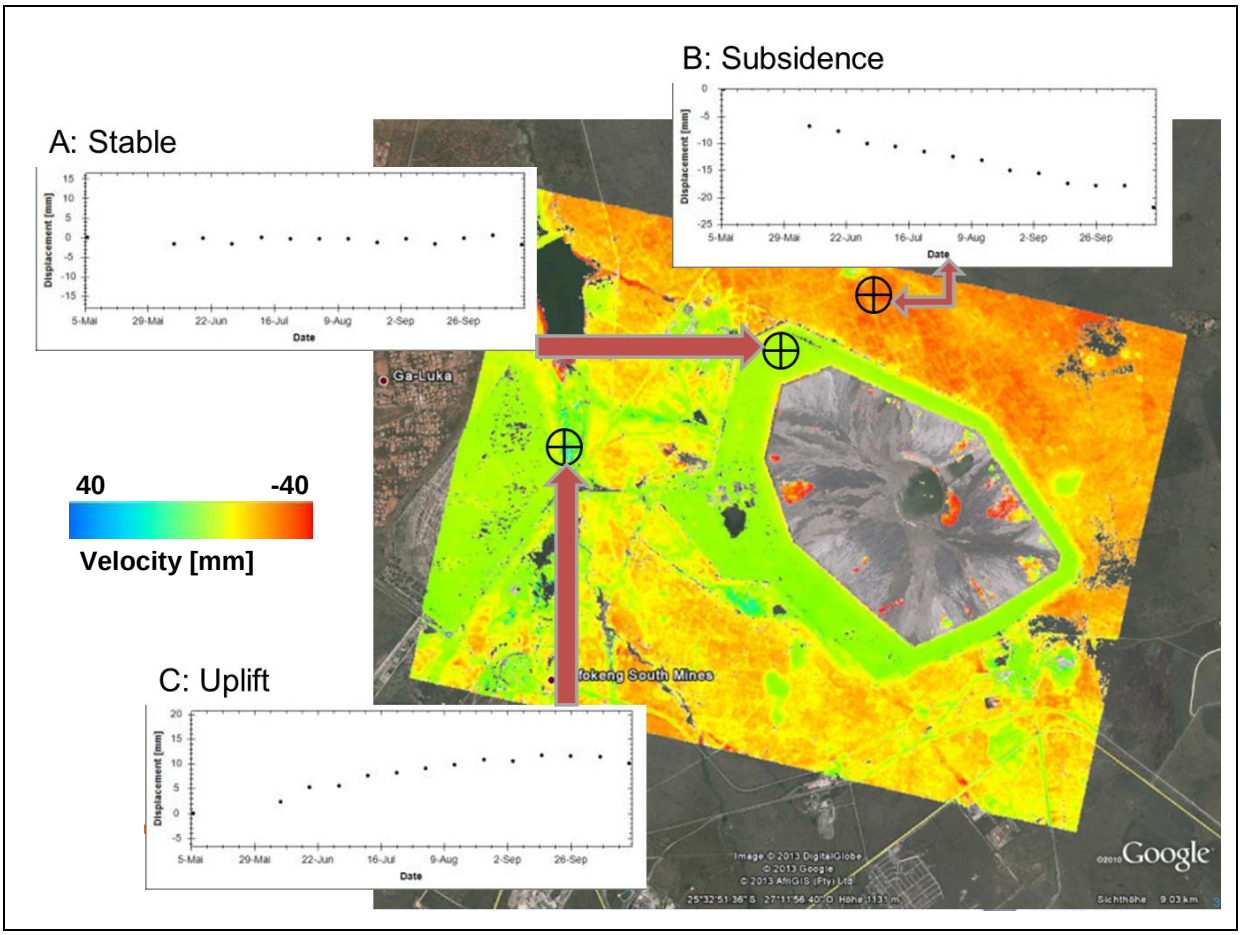

Figure 5.5: Vertical movement velocity and corresponding time series plot measured at a specific pixel, 14 scenes. A: Stable pixel, B: Subsidence pixel, C: Uplift pixel.
Source: © Airbus DS Geo GmbH, © Google Earth 2016

In conclusion it can be highlighted that the measurement of the surface change, up to 2.5mm, occurred using TerraSAR-X High Resolution SpotLight data. The high sensitivity of interferometric results regarding the swelling and shrinkage of soil was confirmed during this case study. The tailings pond walls are stable and no subsidence or upliftment that might cause any specific concern was detected.

5.3 Chuquicamata Mine case study

Chuquicamata open-pit mine is - by excavated volume - the largest open pit copper mine in the world, located in the north of Chile, just outside Calama at 2 850m above sea level, 215km northeast of Antofagasta and 1 240km north of the capital, Santiago. Flotation and smelting facilities were installed in 1952 and expansion of the refining facilities in 1968 made 500 000 ton annual copper production possible in the late 1970s. The mine has been owned and operated by Codelco, a Chilean state enterprise, since the Chilean nationalization of copper in the late 1960s and early 1970s. Its depth of 850m makes it the second deepest open-pit mine in the world (after Bingham Canyon Mine in Utah, United States). The strip map scene footprint of the TerraSAR-X imagery used during this analysis was illustrated in Figures 5.6 and 5.7.

The rationale for generating a SMM result over this area was to determine the following:

i. Stability of the ground surface area above the open-pit mine; and
ii. Stability of its dumping side walls.

Figure 5.6: TerraSAR-X SM footprint coverage (yellow polygon) of the study area (blue polygon). Source: © Google Earth 2016

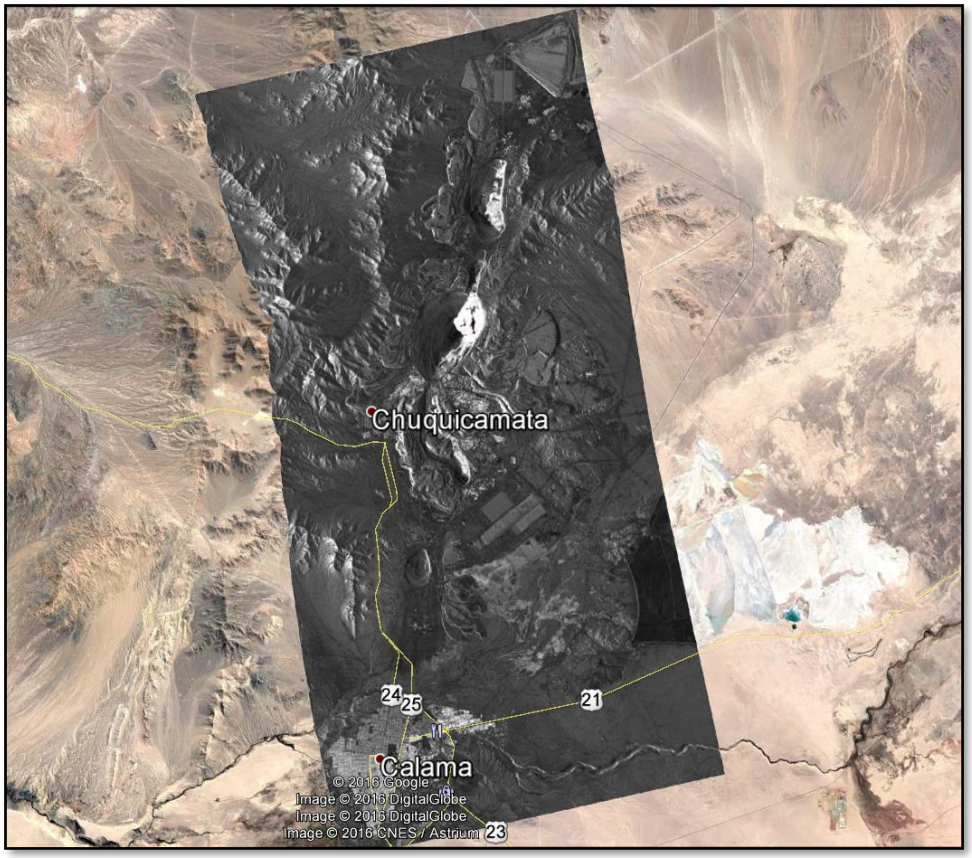

Figure 5.7: TerraSAR-X Strip Map scene, 17km x 34km subset over the study area. Source: © DLR e.V. 2014 and © Airbus DS / Infoterra GmbH 2014. Background imagery from Google Earth, © Google Earth 2016

In total, 52 scenes were acquired for the coverage in HH polarization for the time interval 18/06/2014 to 06/03/2016, see Tables 5.1 and 5.2 as well as Graph 5.2. All data were quality checked prior to their usage for the processing. Scientific TerraSAR-X orbit data with maximum accuracy were used for processing. For the interferometric TerraSAR-X SM data processing a multi-looking factor of 2 x 2 was applied and the final results were geocoded to 5m ground pixel size. The unique WorldDEM™ height model was chosen for initial height estimate.

Nr.	Date	Nr.	Date	Nr.	Date
1	18/06/2014	19	13/01/2015	37	21/08/2015
2	29/06/2014	20	24/01/2015	38	01/09/2015
3	10/07/2014	21	04/02/2015	39	12/09/2015
4	21/07/2014	22	15/02/2015	40	23/09/2015
5	01/08/2014	23	26/02/2015	41	04/10/2015
6	23/08/2014	24	09/03/2015	42	06/11/2015
7	03/09/2014	25	20/03/2015	43	17/11/2015
8	14/09/2014	26	31/03/2015	44	28/11/2015
9	25/09/2014	27	11/04/2015	45	09/12/2015
10	06/10/2014	28	22/04/2015	46	20/12/2015
11	14/10/2014	29	25/05/2015	47	31/12/2015
12	28/10/2014	30	05/06/2015	48	11/01/2016
13	08/11/2014	31	16/06/2015	49	22/01/2016
14	19/11/2014	32	27/06/2015	50	02/02/2016
15	30/11/2014	33	08/07/2015	51	24/02/2016
16	11/12/2014	34	19/07/2015	52	06/03/2016
17	22/12/2014	35	30/07/2015		
18	02/01/2015	36	10/08/2015		

Table 5.1: TerraSAR-X Strip Map scene dates used for the SMM analysis

	Orbit	Beam	Incidence angle	Polarization	Mode
TerraSAR-X	Asc 134	strip_009	~35°	HH	SM

Table 5.2: TerraSAR-X acquisition parameters

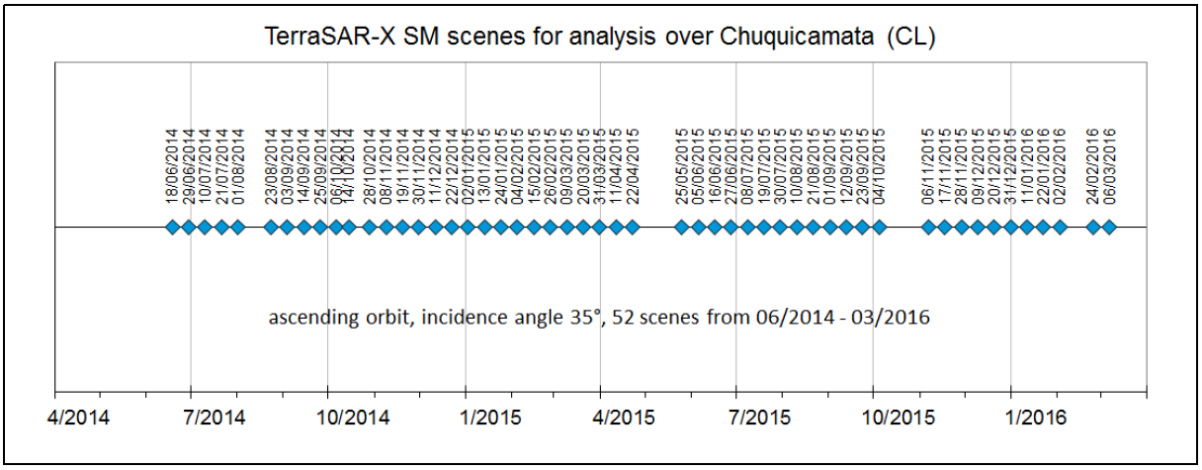

Graph 5.2: Scene time plot of TerraSAR-X SM scenes acquired for the Chuquicamata SMM analysis 06/2014 to 03/2016 (depicted as blue diamonds)

5.3.1 Processing conditions applied during the Chuquicamata SMM analysis

A multi-looking factor of 2 x 2 has been selected in order to prepare the data for SBAS processing. Therefore the intermediate processing results have a ground resolution of approximately 5m x 5m. Based on usable TerraSAR-X SM scenes the following SBAS network connections result (see Table 5.3, Graphs 5.3 and 5.4). Each connection between two points represents one interferogram. The time-position plot shows a normally distributed and highly redundant connection graph.

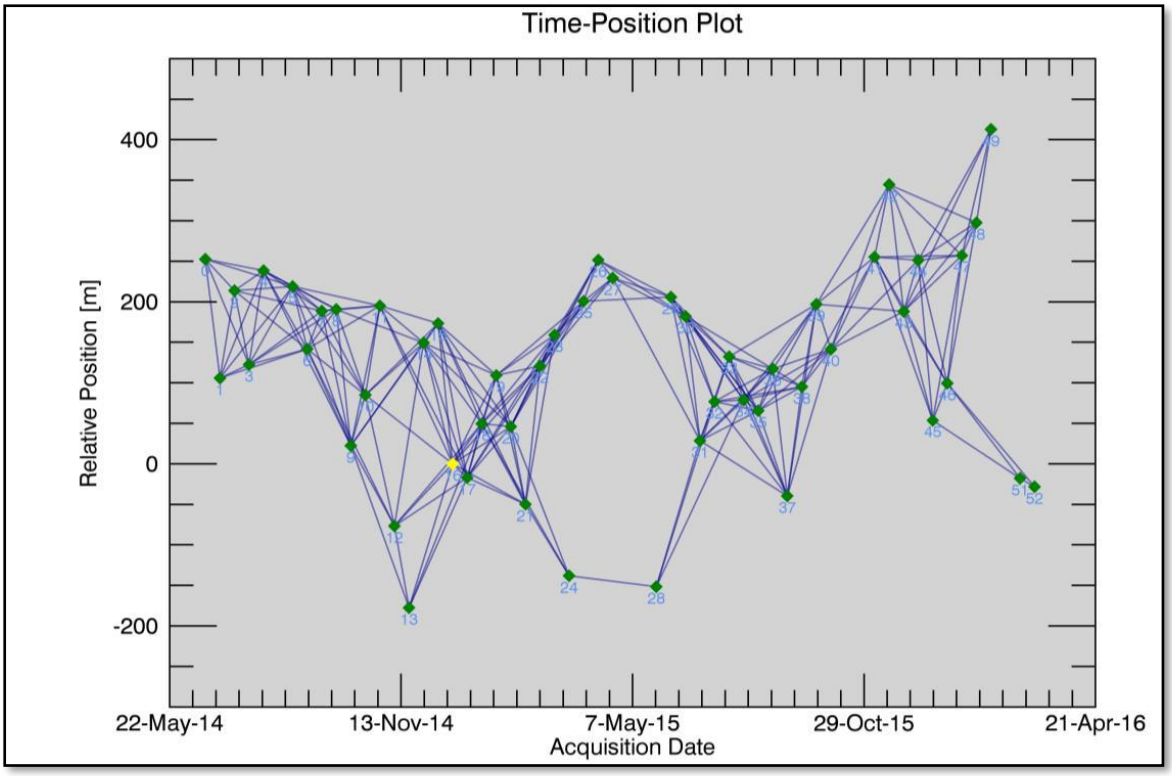

Graph 5.3: Time-Position Plot of SBAS connection graph for the process

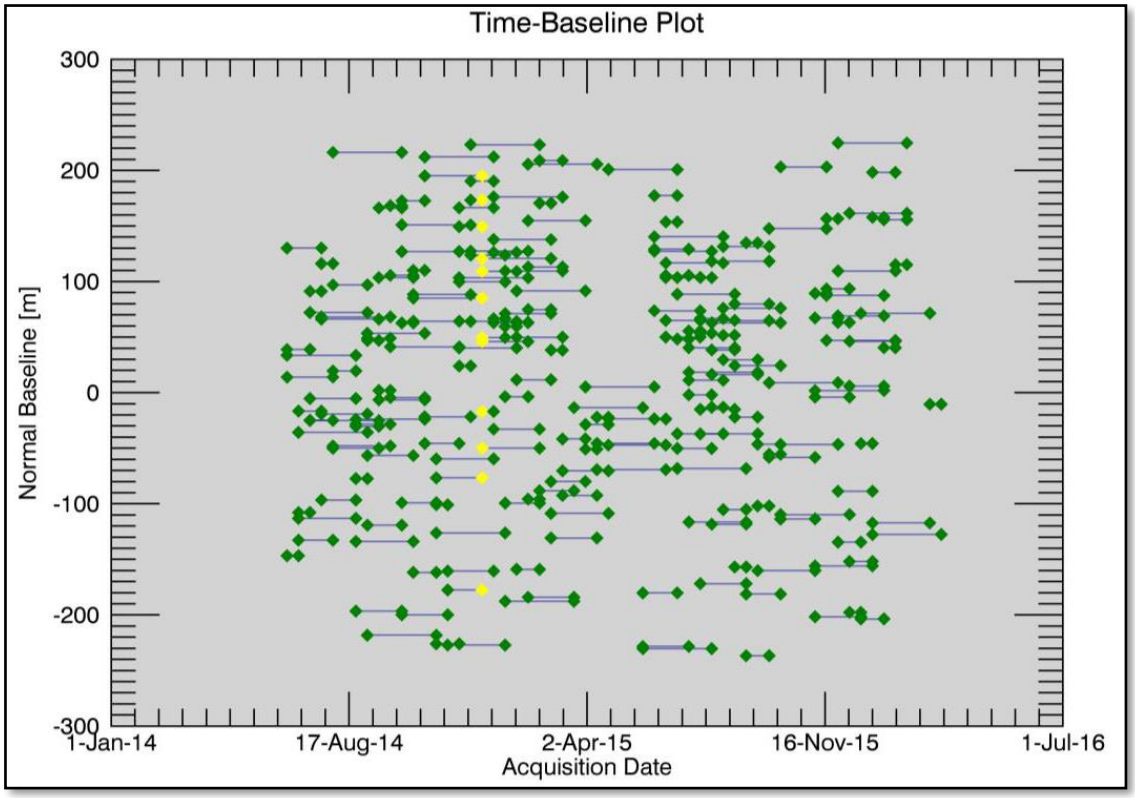

Graph 5.4: Time-Baseline Plot of SBAS connection graph for the process

Number of input images	Number of interferograms	Maximum absolute baseline [m]	Minimum absolute baseline [m]	Maximum temporal separation [d]	Minimum temporal separation [d]
52	223	233	5	66	11

Table 5.3: A summary of the processing parameters used for the Chuquicamata SMM analysis

5.3.2 Results and analysis of the SMM over the Chuquicamata mine

The result of processing as shown in Figures 5.8 and 5.9 was delivered as an average velocity map. A very high overall measurement pixel density was derived. Known constraints were present in areas with vegetation, where only a few measurement pixels existed. The overall characteristics of the results are summarised in Table 5.4 below.

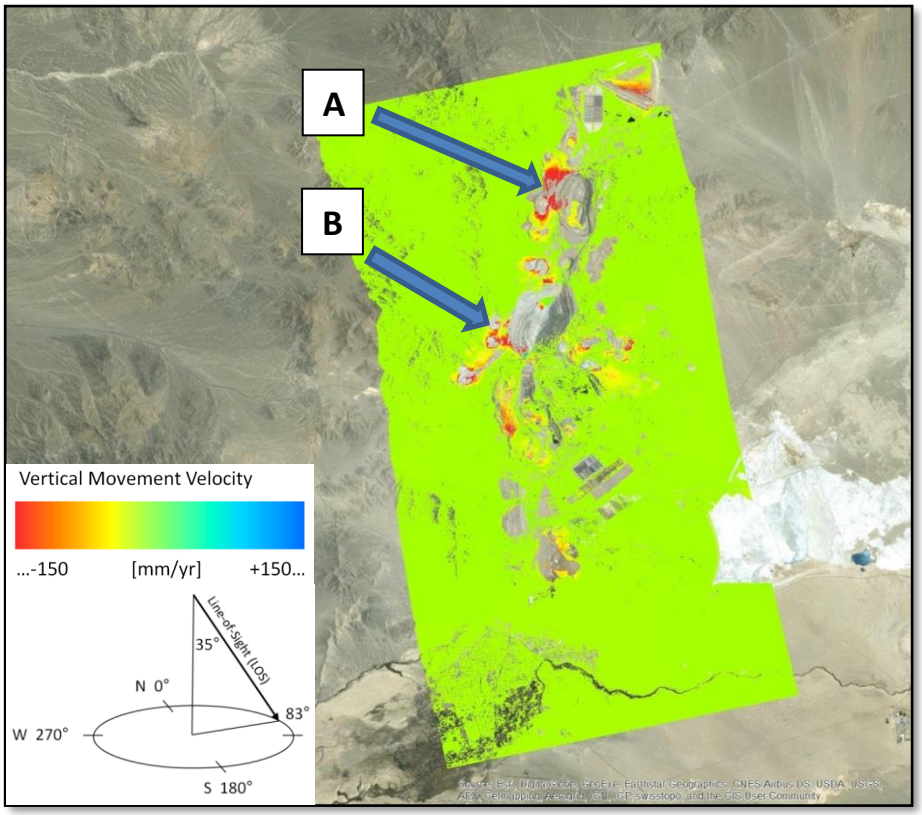

Figure 5.8: Vertical surface movement map of the area of interest (18/06/2014 to 06/03/2016) Source: © DLR e.V. 2016 and © Airbus DS Geo GmbH 2016. Background: Optical image from ArcGIS Online © ESRI 2016

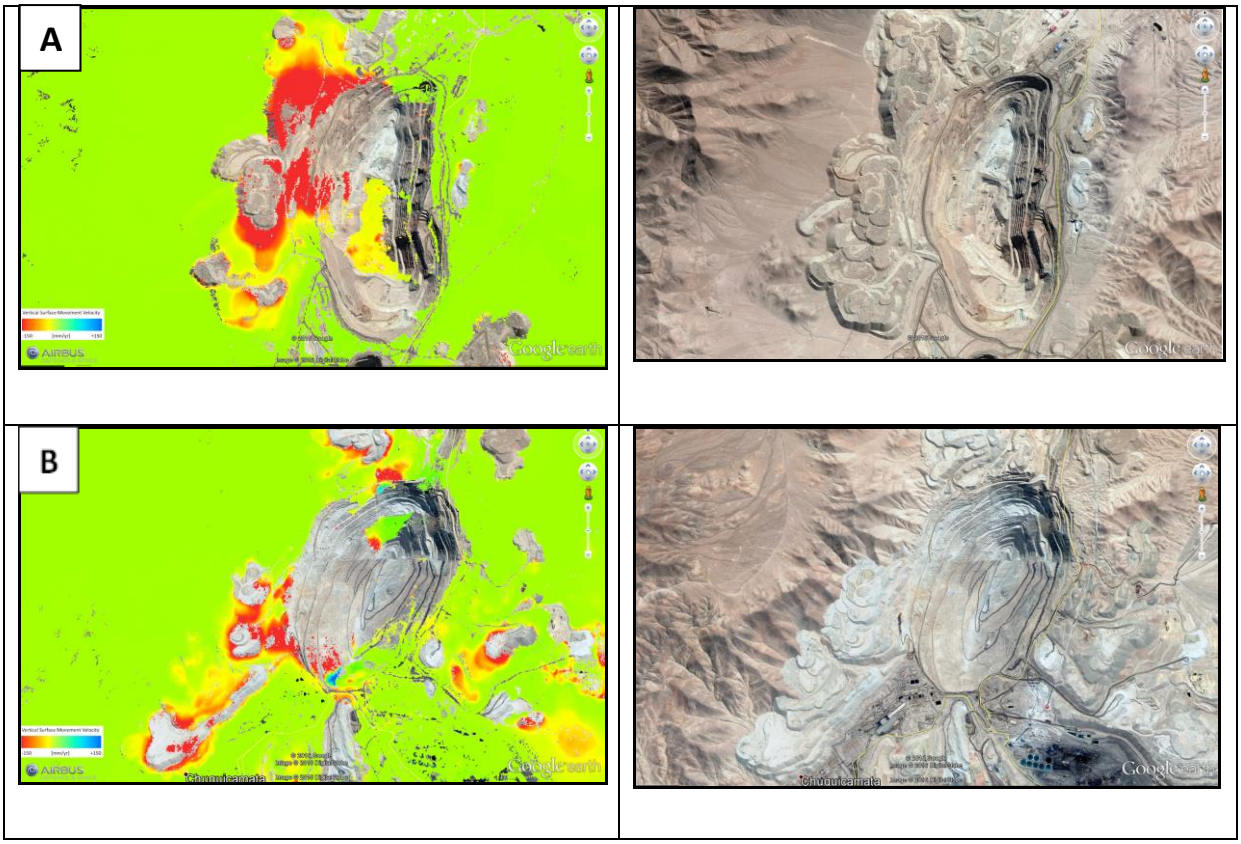

Figure 5.9: Vertical surface movement map of zoomed-in areas of interest [A] and [B] (18/06/2014 to 06/03/2016), as per Figure 5.8.
Source: © DLR e.V. 2016 and © Airbus DS Geo GmbH 2016. Background: Optical image from ArcGIS Online © ESRI 2016

Monitoring period	18/06/2014 – 06/03/2016
Average annual velocity	-0.7 mm/year
Maximum subsidence (annual velocity)	-1701 mm/year
Maximum uplift (annual velocity)	+202 mm/year
Measurement pixel density	ca. 40,850 pixel/km²

Table 5.4: Characteristics of the SMM result

In Figure 5.10 below, a three month time series interval over a zoomed-in area in the Chuquicamata mine illustrates the behaviour of subsidence and upliftment during this 21 month period analysis. The SMM time series plot diagrams in Figure 5.11 illustrate the displacement measured in mm over three pixels. Each pixel shows a continuous decrease from measurement point 0mm to -1 400mm from June 2014 until March 2016. Pixel [A] subsided to a measurement point of -350mm, pixel [B] to -1 350mm and pixel [C] subsided to -400mm. In Figure 5.12 another three pixels

were measured. The pixel [D] subsided to a measurement point of -250mm, pixel [E] provides a reversed result of an upliftment surface area and was measured at 400mm. Pixel [F] is another subsided result and was measured at -360mm. In Figure 5.13 measurements were done over another area within the Chuquicamata mine compared to Figures 5.11 and 5.12. All three areas resulted in subsidence curves on the plot diagrams. The pixel [G] subsided by -230mm, pixel [H] subsided by a significant -1 900mm and pixel [I] subsided by -330mm.

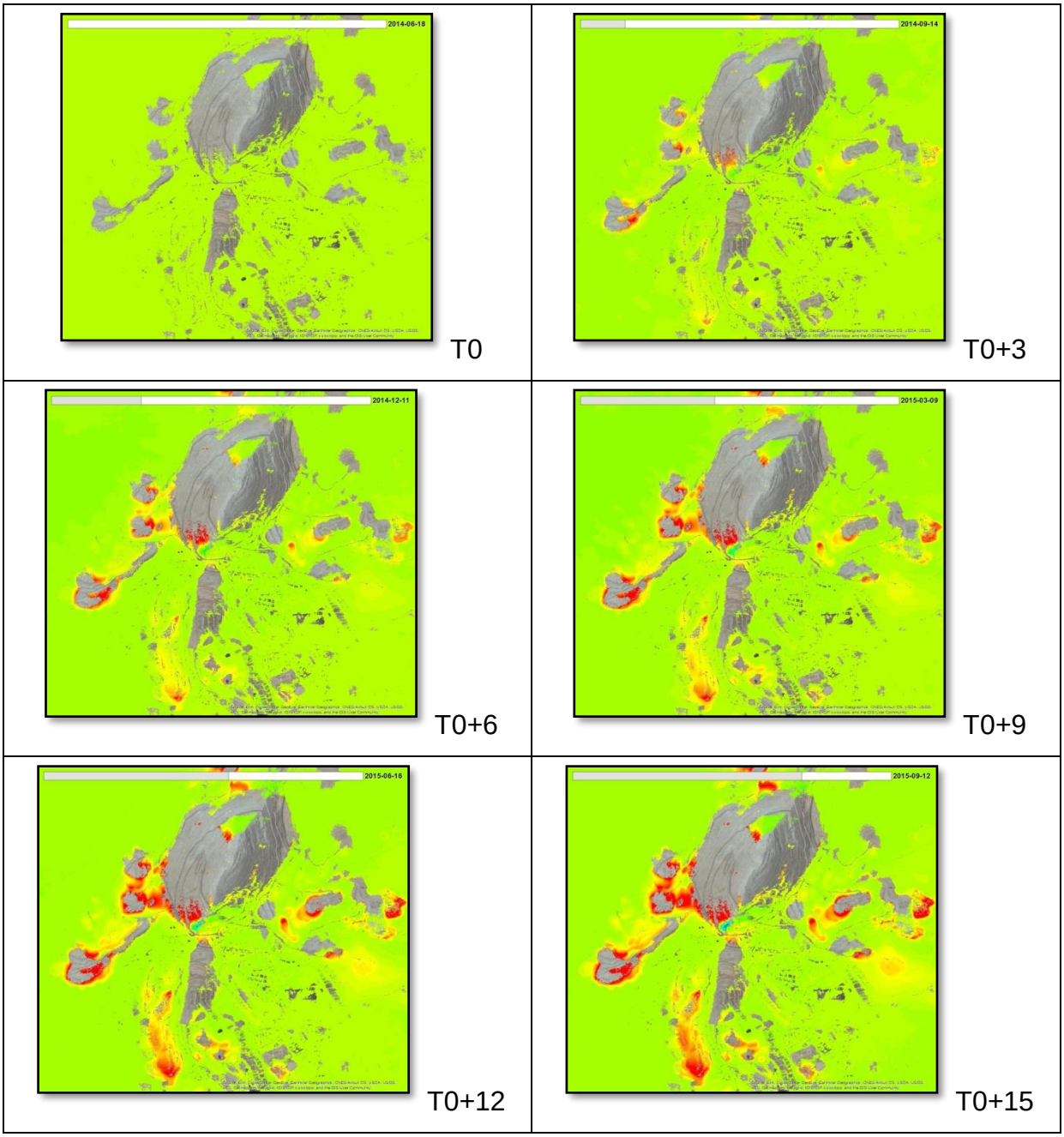

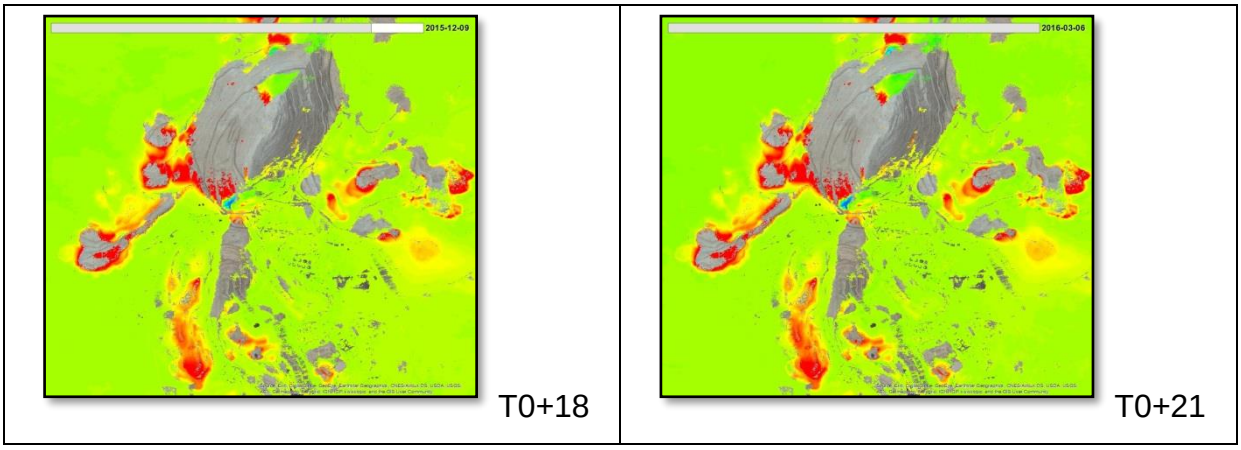

Figure 5.10 Time series SMM analysis for over 21 months (T0 to T21) [Jun 2014 to March 2016], Movement scale (mm): Blue upliftment, Green stable or low upliftment, Yellow low subsidence, Red high subsidence.
Source: © Airbus DS Geo GmbH

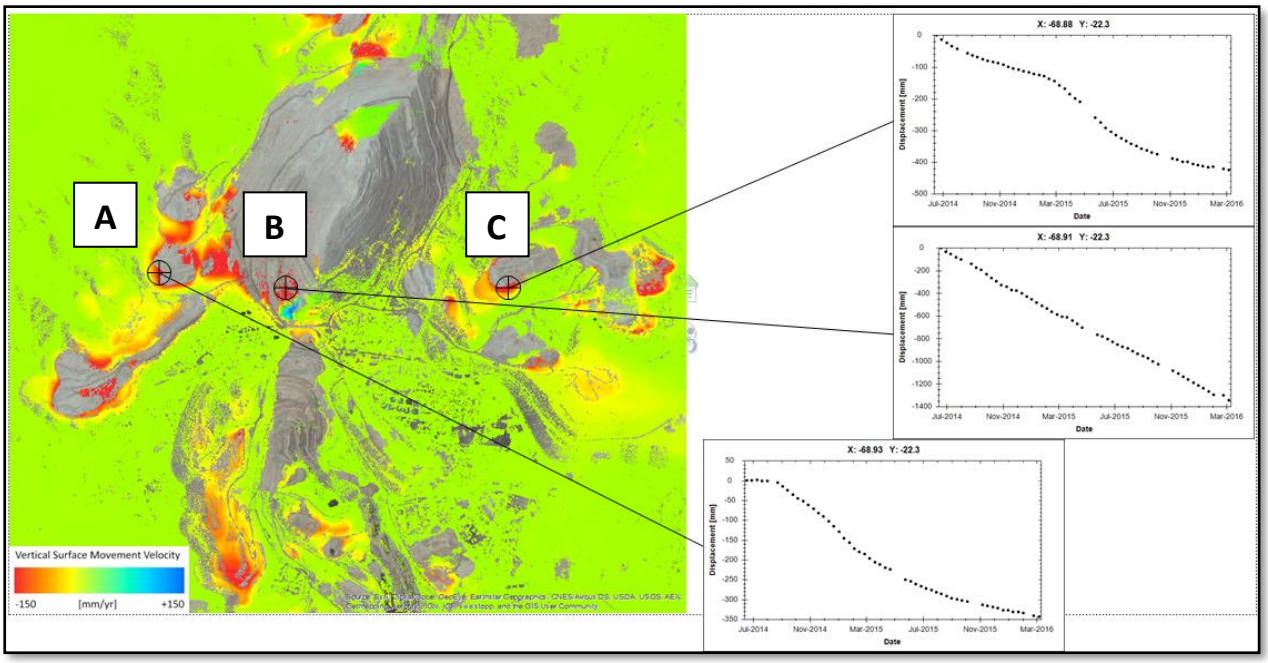

Figure 5.11: First SMM Time series plot diagrams over three pixels illustrating subsidence areas over the Chuquicamata mine.
Source: © Airbus DS Geo GmbH

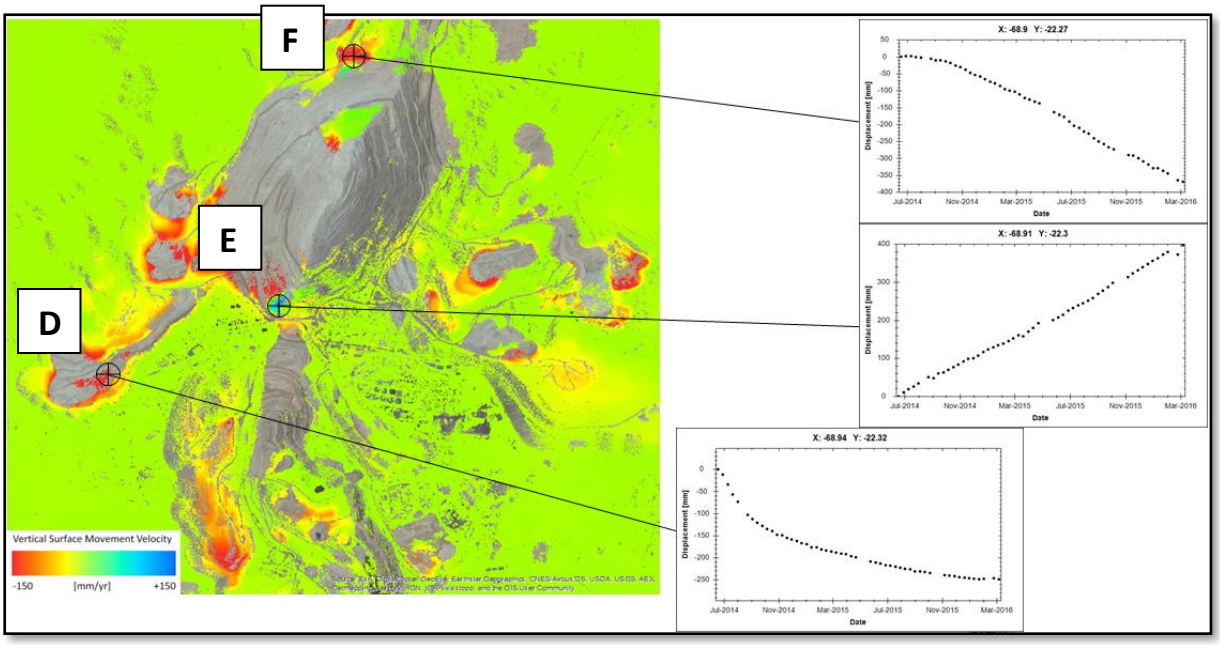

Figure 5.12: Second SMM Time series plot diagrams over three pixel areas, 2 subsided [D,F] areas and 1 upliftment [E] area over the Chuquicamata mine.
Source: © Airbus DS Geo GmbH

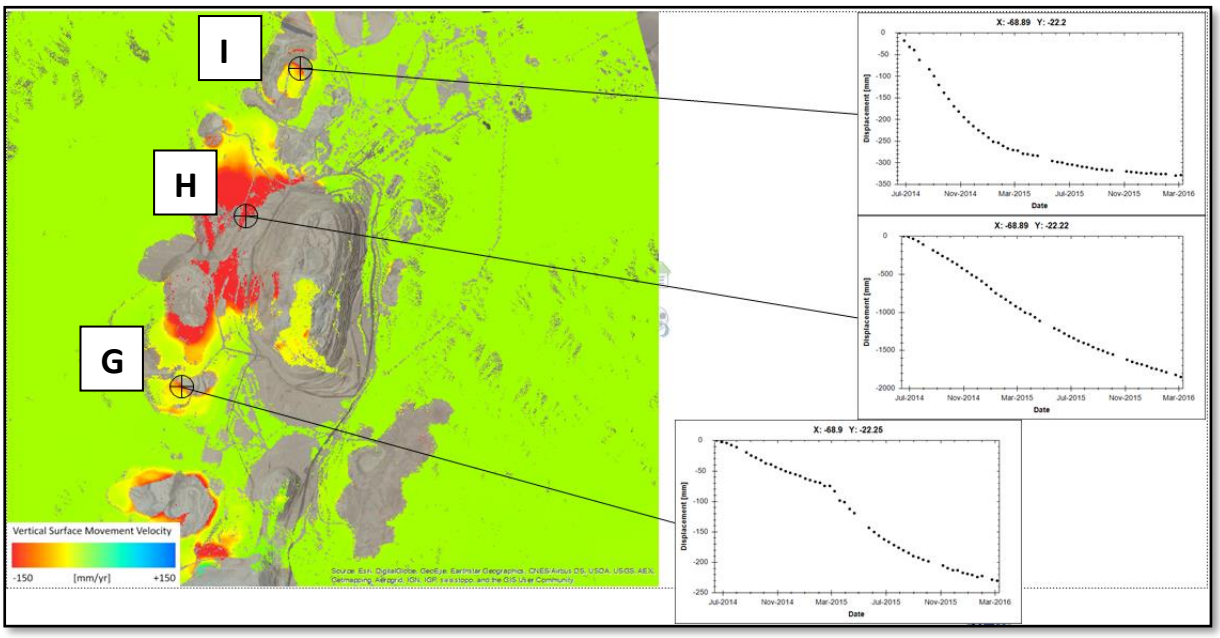

Figure 5.13: Third SMM Time series plot diagrams over three pixel areas, all three illustrate subsidence [G,H,I] over the Chuquicamata mine.
Source: © Airbus DS Geo GmbH

The results and analysis over the Chuquicamata mine using 52 Strip Map scenes from TerraSAR-X to generate a SMM product, illustrated by using a vertical movement map, highlighted interesting facts over the area. Various surface areas above the open pits showed moderate to significant subsidence. It was also evident that some of the side walls (slopes) of the open pits showed subsidence [B,F,H], thus a level of instability. The subsidence measured at pixel [B] showed an upliftment at pixel [E] only a few metres away in a southern direction. The explanation for this might be that as the soil subsides at [B] it pushes the soil upwards at [E], thus the potential reason for the upliftment. Subsidence at some of the mine heaps was also detected, especially their side walls as per pixels [A,C,D,G,I]. The explanation for the latter might be the dumping of soil onto these heaps, introducing extra mass and pressure, resulting in the subsidence of their side walls or adjacent areas (see Figure 5.14).

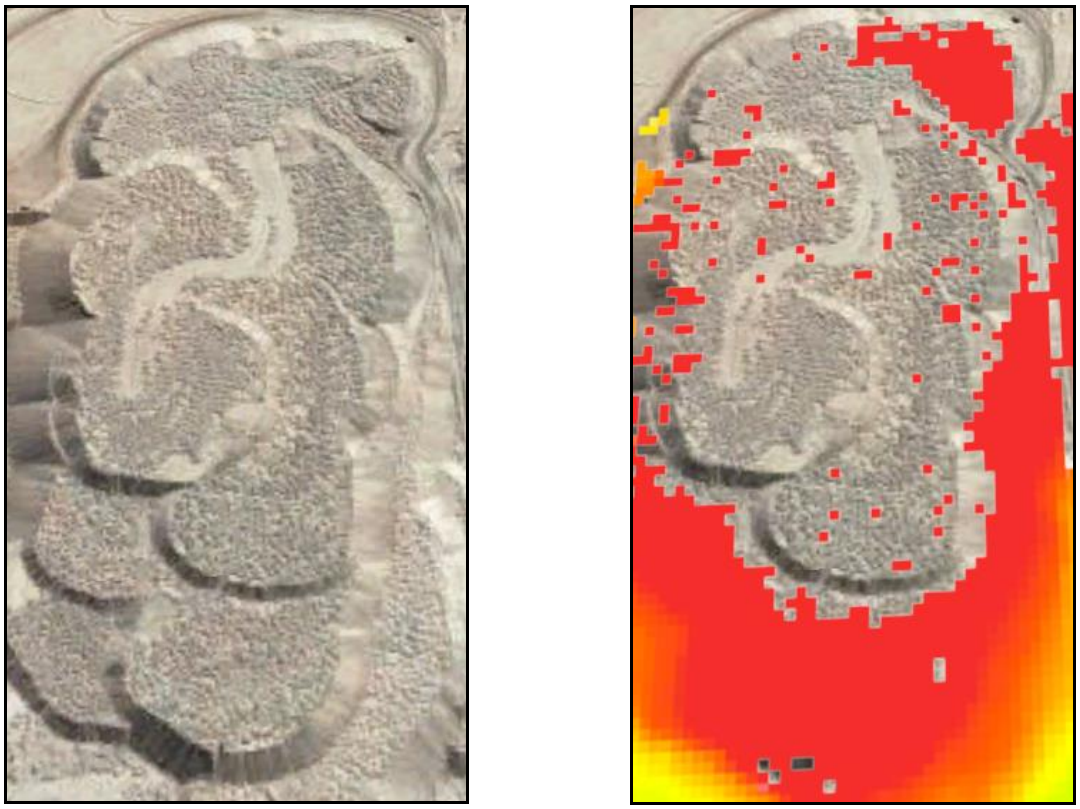

Figure 5.14: Mine heaps at Chuquicamata mine illustrating the high subsidence detected over these areas during the SMM analysis.
Source: © Airbus DS Geo GmbH. Background image from Google Earth © Google Earth 2016

5.4 Conclusion

In this chapter SAR technology from the TerraSAR-X satellite was introduced and applied over two case studies. The first case study was over the Royal Bafokeng tailings pond near Rustenburg, South Africa, followed by the open copper surface mine Chuquicamata Mine located in Chile. These case studies showed evidence that SAR technology available from a satellite platform such as TerraSAR-X can contribute significantly to providing large area surface measurements within the range of millimetres. The accuracy of these measurements over a specific period of time creates a baseline of geo-spatial information for mines to understand the behaviour of the surface stability within the open pit mine as well as its surrounding areas. The stability of side walls, heap dumps as well as the effect of blasting over certain areas can be measured over time. This technology is also relevant to the monitoring of the geological stability of the surface that surrounds a mine, for example the formation of sinkholes due to dolomite.

The applied SMM product from TerraSAR-X is an accurate and consistent measurement system that provides an excellent large area surface stability overview over an area such as a mine with millimetre accuracy. SAR is a technology solution that can complements optical applications. Combining SAR and optical solutions provides a wealth of spatial information solutions for mine monitoring.

CHAPTER 6: DISCUSSIONS, RECOMMENDATIONS AND LIMITATIONS

6.1 Introduction

In this chapter the researcher will share some thoughts in order to put the results of previous analytical chapters into perspective. The perspective of RS as an aid to support mine operations and a tool to monitor primary and secondary environmental factors caused by the mine, directly or indirectly, will be highlighted. Limitations within the study are pointed out as well. This chapter will finally conclude with some recommendations for mine and environmental monitoring as well as a futuristic outlook for RS technologies and their potential to influence further research on this topic.

6.2 Discussions

6.2.1 Contribution of remote sensing to mine operations

RS as a technology to observe an object from a distance from space enables an instantaneous bird's eye view over large areas. The optical satellite sensors provide various combinations of spectral and radiometrical values that can be applied to classify specific features on the land surface (Mather and Koch, 2011; Lillesand et al, 2007; Kramer, 2002; Floyd and Sabins, 1986; Chen, 2012; Weng, 2011).

SAR satellites provide interferometric time series analysis that exploits phase information of the SAR satellite active signal. The X-band signal of the TerraSAR-X satellite provides measurement accuracies of 2mm to 4mm, based on at least 15 images (Anderson, 2016).

With the focus on open pit mining operations *inter alia* include the following key activities, as discussed in section 2.2.2 (Hustrulid and Fernberg, 2010):

- Drilling
- Blasting
- Loading
- Hauling
- Primary crushing
- Secondary crushing
- Grinding

6.2.2 The contribution of optical satellite RS to open pit mine operations

Landsat 8 as a medium resolution satellite provides a 180km x 180km scene size with a 16 day revisit cycle. The spectral bands available from this satellite include 10 multispectral bands which include wavelengths in the visible, NIR, SWIR and thermal range, further complemented by a panchromatic band. This satellite is an ideal sensor for macro level land cover classification (Thompson, 2015). The contribution of this satellite is not so much directly at mine operations level, thus to measure a single heap of ore as example. Its contribution is during mineral exploration (Ali and Pour, 2014; Ducart et al, 2016) and planning (Hustrulid and Kuchta, 2013). The value of Landsat 8 was further discussed in section 6.2.4 as a contributor within the methodology that was introduced during this study.

The contribution of RS to open pit mine operations is primarily embedded in the very high resolution optical satellites. The Pléiades 1A and 1B satellites of Airbus Defence and Space were introduced in sections 3.3.2, 3.3.3 and 4.3. Applying different acquisition modes such as monoscopic and stereoscopic image collection to the satellite produces different products relevant to mine operations. The monoscopic acquisition is a single image acquired over the area of interest, such as the mining area. These monoscopic acquisitions can be acquired at high temporal intervals, for example, the study areas were monitored weekly as from mid-2014. This stack of temporal data provides a spatial library for the mine management to plan and confirm specific mine operations. In section 4.3.2.3 the spatial confirmation of these mine activities was highlighted using five monoscopic Pléiades imagery over each mine to visually confirm drilling activities, excavations, hauling, waste dumps and

iron ore dumps. The satellite image provides a snapshot in time over the whole mine area. Each pixel of the satellite image is spatially georeferenced using the various GCP surveyed points that were established at each mine. The latter provides high geometrical accuracies that are relevant to the mine operations (Lůck, 2015).

As a practical example, a mine manager can visually interpret drilling holes on the satellite image as well as obtaining its coordinates. This spatial reference then confirms the blasting activities within an allocated zone in the mine area during a specific period. Using the temporal data stack the mine manager can then further confirm the correct placement of the excavators (shovels), loader and dumping activities. Furthermore, mines do sometimes sub-contract companies to move waste dumps from one area to another. Using the temporal data stack of this very high resolution satellite imagery makes it possible for the mine management to confirm if a sub-contractor is indeed moving the soil correctly as well as the progress of such an activity.

The stereoscopic collection of data enables the technical capability to create a very high resolution elevation model over a specific area of interest. In section 4.3.3 this concept was discussed in detail with several area examples to demonstrate the value of such a dataset. Stereoscopic data provides the opportunity to create a digital surface model (DSM) and/or digital terrain model (DTM) over the area. During this study three one metre DTMs were created, two over Sishen mine and one over Kolomela mine. The primary contribution of these DTMs was their use for volumetric calculations. Mines can use this RS elevation product to measure in relevant accuracy terms the volume over various types of areas, as discussed in section 4.3.3.2. These calculations complement the traditional mine surveying activities done at mine level. Applying stereoscopic satellite imagery to generate DTMs for the volumetric calculation of a specific area can be used as interim measurement solution. This will reduce the number of actual ground surveying work necessary during each operational year at the mine. Comparing periodic DTM datasets creates accurate volume change products. These products will highlight the changes in height values between different time stamps. Such change products can for example indicate if a specific dumping area recessed or if it increased over time, as per section 4.3.3.4.

6.2.3 The contribution of SAR satellite remote sensing to open pit mine operations

In chapter five two case studies of SAR applications were demonstrated. Applying a time series interferometric analysis over the Royal Bafokeng tailings pond near Rustenburg, South Africa and the open surface mine Chuquicamata Mine in Chile introduced valuable spatial information about the surface stability over a mine area and its surroundings. Activities such as drilling, blasting, hauling of soil and the dumping of it onto large heaps pose the risk of subsidence and upliftment of the surface. These subsidence and upliftment measurements can be early indicators of a stable/unstable surface (Anderson, 2016). The absolute measurement accuracy of the TerraSAR-X satellite as described by Anderson (2016) in section 3.3.4 to provide a SMM product of 2mm to 4mm in vertical velocity measurement can be described as cutting edge technology.

The value of the SMM product for mine operations is to measure and to know what is the stability of the surface over specific topographic features within the mining area and its surroundings. As per section 5.2, is the side wall of a slime dam stable or is the wall subsiding, thus posing a risk of collapse as in the profound cases of the Merriespruit tailings dam and Bafokeng tailings dam disasters as local examples refers. The Merriespruit tailings dam disaster occurred on the night of 22 February 1994 when a tailings dam failed and flooded the suburb of Merriespruit, Virginia, South Africa, destroying eighty homes and killing seventeen people. When the Bafokeng platinum tailings dam in Rustenburg, South Africa failed in 1974, liquefied tailings flowed into an adjacent shaft, killing 13 people underground.

The Chuquicamata Mine in Chile is a good example to illustrate the monitoring of the stability of mine heaps. Several heaps that were measured showed subsidence. Slope subsidence and upliftment in specific areas within the open cut mine area were also detected. Several case studies are available that describe the effects of collapsed slopes of open cut mines, collapsed waste dumps and collapsed surface areas (Harries *et al*, 2006; Szwedzicki, 2010; Gu *et al*, 1998). Applying the SMM product solution over mining areas certainly contributes to the management of risks and the understanding of the overall surface stability within the mining area and its surroundings.

6.2.4 Remote sensing as an aid to environmental impact monitoring

In section 2.2.3 detailed discussions around primary and secondary environmental factors that are influenced by mine activities were introduced. The importance of environmental impact assessment (EIA) studies during the exploration and pre-establishment phase was also highlighted, yet continuous monitoring and assessment during mining and rehabilitation phases are certainly equally important (Emuze and Hauptfleisch, 2014; Maystadt *et al,* 2014; Ongondo, *et al,* 2015; Hendryx, 2015; Gwimbi and Nhamo, 2016; Zhang *et al, 2015;* Appiah and Osman, 2014).

The availability of Landsat series data since the 1970s provides a wealth of historical data for temporal change detection products. These products have been an ideal baseline to understand changes over large areas for more than 40 years (Floyd and Sabins, 1986). During this study Landsat 8 imagery was used to build a composite of land cover classes using at least 18 datasets collected during 2013 – 2014. These images enabled 72 national land cover classes and were then used to select a primary of 14 classes to be evaluated during this study (Thompson, 2015). The contribution of this RS data at medium resolution level provides a sufficient fundamental baseline layer to understand the dominance of specific land cover classes over a specific area.

These classes over the Kolomela mine, as discussed in section 4.2.2.1 revealed that over the 1 755km² area a dominance of SHRUBLAND/GRASS surrounds the open pit mine and has a coverage of at least 94% over the area. This can also be interpreted as a large open area and natural land which surrounds the majority of area around the open pit. Closer to the actual open pit mine an estimated 2.56% of this area is the actual open pit mine. Thus, the primary environmental impact of the soil removal for mining purposes compared to the greater study area is only 44.9km². Combined with MINE_WATER and MINE_BUILDINGS a total of 46km² (2.6%) was calculated.

Compared to the above, the Sishen mine, as discussed in section 4.2.2.2, revealed that over the 1 680km² area a dominance of SHRUBLAND/GRASS also surrounds the open pit mine and has a coverage of at least 90.25% over the area. This can

also be interpreted as a large open area and natural land which surrounds the majority of area around the open pit. The actual open pit mine calculates to an estimated 4.82% of this area. Thus, the primary environmental impact of the soil removal for mining purposes compared to the greater study area is 81km², almost double the size of Kolomela. Combined with MINE_WATER and MINE_BUILDINGS a total of 84km² (5%) was calculated.

The understanding of human activities that had an impact on the environment was calculated as the sum of all the BUILT_UP classes. Thus, activities not related to the primary mine operations. These classes define townships, industrial and commercial areas, residential areas, schools and sport facilities and other related manmade objects as discussed in section 4.2.2. Kolomela mine's secondary impact classes calculate to 9.07km² (0.52%) and Sishen mine's calculate to 13.24km² (0.79%) over each study area. The question that can be asked is if a positive correlation exists between the size of the primary open pit mine area and its relationship to the size of the BUILT_UP classes. Thus, the larger the open pit mine, the higher the likelihood for larger BUILT-UP areas, thus more secondary environmental impact within a mining area. The Sishen mine area is 81km² compared to the 44.9km² of Kolomela mine, thus 80.4% larger. The Sishen mine BUILT_UP classes cover an estimate of 13.24km² compared to the 9.07km² of Kolomela, thus 45.98% more BUILT_UP class areas. To prove this correlation further studies are required over more open pit mine areas, thus offering an opportunity for further research.

Applying medium resolution satellite imagery to create a fundamental baseline land cover layer provides a wealth of spatial information enabling the mine management team to understand the relationship between primary and secondary activities and their impact on the environment. In the next few paragraphs the contribution of very high resolution optical imagery will be discussed as an aid to environmental impact monitoring.

The very high resolution imagery used during this study was acquired from the Pléiades 1A and 1B satellites. The specifications for these satellites were shared in section 4.3. The study analysed the monoscopic time series data and the products that can be derived from stereoscopic data. The monoscopic data provides the opportunity to derive very high resolution land cover classes over the study areas

and then to calculate the changes over time. These land cover change products illustrate the behaviour of an area over time in order to understand if natural vegetation increases, decreases or recovers *versus* the stress factors of manmade features and/or activities. The land cover classes evaluated during this study were described in section 4.3.2.2 and focused on bare soil, vegetation, asphalt/mine and waterbodies classes. The calculations focused on the bare soil and asphalt/mine classes due to the dominance of these classes within both mining areas. During this evaluation four case studies were introduced to illustrate the monitoring of changes in a specific class type due to specific activities. These changes were primarily a decrease in bare soil and an increase in the asphalt/mine class due to human activities such as introducing a new power plant, new mining dumping sites and a new parking area.

The monoscopic change products based on automated algorithms and processing chains were illustrated in section 4.3.3.4. These change products include vegetation change, brightness change and absolute activity change. Applying these algorithms over at least two timestamp satellite scenes provides useful information to detect and interpret changes. These products provide fast solutions to detect changes such as vegetation growth over newly rehabilitated areas and fresh soil exposed due to the removal of vegetation (newly cleared areas); and enable the monitoring of newly established infrastructure such as roads, buildings, slime dams, etc.

The stereoscopic data introduced height products in the form of digital elevation products. These products add a third dimension to the data structure and enable the calculation of volume as well as the detection of changes in height values over specific features such as mine waste dumps and/or stock piles when compared in different time periods, referred to in sections 4.3.3 and 4.3.3.4.4. Elevation models provide insight into the mine operations from *inter alia* a productivity point of view. The volumetric calculation of the movement of soil, the growth of valuable stock piles such as coal or iron ore *versus* waste dumps, the changes in volume over recessed areas due to excavations are all examples of relevant mine monitoring solutions. Using this third dimension of calculation also provides the opportunity to calculate the volume of top soil removal, the volume of mine water in slime dams/tailings dams, hydrological simulations which can be useful to determine the flow of water

during the collapse of a mine dam or during natural floods and the potential effect of water contamination during such an event.

The contribution of SAR to environmental monitoring is *per se* its SMM product. If a SMM result of a slime dam indicates that the side wall is showing high subsidence and might collapse, then the effect of such a disaster can be pro-actively calculated to determine the affected areas during such an event. The latter can be achieved by adding an elevation model to the area, thus the concept of technology integration. Furthermore, the monitoring of the stability after recovery plans have been introduced to stabilise such a side wall can then also be monitored by SMM to determine whether they have been successful or not. The same concept can be applied to side walls of open cut mines and waste dump areas. Thus, SAR can contribute pro-actively to determine if a disaster might happen due to instability over certain surface areas. Acting against such instability in time can avoid a potential environmental disaster and the loss of life.

6.3 Limitations during this study

The researcher is of the opinion that this study contributed to the realization that SAR and optical data from satellites can contribute as an aid to monitor mines and the impact of its activities on the natural environment. The focus of this study was to develop a methodological workflow as an aid for mine operational monitoring and detection of environmental changes. The study was based on literature and an analysis based on satellite imagery and software image processing. It was recognised that further field work verification of the analytical results would have contributed further to this study and its methodology. Such field work over these operational mining areas was not possible due to safety and security regulations. Another point to be highlighted is that the open pit mines within this study are located in established areas with good infrastructure and residential towns nearby. Applying this methodology also over more remote and underdeveloped countries to understand the primary and secondary impact factors within these environments creates the opportunity for further research.

The study focused primarily on open pit mines with limited temporal analysis. The Landsat 8 classification was based on 2014/2015 imagery, yet its purpose was to extract a reliable land cover baseline from multiple scenes as opposed to a change detection product. The monoscopic imagery from Pléiades was acquired during 2015/2016 with a selection of 5 scenes per mine. The aim was to select the scenes within a quarterly period to include seasonal vegetation changes, yet a perfect stack of data over Kolomela mine was not available, especially the time difference between the 30/03/2016 and 28/12/2016 scenes. The prime focus of this study was to detect environmental changes due to human impact opposed to natural changes. Analysing environmental changes based on monthly comparisons would have been the ideal, yet the intense image processing requirements from a data volume perspective was not practical for the researcher. The radiometrical values available in the Pléiades imagery during classification introduced typical challenges such as the mix of waterbodies and certain shadow classes. The predominantly arid conditions over each mine area made it difficult to ensure an absolute classification between bare soil and sparsely spread vegetation. It is recognised that improvement within the distinction between bare soil and vegetation could have been achieved through detailed segmentation classification using object orientated classification methods. Such software, however, was not available to the researcher but holds potential for further future studies.

The stereoscopic contribution from Pléiades was demonstrated with a limitation of two comparison pairs over Sishen mine (2014 *versus* 2016*)* and one stereoscopic acquisition over Kolomela mine (2016). The availability of stereoscopic imagery within the Airbus Defence and Space archive was limited as it requires to be collected specifically within a stereoscopic programming collection mode. The processing and generation of a very high resolution elevation model is an intense and technically advanced image processing technique. Thus, it is recognised that additional stereoscopic data collected quarterly over at least a one year period would have provided useful additional results, yet this was not possible during this study due to the potential costs involved.

It is recognised by the researcher that not only open pit mining (surface mining) exists, but that sub-surface (underground) mining is also important, for example room and pillar mining. The potential to apply SAR technology to monitor the stability

of the surface over these underground mines was not addressed. The problem of acid mine drainage (AMD) holds a serious threat to the environment (Mwiinga, 2011; Akcil and Koldas, 2006; Harries, 1997). Applying satellite surface monitoring technology such as Surface Movement Monitoring (SMM) to address AMD and its potential value from a spatial information perspective was not addressed during this study.

The limitations of satellite monitoring services, due to high costs, will be discussed in the next paragraphs. To enable a satellite monitoring programme over a mine is costly as most of these dedicated satellite programming services are offered on a commercial basis. It is known that various space agencies provide earth observation satellites at no cost (http://gisgeography.com/free-satellite-imagery-data-list/). Most of these services can be accessed through an online archive catalogue. Thus, archive data can be selected and downloaded and is certainly valuable from a research perspective. The latter is however limited from an operational point of view. These “data democracy” programmes are not designed to address various *ad hoc* customised target monitoring requests opposed to commerical service providers. It is important that each mine should consider a monitoring programme that is suitable and sustainable within its avilable budget. Environmental, health and safety monitoring for mines in South Africa is mandatory and must be addressed through their Environmental Management Plans (DEAT, 2004).

It is important to do responsible market research and to consider various technological options available in the market. Cost associated with traditional environmental and operational surveys/ inspections needs to be measured against time, consistancy, resource availability, safety, extent of the obeservation/measurement, etc.

In conclusion, although budgets are a limiting factor for various mines due to the fluctuation in various commodity prices over the past few years, perceptions of unaffordable services from space technology platforms need to be appropriately investigated and awareness of these solutions will certainly be relevant in order to modernise environmental monitoring activities in the future.

6.4 Recommendations

During this study various principles of RS were addressed. The contribution of optical as well as SAR space based technologies as an aid for mine monitoring and environmental change assessment was highlighted. These technologies provide the capability to capture large area snapshots over the full mining area and its surroundings. Monitoring these areas can be done in a high temporal mode, such as daily, weekly, monthly or quarterly frequencies. The temporal acquisition is rather a question of affordability opposed to limitation of the satellite accessibility. It is recommended that mine management collaborate with experts in the field of geo-information and appropriate service providers of such a satellite observation service to gather factual information to establish an appropriate business model that will fit the requirements of the mine.

The designed workflow model introduced in this study as per section 3.2, Figure 3.1 provides the rationale for a multi-sensor approach and for combining satellite technologies to produce a holistic spatial result. Such a result can empower mine management during decision making procedures that affect mine operations, as well as provide them with a bird's eye view of the mine's surroundings and associated changes.

Although this study focused on satellite earth observation technologies, it is recognised and recommended that an integrated approach to technology systems should be performed. Technologies such as airborne LIDAR for precision reference data, drone technologies, ground measurement and scanning systems all complement each other. These technologies are certainly not disregarded by the researcher. The challenge is rather to design a technological approach that will fit the mine requirements and to ensure a sustainable integrated approach that is feasible. It is certainly recommended that satellite observation technologies also be considered to form part of such an integrated approach.

CHAPTER 7: SUMMARY, FUTURISTIC OUTLOOK AND CONCLUSION

7.1 Summary

This study declared a problem statement that mining introduces several primary and secondary environmental challenges within its geographical area. Thus, the rationale for this study was to determine if satellite based RS as a spatial source of information can contribute, through a designed methodological approach, as an aid to understanding open pit mine operations and monitoring their impact on the environment. Applying RS imagery over open pit mines and analysing temporal changes over it constitute the aim of this research.

The six objectives declared in chapter one guided the researcher during this study. These objectives were addressed in a systematic workflow during this study with the core results provided in chapters four and five. The temporal data collected from Landsat 8, Pléiades and TerraSAR-X provided a suitable stack of information to analyse specific changes over the two selected open pit mines, Sishen and Kolomela. The data image processing required diverse approaches; and experts in this field such as the Landsat 8 image processing and land cover classification produced by GEOTERRAIMAGE and the advance image processing system designed by Pinkmatter Solutions, FarEarth, ensured high quality results suitable for further spatial analysis suitable for this study. The Landsat 8 land cover classification derived from an 18 month data stack produced an accurate medium resolution land cover base map. This base map provided the necessary spatial information to understand the predominant land cover classes that exist over each study area. Followed by the Pléiades monoscopic land cover classification, it produced a more micro scale assessment of specific temporal changes over selected targets. These changes enabled the researcher to measure and calculate the class changes over time to illustrate their value for mine operational and environmental monitoring.

Applying the stereoscopic data collected with the Pléiades satellites produced accurate very high resolution elevation models. These elevation models serve as the source information for volumetric calculations. During this study several examples were demonstrated over diverse topological areas such as flat and recessed areas as well as medium and large sized mine waste dumps. Comparing the volumetric calculations from different timestamp stereoscopic datasets resulted in the measurement of volume changes over specific target areas. This is a relevant aid for the mine to determine its estimated production outputs over certain areas, complementary to traditional field surveying activities.

The SAR technology applied over the Royal Bafokeng tailings pond area and the Chuquicamata open-pit mine demonstrated the value of the high precision vertical measurements of surface changes using a temporal stack of interferometric radar data. The measurement accuracies achieved were between 2.5mm to 4mm to detect either subsidence or upliftment over the study areas. This SMM application was a relevant application to determine vulnerable points within a mining area as an aid to surface stability risk assessment and management.

The final objective was to provide recommendations on how satellite based RS can be used to effectively contribute to the monitoring of mine operations and the surrounding environmental conditions. Such recommendations can be derived from the methodological workflow diagram provided, see Figure 3.1. From a satellite earth observation perspective, an integrated approach using multi-sensor platforms such as medium resolution, very high resolution mono- and stereoscopic imagery as well as SAR applications together provides relevant spatial information layers for mine management. Combining all these application results with further complementary technologies, when appropriate, such as airborne LIDAR campaigns and drone micro scale data, provides the ultimate spatial information solution for mine monitoring and the detection of changes within its surrounding environment. Using the combination of all these technologies requires an in depth requirement assessment to fit with the mine operations and a feasibility study to ensure a sustainable approach for the mine. No generic approach is recommended as each mine has different challenges and geographical surroundings.

7.2 Remote sensing: a futuristic outlook and opportunities for future research

In section 2.2.4 some reference was made to futuristic trends in the RS technology and how this industry is changing. An increase in microsatellite capabilities through continuous improvement in space equipment establishes the possibility to increase the number of constellations and therefore the monitoring of Earth resources. This improvement includes scientific and engineering breakthroughs in Ground Sampling Distance (GSD), Instantaneous Field Of View (IFOV), Time Delay Integration (TDI), to mention only a few (Astrium, 2012).

The GSD is the distance at ground view by two consecutive pixels (in meters) along both directions. The IFOV in a scanning system refers to the solid angle subtended by the detector when scanning motion is stopped. Instantaneous field of view is commonly expressed in milliradians or picoradians. A time delay integration charge-coupled device (CCD) is widely used for the observation of objects moving at high speed, undetectable by classic CCD. This technique senses charge patterns and shifts them across the CCD array in sync with the movement of the image, to integrate more light from the scene (Astrium, 2012). The purpose of this study is not to highlight all the details of the space systems engineering concepts, yet the relevance of mentioning a few confirms the human understanding of this science and the continuous excelsior of satellite performance during engineering and operations.

The science of spectroscopy is not new, yet the improvement of this science and use of automated identification and mapping algorithms with expert systems such as the Tetracorder of the USGS serve as a good example. This spectroscopy is much more sophisticated than conventional broadband RS analysis. The Tetracorder can identify and map automatically for example minerals; it can detect sources of acid rock drainage, and map vegetation species, ice, melting snow, water, and water pollution, all with one set of expert system rules (Clark et al, 2003).

Spectroscopy technology is not new. What then is its relevance for the future? Most of these platforms are used at ground level or are airborne. The HyMap system of Australia is a good example of an advanced airborne hyperspectral system. With almost contiguous spectral coverage across the wavelength interval 0.45μm –

2.5µm, the HyMap sensors have achieved high performance levels in terms of signal to noise ratio, band to band registration and image quality (Cocks et al, 1998).

Applying this technology into future spaceborne systems brings a new dimension to RS classification, object orientated feature detection and its changes during time series analysis. High spatial resolution combined with wide swath hyperspectral instruments path the way for improved land cover and land use classification.

To conclude, the futuristic outlook of satellite RS certainly holds great potential and excitement for the geo-informatics community. Improvements in its technical specifications, temporal revisit and increase in competition between service providers are all positive signs for the geo-informatics consumer. Furthermore, the entrance of drone and UAV solutions in the market as well as advanced airborne platforms cannot be excluded from the current and future outlook of spatial technologies in the market (Rawlins, 2017; Brown, 2017).

Embracing the concept of cradle-to-gate to define the Life Cycle Assessment (LCA) of a mine (Durucan, Korre and Munoz-Melendez, 2006), further research opportunities still exist. The LCA model integrates the mine production, processing, waste treatment and disposal, rehabilitation and aftercare stages of a mine's life (Durucan et al, 2006). Thus, during this research focus was primarily on the mines during their production, processing, waste treatment and disposal phases. Applying satellite based RS to monitoring and assessing the progress of rehabilitation and aftercare stages of a mine certainly holds much potential. It is also recommended that a complete coverage of a new prospect mine area be collected to ensure a very good spatial base map of the natural conditions existing before any mine activities are commenced. During the rehabilitation phase this historical base map can then be used as a guide to measure the success of rehabilitation after mine closure, thus a very good benchmark with which the previously existing natural conditions can be compared.

7.3 Conclusion

The dissertation “Satellite based synthetic aperture radar and optical spatial-temporal information as aid for operational and environmental mine monitoring” had

the aim to reach six objectives, as described in section 1.5. Confirming that these objectives have been reached, the following bulleted answers conclude this study.

- Objective 1: Suitable temporal multi-sensor data have been collected over the Sishen and Kolomela open pit mines using Landsat 8 and Pléiades imagery.
- Objective 2: Pre-processing procedures applied by the FarEarth system ensured high quality orthorectification, top of atmosphere corrections and classification results using the Pléiades temporal mono- and stereoscopic imagery.
- Objective 3: The baseline land cover maps over Sishen and Kolomela mines were derived from a Landsat 8 temporal stack of at least 18 images, period 2014/2015. The advanced land cover modelling procedures, as designed by GeoTerraImage, produced high quality and consistent baseline land cover results.
- Objective 4: The one metre digital terrain model produced from the stereoscopic Pléiades imagery enabled the measurement of elevation changes over various different topological areas as selected during this study. These elevation models enabled volumetric calculation from a selected zero plane value as well as the volume changes between two temporal stereo datasets.
- Objective 5: SMM products as produced from multi-stack interferometric scenes collected from the TerraSAR-X satellite were demonstrated over the Royal Bafokeng Platinum tailings pond and Chuquicamata copper mine in Chile. These SMM results clearly demonstrated high precision measurements (2mm to 4mm) for surface subsidence and upliftment activities within the geographical areas analysed.
- Objective 6: Chapter 6 captured various discussion points as well as recommendations from the researcher to confirm the value of satellite based technology for the monitoring of mine operations as well as the monitoring of environmental impact activities. Integration of spatial information from various platforms and the futuristic outlook of spatial technology were also addressed in Chapter 7.

References

Ahluwalia, S.S., 2007. *Microbial and plant derived biomass for removal of heavy metals from wastewater*. Bioresour Technol: 98:2243-2257.

Akcil, A. and Koldas, K.S., 2006. *Acid Mine Drainage (AMD): Causes, treatment and\ case studies*. Journal of Cleaner Production, December, volume 14, pp1139-1146.

Ali, A.S.O. and Pour, A.B., 2014. *Lithological mapping and hydrothermal alteration using Landsat 8 data: a case study in Ariab mining district, Red Sea Hills, Sudan.* International Journal of Basic and Applied Sciences, volume 3, issue 3, pp 199-208.

Anderson, J., 2016. *Satellite based surface movement monitoring over South of Pretoria and surroundings, South Africa*. Unpublished report. © Airbus DS Geo GmbH.

Appiah, D.O. and Osman, B., 2014. *Environmental Impact Assessment: Insights from mining communities in Ghana.* Journal of Environmental Assessment Policy and Management, December, volume 16, issue 4, pp1-20.

Astrium, 2012. Pléiades Imagery User Guide. October, version 2.0. Unpublished report.

Avery, T.E., and Berlin, G.L., 1992. Fundamentals of remote sensing and air photo interpretation. 5th edition. New York: Macmillan Publishing Company.

Barr, R., and Cook, R. E., 2009. *Mining for operational excellence.* Mining Engineering. November 2009. USA.

Berardino, P., Fornaro, G., Lanari, R., and Sansosti, E., 2002. *A New Algorithm for Surface Deformation Monitoring Based on Small Baseline Differential SAR Interferograms*. IEEE Transaction on Geoscience and Remote Sensing, issue 40, pp2375-2383.

Böhme, C., Goosen, S., Lück, W., and Prinsloo, T., 2014. *A light-weight distributed processing and data handling system for emerging space agencies*. 65th International Astronautical Congress, Toronto, Canada. IAC-14, pp4.2.

Brown, J., 2017. *Robots on the rise.* City Press, 19 February.

Bryceson, D., and MacKinnon, D., 2012. *Eureka and beyond: mining's impact on African urbanisation.* Journal of Contemporary African Studies, Vol. 30, No. 4, p513-537. UK: Routledge.

Buys, A., and Steyn, H. 2010. *Creativity and eureka in science and engineering.* Essays Innovate Vol 5. Pretoria: University of Pretoria.

Cann, C. 2016. *The struggle for survival.* Mining Journal. January 22.

Canon, J.C., 2015. *Mining "tsunami" set to take Africa by storm.* Environmental Management Jul/Aug edition, p20-21.

Casu, F., Manzo, M., and Lanari, R., 2006. *A quantitative assessment of the SBAS algorithm performance for surface deformation retrieval from DInSAR data*. Remote Sensing of Environment, 102, 195-210.

Chen, C.H., 2012. Signal and image processing for remote sensing. 2nd edition. New York: CRC Press.

Clark, R.N., Swayze, G.H., Livo, K.E., Kokaly, R.F., Sutley, S.J., Dalton, J.B., McDougal, R.R., and Gent, C.A., 2003*. Imaging spectroscopy: Earth and planetary remote sensing with the USGS Tetracorder and expert systems.* Journal of geophysical research, vol. 108.

Cocks, T., Jenssen, R., Stewart, A., Wilson, I., and Shields, T., 1998. *The hymap™ airborne hyperspectral sensor: The system, calibration and performance*. Presented at 1st EARSEL Workshop on Imaging Spectroscopy, October: Zurich.

DEAT, 2004. Environmental Management Plans, Integrated Environmental Management, Information Series 12, Department of Environmental Affairs and Tourism (DEAT), Pretoria.

Duckart, F.D., Silva, A.M., Toledo, C.L.B. and de Assis, L.M., 2016. *Mapping iron oxides with Landsat-8/OLI and EO-1/Hyperion imagery from the Serra Norte iron deposits in the Carajas Mineral Province, Brazil*. Brazilian Journal of Geology, volume 43, issue 3, pp 331-349.

Durucan, S., Korre, A. and Munoz-Melendez, G., 2006. *Mining life cycle modelling: a cradle-to-gate approach to environmental management in the minerals industry.* Journal of Cleaner Production, Volume 14, Issues 12–13, pp 1057–1070.

Edwards, D.P., Sloan, S., Weng, L., Dirks, P., Sayer, J., Laurence, W.F., 2014. *Mining and the African Environment.* Conservation Letters Vol.7 Issue 3, p302-311.

Emuze, F., and Hauptfleisch, C., 2014. *The impact of mining induced urbanization: a case study of Kathu in South Africa*. Journal of Construction Project Management and Innovation, December, volume 4, issue 2, pp 882 – 894.

Ferretti, A., Prati, C., and Rocca, F., 2001. *Permanent Scatterers in SAR Interferometry.* IEEE Transaction on Geoscience and Remote Sensing, volume 39, pp 8-20.

Floyd, F., and Sabins, J.R., 1986. Remote Sensing Principles and Interpretation. 2nd edition. New York:Freeman.

Gates, H.L., and Appiah, K.A., 2010. *Minerals and Mining in Africa.* Encyclopaedia of Africa, 1ed. England:Oxford University Press.

Gu, W.H., Morgenstern, N.R., Dawson, R.F., and Robertson, P.K., 1998. *A Case History of Liquefaction Flow Failures in Mountains Mine Waste Dumps*. International Conference on Case Histories in Geotechnical Engineering. Fourth conference, March 8th to March 15th.

Gwimbi, P., and Nhamo, G., 2016. *Translating mitigation measures proposed in environmental impact statements into planning conditions: Promises and practices by multinational platinum mining firms along the Great Dyke of Zimbabwe.* Environmental Science and Policy, March, pp10-21.

Hames, A., 2015. *Mine security in Africa: a G4S perspective on the issues involved*. Mining World, Vol. 12, Issue 1, February, p30-34.

Harries, J. 1997. *Acid mine drainage in Australia: Its extent and potential future liability*. Supervising Scientist Report 125. Supervising Scientist. Canberra.

Harries, N., Noon, D., and Rowley, K., 2006. *Case studies of slope stability radar used in open cut mines.* The South African Institute of Mining and Metallurgy International Symposium on Stability of Rock Slopes.

Hendryx, M., 2015. *The public health impacts of surface coal mining*. In The Extractive Industries and Society, December, volume 2, issue 4, pp 820-826.

Hustrulid, W.A., and Fernberg, H., 2010*. An introduction to surface mining*. Talking technical. Atlas Copco, pp 17-22.

Hustrulid, W.A., Kuchta, M., Martin, R.K., 2013. Open pit mine planning and design. 3rd Edition. USA: CRC Press.

Janneh, A., and Ping, J., 2011. *Minerals and Africa's Development: The international Study Group Report on Africa's Mineral Regimes*. Economic Commission for Africa. Addis Ababa: PCMS.

Jansen, W., 2011. KPMG Mining Operational Excellence Framework. Sweden: KPMG International Cooperative.

Jones, H.G., and Vaughan, R.A., 2010. Remote sensing of vegetation: Principles, techniques and applications. Oxford: University Press.

Kramer, H.J., 2002. Observation of the Earth and Its Environment: Survey of Missions and Sensors. 4th edition. Germany: Springer-Verlag Berlin

Heidelberg. Liang, S., 2004. Quantitative Remote Sensing of Land Surfaces. Canada: John Wiley & Sons.

Liang, S., Li, X., Wang, J. 2012. *Advanced remote sensing.* Terrestrial information extraction and applications. Amsterdam: ELSEVIER.

Lillesand, M.T., Kiefer, R.W., Chipman, J.W., 2007. Remote sensing and image interpretation. 6th edition. USA: Wiley.

Lück, W., 2015. *Evaluation of automatically generated digital terrain models and change products from Pléiades satellite imagery over Sishen Mine*. © Pinkmatter Solutions, unpublished report.

Lundgren, P., Usai, S., Sansosti, R., Lanari, R., Tesauro, M., Fornaro, G., and Berardino, P., 2001.*Modeling surface deformation observed with SAR Interferometry at Campei Flegrei Caldera*. Journal Geophysical. Issue 106, pp19355-19367.

Mapani, B., and Kribek, B. 2012. *Environmental and health impacts of mining in Africa.* Proceedings of the annual workshop IGCP/SIDA No. 594, Windhoek, Namibia, July 5th – 6th. Czech: Czech Geological Survey.

Mather, P.M., and Koch, M., 2011. Computer processing of remotely sensed images: An introduction. 4th edition. England: Wiley-Blackwell.

Maystadt, J., De Luca, G., Sekeris, P.G. and Ulimwengu, J., 2014. *Mineral Resources and Conflicts in DRC: A Case of Ecological Fallacy?.* Oxford Economic Papers, July, version 66, issue 3, pp 721-749.

Moore, J. 2016. The official mining in Africa country investment guide (MACIG). Johannesburg: gbreports.

Morgan, M.J., 2015. *Sector focus: Mining in Africa*. African Business. Edition February, p30-39.

Mwiinga, G. 2011. *Acid mine drainage issues in South Africa.* Water Sector edigest, June, pp1-12.

Myburgh, H.A., Nortje, A., 2014. *Operation and performance of the Sishen jig plant.* Journal of the Southern African Institute of Mining and Metallurgy, volume 114 issue 7, July.

Newman, A.M., Rubio, E., Weintraub, R.C.A., Eurek, K., 2010. *A Review of Operations Research in Mine Planning*. Interfaces, volume 40, issue 3, May-June, pp222-245.

Ongondo, F.O., Williams, I.D., and Whitlock, G., 2015. *Distinct Urban Mines: Exploiting secondary resources in unique anthropogenic spaces.* In Urban Mining, Waste Management, November, pp 45:4-9, Elsevier Ltd.

Peck, J.P., 1999. *Open-pit mining (monitoring and control*). AccessScience. McGraw-Hill Global Education Holdings.

Rawlins, L.K., 2017. *Drastic increase in SA drone traffic*. Defenceweb, Friday 10 February.

Steyn, H. 2012., Design and Entrepreneurship. Pretoria: MultiMedia Access.

Szwedzicki, T., 2010. *Warning Signs to Geotechnical Failure of Mining Structures.* International Journal of Surface Mining, Reclamation and Environment, Volume 18, Issue 2, pp150-163.

Thompson, M. 2015. *2013 - 2014 South African National Land-Cover Dataset*. © GeoTerraImage. Version 5. Unpublished report.

Usai, S., 2001. A new approach for long term monitoring of deformation by differential SAR interferometry, Ph.D. thesis, Delft Univ. Press, Delft, The Netherlands.

Weng, Q., 2011. *Advances in Environmental Remote Sensing*. Sensors, Algorithms and Applications. New York: CRC Press.

Yager, T.R., Bermúdez-Lugo O., Mobbs, Newman, P.M., H.R., Taib, M., Wallace, G.J., and Wilburn, D.R. 2012. *The Mineral Industries of Africa*. Minerals Yearbook. U.S. Geological Survey.

Zhang, Y., Lu, W., Zhao, H., Yang, Q., Chen, M. 2015. *Geo-environmental impact assessment and management information system for the mining area, Northeast China.* Environmental Earth Sciences, November, volume 74, issue 10, pp7173-7185.

Internet references

http://gbreports.com/category/mining-minerals [Date of access: 14 February 2016]

http://gisgeography.com/free-satellite-imagery-data-list/ [Date of access: 10 January 2017]

http://interactive.satellitetoday.com/leo-constellation-announcements-the-industry-reacts/ [Date of access: 30 March 2016]

http://www.angloamerican.co.za/our-operations/iron-ore.aspx [Date of access: 8 April 2016]

http://www.angloamericankumba.com/our-business/operations.aspx [Date of access: 8 April 2016]

http://www.digitalglobe.com/ [Date of access: 30 March 2016]

http://www.esa.int/SPECIALS/Eduspace_EN/SEMF9R3Z2OF_0.html [Date of access: 27 March 2016]

http://www.fao.org/docrep/X5318E/x5318e02.htm [Date of access: 28 February 2016]

http://www.geo-airbusds.com [Date of access: 30 March 2016]

http://www.geo-airbusds.com/en/52-pleiades-very-high-resolution-satellite-imagery [Date of access: 15 April 2016]

http://www.intelligence-airbusds.com/en/7555-discover-stack-insight [Date of access: 10 January 2017]

http://www.intelligence-airbusds.com/one-tasking/ [Date of access: 10 January 2017]

http://www.landsat.gsfc.nasa.gov/landsat-8/landsat-8-overview/ [Date of access: 22 December 2016]

http://www.meoweather.com/history/South%20Africa/na/27.7/23.05/Kathu.html?units=c# [Date of access: 10 January 2017]

http://www.mine-engineer.com/mining/open_pit.htm [Date of access: 28 February 2016]

http://www.miningfacts.org/communities/what-is-artisanal-and-small-scale-mining/ [Date of access: 28 February 2016]

http://www.mining-technology.com/projects/kolomela-iron-ore-mine-northern-cape/kolomela-iron-ore-mine-northern-cape1.html [Date of access: 8 April 2016]

http://www.na.srk.com/en/newsletter/srk-40th-anniversary/africa-bafokeng-tailings-dam [Date of access: 30 December 2016]

http://www.newvision.co.ug/print_article/new_vision/news/1446760/collision-course-rules-drones?print=true [Date of access: 30 December 2016]

http://www.oceanservice.noaa.gov/facts/remotesensing.html [Date of access: 27 March 2016]

http://www.skyboximaging.com/ [Date of access: 30 March 2016]

http://www.visualdirectoryonline.com [Date of access: 15 March 2016]

https://en.wikipedia.org/wiki/Chuquicamata [Date of access: 9 April 2016]

https://en.wikipedia.org/wiki/Environmental_Issues_in_Africa [Date of access: 28 February 2016]

https://en.wikipedia.org/wiki/Merriespruit_tailings_dam_disaster [Date of access: 30 December 2016]

https://en.wikipedia.org/wiki/Mineral_industry_of_Africa Africa [Date of access: 28 February 2016]

https://nisar.jpl.nasa.gov/technology/polsar/

https://spaceflight101.com/events/falcon-9-paz/

https://www.cover.co.za/acid-mine-drainage/ [Date of access: 10 January 2017]

https://www.kpmg.com/Africa/en/IssuesAndInsights/Articlespublications/Documents/Mining%20Indaba%20brochure.pdf [Date of access: 11 March 2016]

https://www.planet.com/press/#facts [Date of access: 30 March 2016]

https://www.urthecast.com/constellation [Date of access: 30 March 2016]

Satellite Data

Optical: Landsat

Data Pre-Processing

Data Import

Image rectification

Atmospheric correction

Image transformation

Image Classification

Unsupervised - Indices

Obiect-based

Land Cover/Use

Optical: Pléiades

Data Pre-Processing

GCPs and markers

Image rectification

Stereo

Mono

Image Enhancement

Custom Projection

DSM & DTM

Volumetric Calculation

Data Packaging & Distribution

SAR: TerraSAR-X

InSAR

Data Pre-Processing

Data download

Data extraction

Data import

Data Assessment

Data Selection

DEM Extraction

Interferometric Time Series Analysis

DInSAR

SBAS

Surface movement

Post-Processing

Ground Truthing

Data Export

Finalisation

Change Detection

Post-classification

Statistical measures

Visualisation

Product SMM

Environmental Impact

Primary

Secondary

Mine monitoring &Environmental impact model

Annexure A: Research design diagram

ANNEXURE B Foundation National Land Cover classes

1. Background

This annexure provides the reader additional descriptive information of each fundamental National Land Cover class. This additional information is referenced to Chapter 4, section 4.2.1 of this study.

2. Water

Water was modelled using a combination of 5 spectral indices, including a burn index, and Digital Elevation Model (DEM) derived solar illumination and slope masks. The burn index was used to minimise any spectral confusion between dark burnt areas and comparable water body reflectance. The solar illumination and slope masks were used to minimise any spectral confusion between dark terrain shadow areas and comparable water body reflectance. Generic spectral water models were developed for both flat (standard) and hilly terrain and for shallow water (pan) dominated landscapes.

Permanent water was classified based on areas of open, surface water, that were detectable on all image dates used in the Landsat 8 based water modelling processes. Permanent water extent typically refers to the minimum water extent, which occured throughout the 2013-14 assessment period. It includes both natural and man-made water features.

Seasonal water describes areas of open, surface water, that are detectable on one or more, but not all image dates used in the Landsat 8 based water modelling processes. Seasonal water extent typically refers to the maximum water extent, which may only occur for a limited time within the 2013-14 assessment period. This includes both natural and man-made water features.

3. Base vegetation

The natural vegetation base classes, namely thicket / dense bush, woodland / open bush, grassland, low shrubland and bare, non-vegetated areas were created by merging selected groups of spectral classes. Generally, selected spectral classes were merged into the required vegetation cover classes without geographical control, using the original spectral class extent and distribution 'as-is'. However in some regions, and for some spectral classes it was necessary for the re-coding and merging process to be geographically controlled, and only to allow the recode procedure within pre-determined geographical regions. Controlled geographical recoding (i.e. masking), used pre-selected SANBI bioregion[1] boundaries to define where and how selected spectral classes were modified. Note that the final vegetative land-cover class boundary was always defined by the original spectral foundation class boundaries contained within the SANBI bioregion boundary, and not by the bioregion boundary itself, other than for the fynbos low shrubland sub-class.

Thicket and dense bush: Natural / semi-natural tree and / or bush dominated areas, where typically canopy heights are between 2m - 5m, and canopy density is typically > ± 75%, but may include localised sparser areas down to ± 60%. These areas include dense bush, thicket, closed woodland, tall, dense shrubs, scrub forest and mangrove swamps. They can include self-seeded bush encroachment areas of sufficient canopy density.

Woodlands and open bush: Natural / semi-natural tree and / or bush dominated areas, where typically canopy heights are between ± 2m - 5m, and canopy densities typically between 40 - 75%, but that may include localised sparser areas down to ± 15 - 20% . These areas include sparse open bushland and woodland, including transitional wooded grassland areas. They can include self-seeded bush encroachment areas if canopy density is within the indicated range. In the arid western regions (i.e. the Northern Cape), this cover class may be associated with a

[1] Sourced from "The Vegetation of South Africa, Lesotho and Swaziland". Eds Mucina L and Rutherford MC. 2006. Strelitzia 19. South African National Biodiversity Institute: associated digital GIS database. Note that SANBI Biome and Bioregion boundaries, whilst generically applicable for 1:250,000 digital map scales, is often *considerably more accurate on a local scale, even down to the nearest 100m in some cases* (refer Section 4.1.2, Mapping Scale. p 15)

transitional bush / shrub cover that is lower than typical open bush / woodland cover but higher and/or denser than typical low shrub cover.

Grassland: Natural / semi-natural grass dominated areas, where the tree and / or bush canopy densities are typically < ± 20%, but that may include localised denser areas up to ± 40%, (regardless of canopy heights). These areas include open grassland, and sparse bushland and woodland areas, including transitional wooded grasslands. They may include planted pasture (i.e. grazing) if not irrigated. Irrigated pastures will typically be classified as cultivated, and urban parks and golf courses etc. will be classified as urban.

Low shrubland (other): Natural / semi-natural low shrub dominated areas, typically with ≤ 2m canopy height. They include a range of canopy densities encompassing sparse to dense canopy covers. Very sparse covers may be associated with the bare ground class. They are typically associated with low, woody shrub, Karoo-type vegetation communities, although they can also represent locally degraded vegetation areas where there is a significantly reduced vegetation cover in comparison to surrounding, less impacted vegetation cover, including long-term wildfire scars in some mountainous areas in the Western Cape. Note that taller tree / bush / shrub communities within this vegetation type are typically classified separately as one of the other tree or bush dominated cover classes.

4. Cultivated

The Department of Agriculture, Forestry and Fisheries' (DAFF) public domain 2013 national field boundary dataset (captured from 2.5m resolution, pan-merge SPOT5 imagery), was the initial source of the cultivated land use classes. This existing dataset was updated nationally to represent the latest cultivated land patterns present on the latest 2014 Landsat 8 imagery used in each image frame. This typically involved capturing the distribution of new, commercially cultivated fields, especially centre pivot irrigation units, although all field types were included in the 2014 updating process, including subsistence cultivation areas, if clearly apparent.

All new cultivated lands (and crop types) mapped from the 2014 Landsat 8 imagery were captured manually using on-screen photo-interpretation techniques, since this

facilitated and maintained similar interpretation accuracies to the source SPOT5 derived field boundary data. Furthermore it also eliminated post-classification editing necessities typically associated with field boundary (as opposed to crop type), classification attempts.

Commercial annuals: Cultivated lands used primarily for the production of rain-fed, annual crops for commercial markets. Typically represented by large field units, often in dense local or regional clusters. In most cases the defined cultivated extent represents the actual cultivated or potential extent.

Commercial pivots: Cultivated lands used primarily for the production of centre pivot irrigated, annual crops for commercial markets. In most cases the defined cultivated extent represents the actual cultivated or potential extent.

5. Forest plantations

Forestry plantations, and sub-class detail were derived from selected classes from within the 51 x spectral foundation cover dataset, which were re-coded and re-grouped within controlled geographical areas, using independently sourced and generated geographic masks.

Mature trees: Planted forestry plantations used for growing commercial timber tree species. The class represents mature tree stands which have approximately 70% or greater tree canopy closure (regardless of canopy height), on all the multi-date Landsat images in the 2013-14 analysis period. The class includes spatially smaller woodlots and windbreaks with the same cover characteristics

6. Mines

Mines and sub-class details were derived from selected classes from within the 51 x spectral foundation cover dataset, which were re-coded and re-grouped within controlled geographical areas, using independently sourced and generated geographic masks. The mine area masks were sourced from previous in-house, provincial mapping projects and national 1:50,000 scale map datasets, all of which were then updated nationally to the mine activity extent visible on the 2014 Landsat

imagery. Note that mine water sub-classes were generated by identifying water classes that were located within the final mine geographical masks.

Note that the final mine class boundaries were always defined by the original spectral foundation class boundaries contained within the geographical masks, and not by the geographical mask boundaries themselves.

Mine bare: Mining activity footprint, based on pure, non-vegetated, bare ground surfaces. It includes extraction pits, tailings, waste dumps and associated surface infrastructure such as roads and buildings (unless otherwise indicated), for both active and abandoned mining activities. The class may include open cast pits, sand mines, quarries, borrow pits etc.

Mine semi-bare: Mining activity footprint, based on semi-bare ground surfaces, which may be sparsely vegetated. It includes extraction pits, tailings, waste dumps and associated surface infrastructure such as roads and buildings (unless otherwise indicated) and surrounding dust-impacted areas, for both active and abandoned mining activities. The class may include open cast pits, sand mines, quarries, borrow pits etc.

7. Bare

The erosion (donga) class was derived from selected classes (representative of bare ground) from within the 51 x spectral foundation cover dataset, which were re-coded and regrouped within controlled geographical areas, using independently sourced and generated geographic masks. The erosion area masks were sourced from previous in-house, provincial mapping projects and other national erosion datasets, all of which were then updated nationally to represent the current extent of major dongas visible on the 2014 Landsat imagery. Note that as a result of spectral modelling sensitivities, and the need to be able to separate the bare ground within donga features from the surrounding non-eroding areas, the final modelled extent of erosion features is significantly better represented both spatially and numerically in the wetter, more vegetatively lush regions of the country, where the non-vegetated erosion surfaces are significantly different from the surrounding vegetation cover (i.e.

bushveld and grassland regions). Donga feature detection in the drier more arid region is not as accurate

Erosion dongas and gullies: Non-vegetated donga and gully features, typically associated with significant natural or man-induced erosion activities along or in association with stream and flow lines. The mapped extent of the dongas and gullies is represented by bare ground conditions in all or the majority of the multi-date Landsat images used in the land-cover modelling. Note that these erosion features are significantly better represented both spatially and numerically in the wetter, more lush regions of the country where the non-vegetated erosion surface is significantly different from the surrounding vegetation cover (i.e. bushveld and grassland regions). In general, sparsely vegetated sheet eroded areas and degraded areas with significantly reduced local vegetation cover are not included in this class, but will be represented by local areas of low shrub or bare ground.

Bare non-vegetation: Bare, non-vegetated ground, with little or very sparse vegetation cover (i.e. typically < ± 5 - 10 % vegetation cover), occurring as a result of either natural or man-induced processes. It includes but is not limited to natural rock exposures, dry river beds, dry pans, coastal dunes and beaches, sand and rocky desert areas, very sparse low shrublands and grasslands, surface (sheet) erosion areas, severely degraded areas, major road networks etc. May also include long-term wildfire scars in some mountainous areas in the Western Cape.

8. Built-up / Settlements

Built-up areas and sub-class details were generated independently of the spectral foundation cover dataset. The primary source for the cover class was several, internally developed GEOTERRAIMAGE urban map products and associated databases. These provided detailed information on the extent, distribution and land-use for all settlements nationally. This was verified in rural areas with the national Dwelling Frame dataset, available from STATS SA. This information was then spatially re-modelled to represent built-up area outlines, and further updated and corrected nationally, using the 2014 Landsat imagery for visual reference. This was especially done in the case of rural village outlines in provinces such as Limpopo, Mpumalanga and North West.

Commercial: Areas containing high density buildings and other built-up structures associated with mainly non-residential, commercial, administrative, health, religious or transport (i.e. train station) activities. Note that in some areas this class may include tall, multi-storey residential flat units.

Industrial: Areas containing buildings and other built-up structures associated with mainly non-residential, industrial and manufacturing activities, including power stations.

Informal: Areas containing high density buildings and other built-up structures typically associated with informal, often non-regulated, residential housing. Note that in some areas this class may include new formal developments within township areas that appear on Landsat imagery as primarily non-vegetated areas with limited infrastructure development.

Residential: Areas containing variable density buildings and other built-up structures typically associated with formal, regulated, residential housing. They include well established suburbs, townhouses, hostel complexes, flats etc.

Schools and sports grounds: Areas containing buildings, other built-up structures and open sports areas typically associated with schools and school sports grounds. Image identification of such features is based on the local spatial relationship between the buildings and the open area, thus small urban schools without adjacent open areas may have been missed.

Smallholding: Areas containing a low density mix of buildings, other built-up structures within open areas, which may or may not be cultivated, that are representative of both formally declared agricultural holdings, and similar smallholdings / small farms, typically located on the periphery of urban areas.

Sports and golf: Areas containing a low density mix of buildings, other built-up structures associated with golf courses. The class includes both residential golf estates and non-residential golf courses, and typically represents the border extent of the entire estate or course.

Township: Areas containing high density buildings and other built-up structures typically associated with formal, regulated, residential housing associated with townships and "RDP" type housing developments.

Village: Areas containing variable density structures typically associated with rural villages, including both traditional and modern building formats.

Built-up other: Areas containing variable densities of buildings, other built-up structures, or no structures at all, that are not clearly identifiable as one of the other built-up classes. May include runways, major infrastructure development sites, holiday chalets, roads, car parks, cemeteries etc.

ANNEXURE C Technical specifications for the Pléiades satellites

Number of satellites	2 -- Pléiades 1A and Pléiades 1B
Launch	Pléiades 1A: 16th December 2012; *Pléiades 1B: Q4 2012*
Altitude	694km
Type	Sun-synchronous, 10:30 AM descending node
Period	98.79 minutes
Inclination	98.2°
Cycle	26 days
Optical system	The telescope is a Korsch type combination with 65cm aperture diameter, focal length of 12.905m, f/20, TMA optics
Spectral bands	Pan: 0.47-0.83 µm; Blue = 0.43-0.55 µm, Green = 0.50-0.62 µm, Red = 0.59-0.71 µm, Near Infrared = 0.74-0.94 µm (NIR)
Detectors	Panchomatic array assembly: 5 x 6000 (30,000 cross-track) pixels Multispectral array assembly: 5 x 1500 (7500 in cross-track) pixels Each pixel having a size of 13 µm in Panchromatic
Ground sampling distance (nadir)	Panchromatic: 0.7m; Multispectral: 2.8m
Product resolution	Panchromatic: 0.5m; Multispectral: 2.0m
Swath width	20km at nadir
Dynamic range at acquisition	12 bits per pixel
NIIRS class	6
Viewing angle	Standard: +/- 30°; Maximum: +/- 47°
Revisit frequency, using both Pléiades 1A & 1B	• with +/- 30° viewing angle, 1.3 days and better above 40° latitude, 1.7 days at equator; • with +/- 45° viewing angle, daily revisit of any point on the globe
Pointing agility	Roll of 60° within 25 seconds; Pitch of 60° within 25 seconds; 200km in 11 seconds including stabilization time
Acquisition capability	450 segments/day (up to 600) – relying on the two main receiving stations, Toulouse (France) and Kiruna
Location accuracy at nadir	Performance (Oct. 2012): 8.5m CE90 with refined attitude data
Onboard storage	600 GB (Solid State Mass Memory)
Instrument TM link rate	The output rate is nominally of 465 MB/sec, on three individual channels of 155 MB/sec each
Mission lifetime	Minimum of 5 years with an estimated life of more than 10 years

Source: Pléiades Imagery User Guide, October 2012, V 2.0

ANNEXURE D Pléiades temporal dataset

1. Background

The Pléiades imagery used during this monostatic imagery time series analysis consisted of five images selected in terms of availability and to take seasonal changes into account. The scene date stamp over each mine was as follows:

	Scene 1	Scene 2	Scene 3	Scene 4	Scene 5
Sishen	10/05/2015	27/07/2015	19/10/2015	5/01/2016	30/03/2016
Kolomela	16/05/2015	19/10/2015	5/01/2016	30/03/2016	28/12/2016

The imagery below illustrates the temporal datasets that were used to detect changes. This imagery was displayed in natural colour using the red, green and blue bands of the Pléiades satellites. The imagery was pansharpened to 0.5m spatial resolution and ortho-rectified to ensure good geometrical co-registration between the images.

A new waste dump area at the Sishen mine was demonstrated in Figures D1 and D2 from the “A1” subset area. The growth is visible from 10/05/2015 until 30/03/2016. The construction of a new power plant area at the Sishen mine was demonstrated in Figures D1 and D3 from the “A2” subset area. The progress of the construction is also visible from 10/05/2015 until 30/03/2016.

The Kolomela mine temporal images ranged from 16/05/2015 to 30/03/2016, see Figure D4. The growth of a new mine dumping area was illustrated in “B1” subset area and can be viewed in Figure D5. The construction of a new asphalt parking area was demonstrated in Figure D6, extracted from the “B2” subset area.

2. Pléiades temporal dataset over Sishen and Kolomela iron ore mines

10/05/2015

27/07/2015

19/10/2015

05/01/2016

30/03/2016

Figure D1: Sishen Mine area illustrated with five Pléiades temporal images, analytical case study areas as per RED squares in scene 30/03/2016

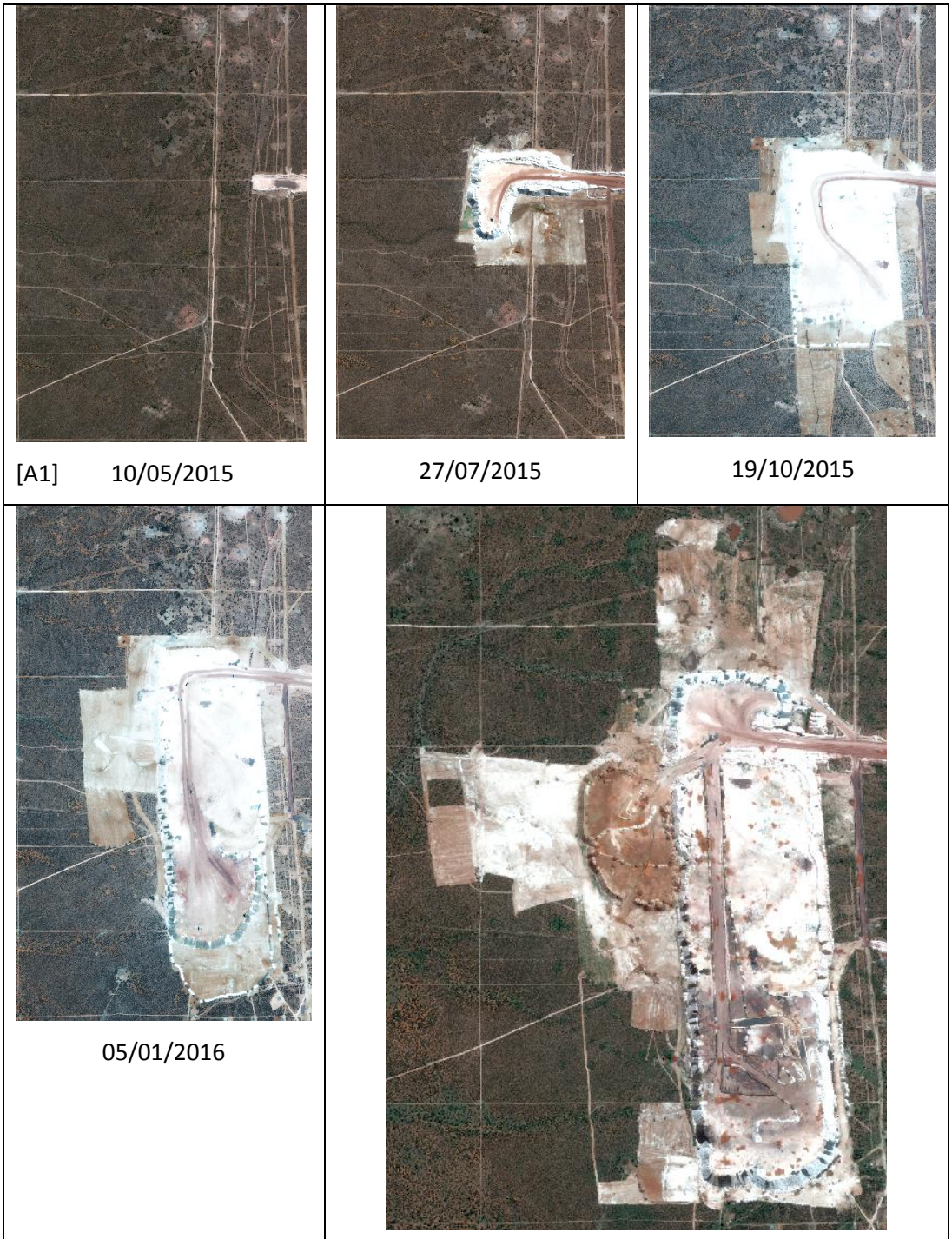

Figure D2: Sishen Mine area illustrated with five Pléiades temporal images, new mining waste dumping site [A1]

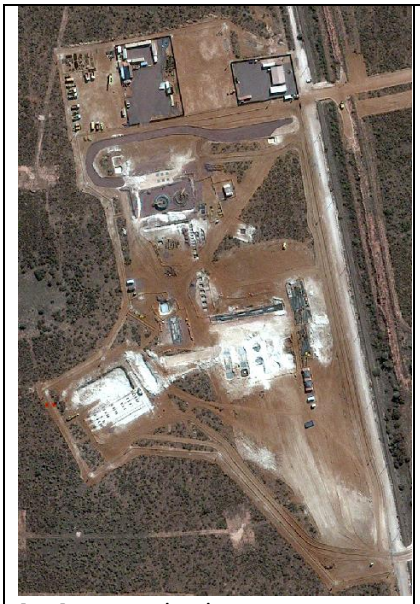

[A2] 10/05/2015

27/07/2015

19/10/2015

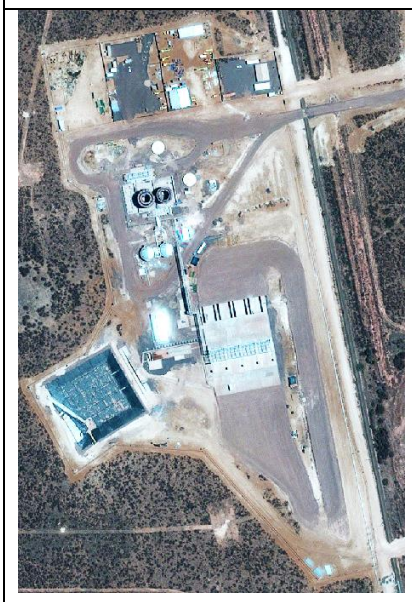

05/01/2016

30/03/2016

Figure D3: Sishen Mine area illustrated with five Pléiades temporal images, new power plant construction site [A2]

16/05/2015

19/10/2015

05/01/2016

30/03/2016

28/12/2016 (Only clipped scene was available)

Figure D4: Kolomela Mine area illustrated with five Pléiades temporal images, analytical case study areas as per RED squares in scene 28/12/2016

[B1] 16/05/2015

19/10/2015

05/01/2016

30/03/2016

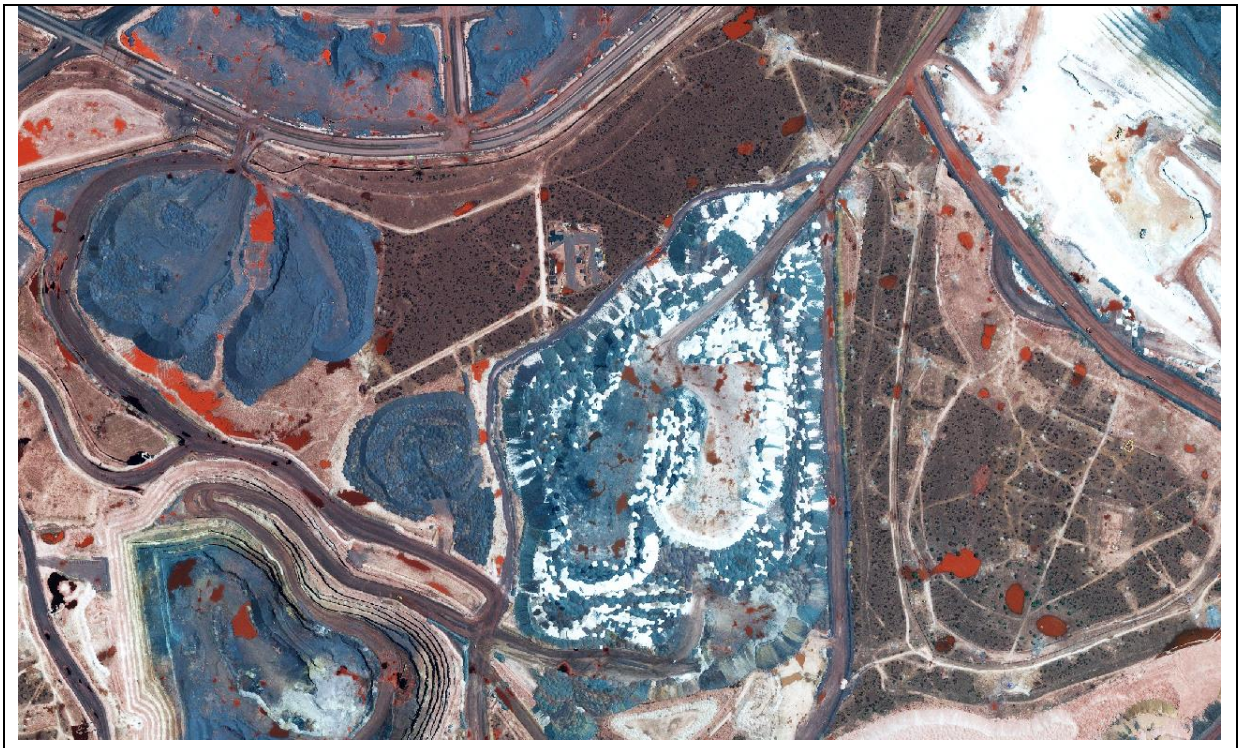

28/12/2016

Figure D5: Kolomela Mine area illustrated with five Pléiades temporal images, new mining dumping site [B1]

[B2] 16/05/2015

19/10/2015

05/01/2016

30/03/2016

28/12/2016

Figure D6: Kolomela Mine area illustrated with five Pléiades temporal images, new parking area [B2]